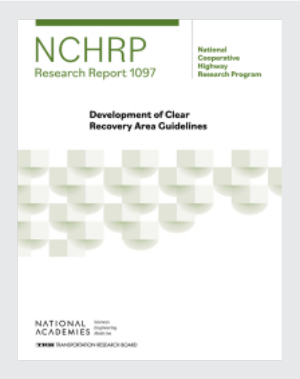

Development of Clear Recovery Area Guidelines (2024)

DETAILS

148 pages | 8.5 x 11 | PAPERBACK

ISBN 978-0-309-70945-3 | DOI 10.17226/27593

CONTRIBUTORS

Roger Bligh, Boniphace Kutela, Sofokli Cakalli, Nauman Sheikh, Raul Avelar; National Cooperative Highway Research Program; Transportation Research Board; National Academies of Sciences, Engineering, and Medicine

SUGGESTED CITATION

National Academies of Sciences, Engineering, and Medicine. 2024. *Development of Clear Recovery Area Guidelines*. Washington, DC: The National Academies Press. https://doi.org/10.17226/27593.

NATIONAL COOPERATIVE HIGHWAY RESEARCH PROGRAM

NCHRP RESEARCH REPORT 1097

Development of Clear Recovery Area Guidelines

Roger Bligh
Boniphace Kutela
Sofokli Cakalli
Nauman Sheikh
Raul Avelar
Texas A&M Transportation Institute
The Texas A&M University System
College Station, Texas

Subscriber Categories
Design • Operations and Traffic Management • Safety and Human Factors

Research sponsored by the American Association of State Highway and Transportation Officials
in cooperation with the Federal Highway Administration

NATIONAL ACADEMIES *Sciences Engineering Medicine*

TRB TRANSPORTATION RESEARCH BOARD

2024

NATIONAL COOPERATIVE HIGHWAY RESEARCH PROGRAM

Systematic, well-designed, and implementable research is the most effective way to solve many problems facing state departments of transportation (DOTs) administrators and engineers. Often, highway problems are of local or regional interest and can best be studied by state DOTs individually or in cooperation with their state universities and others. However, the accelerating growth of highway transportation results in increasingly complex problems of wide interest to highway authorities. These problems are best studied through a coordinated program of cooperative research.

Recognizing this need, the leadership of the American Association of State Highway and Transportation Officials (AASHTO) in 1962 initiated an objective national highway research program using modern scientific techniques—the National Cooperative Highway Research Program (NCHRP). NCHRP is supported on a continuing basis by funds from participating member states of AASHTO and receives the full cooperation and support of the Federal Highway Administration (FHWA), United States Department of Transportation, under Agreement No. 693JJ31950003.

The Transportation Research Board (TRB) of the National Academies of Sciences, Engineering, and Medicine was requested by AASHTO to administer the research program because of TRB's recognized objectivity and understanding of modern research practices. TRB is uniquely suited for this purpose for many reasons: TRB maintains an extensive committee structure from which authorities on any highway transportation subject may be drawn; TRB possesses avenues of communications and cooperation with federal, state, and local governmental agencies, universities, and industry; TRB's relationship to the National Academies is an insurance of objectivity; and TRB maintains a full-time staff of specialists in highway transportation matters to bring the findings of research directly to those in a position to use them.

The program is developed on the basis of research needs identified by chief administrators and other staff of the highway and transportation departments, by committees of AASHTO, and by the FHWA. Topics of the highest merit are selected by the AASHTO Special Committee on Research and Innovation (R&I), and each year R&I's recommendations are proposed to the AASHTO Board of Directors and the National Academies. Research projects to address these topics are defined by NCHRP, and qualified research agencies are selected from submitted proposals. Administration and surveillance of research contracts are the responsibilities of the National Academies and TRB.

The needs for highway research are many, and NCHRP can make significant contributions to solving highway transportation problems of mutual concern to many responsible groups. The program, however, is intended to complement, rather than to substitute for or duplicate, other highway research programs.

NCHRP RESEARCH REPORT 1097

Project 17-11(03)
ISSN 2572-3766 (Print)
ISSN 2572-3774 (Online)
ISBN 978-0-309-70945-3
Library of Congress Control Number 2024931083

COPYRIGHT INFORMATION

NOTICE

The research report was reviewed by the technical panel and accepted for publication according to procedures established and overseen by the Transportation Research Board and approved by the National Academies of Sciences, Engineering, and Medicine.

The opinions and conclusions expressed or implied in this report are those of the researchers who performed the research and are not necessarily those of the Transportation Research Board; the National Academies of Sciences, Engineering, and Medicine; the FHWA; or the program sponsors.

The Transportation Research Board does not develop, issue, or publish standards or specifications. The Transportation Research Board manages applied research projects which provide the scientific foundation that may be used by Transportation Research Board sponsors, industry associations, or other organizations as the basis for revised practices, procedures, or specifications.

The Transportation Research Board; the National Academies of Sciences, Engineering, and Medicine; and the sponsors of the National Cooperative Highway Research Program do not endorse products or manufacturers. Trade or manufacturers' names or logos appear herein solely because they are considered essential to the object of the report.

Published research reports of the

NATIONAL COOPERATIVE HIGHWAY RESEARCH PROGRAM

are available from

Transportation Research Board
Business Office
500 Fifth Street, NW
Washington, DC 20001

and can be ordered through the Internet by going to
https://www.mytrb.org/MyTRB/Store/default.aspx

Printed in the United States of America

NATIONAL ACADEMIES *Sciences Engineering Medicine*

The **National Academy of Sciences** was established in 1863 by an Act of Congress, signed by President Lincoln, as a private, non-governmental institution to advise the nation on issues related to science and technology. Members are elected by their peers for outstanding contributions to research. Dr. Marcia McNutt is president.

The **National Academy of Engineering** was established in 1964 under the charter of the National Academy of Sciences to bring the practices of engineering to advising the nation. Members are elected by their peers for extraordinary contributions to engineering. Dr. John L. Anderson is president.

The **National Academy of Medicine** (formerly the Institute of Medicine) was established in 1970 under the charter of the National Academy of Sciences to advise the nation on medical and health issues. Members are elected by their peers for distinguished contributions to medicine and health. Dr. Victor J. Dzau is president.

The three Academies work together as the **National Academies of Sciences, Engineering, and Medicine** to provide independent, objective analysis and advice to the nation and conduct other activities to solve complex problems and inform public policy decisions. The National Academies also encourage education and research, recognize outstanding contributions to knowledge, and increase public understanding in matters of science, engineering, and medicine.

Learn more about the National Academies of Sciences, Engineering, and Medicine at **www.nationalacademies.org**.

The **Transportation Research Board** is one of seven major program divisions of the National Academies of Sciences, Engineering, and Medicine. The mission of the Transportation Research Board is to mobilize expertise, experience, and knowledge to anticipate and solve complex transportation-related challenges. The Board's varied activities annually engage about 8,500 engineers, scientists, and other transportation researchers and practitioners from the public and private sectors and academia, all of whom contribute their expertise in the public interest. The program is supported by state transportation departments, federal agencies including the component administrations of the U.S. Department of Transportation, and other organizations and individuals interested in the development of transportation.

Learn more about the Transportation Research Board at **www.TRB.org**.

COOPERATIVE RESEARCH PROGRAMS

CRP STAFF FOR NCHRP RESEARCH REPORT 1097

Waseem Dekelbab, *Deputy Director, Cooperative Research Programs, and Manager, National Cooperative Highway Research Program*
David M. Jared, *Senior Program Officer*
Mazen Alsharif, *Senior Program Assistant*
Natalie Barnes, *Director of Publications*
Heather DiAngelis, *Associate Director of Publications*

NCHRP PROJECT 17-11(03) PANEL
Field of Traffic—Area of Safety

Don Jay Gripne, *DJG NW Inc., Olympia, WA* (Chair)
Mark Ayton, *Safe Roads R&D, Inc., Aurora, ON*
Drew A. Boyce, Jr., *Delaware Department of Transportation, Dover, DE*
Mack O. Christensen, *Horrocks Engineers, Pleasant Grove, UT*
Keith A. Cota, *Epsom, NH*
Richard G. McGinnis, *Bucknell University, Lewisburg, PA*
Aurora Meza, *VRX, Inc., Austin, TX*
Aimee Zhang, *FHWA Liaison*

AUTHOR ACKNOWLEDGMENTS

The research reported herein was performed under NCHRP Project 17-11(3) by the Texas A&M Transportation Institute, a member of The Texas A&M University System.

FOREWORD

By David M. Jared
Staff Officer
Transportation Research Board

NCHRP Research Report 1097 presents guidelines to determine a recommended clear recovery distance for a given set of roadway and roadside characteristics. Due to the limitations inherent in using crash data for this purpose, an innovative methodology was used that combined encroachment simulations, crash data, statistical modeling, and risk analysis. The guidelines include a risk-based tool that correlates recommended clear zone distance with the potential for severe injuries or fatalities to motorists. The guidelines should be of interest to road design and safety professionals seeking to specify the safest and most practical clear zone recovery areas for various roadway designs.

The clear zone concept for roadside design emerged in the mid-1960s as a single distance for lateral clearance that reduced the likelihood of an errant vehicle striking a roadside obstacle. Subsequent recovery area guidelines that developed over the next two decades provided a variable distance expressed in terms of traffic volume, design speed, sideslope, and other roadway and roadside factors. However, these values are based on studies from the 1950s through the 1980s that used relatively limited data and extrapolated numbers. User agencies saw a need for updated guidelines to aid designers in better understanding the risk associated with roadside encroachments while recognizing and working within the associated design constraints.

Under NCHRP Project 17-11(03), "Development of Clear Recovery Area Guidelines," Texas A&M Transportation Institute was asked to develop guidelines for roadside clear zones that are expressed in terms of key roadway and roadside design parameters. The research approach combined vehicle dynamics computer simulation results with crash data analyses. The vehicle dynamics simulations permitted consideration of a wide range of encroachment and design variables. Specialized crash datasets with reconstructed crashes were used to develop marginal probabilities for the encroachment variables, which were applied as weight factors to the simulation results. Statistical models were developed from the weighted simulation results. The statistical models were incorporated into an encroachment probability-based risk analysis tool. The analysis tool estimated the probability of a severe injury or fatal crash for a prescribed roadway and roadside configuration for a given lateral offset (i.e., clear zone distance) and a selected fixed object spacing at the clear zone edge. Clear zone guidelines were developed using a relative risk approach, whereby the recommended clear zone distance has a risk of a severe injury or fatal crash that is less than or equal to that of a roadside guardrail. The guidelines were developed using equations and a chart-based format expressed in terms of design variables found to have the most significance on the clear zone risk and hence are suitable for possible incorporation into the AASHTO *Roadside Design Guide*.

CONTENTS

SUMMARY

Development of Clear Recovery Area Guidelines

The clear zone concept for roadside design emerged in the mid-1960s as a single distance for lateral clearance that reduced the likelihood of an errant vehicle striking a roadside obstacle. Subsequent recovery area guidance that evolved over the next two decades provided a variable distance expressed in terms of traffic volume, design speed, sideslope, and other roadway and roadside factors. However, these values are based on studies from the 1950s through the 1980s that used relatively limited data and extrapolated numbers. User agencies recognized a need for updated guidelines to aid designers in better understanding the risk associated with roadside encroachments while recognizing and working within the associated design constraints.

The objective of NCHRP Project 17-11(03), "Development of Clear Recovery Area Guidelines" was to develop updated guidelines for roadside clear zones expressed in terms of key roadway and roadside design parameters. It was recognized that the use of crash data for determining the extent of lateral movement of vehicles encroaching onto the roadside is often limited by a vehicle striking a fixed object or rolling over. Therefore, any lateral extent of encroachment distribution derived from crash data will be a truncated distribution, and the full effect of sideslopes and other variables on the lateral extent of encroachments is only partially observed. Furthermore, detailed information on the roadway and roadside design variable of interest is often lacking in most databases.

A research approach that combined crash data analyses with computer simulation results was developed to overcome this limitation. Use of computer simulation permitted a detailed analysis of vehicle trajectory and resulting vehicle kinematics for a wide range of variables for which data may not otherwise be available. The simulation matrix consisted of over two million unique vehicle encroachment simulations performed using a state-of-the-art vehicle dynamics code. The variables in the simulation matrix included vehicle type, encroachment speed and angle, vehicle orientation at departure (i.e., tracking or non-tracking), driver input (e.g., steering and/or braking), horizontal curvature, vertical grade, shoulder width, foreslope ratio, foreslope width, ditch bottom width, backslope ratio, and backslope width. Simulation output included lateral distance traveled, vehicle stability outcome, trajectory data, and velocity data.

Real-world crash data were used to develop probability distributions for the selected encroachment variables, such as encroachment speed, encroachment angle, vehicle orientation at point of departure from the traveled way (i.e., tracking or non-tracking), and driver input applied during the encroachment (i.e., steering, braking, or a combination of both). The results were used to determine marginal probabilities for the values of the encroachment variables used in the simulation matrix that were applied as weighting factors to the simulation results. These weighting factors essentially define the probability of occurrence for a given set of simulated encroachment conditions and the resulting outcome of the encroachment. A probability

matrix for vehicle type was developed using vehicle sales data by combining sales percentages for the vehicle makes and models corresponding to the platforms of the simulated vehicles.

Encroachment relationships in the form of statistical models were derived in terms of significant roadway and roadside design variables to assist with the determination of the probability and severity of an impact given an encroachment has occurred. Models were developed for lateral distance traveled by the encroaching vehicle, longitudinal distance traveled by the encroaching vehicle, rollover probability, speed versus lateral offset, and vehicular angle or orientation versus lateral offset. These relationships were developed for two categories of posted speed and two facility types.

The encroachment relationships were incorporated into a risk analysis tool to estimate the probability of a fatal or serious injury crash [P(K+A)]. An encroachment-based analysis methodology estimates the conditional probability of a crash given a roadside encroachment has occurred and the probable severity of the crash.

Sensitivity analyses were performed using the risk analysis tool to evaluate the sensitivity of the design variables to the estimation of risk and the relative importance of the variables to the overall determination of P(K+A). The results of the sensitivity analyses were used to determine which variables to retain or exclude from the clear zone guideline development process.

Analyses were parametrically executed using the risk analysis tool to cover combinations of facility type, posted speed limit, roadway and roadside design variables, clear zone distance, and hazard conditions beyond the clear zone edge. A relative risk approach was used to define a clear zone distance for a given design configuration that has a P(K+A) risk equal to that of the guardrail.

The final clear recovery area guidelines were expressed in both chart and equation form in a format that could be considered for incorporation into the American Association of State Highway and Transportation Officials (AASHTO) *Roadside Design Guide*. The guidelines can be used to determine a recommended clear recovery distance for a given set of roadway and roadside characteristics. The guidelines also consider the nature of the hazard that exists beyond the clear zone edge.

CHAPTER 1

Introduction

The clear zone concept for roadside design emerged in the mid-1960s. It was defined as a recovery area that afforded a driver a reasonable opportunity to regain control of an errant vehicle and avoid a crash. It originated as a single lateral distance beyond which a vehicle striking a roadside obstacle was less probable. The default clear zone distance was 30 ft. If obstacles within this lateral distance could not be removed, some form of shielding or protection was introduced.

Acceptance of a single distance for lateral clearance diminished over time. On low-volume, low-speed facilities, the 30-ft lateral clear recovery distance was considered excessive. On the other hand, it was recognized that some roadside slopes could result in increased encroachment distances, and a 30-ft clear zone might be insufficient.

Subsequent recovery area guidance contained in the American Association of State Highway and Transportation Officials (AASHTO) 1977 *Guide for Selecting, Locating, and Designing Traffic Barriers* (Barrier Guide) (*1*) and the AASHTO 1989 *Roadside Design Guide* (RDG) (*2*) was expressed in terms of traffic volume, design speed, sideslope, and other roadway and roadside factors. The clear zone guidance has remained relatively unchanged since those times. The minimum recommended clear zone distance range is 7 to 10 ft, corresponding to a design speed ≤ 40 mph, design average daily traffic (ADT) under 750, and a 1V:4H or flatter foreslope. Conversely, the largest recommended clear zone range of 38 to 46 ft corresponds to a design speed of 65 to 70 mph; a design ADT over 6,000; and a foreslope ratio of 1V:5H to 1V:4H.

Although these guidelines provide a more realistic approach than the application of a single distance, the values are based on studies from the 1950s through the 1980s that used relatively limited data and extrapolated numbers. Further, transportation agencies frequently face difficulties in providing desirable recovery areas because of right-of-way constraints or construction costs. Updated guidelines are needed to aid designers in understanding the risk while recognizing and working within the associated constraints.

The objective of this study was to develop updated guidelines for roadside clear zones expressed in terms of key roadway and roadside design parameters. This report documents the research performed and clear recovery area guidelines developed under this project. The research approach combined crash data with vehicle dynamics computer simulation results to consider a wide range of encroachment and design variables. This data was used to develop clear zone guidelines through an encroachment probability-based, relative risk analysis methodology.

Chapter 2 provides a historical overview of clear recovery area guidance in the United States. Details of the vehicle dynamics encroachment simulations are presented in Chapter 3. The vehicle dynamics simulation matrix consisted of over two million unique vehicle encroachment simulations. The simulations were executed using a state-of-the-art, multi-rigid-body vehicle dynamics code, modified by the project researchers, to include a friction ellipse model to simulate soil

furrowing during vehicle sideslip and a vehicle-body-to-terrain contact algorithm to model contact between vehicle hardpoints and the roadside terrain. Simulation output included lateral distance traveled, vehicle stability outcome, trajectory data, and velocity data.

Chapter 4 documents the development of encroachment variable distributions and marginal probabilities for the values of the encroachment variables used in the simulation matrix. NCHRP Project 17-43, "Long-Term Roadside Crash Data Collection Program" crash database, published as *NCHRP Web-Only Document 341: Roadside Database Coding Manual,* was used to develop univariate distributions for key encroachment parameters (*3*). The research team used these distributions to determine conditional probabilities or weighting factors for the values of the variables used in the simulation matrix. A probability matrix for vehicle type was developed using vehicle sales data by combining sales percentages for the vehicle makes and models corresponding to the platforms of the simulated vehicles.

Chapter 5 describes the development of encroachment relationships from the weighted simulation results. Statistical models were derived in terms of significant roadway and roadside design variables to assist with determining the probability of an impact given an encroachment has occurred and the severity of the impact.

The development of a risk analysis tool, referred to herein as the Clear Zone Guideline Assistance Program (CZ-GAP), is presented in Chapter 6. The encroachment relationships developed from the simulation results were incorporated into the risk analysis tool to estimate the probability of a fatal or serious injury crash [P(K+A)]. An encroachment-based analysis method estimates the conditional probability of a crash given a roadside encroachment has occurred and the probable severity of the crash.

Chapter 7 documents analyses performed to evaluate the sensitivity of encroachment and design variables to the estimation of risk and the relative importance of variables to the overall determination of P(K+A), which is the basis for the development of clear recovery area guidelines. Several design configurations were selected, and the values of individual design parameters were varied to examine the effect of changes in these parameters on risk. The results of the sensitivity analyses were used to retain or exclude variables from the clear zone guideline development process.

The recovery area guideline development process is described in Chapter 8. The CZ-GAP risk analysis tool was used to estimate P(K+A) for various roadway and roadside design configurations. Analyses were parametrically executed to cover combinations of facility type, posted-speed-limit categories, roadway and roadside design variables, clear zone distance, and hazard conditions beyond the clear zone edge. A relative risk approach was used to define a clear zone distance for a given design configuration that has a P(K+A) risk equal to that of the guardrail.

The final clear recovery area guidelines will be made available for consideration for incorporation into the AASHTO RDG. The guidelines can be used to determine a recommended clear recovery distance for a given set of roadway and roadside characteristics. They also consider the nature of the hazard that exists beyond the clear zone edge.

Finally, Chapter 9 presents study conclusions, recommendations, and suggested future research.

CHAPTER 2

Clear Recovery Area Background

Up to the 1960s, little emphasis was placed on roadside safety design. The prevailing philosophy was that reasonable and prudent drivers did not inadvertently leave the travelway, and the penalty for doing so by others was acceptable. Studies by Stonex at the General Motors (GM) Proving Ground in the late 1950s and early 1960s showed that even professionally trained drivers strayed from the travelway and that measures to minimize risks of roadside encroachments were needed and warranted (*4, 5*). Work at the GM Proving Ground contributed significantly to the acceptance by many of the need for a "forgiving roadside." This need was underscored by the alarming number of run-off-the-road, single-vehicle crashes and the high severity associated with these crashes.

Recommended measures to minimize risks to errant motorists included providing (a) flat, unencumbered roadsides of sufficient width to permit an errant driver to safely bring their vehicle under control or to stop; (b) traversable sideslopes, preferably 1:6 or flatter, and safer ditch sections; (c) breakaway or yielding supports for signs and light poles; and (d) improved guardrail systems, including safer treatments at guardrail ends. Results of the GM studies also formed the basis for initial dimensions of recommended "recovery areas" (*6, 7*). These areas were later referred to as "clear zones" (*1, 2*), "clear recovery zones" (*8*), or roadside recovery distance (*9*).

The GM studies provided probability data on lateral extent of vehicular movement for run-off-the-road crashes. Using these data, the American Association of State Highway Officials (AASHO), and subsequently AASHTO, suggested that, where feasible, a clear, unencumbered recovery area should extend 30 ft or more laterally from the travelway (*6, 7*). The GM studies indicated that the lateral extent of vehicular movement would not exceed 30 ft in approximately 80% of run-off-the-road crashes on high-speed highways.

National guidelines continued to recommend a 30-ft clear zone distance up until 1977, although it was recognized that the 30-ft width was somewhat arbitrary and based on accident studies at the GM Proving Grounds where relatively flat roadsides were provided. The 1977 AASHTO *Guide for Selecting, Locating, and Designing Traffic Barriers* (Barrier Guide) contained clear zone recommendations that were dependent on design speed, the slope of the cut or fill section, and whether the hinge at the juncture of the shoulder with the sideslope was rounded (*1*). These guidelines indicated that the width of the clear zone should increase with increasing design speed and increasing steepness of fill slopes (width decreases with increasing steepness of cut slopes). For example, the recommended clearance for a high-speed roadway (60-mph design speed) with a fill section having a 1V:4H unrounded sideslope was approximately 43 ft. For the same example and a 40-mph design speed, the recommended clearance was approximately 18 ft. Clear zone criteria contained in the 1977 AASHTO Barrier Guide were developed by Ross et al. in a study sponsored by the Federal Highway Administration (FHWA) (*10*). In the study, the Highway-Vehicle-Object Simulation Model (HVOSM) computer program was used to determine the lateral extent of vehicular movement for encroachments on fill and cut roadside sections, rounded

6 Development of Clear Recovery Area Guidelines

Table 1. Comparison of clear zone recommendations in 1977 Barrier Guide (*1*) and 1989 RDG (*2*).

1977 Barrier Guide (*1*)		1989 *Roadside Design Guide* (*2*)	
Design ADT	Clear Zone Distance, ft	Design ADT	Clear Zone Distance, ft
All	43	< 750	20–24
		750–1500	26–32
		1500–6000	32–40
		> 6000	36–44

and unrounded, at speeds of 40, 50, and 60 mph (*11*). The assumed driver response for the simulated encroachments included an emergency steer-back-to-the-travelway maneuver and emergency full braking.

The 1989 AASHTO RDG (*2*) contained certain revisions to the clear zone criteria of the 1977 AASHTO Barrier Guide (*1*). In addition to the variables considered in the Barrier Guide, clear zone widths were also defined in terms of traffic volume, and greater ranges of design speed were adopted, but the effects of slope rounding were not considered. Clear zone criteria presented in the 1989 AASHTO RDG were derived from data in the 1977 Barrier Guide, in combination with state practices and the collective judgment of the task force that prepared the RDG. The following statement in the 1989 RDG is noteworthy.

> The numbers obtained from Figure 3.1 or Table 3.1 imply a degree of accuracy that does not exist. Again, the curves are based on limited empirical data, which was then extrapolated to provide data for a wide range of conditions. Thus, the numbers obtained from these curves represent a reasonable measure of the degree of safety suggested for a particular roadside, but they are neither absolute nor precise (*2*).

Users of the 1989 Guide were reminded of the subjective nature of the clear zone recommendations and that engineering judgment was essential in their application.

A comparison of clear zone recommendations in the 1977 Guide and 1989 RDG is shown in Table 1. This example assumes a 60-mph design speed and a 1V:4H foreslope. The 1989 RDG recommends essentially the same clear zone distance as the 1977 Guide for high-volume roadways but recommends considerably lower clear zones for lower-volume roadways. The guidance found in the 2002 and 2011 editions of the AASHTO RDG (*12, 13*) was essentially unchanged from the 1989 RDG (*2*).

NCHRP Project 17-11

It was recognized that updated guidelines were needed to aid designers in determining safe and cost-effective recovery areas, while also recognizing the constraints associated with building or improving the highway system. The objective of NCHRP Project 17-11, "Determination of Safe/Cost Effective Roadside Slopes and Associated Clear Distances" was to develop relationships between recovery area distance and roadway and roadside features, vehicle factors, encroachment parameters, and traffic conditions for a range of highway functional classes that can subsequently be used to establish clear zone guidelines.

It was recognized that the use of crash data for determining the statistics on the extent of lateral movement of vehicles encroaching onto the roadside is often limited by a vehicle striking a fixed object or rolling over. Therefore, any lateral extent of encroachment distribution derived from crash data will be a truncated distribution, and the full effect of sideslopes and other variables on lateral extent of encroachments is only partially observed.

A research approach that combined crash data analyses with computer simulation results was developed to overcome this limitation. Use of computer simulation permits a detailed analysis of

vehicle trajectory and resulting vehicle kinematics for a wide range of variables for which data may not otherwise be available. When combined with real-world crash data, the results can be used to determine the influence of and develop relationships between various encroachment parameters.

Clinical reconstruction and analyses of the National Automotive Sampling System (NASS) Crashworthiness Data System (CDS) data were used to develop probability distributions for the key encroachment parameters for different highway functional classes (*14*). The reconstructed crash data provided key encroachment parameters for ran-off-road crashes, including encroachment speed, encroachment angle, vehicle orientation at encroachment (i.e., tracking, non-tracking), and driver control input (i.e., steering, braking, or both). The probability distributions developed from the weighted NASS-CDS data were applied to each encroachment parameter used in the simulation matrix to obtain a probability for each simulation outcome.

Exceedance curves were developed and used to create lateral extent of movement relationships that combine simulation and real-world crash data such that they are a function of multiple encroachment parameters. The exceedance curves can be used to determine the percentage of encroachments that will exceed a certain lateral distance. The researchers recommended that the guideline development process involve some form of cost-effectiveness or risk analysis procedure.

NCHRP Project 17-11(02)

The objective of NCHRP Project 17-11(02), "Development of Clear Recovery Area Guidelines" was to use the data and relationships generated under NCHRP Project 17-11 to develop guidelines for roadside clear zones expressed in terms of key roadway and roadside design parameters. The research approach was to use the Roadside Safety Analysis Program (RSAP) to perform a benefit-cost analysis. RSAP is an encroachment probability-based analysis tool comprised of various analysis modules that include an Encroachment Probability Module, Crash Probability Module, Severity Prediction Module, and Benefit-Cost Module (*15*).

The analytical methodology incorporated in RSAP uses a series of conditionally independent probabilities to represent a roadside encroachment event. This includes the probability of an encroachment occurring, the conditional probability of a crash given a roadside encroachment has occurred, the probable severity of a crash if one occurs, and the expected benefit-cost ratio of the roadside design configuration being investigated. The design alternative evaluated in the incremental benefit-cost analyses was varying recovery area distances for a given set of roadway and roadside conditions. The benefits of a design alternative are defined in terms of a reduction in crash cost derived from a decrease in crash frequency and/or severity, while the costs are defined by the direct construction and maintenance costs associated with the alternative.

The encroachment exceedance curves and encroachment severity relationships developed under NCHRP Project 17-11 were intended to be used to update the RSAP Crash Prediction and Severity Prediction Modules, respectively. It was discovered that the crash scene diagrams supplied by the National Highway Traffic Safety Administration (NHTSA), and subsequently used by the researchers under NCHRP Project 17-11, were not to scale. Thus, the reconstructed encroachment parameters used to develop the marginal probabilities for weighting the simulation outcomes were not correct. Further research to develop reconstructed run-off-road crash data with various encroachment parameters includes *NCHRP Report 665: Identification of Vehicular Impact Conditions Associated with Serious Ran-off-Road Crashes* (*16*), performed under NCHRP Project 17-22 and *NCHRP Web-Only Document 341* (*3*). The effort initiated under NCHRP Project 17-11(02) was reformulated under NCHRP Project 17-11(03) using this new crash data as well as improved vehicle dynamics simulation and analysis tools.

CHAPTER 3

Vehicle Dynamics Encroachment Simulations

This chapter presents details of the vehicle dynamics encroachment simulations performed under NCHRP Project 17-11(03). Discussion on the selection of appropriate simulation code is presented next. This is followed by details of the vehicle models used in the encroachment simulations. The chapter also includes details of the simulation interface manager (SIM) program used for managing the large number of simulations performed, the various outputs recording for the simulations, and the stopping conditions used for managing the simulations in a batch mode. Details of the various driver inputs used in the simulations are also presented in this chapter.

Simulation Code Selection

The research team selected the multi-rigid-body vehicle dynamics analysis method for performing the large number of simulations needed in this project. CarSim, which is a commercially available vehicle dynamics code, was used for all the simulations performed. There were several considerations that weighted in favor of selecting the vehicle dynamics simulation method using CarSim as the analysis tool. These are discussed next.

Computational Time

Multi-rigid-body vehicle dynamics simulations have very short computational time requirements. A 5-second encroachment event can usually be simulated in 3 to 5 seconds on a standard desktop computer. In contrast, simulation analysis methods, such as finite element analysis, can take more than 24 hours to complete the analysis of a similar event, using multiple CPU cores on a supercomputing machine. Since the research team anticipated performing more than a million vehicle encroachment simulations, the vehicle dynamics analysis method was selected for the simulation analysis.

Accuracy

Vehicle dynamics analysis makes simplifying assumptions about the vehicle and uses mostly lumped masses, springs, dampers, and nodal constraints to reasonably capture the dynamic response of the vehicle. While other analysis methods, such as the finite element method, can provide a lot more information about the stresses, strains, deformations, loads, etc. in different parts of the vehicle, that type of information is not needed to meet the objectives of this project. The simulation analysis was to be used to determine the overall trajectory, kinematics (i.e., vehicle roll, pitch, and yaw angles), and motion time histories (i.e., vehicle accelerations, speeds, etc.). For these, vehicle dynamics codes are known to provide reasonable and comparable results to the more advanced finite element simulation analysis (*17*).

Vehicle Modeling and Design Characteristics

CarSim, the vehicle dynamics code used for this project, provides many pre-built vehicle models in various vehicle classes. These pre-built vehicle models can be modified with relative ease using the basic vehicle geometric data and vehicle inertia and mass distribution. Reasonably accurate suspension properties can also be incorporated as needed. Since this project was going to develop more than one vehicle model, the ability to use pre-built models and customize them to specific vehicle makes and models was a significant advantage for using vehicle dynamics analysis with CarSim.

Terrain Modeling

CarSim also allows constructing roadway and roadside terrains with relative ease. This feature enabled the researchers to develop the several hundred roadway and ditch terrains that were analyzed in the project.

Vehicle-Body-to-Terrain Contact

Most vehicle dynamics codes are limited in the capability to simulate contact between two bodies. For vehicles encroaching onto roadsides with various steep foreslope and backslope combinations, vehicle body-to-terrain contact can significantly influence the trajectory and overall stability of the vehicle.

CarSim does not have a vehicle body-to-terrain contact by default. However, Texas A&M Transportation Institute (TTI) researchers previously developed a user subroutine for the commercial CarSim package that incorporates the vehicle body-to-terrain contact. This contact has been successfully used in several past research studies (*18, 19*). The contact subroutine checks if the vehicle's body contacts the terrain during the simulation run time. If contact is detected, the subroutine applies contract forces to the vehicle to account for the terrain reaction. The contact subroutine tracks several user-defined points on the body of the vehicle and determines whether any of those points have penetrated the local terrain. If penetration is detected for a specific point, corrective forces are applied to the vehicle.

Incorporating the vehicle body-to-terrain contact significantly improves the reliability of the simulation results in off-road conditions such as the roadside ditches modeled under this project.

Soil-Furrowing Forces

The default method in CarSim and most other vehicle dynamics analysis codes for applying road forces on vehicle tires is adequate for roadway surface conditions under normal vehicle turning and maneuvering on paved surfaces. In case of vehicle encroaching on roadside ditches, soil-furrowing forces that apply lateral force on the vehicle's tires as it sideslips on wet soils are a significant source of vehicle rollover due to soil tripping. In previous studies, TTI researchers developed a surrogate method to successfully incorporate soil-furrowing forces into vehicle dynamics simulations using a friction ellipse model (*18, 19, 20*). This surrogate method was implemented as a user subroutine that interacts with CarSim during each simulation runtime.

The subroutine determines whether the vehicle is traversing a terrain marked as soil, and if so, calculates and applies lateral forces to the tire using the friction ellipse method. The effective lateral friction coefficient, m_{soil}, is determined using the formulation shown in Figure 1. The lateral friction coefficient is higher for a vehicle sideslipping on soil than the default lateral friction coefficient on a paved roadway. The higher friction coefficient results in higher lateral force on the tires, which acts as a surrogate for the soil-furrowing force. The lateral friction coefficient is a

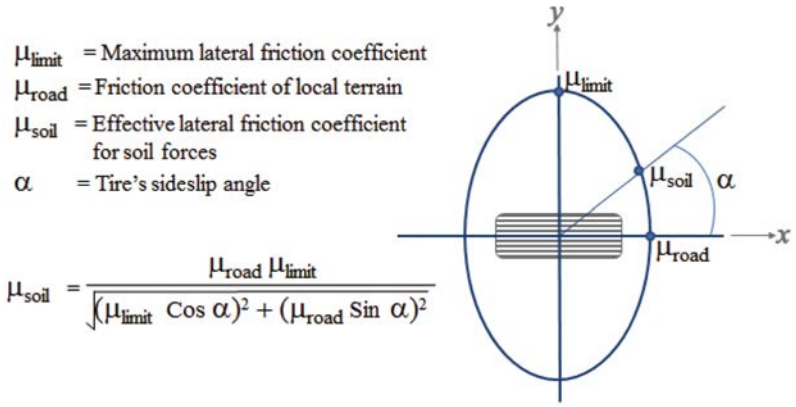

Figure 1. Friction ellipse model for modeling tire forces due to soil furrowing.

function of the tire's sideslip angle and is the same as the default roadway coefficient when there is no sideslipping. However, it increases with sideslipping and reaches a maximum value of m_{limit} when the vehicle is sideslipping at 90 degrees. Based on past research, the researchers used the m_{limit} value of 2.0 for the simulations (*18,19*).

The researchers coded the ability to incorporate soil-furrowing forces only when the vehicle is traversing a terrain marked by the user as soil. This implies that when the vehicle is on a paved road or shoulder, the default CarSim friction formulation is used. The soil-furrowing forces are used only on the ditch terrain after the shoulder, which is more realistic.

Driver Input Capability

Another significant advantage of using CarSim vehicle dynamics simulations is the ability to apply realistic driver inputs to the vehicles during the simulations. Steering and braking inputs can be applied in a consistent manner for the simulations. Driver inputs used in this research are described in detail later in this chapter.

Due to the many advantages described above, the vehicle dynamics simulation method using CarSim was a good choice for the simulation tool for this research project.

Vehicle Model Selection

The vehicle models used in the dynamic encroachment simulations were selected as representative of four categories: passenger car, pickup truck, compact utility vehicle (CUV), and sport utility vehicle (SUV). These categories were developed based on the statistical analysis of the 2019 U.S. vehicle sales data. Details on the classification of the 2019 vehicle sales data are presented in Chapter 4. The selected vehicles were modeled in CarSim and were used to perform the simulations.

The passenger sedan category was represented by the 2019 Toyota Camry, which was the best-selling model in this category for 2019. Its average weight of 3,407 pounds also happens to be in the acceptable range for the *Manual for Assessing Safety Hardware* (MASH) 1500A midsize passenger vehicle (*21*).

The pickup truck category was represented by the 2019 Ram 1500 Crew Cab 4-Door. While Ram pickups were collectively the second best-selling model in this category for 2019, a specific

breakdown of sales for the half-ton class was not available. Preference was thus given to the use of the Ram 1500 as it is also the most used design vehicle for testing and evaluating crashworthiness of roadside safety hardware.

The CUV category was represented by the Toyota RAV4, which was the best-selling model in this category for 2019. The SUV category was represented by the Jeep Grand Cherokee, which was the best-selling model in this category for 2019.

Vehicle Model Development

The research team developed vehicle dynamics models of the selected vehicle makes and models. The specifics of the selected vehicles and some of their key properties are presented in Table 2. The research team's vehicle model development process is explained next.

The process of modeling a vehicle model involved an evaluation of the "preset" vehicle models included with the CarSim software. The preset vehicle models in CarSim cover a wide range of vehicle designs and classes. For each of the selected vehicle makes and models, the researchers compared the vehicle properties of the selected model to those of the various preset CarSim models. Based on this comparison, the closest CarSim vehicle model was selected as a baseline, to which changes were made to match the specific vehicle of interest more closely.

In addition to the vehicle properties listed in Table 2, other properties that were incorporated into the vehicle models were the front and rear suspension types; steering type; antilock braking system (ABS); horizontal and lateral location of the vehicle's center of gravity (CG); distribution of the vehicle's curb mass between the front and rear axle; overall height, width, and ground clearance; front and rear overhang distances; and the yaw, pitch, and roll moments of inertia.

Vehicle properties were obtained using the Expert AutoStats software database, which contains data for cars, pickups, vans, and utility vehicles (*22*). The Expert AutoStats software database is commonly used in the accident reconstruction field. Most of the design parameter values in the database are measured values, except the roll, pitch, and yaw moments of inertia. The values reported for moments of inertia are approximate and based on analytical calculations.

In addition to incorporating design characteristics and properties of the vehicles, the researchers added coordinates of six hardpoints underneath the vehicle. These hardpoints are approximate locations of relatively stiff structural points underneath the vehicle that may engage the roadside terrain and apply terrain contact forces to the vehicle. TTI's SIM program tracks these hardpoints

Table 2. Vehicle makes and models selected for simulation model development.

Vehicle Year/Make/Model	Representing Vehicle Class	Curb Weight (lb)	Wheelbase (in.)	Track Width (front) (in.)	Track Width (rear) (in.)	CG Height (in.)
2019 Toyota Camry (L4) 4-Door Sedan	Passenger sedan	3,492	111	62	63	22.37
2019 Ram 1500 (Classic) Crew Cab 4-Door 4x2	Pickup truck	5,360	149	68	68	29.61
2019 Toyota RAV4 4-Door 4x2	Compact utility (CUV)	3,492	106	63	64	26.73
2019 Jeep Grand Cherokee 4-Door 4x2	Sport utility (SUV)	4,650	115	64	64	27.13

CG = center of gravity.

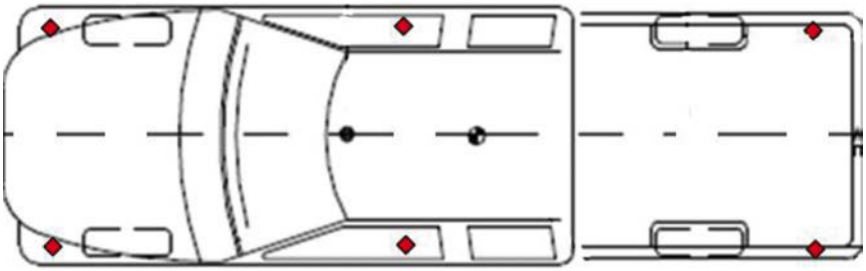

Figure 2. Approximate locations of hardpoints for vehicle body-to-terrain contact (denoted by diamond shapes).

after each timestep during a CarSim simulation and determines whether any of them contacted the terrain surface. If contact is detected, terrain forces are computed and applied to the corresponding hardpoint(s) on the vehicle. The general locations of these six hardpoints are listed below and shown in Figure 2.

1. Driver-side, bottom of the front bumper.
2. Passenger-side, bottom of the front bumper.
3. Driver-side, middle of the vehicle.
4. Passenger-side, middle of the vehicle.
5. Driver-side, bottom of the rear bumper.
6. Passenger-side, bottom of the rear bumper.

Simulation Interface Manager

The TTI research team used an internally developed SIM program that generates various input files for the CarSim solver, runs CarSim in automated batch mode to perform analysis of all selected simulation cases, and generates the needed outputs for further analysis for research. The use of SIM greatly facilitated performing simulations of more than two million cases analyzed under this project. SIM performs the following functions.

1. Generates the needed CarSim input files, which include road/terrain profiles and events files (which include information about the vehicle's encroachment speed, angle, and sideslipping and the driver's steering, braking, and throttle information, etc.).
2. Runs CarSim in loop to perform analysis for all simulation cases in a defined simulation matrix. In doing so, the SIM program checks for vehicle body-to-terrain penetrations using TTI's contact algorithm and applies terrain contact forces to the vehicle as needed.
3. Applies soil-furrowing forces to the vehicle tire if it determines that the tire is sideslipping while traversing on a wet soil terrain defined by the user.
4. Manages each simulation run time and terminates the simulations based on various termination criteria, such as if the vehicle returns to the road, travels too far, overturns, etc.
5. Generates output logs for all simulation cases, recording key simulation outcomes for further use in data analysis of the simulation outcomes.

Further details of the SIM program can be found in previous work by Sheikh et al. (*18, 19*).

Simulation Stopping Conditions

Using SIM, the researchers set several conditions for determining whether a simulation should be stopped after the outcome of an encroachment case has been determined. This prevented the simulations from running longer than needed and saved time when a large number of

simulations needed to be performed. A simulation was stopped if any of the following conditions were met.

1. Vehicle's CG came back to its initial lateral position, indicating that the vehicle had returned to the roadway.
2. Vehicle traveled beyond a specified lateral offset (set at 105 ft from the roadside edge of the travel lane).
3. Vehicle's speed reduced below a specified minimum (set at 5 mph).
4. Vehicle rolled more than a specified maximum roll (set at 65 degrees). The vehicle was considered to have initiated an overturn at this point.
5. Vehicle pitched more than a specified maximum pitch (set at 90 degrees). The vehicle was considered to have overturned at this point.
6. Vehicle traveled for more than 10 seconds without any other significant outcome occurring.

Simulation Outputs

Even though CarSim generates outputs of individual simulations that include time histories of a large number of vehicle and terrain variables, to analyze more than two million simulation outcomes, there was a need to generate a single aggregated output of key variables from all simulations. Such aggregated output was to be used for statistical analysis in subsequent tasks of the research project.

This was made possible using the output module of the SIM program, which generates an aggregated output table containing only selected output parameters from each simulation. Table 3 lists the aggregated outputs recorded by SIM. Additionally, vehicle trajectories of individual simulation cases were saved for further analysis.

Table 3. Simulation outcomes recorded in the aggregate outcomes table.

Label	Description
Run No.	Simulation case number. Unique for a single-vehicle type only.
Termination	Describes if the simulation terminated normally or if the simulation crashed. It has values of "Normal" or "ERROR."
Outcome	Stopping condition that caused the run to stop has the following values. - Time Exceeded - Returns - Stops - Gone Far - Overturns
Description	A brief description of the outcome.
High Roll	Flag for high roll (> 55 deg.). It has a value of 1 or 0 (1 = high roll).
Max Roll	Maximum vehicle roll during simulation (deg.).
High Pitch	Flag for high pitch (> 55 deg.). It has a value of 1 or 0 (1 = high pitch).
Max Pitch	Maximum vehicle pitch during simulation (deg.).
Sideslip	Flag for sideslipped vehicle (> 20 deg.). It has a value of 1 or 0 (1 = vehicle sideslip).
Max Slip	Maximum sideslip angle during simulation (deg.).
Spinout	Flag for vehicle spinout. It has a value of 1 or 0 (1 = vehicle spins out).
Max Lat. Vel	Maximum lateral vehicle velocity during simulation (km/h).
Max Lat. Travel	Maximum distance vehicle travels laterally from the edge of the roadway (m).
Xcg at sim. Stop	X-coordinate of vehicle's sprung mass CG when simulation stops (m).
Ycg at sim. Stop	Y-coordinate of vehicle's sprung mass CG from origin when simulation stops (m).
Lateral Offset at sim. Stop	Lateral distance of vehicle's sprung mass CG from the edge of travel lane when simulation stops (m).

Non-Tracking Encroachments

When a vehicle leaves the roadway in a non-tracking manner, there is very limited crash data available to fully characterize the vehicle's kinematic behavior. A vehicle is in a non-tracking condition when the heading vector is substantially different than the path of the vehicle's CG. In several past research studies, non-tracking encroachments have been modeled by applying an initial yaw rate to the vehicle at the time of encroachment (e.g., 15 degrees/sec) as shown in the left illustration of Figure 3 (*18, 19, 20*). Yaw rate is the rotational velocity of the vehicle as it rotates about its vertical axis. In this scenario, the vehicle's heading vector ***H*** and the path of the CG defined by the encroachment velocity ***V*** are initially aligned. A yaw rate (*R*) is applied at the start of the simulation, which initiates a sideslip mode resulting in a non-tracking encroachment.

While this approach of modeling non-tracking encroachments is reasonable, the researchers felt that it could be improved and made more realistic by adding sideslip angle β to the non-tracking vehicle from the onset of the simulation as shown in the right illustration of Figure 3. This would be more realistic because in a non-tracking encroachment, a vehicle is expected to already be sideslipping as it leaves the travelway.

Analysis of the *NCHRP Web-Only Document 341* crash database was used to select a sideslip angle of 21 degrees for modeling the non-tracking encroachments (details in the next chapter) (*3*). As shown in the right side of Figure 3, the vehicle is now initialized with a heading vector, ***H***, oriented away from the vehicle's CG velocity vector, ***V***, by the sideslip angle β of 21 degrees. The yaw rate, *R*, is still applied to the vehicle because it is expected that the vehicle will have some rotational velocity about its vertical axis that initiated the sideslip condition.

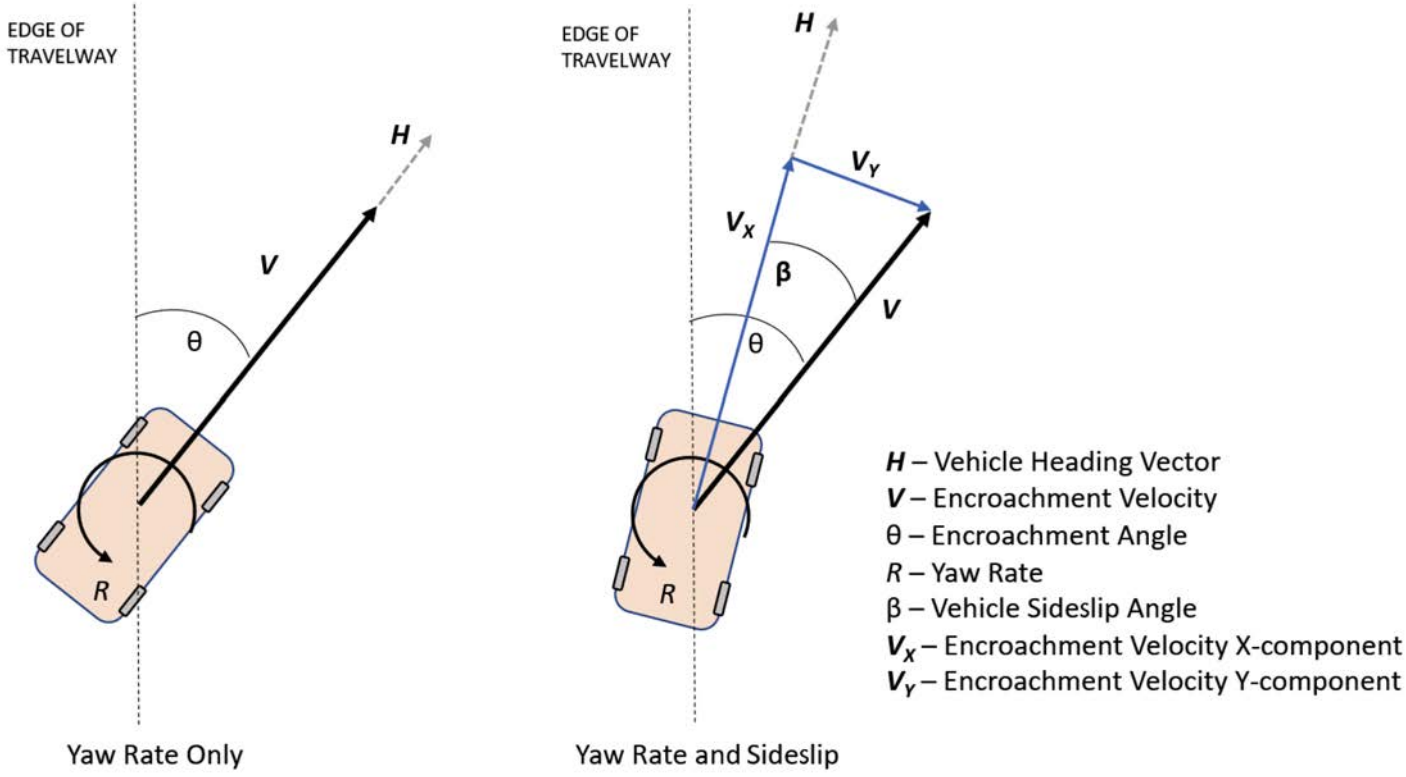

Figure 3. Non-tracking encroachment models without sideslip (left) and with sideslip (right).

Table 4. Matrix for yaw rate sensitivity study.

Slip Angle (degrees)	21
Yaw Rate (degrees/s)	0, 15, 30, and 45
Speed (mph)	45, 55, and 65
Angle (degrees)	10, 20, and 30
Foreslope	1V:6H
Foreslope Width (ft)	30
Backslope	1V:6H
Backslope Width (ft)	30
Ditch Bottom Width (ft)	0
Vehicle Type	SUV
Shoulder Width (ft)	6

With the introduction of the sideslip angle to the non-tracking encroachment condition, the researchers felt it would be appropriate to conduct a small sensitivity study to assess if the 15-degrees/sec yaw rate from previous studies would still be appropriate. Several values of the yaw rate were simulated in the sensitivity study. The goal was to check that the 15-degrees/sec yaw rate, in combination with the sideslip angle, does not unrealistically destabilize the vehicle.

The simulation matrix for assessing the sensitivity to yaw rate in non-tracking vehicle encroachments is presented in Table 4. A symmetric V-ditch with 1V:6H foreslope and backslope was selected as the terrain for the sensitivity study. Simulations were performed for three encroachment angles and three encroachment speeds (nine combinations). Four yaw rates were simulated for each of the nine encroachment speed and angle combinations. Figure 4 shows the maximum

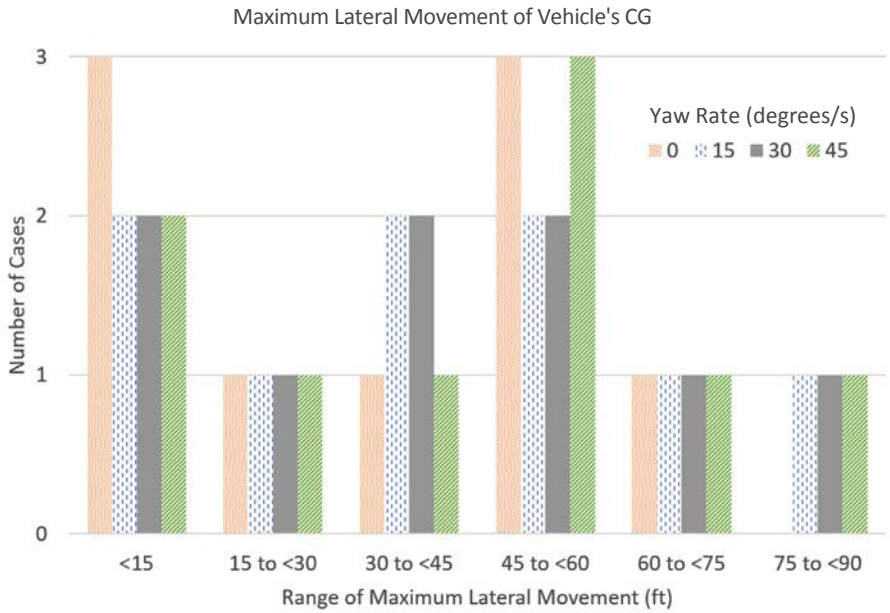

Figure 4. Influence of yaw rate on the vehicle's maximum lateral movement.

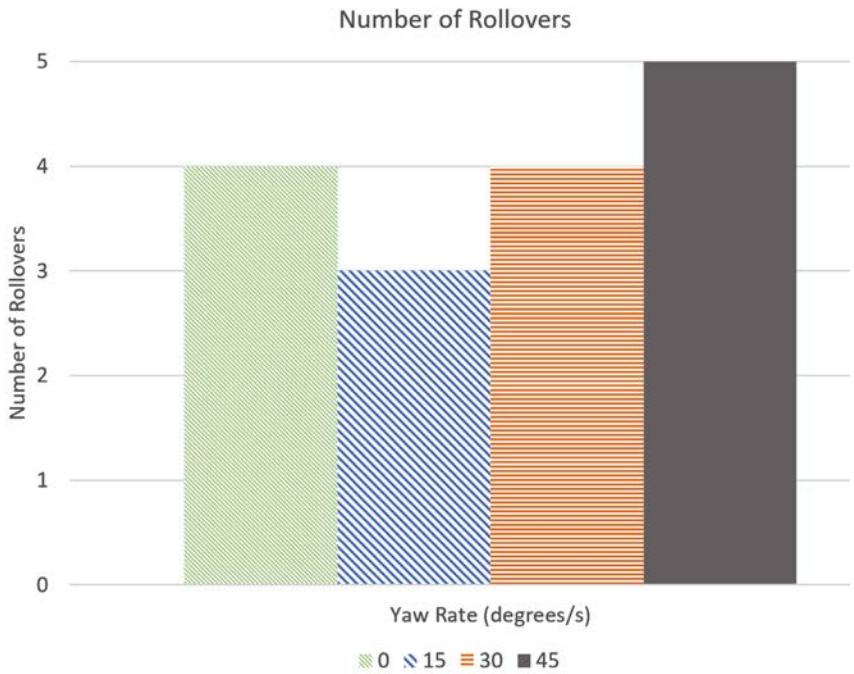

Figure 5. Influence of yaw rate on number of vehicle rollovers.

lateral movement of the encroaching vehicles for the different yaw rates. Figure 5 presents the number of rollovers associated with each of the simulated yaw rates.

Even though the number of cases simulated was small, the results indicated that the previously used yaw rate of 15 degrees/sec is still a reasonable choice. It did not excessively destabilize the vehicle, which is indicated by the number of rollovers remaining lower than the other yaw rates simulated (see Figure 5). The results also suggested that the non-tracking encroachments are not highly sensitive to the yaw rate. This can be concluded by noting that doubling the yaw rate from 15 degrees/sec to 30 degrees/sec resulted in only one additional rollover. Furthermore, the extent of lateral movement distribution remained the same for these two yaw rates as shown in Figure 4.

Based on these observations, the researchers selected a 15-degrees/sec yaw rate combined with a sideslip angle of 21 degrees for simulating the non-tracking encroachments in the simulation matrix.

Driver Inputs

Response of the driver at the time of and during the roadside encroachment is a complex phenomenon with many possible variations in driver response. The research team developed five driver inputs for simulating a broad spectrum of driver responses that can be expected. Since driver response at the time of the encroachment is expected to depend on whether the vehicle is tracking or non-tracking, the research team incorporated the tracking/non-tracking vehicle condition as part of the driver inputs.

The five driver inputs used in this research are presented in Table 5. Driver Input 1 simulated a driver who is asleep or impaired and does not apply any driver input. Inputs 2, 3, and 4 were tracking encroachments in which the driver reacts after a perception-reaction time (PRT) of 1 second. The 1-second PRT has been used in previous research and was considered reasonable for this research (*18, 19*).

Table 5. Driver inputs for the encroachment simulations.

Driver Input	Details
1	*No input (tracking).*
2	*Panic steer to return to road (R2R), no braking (tracking).* After 1.0 sec PRT delay on leaving the edge of the travel lane, a 360-deg steer toward the roadway is applied at the rate of 720 deg/s.
3	*Full braking, no steering (tracking).* After 1.0 sec PRT delay on leaving the edge of the travel lane, sudden brakes are applied. Brakes are modeled as ABS brakes.
4	*Panic R2R steer and full braking (tracking).* After 1.0 sec PRT delay on leaving the edge of the travel lane, sudden brakes and a 360-deg steer toward the roadway are applied at the rate of 720 deg/s. Brakes are modeled as ABS brakes.
5	*Constant steer and full ABS brake (non-tracking).* Vehicle encroaches with a yaw rate of 15 deg/s (yawing toward the roadway) and a sideslip angle of 21 degrees, with a constant steer angle of 360 deg and fully applied ABS brakes.

Input 2 depicts a panic steer back to the roadway without brakes being applied. Input 3 depicts a panic braking response without any steering input. Input 4 depicts both, a steer back to the roadway and braking.

Input 5 was a non-tracking encroachment. In this case, the driver was assumed to have already reacted to some event on the roadway and had applied the steering and/or braking inputs prior to encroaching. Thus, no PRT was used for this input at the start of the encroachment.

For all the tracking steering inputs, the rate for panic steer was determined based on NHTSA's Fishhook maneuver guidelines, which have a recommended steering rate of 720 degrees/second. This rate was used to develop a maximum steer of 360 degrees after the passage of PRT.

Simulation Matrix

Table 6 presents the vehicle dynamics encroachment simulation matrix used in this research. The variables in the matrix include vehicle type, encroachment speed and angle, vehicle orientation at departure (i.e., tracking or non-tracking), driver input (e.g., steering and/or braking),

Table 6. Vehicle dynamics encroachment simulation matrix.

Variable	Values
Vehicle Type (also see Table 2)	Passenger sedan Pickup truck Compact utility Sport utility
Encroachment Speed	35, 45, 55, 65, and 75 mi/h.
Encroachment Angle	5, 10, 15, and 25 degrees.
Driver Input and Vehicle Orientation (also see Table 5)	1 – No input – tracking 2 – Steering only after PRT – tracking 3 – Braking only after PRT – tracking 4 – Steering and braking after PRT– tracking 5 – Fixed steer and full brakes without PRT – non-tracking
Shoulder Width (ft)	2, 6, and 12. Shoulder slope of 4% on all shoulders.
Foreslope Ratio	1V:10H, 1V:6H, 1V:4H, and 1V:3H.
Foreslope Width (ft)	8 and 16.
Ditch Bottom Width (ft)	0, 4, and 10.
Backslope Ratio	1V:6H, 1V:4H, 1V:3H, and 1V:2H.
Backslope Width (ft)	8 and 16.
Horizontal Curvature (degrees)	0, 4, and 6. Superelevation of 2% on all curves.
Vertical Grade (percent)	0, 4, and 6. All downgrade.

horizontal curvature, vertical grade, shoulder width, foreslope ratio, foreslope width, ditch bottom width, backslope ratio, and backslope width. The roadway and roadside design parameters were selected to represent a range of typical roadside conditions.

Even though superelevation and shoulder slope were not selected to be part of the final clear zone guidelines, the researchers incorporated typical mild values for these slopes so that the simulated roadway configurations were more representative of the field conditions. The researchers examined various state standards and selected a shoulder slope of 1:25 and a superelevation of 2% for the road profile modeled in this research. Other than the horizontal curves, the simulated roadway profile was flat and level.

The selected simulation matrix consisted of 2,073,600 individual simulation cases. The researchers used SIM and CarSim to perform all the simulations. The output generated from the simulations was further used in the statistical analysis and clear zone guideline development, as presented in the subsequent chapters of this report.

CHAPTER 4

Encroachment Variable Distributions and Marginal Probabilities

NCHRP Web-Only Document 341 Crash Database

The research team used the crash database from *NCHRP Web-Only Document 341* to develop univariate distributions for the encroachment parameters in the simulation matrix (*3*). *NCHRP Web-Only Document 341* crash records originated with the NASS-CDS database. The developers used a scaled scene diagram and other available information (e.g., vehicle crash data) to clinically reconstruct both impact and encroachment conditions. Additional supplemental roadway and roadside site data were also collected. Based on the sampling scheme developed for the NASS-CDS, each crash record has a sampling weight that indicates the number of crashes the investigated crash represents. These sampling weights are intended to be used in any analyses of the crash data. Thus, before any analyses were performed or encroachment variable distributions developed, crash records from *NCHRP Web-Only Document 341* were linked to their corresponding NASS-CDS sampling weights.

The research team reviewed both *NCHRP Web-Only Document 341* and NASS-CDS coding manuals and determined the keys to link the tables in the *NCHRP Web-Only Document 341* database (*3*) to the NASS-CDS case files. All the 2,151 crash records from *NCHRP Web-Only Document 341* database were matched to the corresponding crash records in the NASS-CDS data files. After merging all events to the NASS-CDS, it was found that the sampling weights assigned to the 2,151 crash records had the following features:

- Range = 1.5 to 5,155.09.
- Median = 107.75.
- Mean = 338.99.
- Standard Deviation = 594.57.

The resulting distribution, which has a heavy right tail, is shown in Figure 6.

In addition, *NCHRP Web-Only Document 341*crash records were filtered for the facility types of interest in this project, which were 2-lane undivided (2U) and 4-lane divided (4D) roadways (*3*). The crash records were filtered for facility type by using the median width and number of lanes. The identification of 2U roads was 1 lane in each direction of travel and a median width of zero. The 4D roads were similarly identified by the number of lanes and the presence of a median. Roadways with a two-way left-turn lane were excluded from the analysis.

Encroachment Parameter Distributions and Marginal Probabilities

The encroachment parameters included in the computer simulation matrix are encroachment speed, encroachment angle, vehicle orientation at departure (i.e., tracking or non-tracking), and driver input (e.g., steering and/or braking). The researchers developed univariate distributions

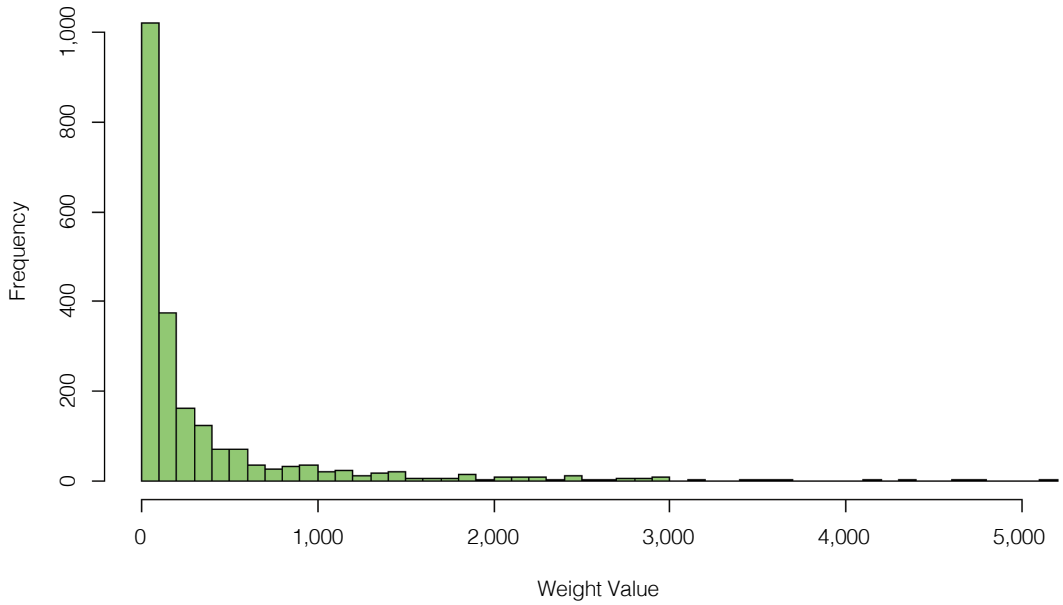

***Figure 6. Distributions of sampling weights for* NCHRP Web-Only Document 341 *database crashes* (3).**

for the selected encroachment parameters for both 2U and 4D roadways. These distributions were used to determine conditional probabilities for the values of the variables used in the simulation matrix. The marginal probabilities were used as weighting factors to support the aggregation of simulation results for the development of lateral extent of encroachment and encroachment severity relationships.

Encroachment Speed

The research team used the *NCHRP Web-Only Document 341* crash data to develop weighted distributions for encroachment speed for the two facility types of interest—2U and 4D roadways. The weighted distributions of encroachment speeds and select percentiles and quantiles are shown in Figure 7, where the speeds are given in km/h, the original units in the dataset (*3*).

In Figure 7, the distributions of encroachment speeds for 2U roadways significantly differ from the distribution for 4D roadways. There is a distinct shift of the distribution to the right for 4D roadways, indicating higher encroachment speeds for 4D roadways compared to 2U roadways. The reason for this difference is likely associated with higher speed limits for 4D facilities coupled with geometric design in accordance with higher design speeds. However, it is interesting to note that although the lower percentiles are clearly higher for 4D facilities (e.g., the 50th percentile is 20 km/h or 12.4 mph higher for 4D facilities), the two facility types tend to become more similar at their extreme values on the right. The difference between 95th percentile encroachment speeds is reduced to about 10 km/h or 6.2 mph.

The team used the weighted distributions of encroachment speed shown in Figure 7 to evaluate marginal probabilities associated with different sets of selected encroachment speed ranges for use in the simulation matrix. The researchers decided to move forward with the encroachment speed bins presented in Table 7. The encroachment speed values presented in Table 7 provided the most balanced set of probabilities across both 2U and 4D roadways.

These probabilities were used as weighting factors for the encroachment speeds used in the simulation matrix. The 25-mph bin represents all crashes with a reported encroachment speed of less than 30 mph. The 35-mph bin represents all crashes with a reported encroachment speed greater

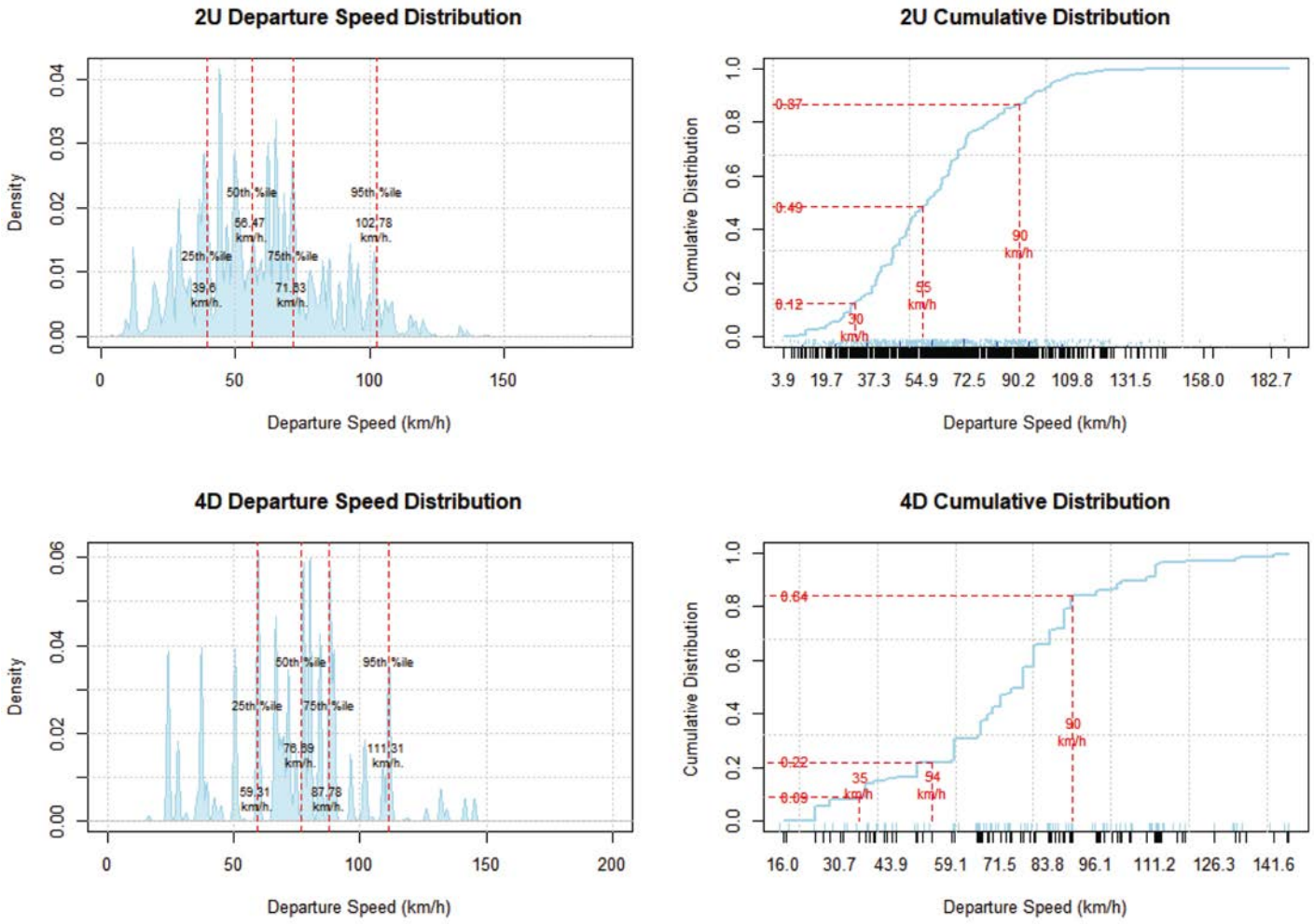

Figure 7. Weighted distribution of encroachment speeds.

Table 7. Marginal probabilities for encroachment speeds to be used in simulation study.

	Speed (mph)				
	25	**35**	**45**	**55**	**65**
Facility Type	P(x < 30 mph)	P(30 mph <= x < 40 mph)	P(40 mph <= x < 50 mph)	P(50 mph <= x < 60 mph)	P(x >= 60 mph)
2U	0.372	0.230	0.205	0.107	0.086
4U	0.164	0.143	0.346	0.205	0.141

NOTE: P= probability.

22 Development of Clear Recovery Area Guidelines

or equal to 30 mph and less than 40 mph. The 45-mph bin represents all crashes with a reported encroachment speed greater or equal to 40 mph and less than 50 mph. The 55-mph bin represents all crashes with a reported encroachment speed greater or equal to 50 mph and less than 60 mph. The 65-mph bin represents all crashes with a reported encroachment speed of 60 mph or greater.

Encroachment Angle

The encroachment angle of the vehicle relative to the roadway was extracted from the *NCHRP Web-Only Document 341* database for each crash record. For left-side departures, the encroachment angle was reported between 180 and 360 degrees in the database. These values were adjusted and combined with the right-side encroachment angles to develop the weighted distributions and select percentiles for both 2U and 4D roadways as shown in Figure 8. The distributions suggest that the encroachment angle for 2U facilities is slightly higher than for 4D facilities.

The team used the weighted distributions of encroachment speed shown in Figure 8 to evaluate marginal probabilities associated with different sets of selected encroachment angle ranges for

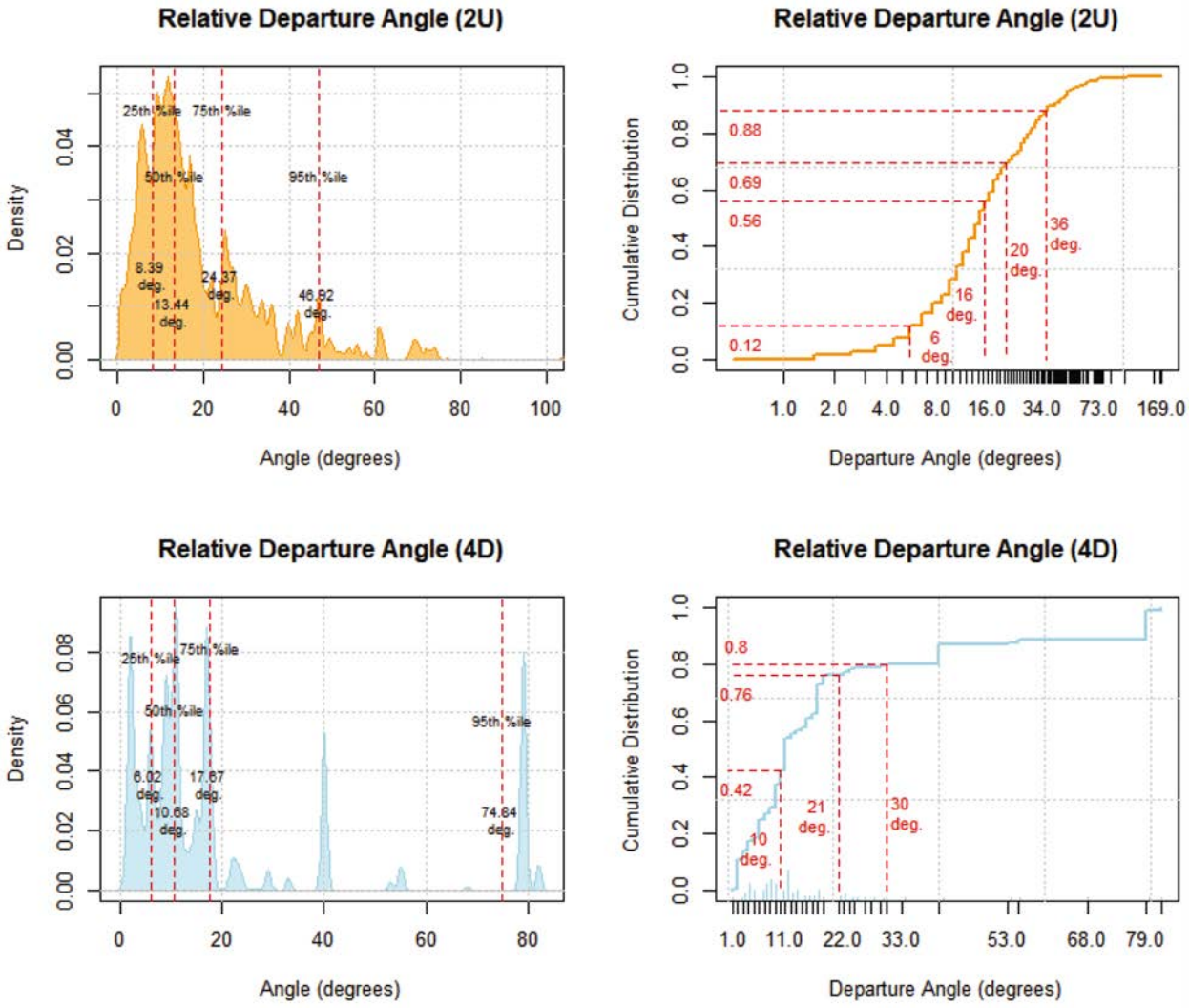

Figure 8. Weighted distributions and percentiles of encroachment angle.

use in the simulation matrix. The research team considered different sets of encroachment angle values and concluded those presented in Table 8 provided a reasonably balanced set of marginal probabilities across both 2U and 4D roadways.

These probabilities were used as weighting factors for the encroachment angles used in the simulation matrix. The 5-degree bin represents all crashes with a reported encroachment angle of less than 10 degrees. The 15-degree bin represents all crashes with a reported encroachment angle greater or equal to 10 degrees and less than 20 degrees. The 25-degree bin represents all crashes with a reported encroachment angle greater or equal to 20 degrees and less than 30 degrees. The 35-degree bin represents all crashes with a reported encroachment angle of 30 degrees or greater.

Sideslip Angle

The simulation matrix includes both tracking and non-tracking encroachment conditions. A tracking condition is generally defined as the vehicle heading angle (i.e., vehicle orientation) and encroachment angle (i.e., the path of the vehicle's CG) being aligned as the vehicle leaves the traveled way. A non-tracking encroachment can be generally defined as the encroaching vehicle having a sideslip angle as it leaves the roadway, where the sideslip angle is defined as the difference between the vehicle heading angle and the encroachment angle. Crash records from *NCHRP Web-Only Document 341* were analyzed to help with the selection of a reasonable sideslip angle for the non-tracking encroachments in the simulation matrix.

The research team calculated the sideslip angle by computing the difference between the heading angle and the encroachment angle. The sideslip angle calculation considered four different cases: both heading and encroachment angles are toward the right; both heading and encroachment angles are toward the left; the encroachment angle is toward the right, but the heading angle is toward the left; and the encroachment angle is toward the left, but the heading angle is toward the right. A positive sideslip angle indicates a larger encroachment angle than the heading angle in the direction of encroachment, and a negative sideslip angle indicates the opposite. Figure 9 and Figure 10 show the weighted histograms for right-side and left-side departures, respectively.

For right-side departures, the mean sideslip angle is 4.02 degrees, and the three relevant quartiles (i.e., 25th, 50th, and 75th percentiles) are −1.52, 0.62, and 6.08 degrees, respectively. For left-side departures, the mean sideslip angle is 0.18 degrees, and the three relevant quartiles (i.e., 25th, 50th, and 75th percentiles) are −3.62, 1.92, and 10.72 degrees, respectively.

Further statistical analysis of the sideslip angle was conducted to assist with the determination of a suitable threshold or definition between tracking and non-tracking encroachments. For this analysis, the team used a distribution of the absolute sideslip angle as a basis rather than relative to the direction of departure. Figure 11 shows the distribution for the absolute sideslip angles and key quantiles of that distribution.

Table 8. Marginal probabilities of encroachment angles in the simulation matrix.

	Encroachment Angle (degrees)			
	5	**15**	**25**	**35**
Facility Type	P(x < 10)	P(10 <= x < 20)	P(20 <= x < 30)	P(x >= 30)
2U	0.283	0.399	0.140	0.178
4D	0.377	0.383	0.037	0.203

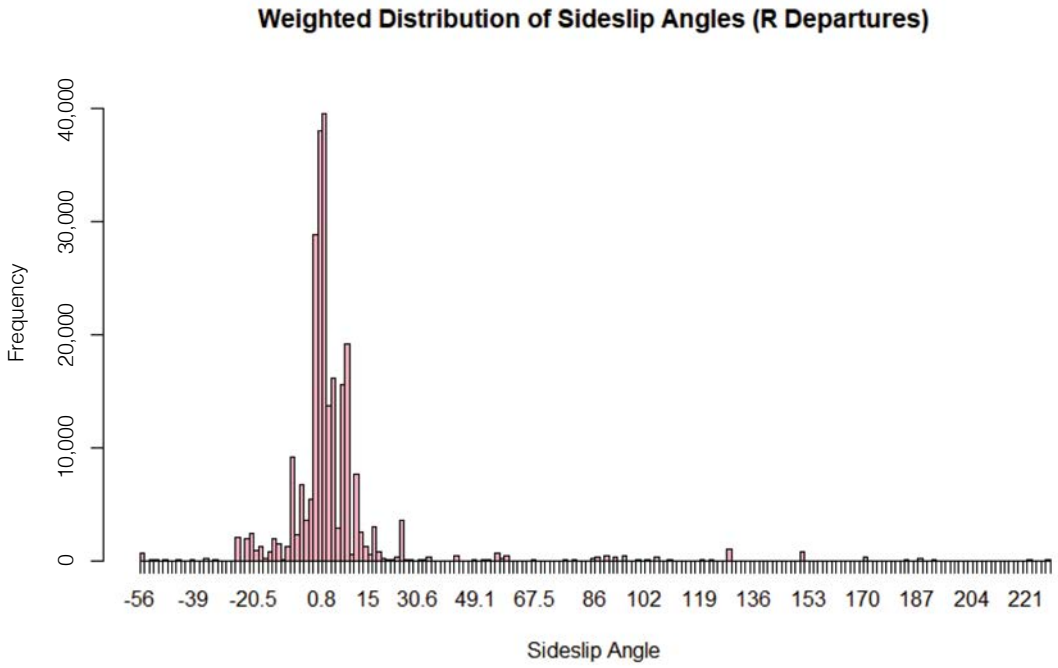

Figure 9. Weighted distribution of sideslip angles (right-side departures).

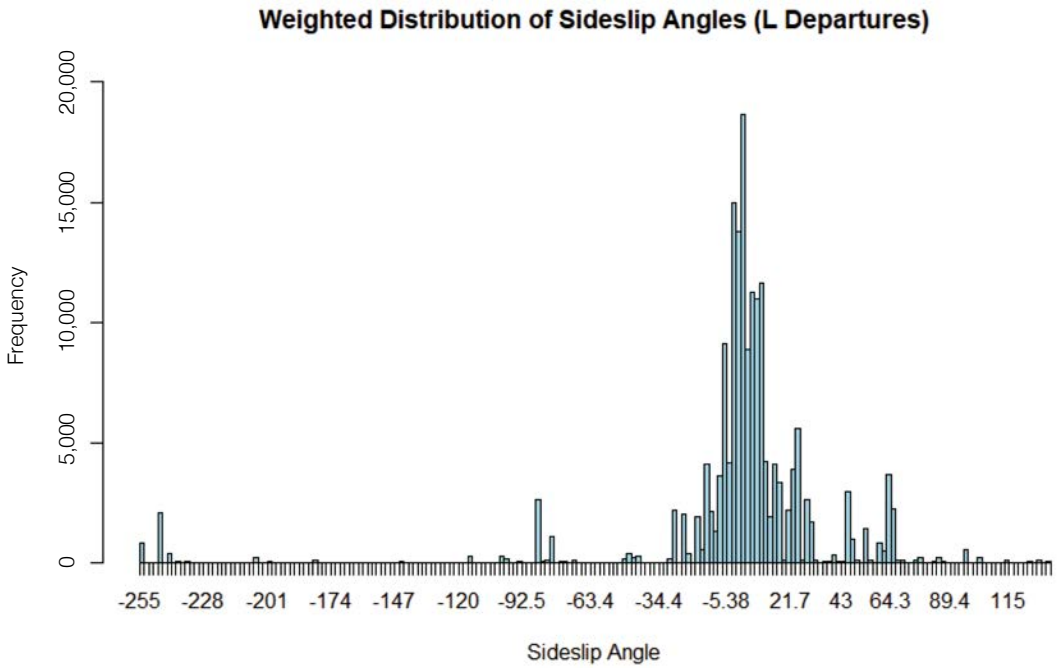

Figure 10. Weighted distribution of sideslip angles (left-side departures).

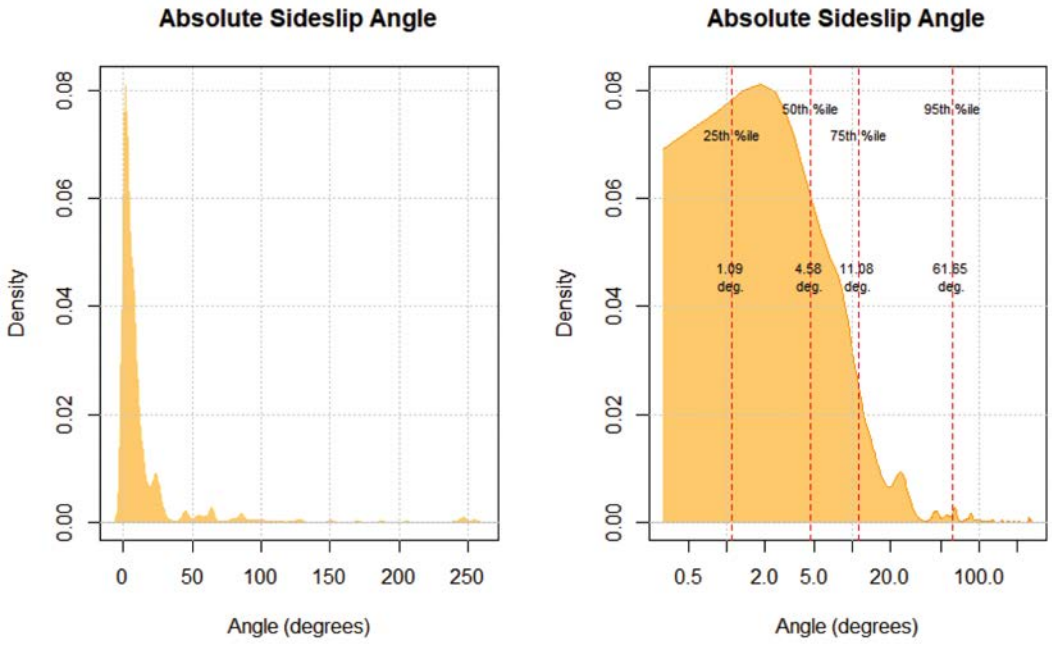

Figure 11. Absolute sideslip angles (left) and quantiles (right).

A clear observation is that a large proportion of the sideslip angles are small (75% of the data has absolute sideslip angles smaller than 11.08 degrees). Current vehicle technology often allows vehicles to recover from small sideslip angles. The selected definition or threshold between tracking and non-tracking is intended to represent a significant non-tracking condition from which the ability to recover is not certain.

The research team considered different values of sideslip angles for the non-tracking threshold. Figure 12 shows the cumulative distribution of the absolute sideslip angles of interest for defining a non-tracking encroachment threshold and the corresponding percentage of tracking

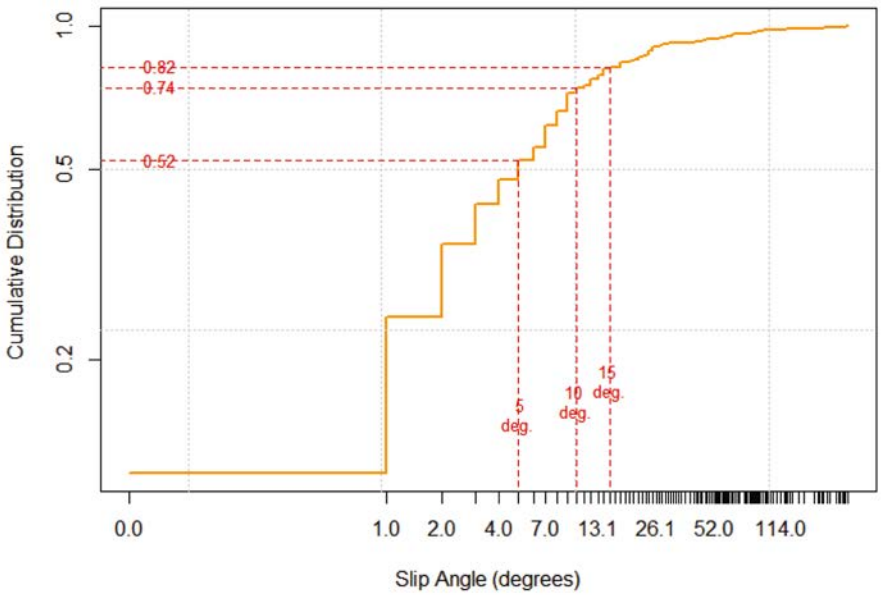

Figure 12. Cumulative distribution of absolute sideslip angles and thresholds of interest.

encroachments that would result for each value. For example, Figure 12 indicates that 82% of the sideslip angles are smaller than or equal to 15 degrees. Thus, if a 15-degree sideslip angle were to be selected as the threshold between tracking and non-tracking encroachments, it would result in 82% tracking encroachments and only 18% non-tracking encroachments.

The researchers selected a sideslip angle of 10 degrees to serve as the definition between tracking and non-tracking encroachments. Using the sideslip angle distribution presented in Figure 12, this results in 74% tracking encroachments and 26% non-tracking encroachments. The research team considered these distributions as a reasonably representative condition. Selecting smaller sideslip angles would have resulted in a more conservative rather than representative condition. Also, most of the U.S. vehicle fleet is now equipped with electronic stability control, which is very effective at helping drivers recover from smaller sideslip angles.

Figure 13 shows the truncated distributions at various thresholds and the key quantiles for each. The corresponding quantiles for the 10-degree sideslip angle are shown in the lower left truncated distribution. The 50th percentile sideslip angle of this truncated distribution would be approximately 21 degrees. This was considered a reasonable sideslip angle to use for the non-tracking encroachment condition defined in the simulation matrix. The intent was to define a representative rather than a worst-case non-tracking condition, and the 50th percentile fulfills that intent. Therefore, the non-tracking encroachments in the simulation matrix were defined using a sideslip angle of 21 degrees and yaw rate of 15 degrees/sec as the vehicle departs the travelway.

Driver Input

Statistical analysis of driver input provided during the encroachment (i.e., none, steering, braking, or combined steering and braking) was conducted to develop marginal probabilities

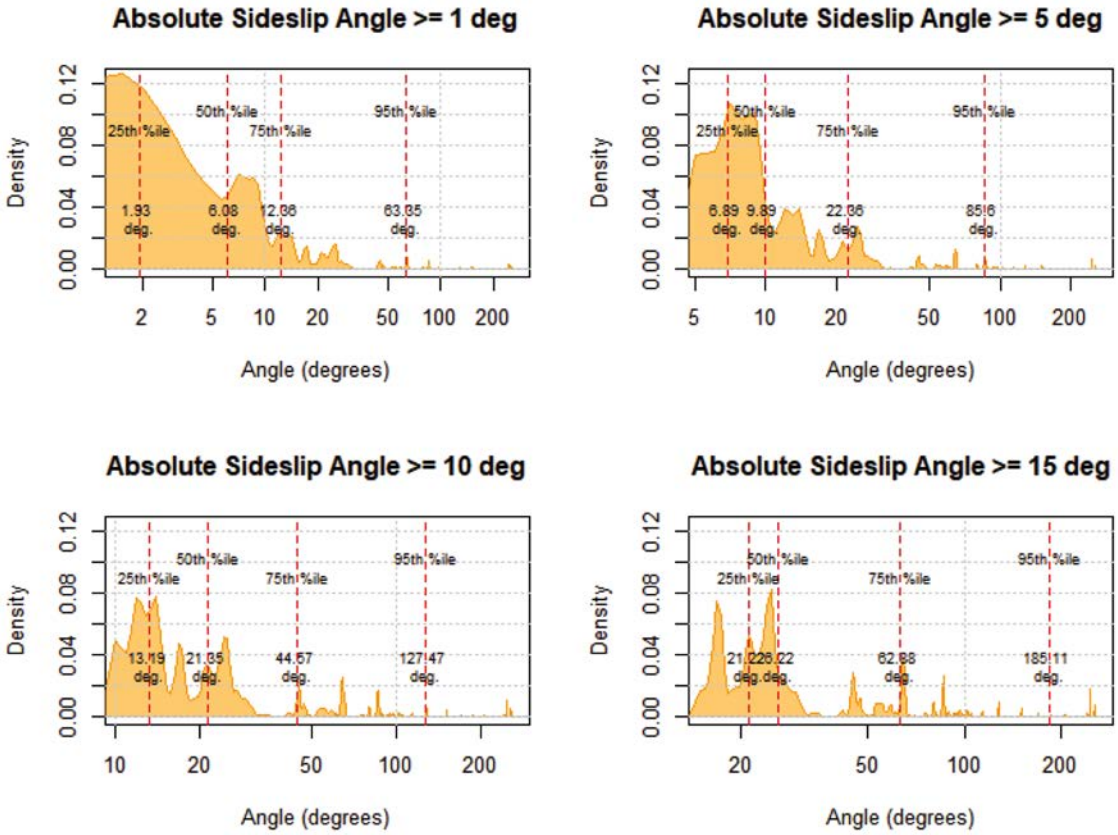

Figure 13. Various truncated distributions for absolute sideslip angles and quantiles.

for each driver input category. Additional data elements were extracted from the NASS-CDS database and merged with the *NCHRP Web-Only Document 341* database (*3*) for this purpose. More specifically, the field "Attempted Avoidance Maneuver" was accessed in the "Pre-Crash" tab as follows: "Vehicle 1" >>> "General Vehicle" >>> "Pre-Crash."

Tracking encroachments have been defined for purposes of this project as those that have a sideslip angle less than or equal to 10 degrees. Current vehicle technology permits vehicles to readily recover from shallow sideslip angles. In non-tracking encroachments, the driver has already reacted and lost control of the vehicle. Thus, it is not significant to analyze driver input for these encroachments.

Using all the data in the *NCHRP Web-Only Document 341* database, the percent of encroachments reported as having no driver input is very high as shown in Figure 14 and Figure 15 for

Figure 14. Weighted distribution of driver inputs for 2U roadways.

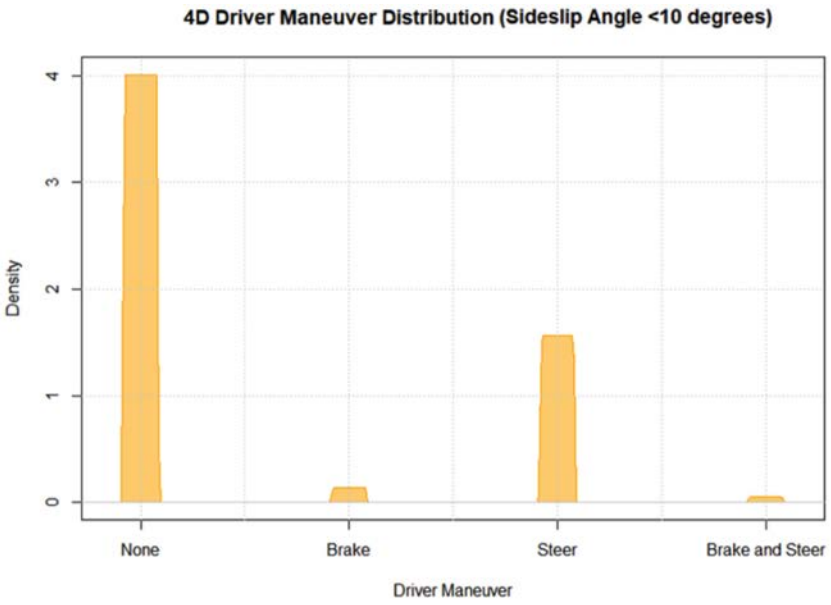

Figure 15. Weighted distribution of driver input for 4D roadways.

2U and 4D roadways, respectively. This percentage of no driver response is not consistent with driver input responses derived from the older database in *NCHRP Report 665* (*16*). The researchers investigated these differences to determine the most appropriate values for marginal probabilities to weight the simulation outcomes.

Assuming the driver is not impaired or asleep, there is a perception-reaction event that occurs after a driver inadvertently leaves the travelway. The driver perceives the departure from the road and reacts to it by steering and/or braking the vehicle. If an object is present close to the roadway, it will likely be impacted before completion of the perception-reaction phase, and the crash would be coded as "no driver input." However, this creates a truncated distribution. In the absence of striking an object so quickly, the driver may have reacted by steering and/or braking their vehicle. In this project, interest lies in the driver's behavior during unencumbered encroachments onto the roadside.

To further investigate these cases, distributions of the lateral offset of objects struck were developed. As shown in Figure 16 and Figure 17 for 2U and 4D roadways, respectively, a high percentage of objects struck have a lateral offset of less than 10 ft. The lateral distance traveled during a PRT of 1 second or greater will vary with the speed and angle of the encroaching vehicle. However, in many, if not most scenarios, a lateral distance of 10 ft will be traveled prior to completion of the PRT. For example, if a vehicle leaves the travelway at a speed of 40 mph, it will travel 59 ft in 1 second. Even at an encroachment angle of only 10 degrees, the vehicle will travel a lateral distance of 10.2 ft during that time. A higher encroachment speed and/or angle will increase the lateral distance traveled during a 1 second PRT beyond 10 ft.

The histograms in Figure 16 and Figure 17 demonstrate that most of the events in the database have very small lateral offsets, suggesting that the drivers probably did not have a chance to react before hitting a roadside object.

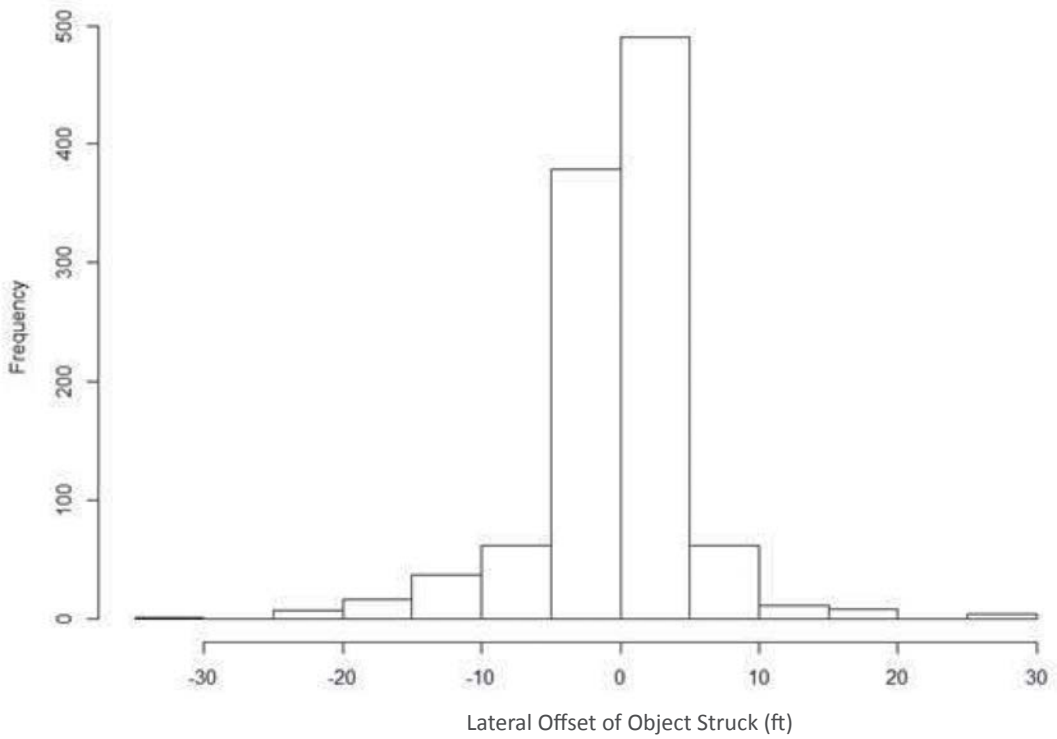

NOTE: Left-side departures are negative and right-side departures are positive.

Figure 16. Weighted distribution of lateral offset of object struck for 2U roadways.

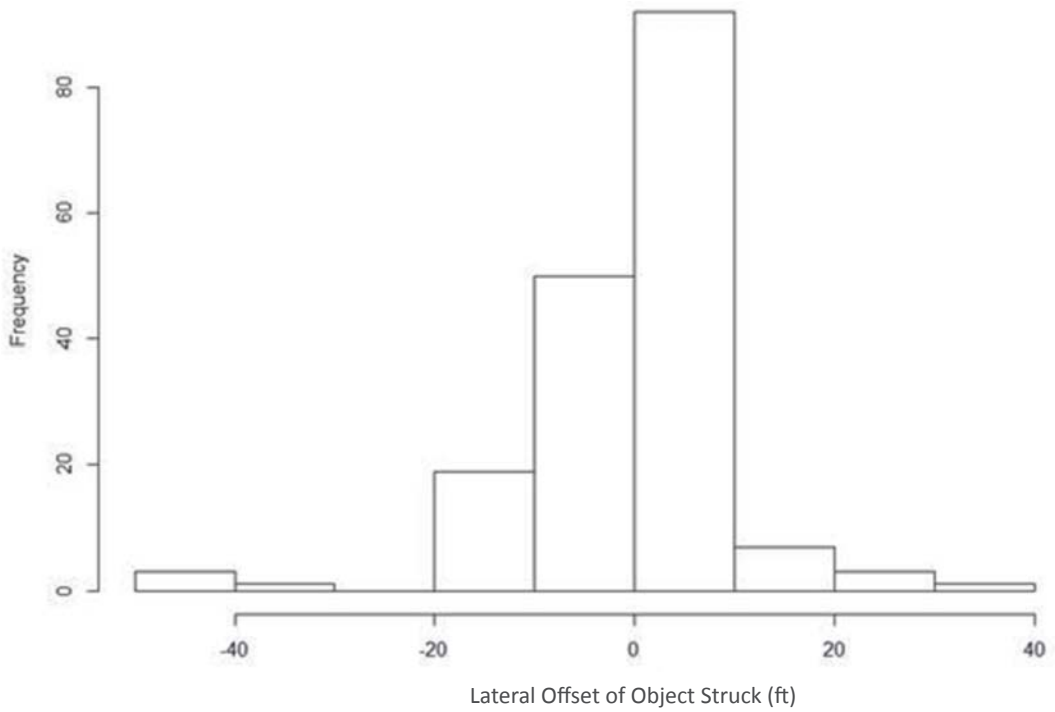

NOTE: Left-side departures are negative and right-side departures are positive.

Figure 17. Weighted distribution of lateral offset of object struck for 4D roadways.

The maneuver distributions associated with crash events that occurred greater than 10 ft off the roadway are shown in Figure 18 and Figure 19 for 2U and 4D roadways, respectively.

Comparing Figure 18 and Figure 19 with the respective distributions in Figure 14 and Figure 15, a significant drop in the percentage of no driver response is observed for both 2U and 4D roadways.

Due to the small number of cases with objects struck beyond 10 ft, the researchers decided to combine the data for 2U and 4D roads to develop the marginal probabilities. The marginal probabilities associated with driver inputs used in the simulation (Table 5), including the non-tracking condition, are presented in Table 9.

While these values are more consistent with the data in *NCHRP Report 665*, particularly for the no-response category, there are still differences (*16*). Most notable is the lower percentage of braking responses in the *NCHRP Web-Only Document 341* data in the form of braking only as well as combined braking and steering (*3*).

This difference may be due to the increased use of ABSs. *NCHRP Report 665* data covers a period from 1996 through 2002 (*16*). Federal Motor Vehicle Safety Standard Number 135, *Light Vehicle Brake Systems* (49 CFR 571.135), requires an ABS on passenger cars manufactured on or after September 1, 2000, and on multipurpose passenger vehicles, trucks, and buses with a gross vehicle weight rating of 7,716 pounds that are manufactured on or after September 1, 2002. Although many vehicles would have had an ABS before this compulsory date, it stands to reason that many of the vehicles in the older *NCHRP Report 665* database would not, while virtually all of the vehicles in the more recent *NCHRP Web-Only Report 341* database would (*16, 3)*. Because ABSs prevent wheel lockup, physical evidence of braking is much more difficult to discern. It is possible that crash investigators are not able to detect some braking responses as a result. Thus, the differences in driver response noted between the two datasets may be attributed to difficulty detecting braking with ABSs more than as a result of actual differences in driver response.

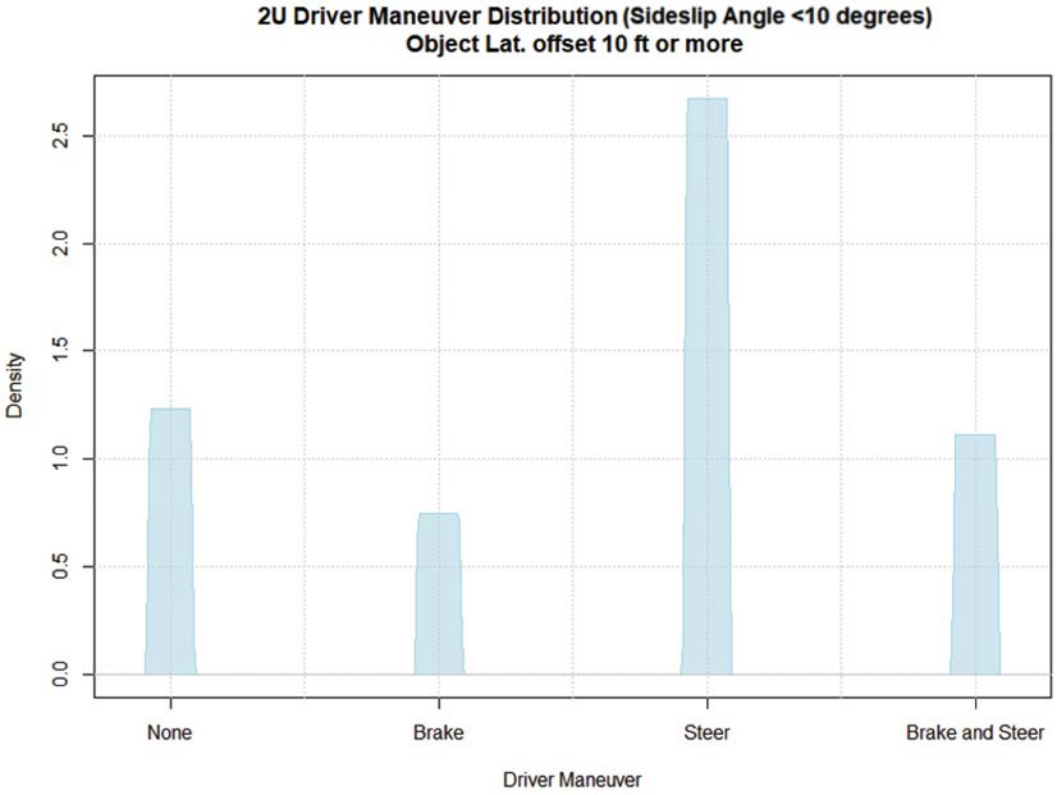

Figure 18. Distribution of driver input for objects struck greater than 10 ft off roadway (2U roadways).

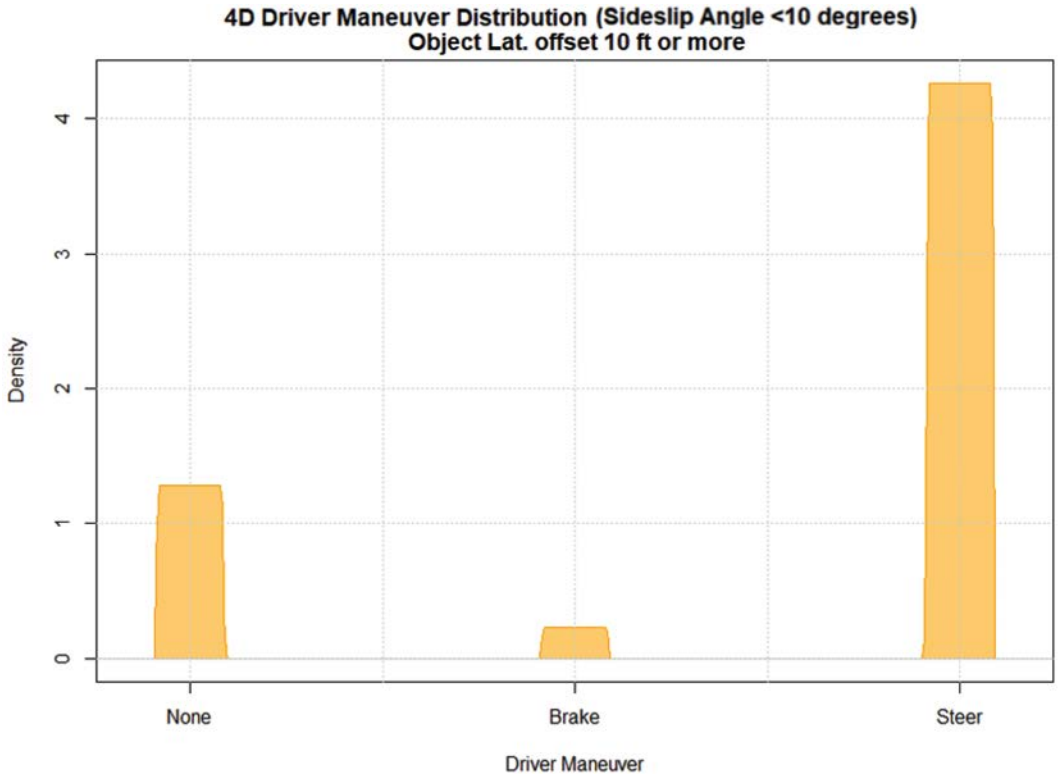

Figure 19. Distribution of driver input for objects struck greater than 10 ft off roadway (4D roadways).

Table 9. Weights for driver inputs used in the simulation matrix.

Input Number	Driver Type	Weight
1	No driver input (tracking)	0.223
2	Steering (tracking)	0.061
3	Braking (tracking)	0.113
4	Steering and braking (tracking)	0.343
5	Steering and braking (non-tracking)	0.260

Vehicle Probability Matrix

The researchers analyzed vehicle sales data to determine the marginal probability for each vehicle platform category of interest and selected a representative vehicle from each class for use in the encroachment simulation analyses. The researchers used 2019 U.S. sales data from Goodcarbadcar.net for the analysis. Although 2020 data was available at the time of the analysis, it was dramatically influenced by the COVID-19 pandemic, and the heavily skewed numbers were not considered reflective of anticipated vehicle sales moving forward. The top 10 best-selling models of 2019 and the respective vehicle platform categories they represent are presented in Table 10.

The vehicle types initially considered for the simulation matrix included a small passenger car, midsize sedan, SUV, and pickup truck. To develop the marginal probabilities or weights for the different simulated vehicle platforms, a classification scheme was needed to assign each vehicle make and model to its most appropriate platform. The classification criteria of the Highway Loss Data Institute were used to group each vehicle make and model into their representative categories (*23*).

The classification scheme presented in Figure 20 was used to classify passenger car make and models into the midsize sedan and small car model platforms. The length, width, curb weight, and other specifications were obtained from the respective official websites of the vehicle makes and two other trusted sites: www.edmunds.com and www.cars.com.

For this project, the small passenger car classes (i.e., S1, S2, and S3) were grouped to represent the small car vehicle category, and all midsize and large passenger car classes (i.e., M, L1, and L2) were included in the midsize sedan category.

Table 10. Top 10 best-selling vehicle models in 2019.

Rank	Vehicle	Classification	Sales 2019
#1	Ford F-Series	Pickup	896,526
#2	Ram Pickup	Pickup	633,694
#3	Chevrolet Silverado	Pickup	575,569
#4	Toyota RAV4	CUV	448,068
#5	Honda CR-V	CUV	384,168
#6	Nissan Rogue	CUV	350,447
#7	Chevrolet Equinox	CUV	346,049
#8	Toyota Camry	Passenger Car	336,978
#9	Honda Civic	Passenger Car	325,650
#10	Toyota Corolla	Passenger Car	304,850

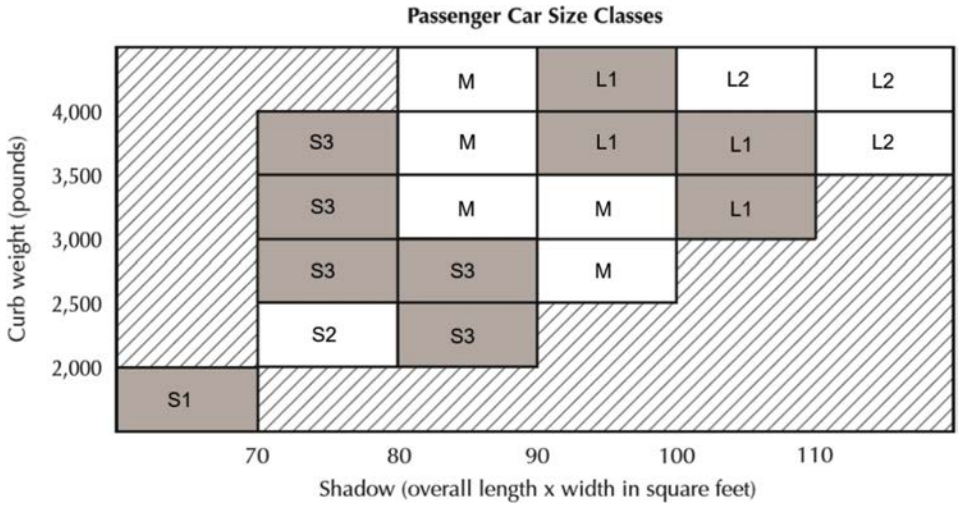

Figure 20. Passenger car classification scheme.

The Insurance Institute for Highway Safety (IIHS) has three classifications for pickups based on carrying capacity and curb weight as follows:

- **Small (P1):** curb weight of 4,000 pounds or less.
- **Large (P2):** curb weight of more than 4,000 pounds and a carrying capacity of one-half ton.
- **Very Large (P3):** curb weight of more than 4,000 pounds and a carrying capacity of three-quarters or 1 ton.

Sales data segregated by carrying capacity is not readily available. As shown in Table 10, the available sales data tends to aggregate the different models (e.g., Ford F-Series) rather than report them by model trim (e.g., F-150, F-250, F-350). However, since all pickup trucks were included in the pickup truck category, this did not affect the outcome of the classification.

IIHS divides SUVs into five classes. The smallest and largest classes of SUVs (U1 and U5, respectively) are classified on vehicle shadow (the overall length x width) and curb weight. The other classes are based only on curb weight as follows:

- **Mini (U1):** curb weight of 3,000 pounds or less and a shadow less than 75 square feet.
- **Small (U2):** curb weight between 3,001 and 3,750 pounds.
- **Midsize (U3):** curb weight between 3,751 and 4,750 pounds.
- **Large (U4):** curb weight between 4,751 and 5,750 pounds.
- **Very Large (U5):** curb weight of more than 5,751 pounds or a shadow of more than 115 square feet.

All these classes were included in the SUV model category for purposes of developing probabilities for this project.

Regarding vans, the research team classified minivans as V1 and full-size vans as V2 based on size and weight. For probability distribution purposes, both of these classes were included in the SUV category.

After some statistical analysis of the 2019 vehicle sales data, the research team developed the percentage allocations for the vehicle categories of interest as shown in Figure 21. Using this approach, the results suggested that approximately 51% of the 2019 U.S. vehicle market fell into the SUV category.

Looking deeper into the SUV category data, the research team noticed a large range of curb weights and vehicle dimensions that would make it difficult for a single-vehicle model to

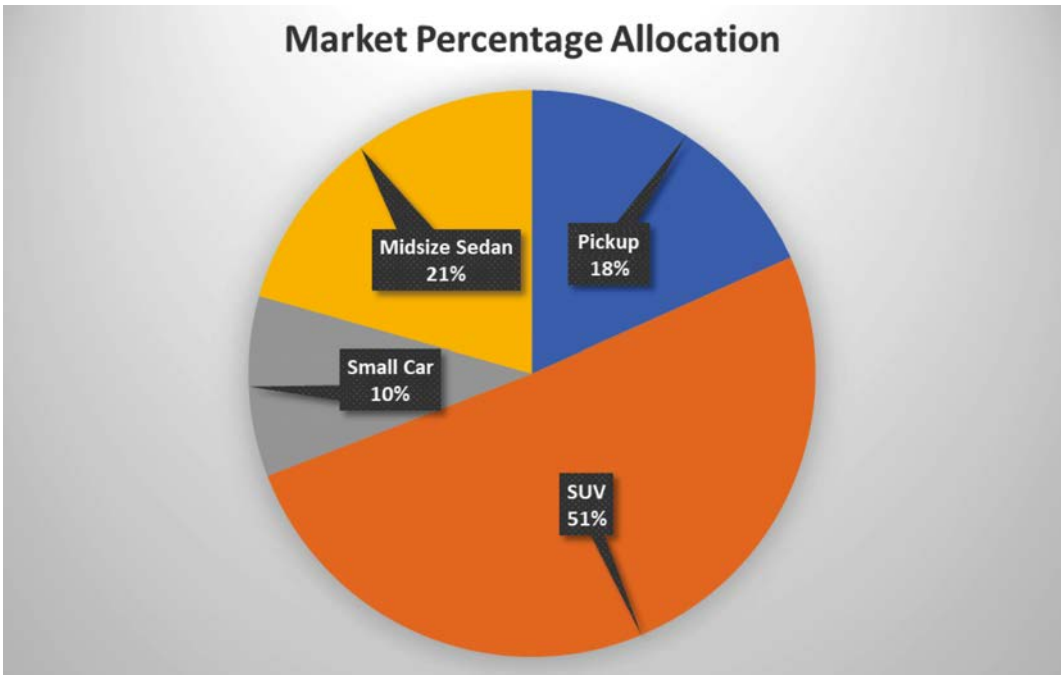

Figure 21. Marginal probabilities for initial vehicle categories selected for simulations.

adequately represent this category in the simulations. Of particular note is the rapidly growing vehicle category that is being referred to by the manufacturers as either CUV or crossover. Such vehicles are commonly smaller and tend to be more stable than midsize or large SUVs. Thus, if this large class was to be modeled using a midsize SUV, the resulting guidelines may have tended to be overly conservative.

The researchers performed additional literature reviews to further examine this issue and develop vehicle model categories that would be more representative of the changing vehicle fleet. It was decided that the SUV category would be separated into two categories. One category would be comprised of CUVs, also known as crossovers, and the second category would include more traditional SUVs. To distinguish between these two vehicle classes, researchers used the Wards' vehicle classification criteria and information from Midwest Roadside Safety Facility (MwRSF) Research Report No. TRP-03-427-20 that resulted from NCHRP Project 20-7 Task 372, "Evaluation of MASH Test Vehicles" (*24*). This classification is based on vehicle body style and size. CUVs have a unibody construction, while SUVs have a constructed body on a frame.

Adding another vehicle category in the matrix would have increased the simulation matrix and subsequent analysis effort beyond available resources. Therefore, the research team decided to merge the small car and midsize sedan categories into the passenger car category. It was noted that all of the highest-selling small car makes and models were part of the larger S3 class and had curb weights and shadows that were not appreciably different from the highest-selling midsize sedan.

The reclassification of the 2019 U.S. vehicle sales data is shown in Figure 22. These are the weight factors or marginal probabilities that were assigned to the selected simulated vehicle categories. While the CUV category has the largest allocation, it is consistent with sales trends in the U.S. vehicle market.

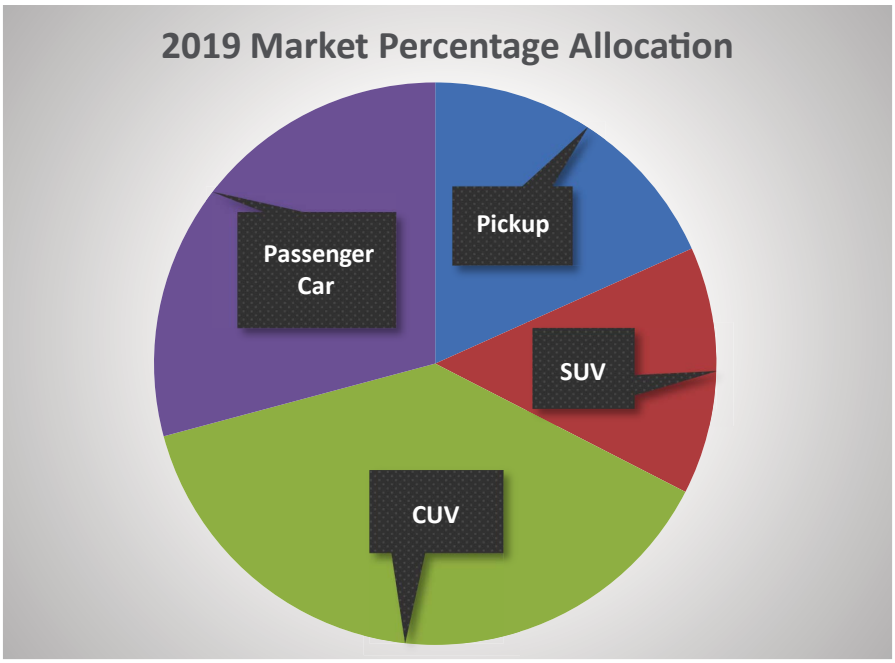

Figure 22. Sales-based probabilities for the selected vehicle categories.

CHAPTER 5

Encroachment Relationships

The simulation results generated from the large vehicle encroachment simulation matrix were weighted using the marginal probabilities developed in Chapter 4. This methodology permitted the probability of a discrete simulation to be determined through the application of observed crash data.

The research team used the weighted simulation outcomes to develop various encroachment distance and severity relationships for 2U and 4D facility types. The developed relationships included rollover probability, lateral extent of encroachment and longitudinal distance traveled, impact speed, and impact angle at a given lateral distance.

Statistical Model Specifications and Data Generation Process

Since the planned risk analysis procedure was intended to evaluate a given clear zone distance for a roadway and roadside configuration of interest, the likelihood of reaching a certain lateral distance was a key aspect of the model development process. Determining the probability of an impact with hazards at the clear zone edge and the severity of such impacts was equally important to the risk analysis methodology. This involves modeling both longitudinal distance and speed at the defined lateral clear zone distance.

Such data analysis processes call for complex models, such as mixed-effect models that take care of the repeated measures for the same simulation. Thus, the model development process involved structuring the encroachment simulation data for the mixed-effect models. Thus, for each simulation, the maximum lateral distance reached was determined, along with the vehicle speed and longitudinal distance traveled at different lateral offset distances ranging from 10 ft to 70 ft in 10 ft increments.

There are a total of 2,073,600 simulations, with each vehicle type having a total of 518,400 observations. The data regeneration resulted in a total of 3,628,800 observations for rollover probability and the probability of reaching a certain clear zone distance. This was based on some simulations reaching multiple clear zone distances without steering back, stopping, or rolling over. Similarly, the following number of observations was available for speed and longitudinal distance modeling.

- Passenger sedan: 1,697,198 observations.
- Pickup truck: 1,892,359 observations.
- Crossover or CUV: 1,748,198 observations.
- SUV: 1,568,715 observations.

The statistical models developed depended on the nature and distribution of the dependent variables. The team utilized logistic regression for the probability of reaching a certain clear zone as well as the likelihood of rollover at a given lateral distance. This is due to the binary nature of the outcome

variable (rollover—yes/no, and reaching a clear zone distance—yes/no). On the other hand, the research team utilized a multiple linear regression for the speed distribution model and the impact angle model; a gamma regression was used for the longitudinal distance distribution model.

Lateral Extent of Encroachment Models

The lateral extent of encroachment defines how far a vehicle can travel in the lateral direction relative to the edge of the traveled way for a given set of roadway and roadside design conditions. As mentioned earlier, the research team utilized logistic regression models to predict the lateral extent of encroachment. Table 11 through Table 18 present the models for the likelihood of an encroaching vehicle reaching or crossing a given lateral distance (clear zone) threshold. The negative coefficient of the clear zone distance variable suggests that the probability of reaching a certain threshold declines as the lateral distance increases. The magnitude of the decrease of the probabilities varies by vehicle type.

Other variables of interest that were found to be statistically significant in terms of the probability of reaching a certain lateral distance include horizontal curvature, shoulder width, foreslope width, backslope ratio, backslope width, and ditch bottom width. The model indicates that an increase in shoulder width, foreslope width, and ditch bottom width correspond to an increase in the probability of reaching a certain lateral distance. The model indicates that a flatter

Table 11. Lateral distance crossing probability model for 2U roads for CUV.

	Estimate	Standard Error	z-Value	P-Value
Intercept	0.080	0.069	1.16	0.246
Degree of Horizontal Curvature	0.729	0.027	26.54	<0.001
Shoulder Width	0.018	0.003	6.17	0.000
Foreslope Width	0.037	0.003	12.41	<0.001
Backslope	0.131	0.008	16.46	<0.001
Backslope Width	–0.015	0.003	–5.06	0.000
Bottom Ditch Width	0.027	0.003	9.59	<0.001
Clear Zone Distance	–0.046	0.001	–72.16	<0.001
Model Summary				
Number of Observations	3,628,800			
AIC	18			

NOTE: AIC = Akaike information criteria.

Table 12. Lateral distance crossing probability model for 4D roads for CUV.

	Estimate	Standard Error	z-Value	P-Value
Intercept	–0.224	0.067	–3.33	0.001
Degree of Horizontal Curvature	0.850	0.027	31.34	<0.001
Shoulder Width	0.016	0.003	5.80	0.000
Foreslope Width	0.039	0.003	13.37	<0.001
Backslope	0.137	0.008	17.55	<0.001
Backslope Width	–0.016	0.003	–5.48	0.000
Bottom Ditch Width	0.027	0.003	9.54	<0.001
Clear Zone Distance	–0.044	0.001	–71.18	<0.001
Model Summary				
Number of Observations	3,628,800			
AIC	18			

NOTE: AIC = Akaike information criteria.

Table 13. Lateral distance crossing probability model for 2U roads for pickup.

	Estimate	Standard Error	z-Value	P-Value
Intercept	0.292	0.068	4.31	0.000
Degree of Horizontal Curvature	0.843	0.027	31.20	<0.001
Shoulder Width	0.008	0.003	2.97	0.003
Foreslope Width	0.028	0.003	9.77	<0.001
Backslope	0.131	0.008	16.73	<0.001
Backslope Width	–0.014	0.003	–4.99	0.000
Bottom Ditch Width	0.022	0.003	7.89	0.000
Clear Zone Distance	–0.043	0.001	–69.03	<0.001
Model Summary				
Number of Observations	3,628,800			
AIC	18			

NOTE: AIC = Akaike information criteria.

Table 14. Lateral distance crossing probability model for 4D roads for pickup.

	Estimate	Standard Error	z-Value	P-Value
Intercept	–0.062	0.066	–0.94	0.347
Degree of Horizontal Curvature	0.975	0.027	36.47	<0.001
Shoulder Width	0.008	0.003	3.02	0.003
Foreslope Width	0.031	0.003	11.05	<0.001
Backslope	0.137	0.008	17.81	<0.001
Backslope Width	–0.014	0.003	–5.05	0.000
Bottom Ditch Width	0.023	0.003	8.50	<0.001
Clear Zone Distance	–0.042	0.001	–69.00	<0.001
Model Summary				
Number of Observations	3,628,800			
AIC	18			

NOTE: AIC = Akaike information criteria.

Table 15. Lateral distance crossing probability model for 2U roads for SUV.

	Estimate	Standard Error	z-Value	P-Value
Intercept	–0.150	0.071	–2.12	0.034
Degree of Horizontal Curvature	0.829	0.029	29.03	<0.001
Shoulder Width	0.020	0.003	6.77	0.000
Foreslope Width	0.034	0.003	11.27	<0.001
Backslope	0.154	0.008	18.68	<0.001
Backslope Width	–0.008	0.003	–2.68	0.007
Bottom Ditch Width	0.039	0.003	13.19	<0.001
Clear Zone Distance	–0.052	0.001	–76.68	<0.001
Model Summary				
Number of Observations	3,628,800			
AIC	18			

NOTE: AIC = Akaike information criteria.

Table 16. Lateral distance crossing probability model for 4D roads for SUV.

	Estimate	Standard Error	z-Value	P-Value
Intercept	–0.459	0.070	–6.56	0.000
Degree of Horizontal Curvature	0.983	0.029	34.46	<0.001
Shoulder Width	0.020	0.003	6.94	0.000
Foreslope Width	0.035	0.003	11.63	<0.001
Backslope	0.151	0.008	18.68	<0.001
Backslope Width	–0.008	0.003	–2.57	0.010
Bottom Ditch Width	0.037	0.003	12.79	<0.001
Clear Zone Distance	–0.051	0.001	–76.08	<0.001
Model Summary				
Number of Observations	3,628,800			
AIC	18			

NOTE: AIC = Akaike information criteria.

Table 17. Lateral distance crossing probability model for 2U roads for sedan.

	Estimate	Standard Error	z-Value	P-Value
Intercept	0.051	0.069	0.74	0.461
Degree of Horizontal Curvature	0.892	0.028	32.11	<0.001
Shoulder Width	0.014	0.003	4.72	0.000
Foreslope Width	0.027	0.003	9.10	<0.001
Backslope	0.148	0.008	18.55	<0.001
Backslope Width	–0.019	0.003	–6.44	0.000
Bottom Ditch Width	0.022	0.003	7.50	0.000
Clear Zone Distance	–0.045	0.001	–70.67	<0.001
Model Summary				
Number Of Observations	3,628,800			
AIC	18			

NOTE: AIC = Akaike information criteria.

Table 18. Lateral distance crossing probability model for 4D roads for sedan.

	Estimate	Standard Error	z-Value	P-Value
Intercept	–0.255	0.068	–3.76	0.000
Degree of Horizontal Curvature	1.042	0.028	37.63	<0.001
Shoulder Width	0.012	0.003	4.25	0.000
Foreslope Width	0.030	0.003	10.21	<0.001
Backslope	0.145	0.008	18.51	<0.001
Backslope Width	–0.019	0.003	–6.50	0.000
Bottom Ditch Width	0.020	0.003	7.13	0.000
Clear Zone Distance	–0.044	0.001	–70.05	<0.001
Model Summary				
Number of Observations	3,628,800			
AIC	18			

NOTE: AIC = Akaike information criteria.

backslope ratio is also associated with a greater probability of reaching a given lateral distance, while a larger backslope width results in a lower likelihood of reaching that lateral distance. An increase in the degree of horizontal curvature (i.e., a sharper curve) results in an increased probability of reaching a certain lateral distance.

Longitudinal Distance Models

To predict the occurrence of crashes with fixed objects (e.g., trees) at the clear zone edge, it is necessary to understand the longitudinal distance (along the roadway segment) that an encroaching vehicle has traveled when it reaches the given lateral offset. This permits the interaction to be predicted between the encroaching vehicles and the hazards defined along the clear zone edge. Thus, the encroachment simulation trajectories were used to develop models for longitudinal distance distributions as a function of the lateral extent of encroachment. Although the process described in this section was followed to develop longitudinal distance models for each of the vehicle types and facility types being considered under this study, the plots presented for discussion correspond to the pickup data weighted to represent 2U roadways.

Figure 23 presents the distributions of longitudinal distances observed for selected ranges of lateral distance for pickup trucks corresponding to a sample of 50,000 simulated trajectories. It

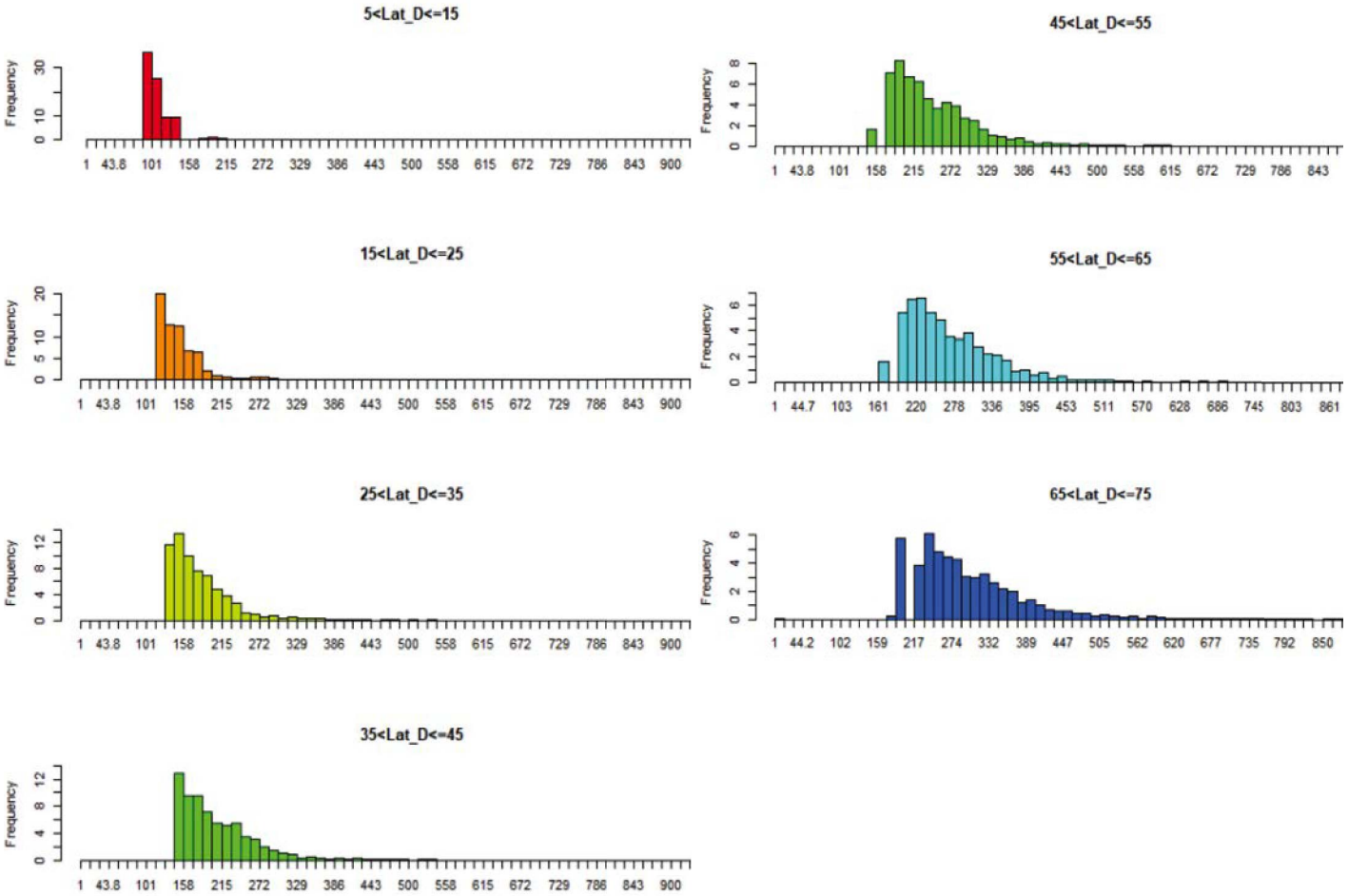

Figure 23. Longitudinal distance marginal distributions for pickups on 2U roads. The x-axis is the longitudinal distance from the departure point in feet. Lat_D = lateral distance.

can be seen that, in general, these distributions start with an accentuated spike on their leftmost side and then quickly decay as the longitudinal distance increases. A key feature observed in the data is that the spread of the longitudinal distance distribution increases with increasing lateral distances. This is logical given that the influence of encroachment speed, angle, and driver inputs (e.g., steering) on the trajectory of an encroaching vehicle will increase with lateral distance traveled.

Another key feature is a noticeable softening of the leftmost spike as the lateral distance increases, moving the mode of the distribution slightly to the right for greater lateral distances (most notable for lateral distances beyond 45 ft). In other words, three features are apparent: positive skewness of the distributions in general, increasing spread of the distribution with increasing lateral distances, and high kurtosis (i.e., peakness) of the distributions that decreases with increasing lateral distances.

Next, the research team fitted a preliminary model of the gamma distribution, where the scale parameter varies with the design variable, and the dispersion parameter is estimated as a flat average. The purpose of this exercise was to compare the marginal distributions from the raw data for lateral distance classes slightly different than in Figure 23, to the distributions produced by the model. The comparison result is shown in Figure 24.

The general trend of the marginal distributions is well-captured, with the mode of each distribution roughly in the correct location. However, regarding the kurtosis observed in the marginal distributions, a mismatch is observed at the smaller lateral distances that tends to dissipate at larger lateral distances. The comparison, however, is not necessarily expected to be direct, as the marginal distributions from the raw data represent the aggregate of all simulations that had data within the range of lateral distances, while the model conditional distribution is calculated at the average lateral distance of each interval shown.

The exploratory analysis identified the shape, location, and spread of the distributions change with lateral distance. A model that parameterizes only the scale parameter responds well to the need to model varying spread and location but seems rigid in capturing changes in shape. The research team determined that parameterizing both scale and dispersion parameters in terms of the design variables would provide more flexibility to the modeling process to capture the changes observed in the distributions.

Modeling the Scale and Shape of Lateral Distance Distributions

As an initial step of the modeling effort, the research team took a random sample of 12,000 simulated runs from the pickup truck dataset (containing approximately 44,500 longitudinal distances at different lateral distance thresholds). The team programmed an iterative estimation algorithm to estimate both distributional parameters for the conditional gamma distribution.

Table 19 shows the parameter estimates for the scale submodel fitted to the sample of simulated pickup encroachments. It can be seen that lateral distance, vertical grade, horizontal curvature, shoulder width, foreslope ratio, foreslope width, backslope ratio, backslope width, and ditch bottom width all play a role in determining the reach and spread of the longitudinal distance distribution.

In addition to the parameter estimates, Table 19 also summarizes the estimated variation between simulation runs that remain unaccounted for among the parameters, compared to the residual variation in the data beyond the model estimates.

Similarly, Table 20 shows the estimates corresponding to the shape parameter of the longitudinal distance distribution. It can be seen that only a subset of the factors that influence scale has an impact on the shape of the distribution. Most notably, lateral distance, horizontal curvature,

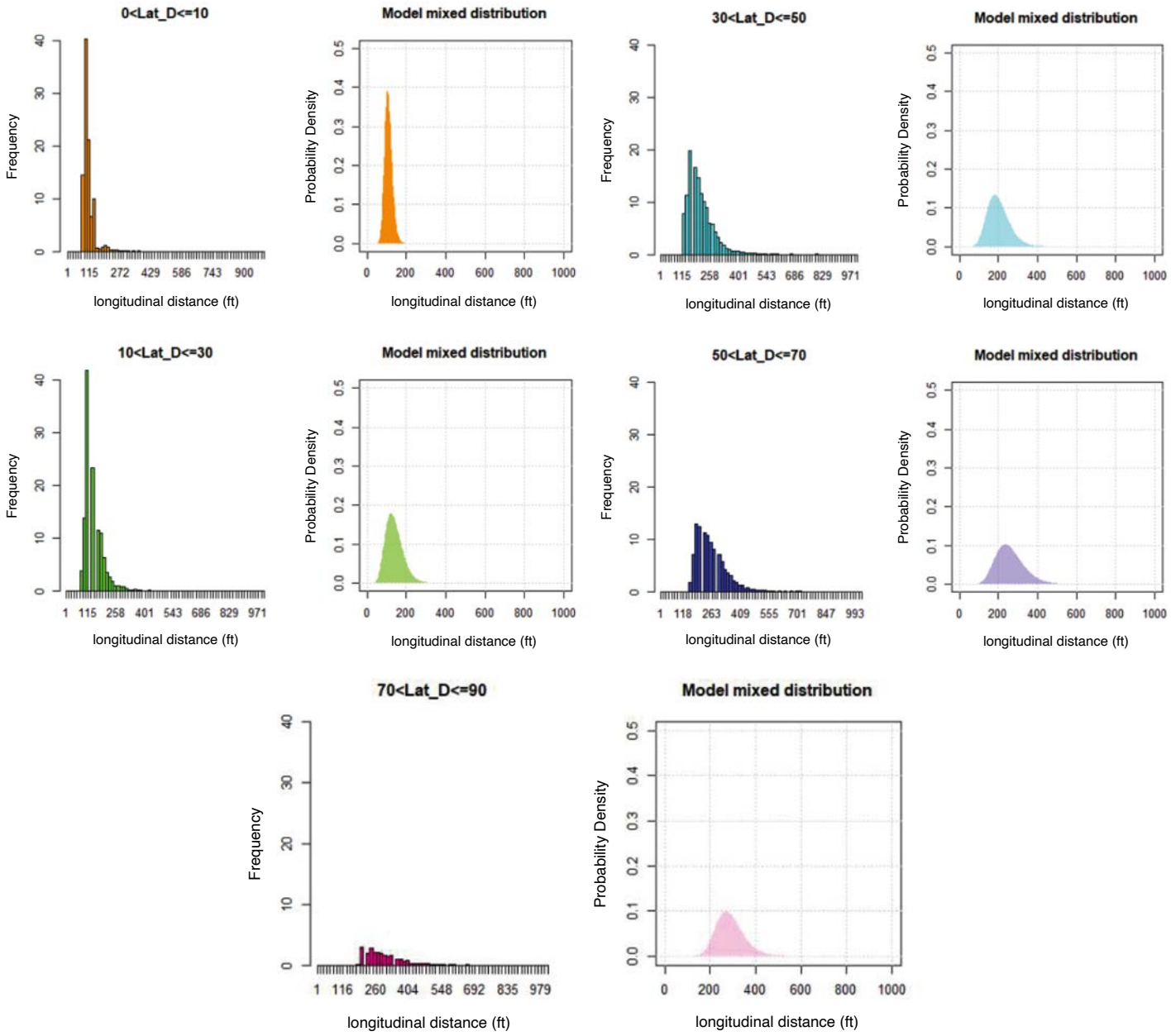

Figure 24. Longitudinal distance marginal distributions compared to the conditional distributions from a preliminary model of longitudinal distances for pickups and 2U roads.

backslope ratio, and backslope width. Shoulder width, foreslope ratio, and foreslope width have only a mild impact on the shape of the distribution.

To have an initial visualization of how this complex model performs in capturing the observed longitudinal distances, the research team prepared a set of graphs, shown in Figure 25, comparing the model-predicted distribution shapes and the observed longitudinal distances for a few randomly sampled simulation runs in the data.

As expected, the observations tend to fall both on the lower and upper half of the distributions, except for one case for which the observation is further to the right of the range. However, this plot does not provide further insights into the correctness of the shape and location of the

Table 19. Parameter estimates for the scale of longitudinal distance distribution for pickups at 2U roadways.

Variable	Estimate	Standard Error	z-Value	P-Value
Intercept	4.63E+00	2.32E-02	199.791	< 2e-16
Lateral Distance	3.04E-02	2.02E-04	150.714	< 2e-16
Lateral Distance Squared	–1.40E-04	1.21E-06	–115.709	< 2e-16
Vertical Grade	4.13E-05	1.81E-04	0.228	0.81927
Degree of Horizontal Curvature	–1.89E-01	4.29E-03	–44.108	< 2e-16
Shoulder Width	–8.32E-04	4.56E-04	–1.826	0.06785
Foreslope Squared	9.42E-04	3.43E-04	2.748	0.00599
Foreslope	–1.50E-02	5.33E-03	–2.815	0.00488
Foreslope Width	–3.57E-03	4.25E-04	–8.391	< 2e-16
Bottom Ditch Width	–3.79E-03	4.09E-04	–9.265	< 2e-16
Backslope	5.72E-03	3.07E-03	1.864	0.06239
Backslope Width	–1.74E-03	1.03E-03	–1.681	0.09273
Lateral Distance* Vertical Grade	1.64E-05	2.13E-06	7.680	1.59E-14
Lateral Distance* Shoulder Width	–5.10E-05	5.38E-06	–9.477	< 2e-16
Backslope* Foreslope	1.21E-03	4.75E-04	2.539	0.01110
Backslope Width * Foreslope	–1.40E-04	1.59E-04	–0.882	0.37795
Lateral Distance* Backslope	–6.86E-04	3.64E-05	–18.872	< 2e-16
Lateral Distance* Backslope Width	5.05E-05	5.55E-06	9.107	< 2e-16
Lateral Distance* Foreslope	–1.56E-04	2.37E-05	–6.610	3.85E-11
Lateral Distance* Backslope* Foreslope	1.21E-05	5.37E-06	2.258	0.02397

Random Effects and Residual Variation		
	Variance	Standard Deviation
Groups Run_Number	0.018241	0.13506
Residual	0.006338	0.07961

NOTE: *indicates interaction between the variables.

predicted distributions. To help with this, a graph was made of 850 predictions from the distributional model (i.e., the overlapping predicted distributions for 850 randomly picked pickup simulations). In Figure 25, each graph represents a randomly selected encroachment simulation. The vertical line represents the observed longitudinal travel distance for the encroachment. The colored area is the distribution generated by the model for the design condition associated with the selected encroachment. The closer the observed is to the mean of the predicted distribution, the better the correlation. The overlapped distributions should roughly correspond to the spread and concentration areas of the corresponding observed longitudinal distances.

Next, for a more formal assessment against the fit of the predicted distributions, the research team calculated the percentile of each observation from the corresponding predicted (conditional)

Table 20. Parameter estimates for the shape of longitudinal distance distribution for pickups at 2U roadways.

Variable	Estimate	Standard Error	z-Value	P-Value
Intercept	–4.002880	0.181441	–22.062	< 2e-16
Lateral Distance	–0.051700	0.005941	–8.703	< 2e-16
Lateral Distance Squared	0.000717	6.71E-05	10.679	< 2e-16
Degree of Horizontal Curvature	–0.669750	0.058879	–11.375	< 2e-16
Shoulder Width	–0.009770	0.005658	–1.726	0.08430
Foreslope	–0.008140	0.018731	–0.434	0.66400
Foreslope Width	–0.012430	0.005825	–2.135	0.03280
Backslope	–0.091920	0.023145	–3.972	7.15E-05
Backslope Width* Backslope	0.000721	0.001383	0.521	0.60210
Lateral Distance* Foreslope	–0.000490	0.000431	–1.140	0.25450

NOTE: *indicates interaction between the variables.

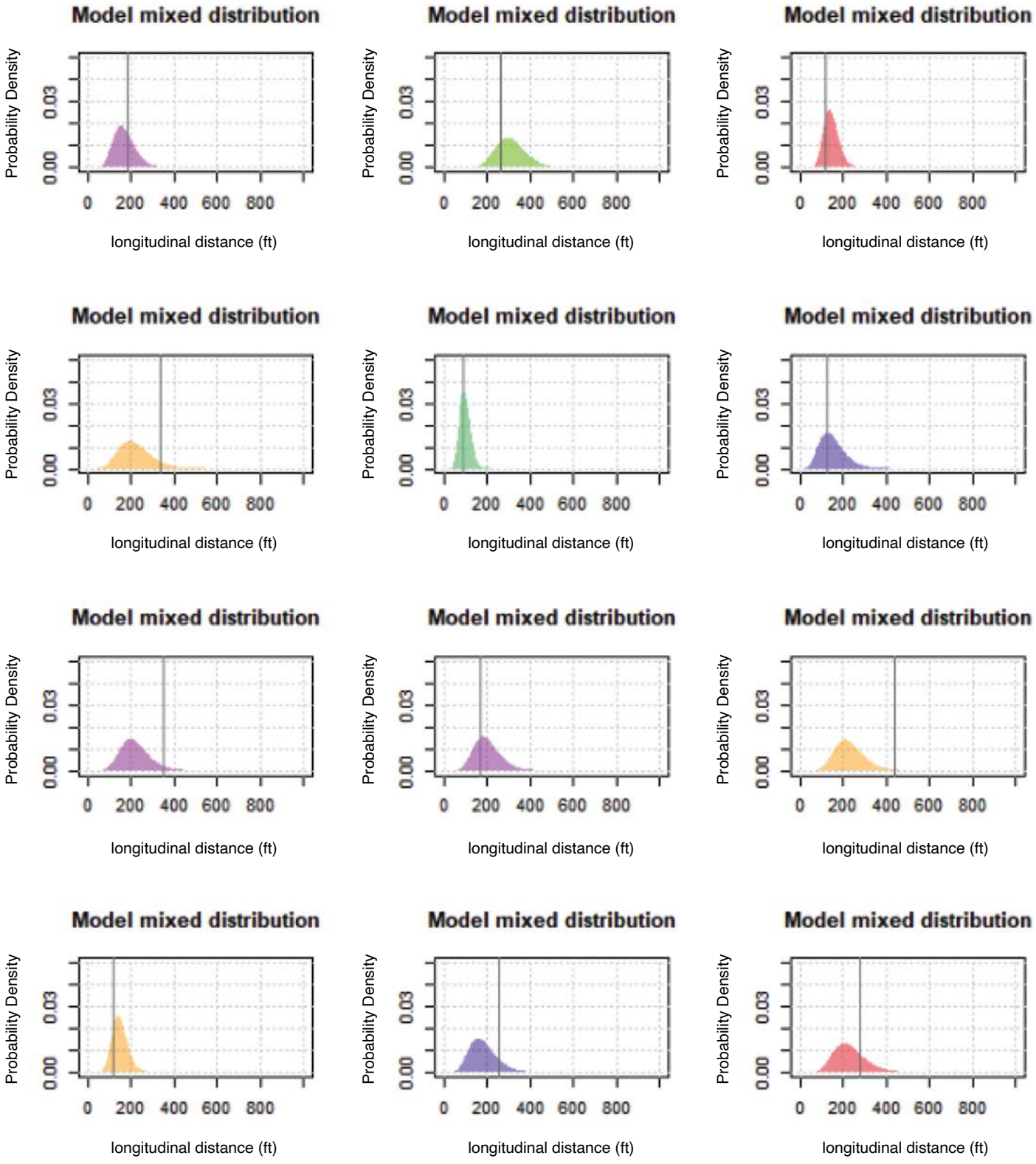

Figure 25. Longitudinal distance predicted distributions compared to actually observed longitudinal distance for pickup simulations at 2U roads selected at random.

distribution and made a histogram and quantile-to-quantile (q-q) plot. The expectation is that the histogram should look relatively flat from the minimum of zero on the left to the maximum of 1.0 on the right, and the q-q plot should fall along the 1:1 line if the observed and predicted quantiles correspond to each other. This result is shown in Figure 26.

There is an obvious area of discrepancy on the left extreme of the two plots between 0 and about 0.15. This gap corresponds to the gap noticed in the superposition of distributions noted in Figure 26. Similarly, the q-q plot on the right shows a poor fit between the distributions at the lower percentiles, but the distributions catch up to each other eventually, as the plot tends toward the expected line of 1:1 (the dotted line) with increasing percentiles.

Post Hoc Adjustment of Predicted Distribution

Given the mismatch between the observed and predicted distributions of longitudinal distances, the research team implemented an algorithm that applies a post hoc adjustment to the predicted distribution to attempt to close the gap between the predicted and observed distributions. The following potential adjustments were included in the search for an optimized estimate in this algorithm.

1. An initial right shift with exponential decay to the domain of the distribution (meaning, the predicted longitudinal distance quantiles are shifted to the right by a threshold that decays with larger longitudinal distance quantiles). The adjustment is such that the order of predicted quantiles does not change. This adjustment is controlled by new parameters defined as the right shift (a), and the rate of decay (b).
2. A flat shift in the predicted quantile equivalent to relocating the origin of the reference system, denoted by a new parameter (c).

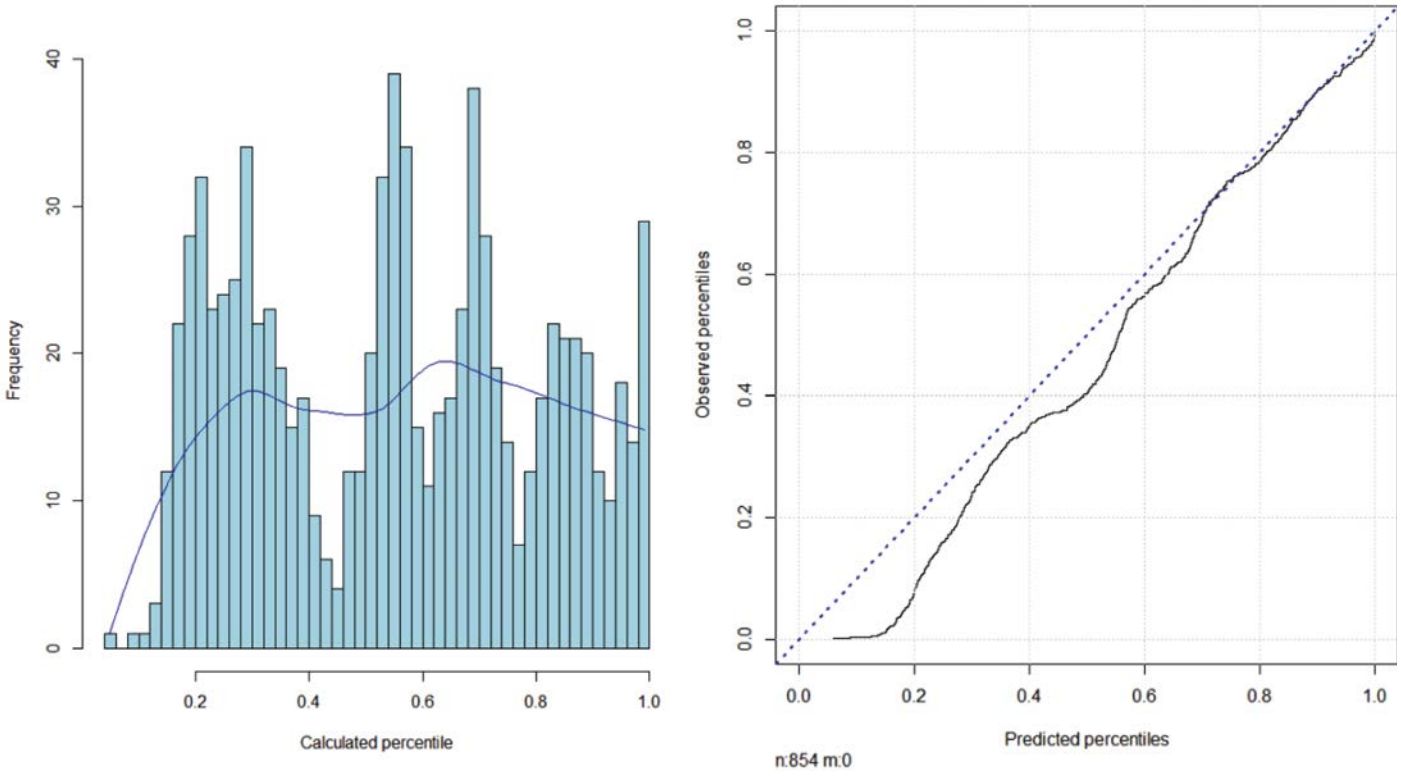

Figure 26. Histogram (left) and q-q plot (right) for observed versus predicted longitudinal distance quantiles for pickups at 2U roads. Note: In the histogram, the blue line represents the density plot for the distribution.

3. To try to address the kurtosis and left-tail issues, the algorithm also searched for a truncation point of the predicted distributions at a given flat percentile (defined as parameter trun). The new quantiles are calculated from the remaining truncated distribution, discarding the lower portion of the predicted distribution.

A genetic algorithm was implemented to find the best combinations of the adjustments above, stated as an optimization problem that minimizes the deviation between the predicted and observed percentiles. The graphs in Figure 27 show the results after optimizing the above adjustments to different lateral distances.

It can be seen in the plots in Figure 27 that roughly the same combination of adjustments to the predicted distributions yields a significant improvement in the correspondence between the predicted and the observed percentiles.

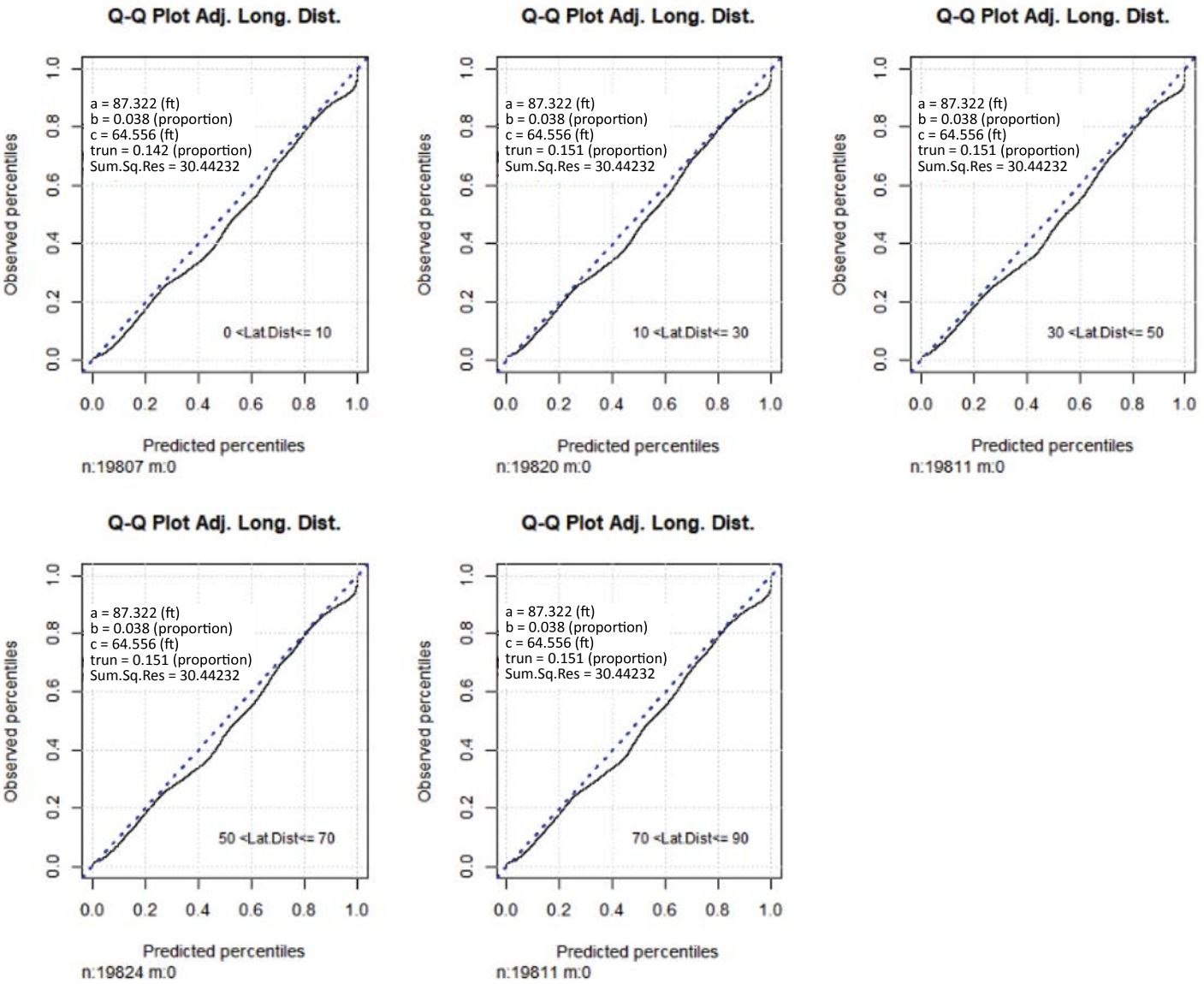

Figure 27. Q-q plots for observed versus adjusted predicted longitudinal distance distributions (sample model) for pickups at 2U roads. Sum.Sq.Res. = sum of the squares of the residuals (estimate of the error between the observed and predicted).

Next, the research team refitted the distributional model to the complete dataset of pickup simulations, with the expectation that a more comprehensive database would yield a better prediction. The results are shown in Figure 28. When applying the adjustments described above to the predictions of this model, it is apparent that the performance of the adjusted models is marginal compared to the adjusted predictions on the model fitted to a large random sample of the data. Upon reviewing the comparative performances, the research team decided to move forward with using the model fitted to the sample of runs.

Models and Adjustments for Facility Types and Additional Vehicles

The research team followed a similar process to the one described in the previous sections to arrive at longitudinal distance models and adjustments for the rest of the vehicle types for both

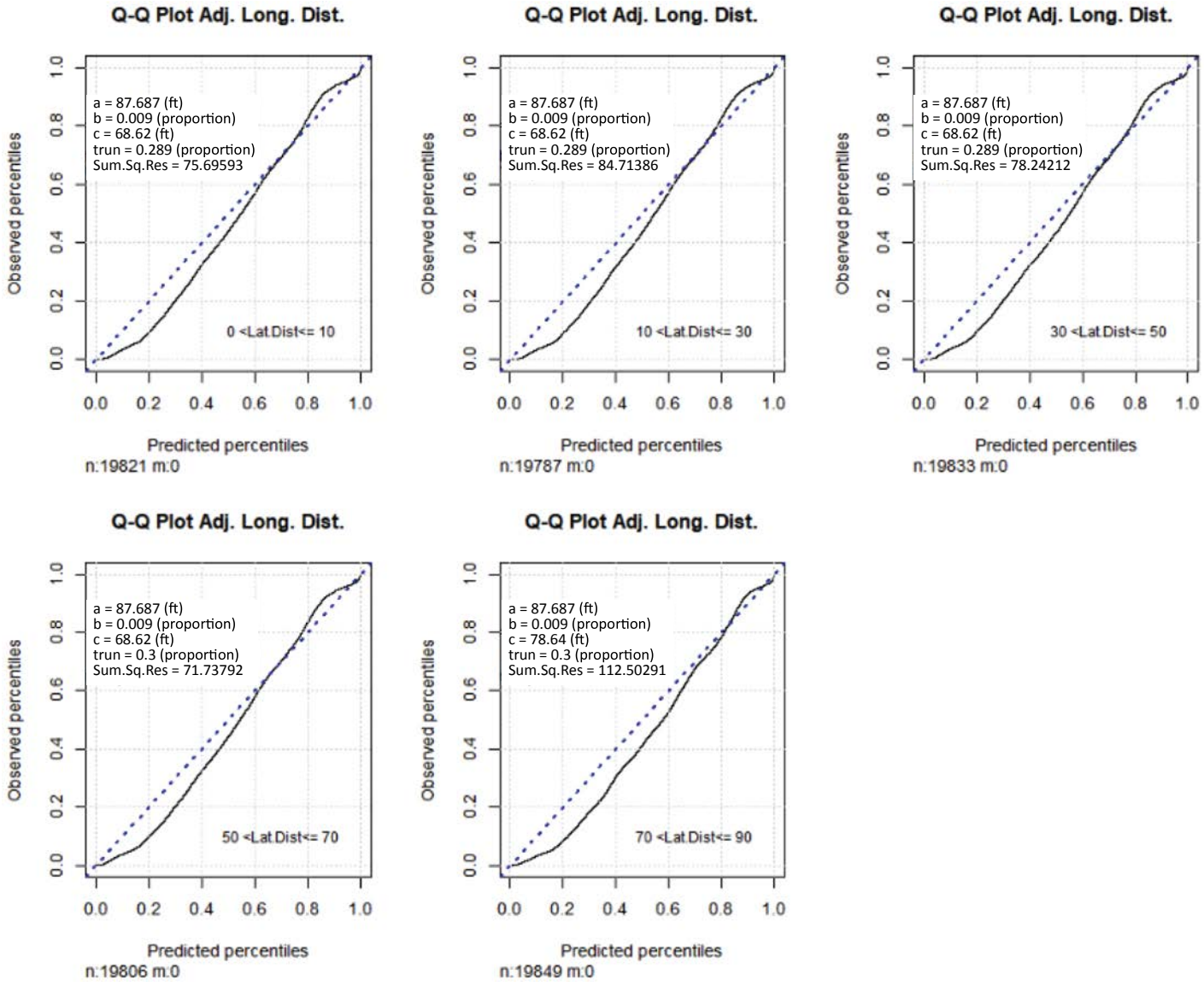

Figure 28. Q-q plots for observed versus adjusted predicted longitudinal distance distributions (full data model) for pickups at 2U roads. Sum.Sq.Res. = sum of the squares of the residuals (estimate of the error between the observed and predicted).

facility types of interest after confirming very similar trends from the raw data. The following sections document the performance of the adjusted distributional predictions.

Figure 29 shows the performance of the final adjusted models for pickup trucks on 4D roads. Similar to the performance at 2U sites, the expectation is that roughly the same set of adjustments should produce acceptable performance for the model, regardless of the lateral distance.

Figure 30 shows the performance of the final adjusted models for sedans on 2U roads, and Figure 31 presents the corresponding performance for 4D roads. Figure 32 shows the performance of the final adjusted models for CUVs on 2U roads, while Figure 33 presents the corresponding performance for 4D roads. Figure 34 shows the performance of the final adjusted models for SUVs on 2U roads, while Figure 35 presents the corresponding performance for 4D roads. Similar to the performances for the pickup truck, the expectation is that roughly the same set of adjustments should produce acceptable performance for the model, regardless of the lateral distance.

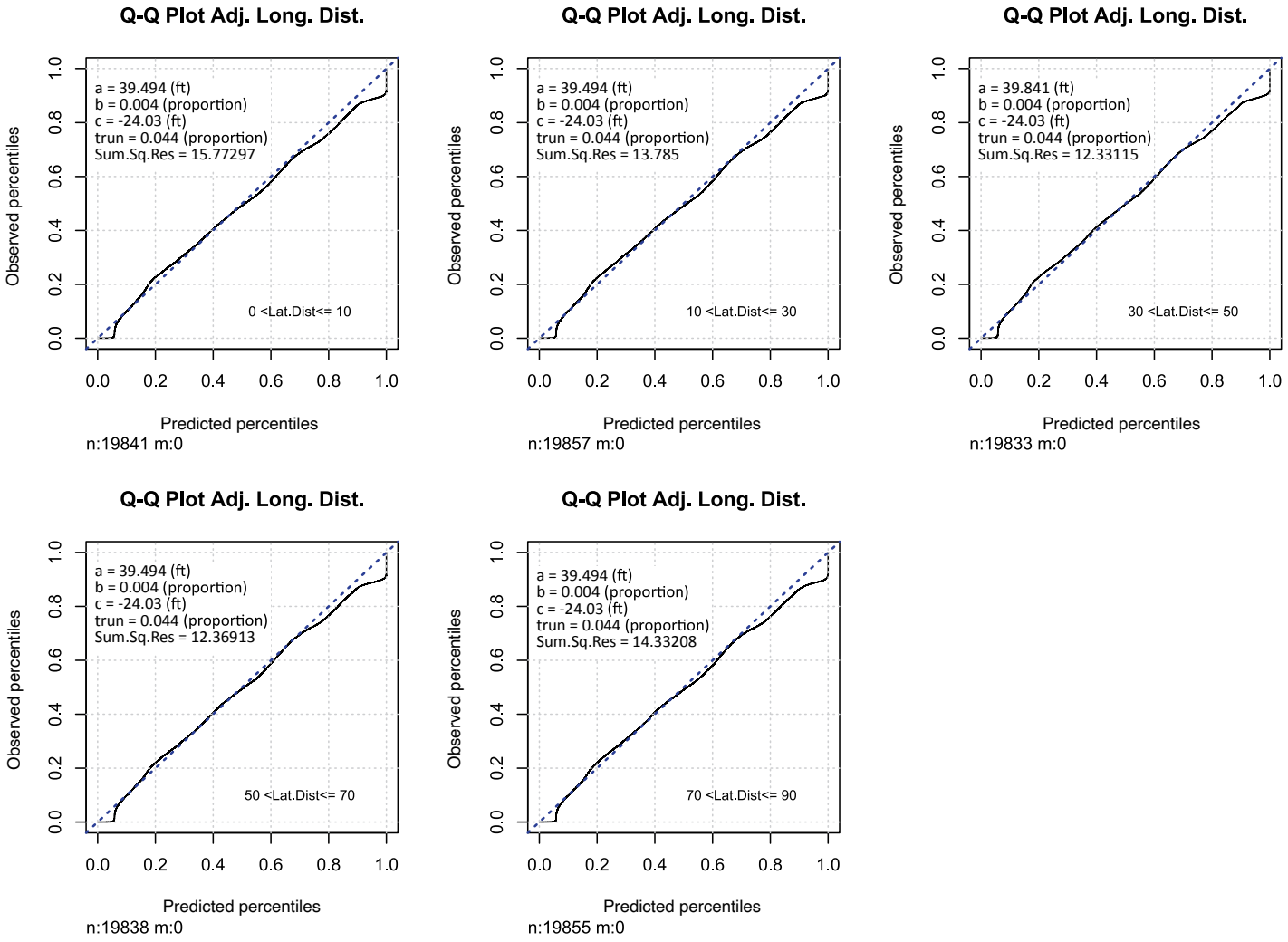

Figure 29. Q-q plots for observed versus adjusted predicted longitudinal distance distributions (sample model) for pickups at 4D roads. Sum.Sq.Res. = sum of the squares of the residuals (estimate of the error between the observed and predicted).

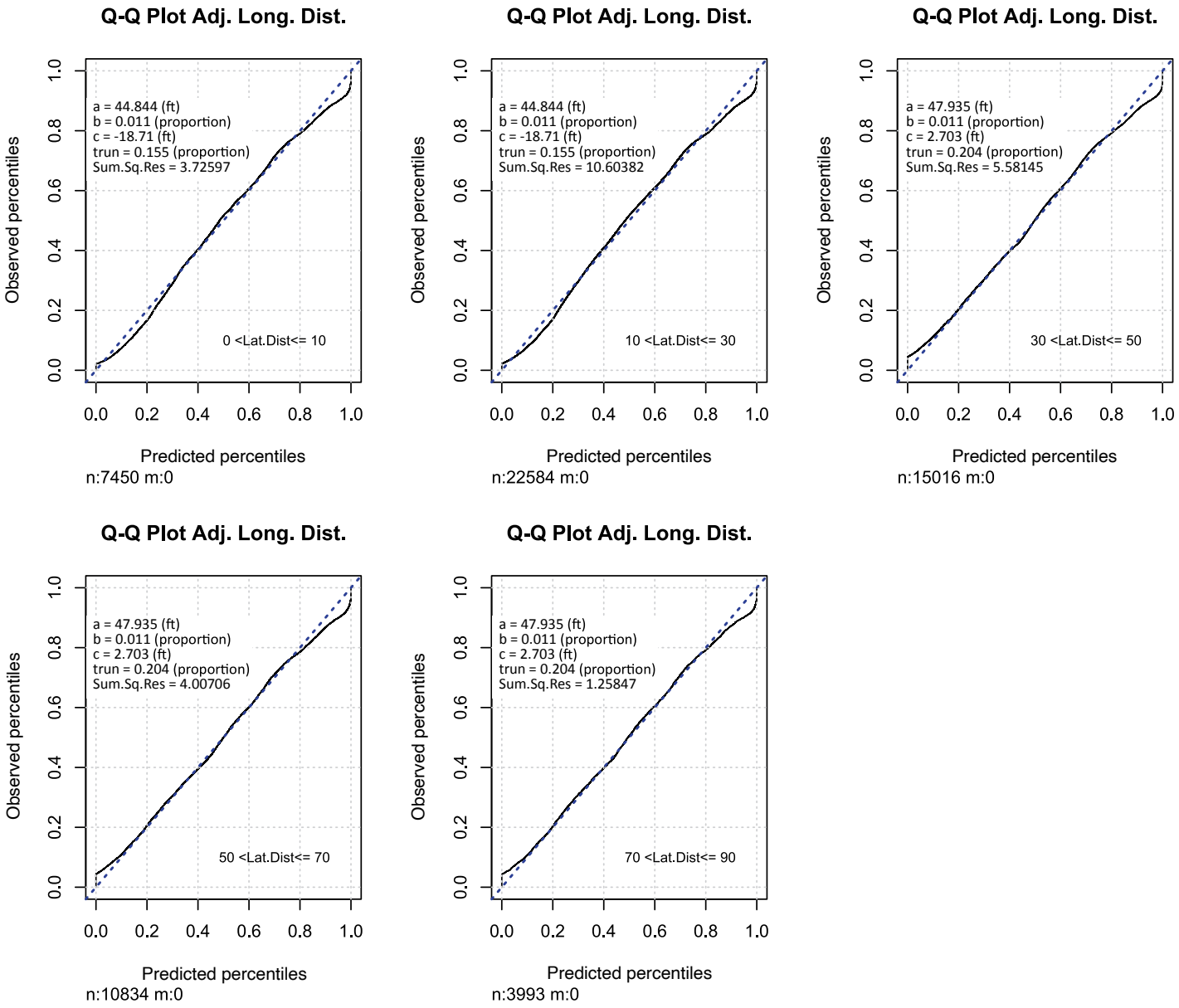

Figure 30. Q-q plots for observed versus adjusted predicted longitudinal distance distributions (sample model) for sedans at 2U roads. Sum.Sq.Res. = sum of the squares of the residuals (estimate of the error between the observed and predicted).

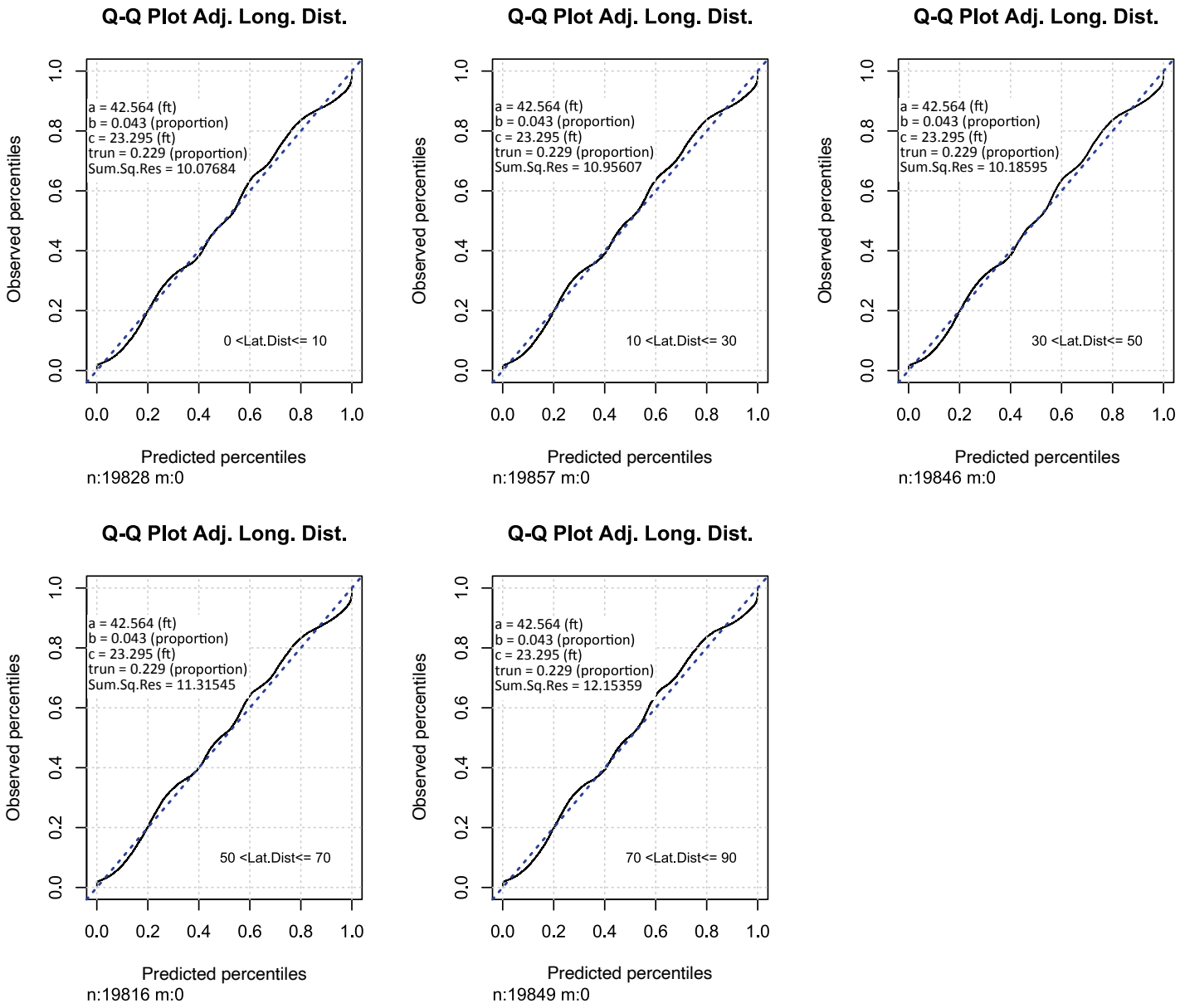

Figure 31. Q-q plots for observed versus adjusted predicted longitudinal distance distributions (sample model) for sedans at 4D roads. Sum.Sq.Res. = sum of the squares of the residuals (estimate of the error between the observed and predicted).

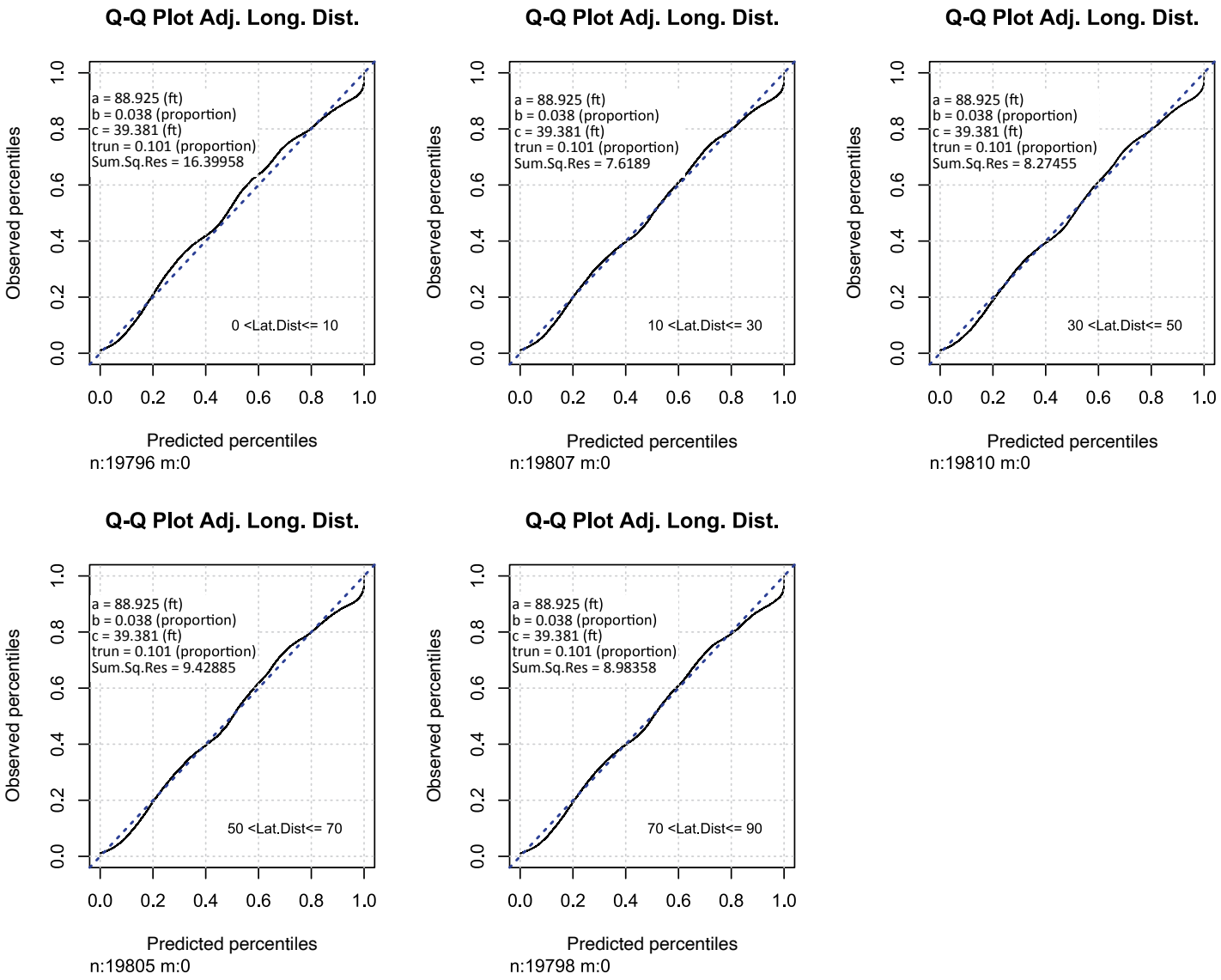

Figure 32. Q-q plots for observed versus adjusted predicted longitudinal distance distributions (sample model) for CUVs at 2U roads. Sum.Sq.Res. = sum of the squares of the residuals (estimate of the error between the observed and predicted).

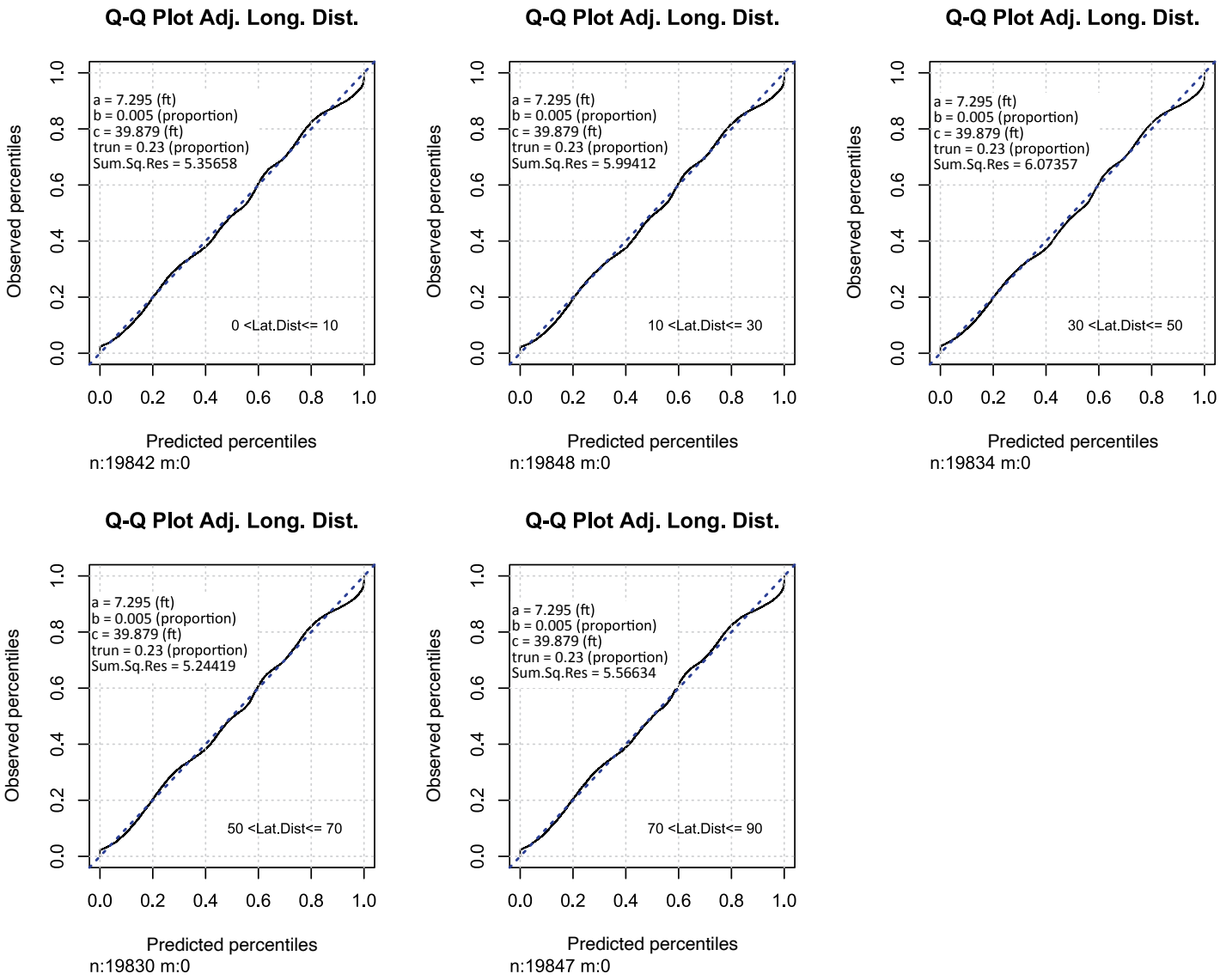

Figure 33. Q-q plots for observed versus adjusted predicted longitudinal distance distributions (sample model) for CUVs at 4D roads. Sum.Sq.Res. = sum of the squares of the residuals (estimate of the error between the observed and predicted).

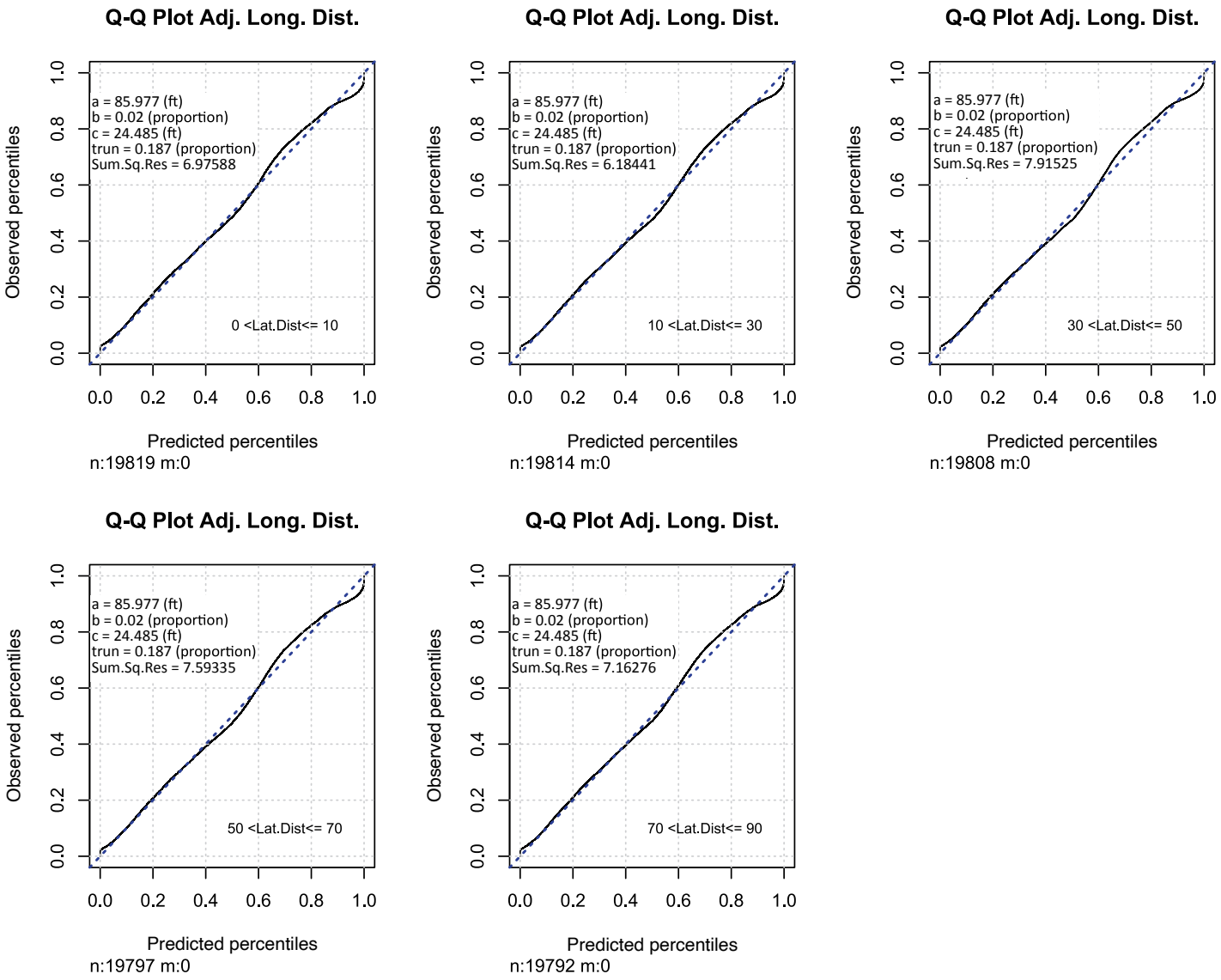

Figure 34. Q-q plots for observed versus adjusted predicted longitudinal distance distributions (sample model) for SUVs at 2U roads. Sum.Sq.Res. = sum of the squares of the residuals (estimate of the error between the observed and predicted).

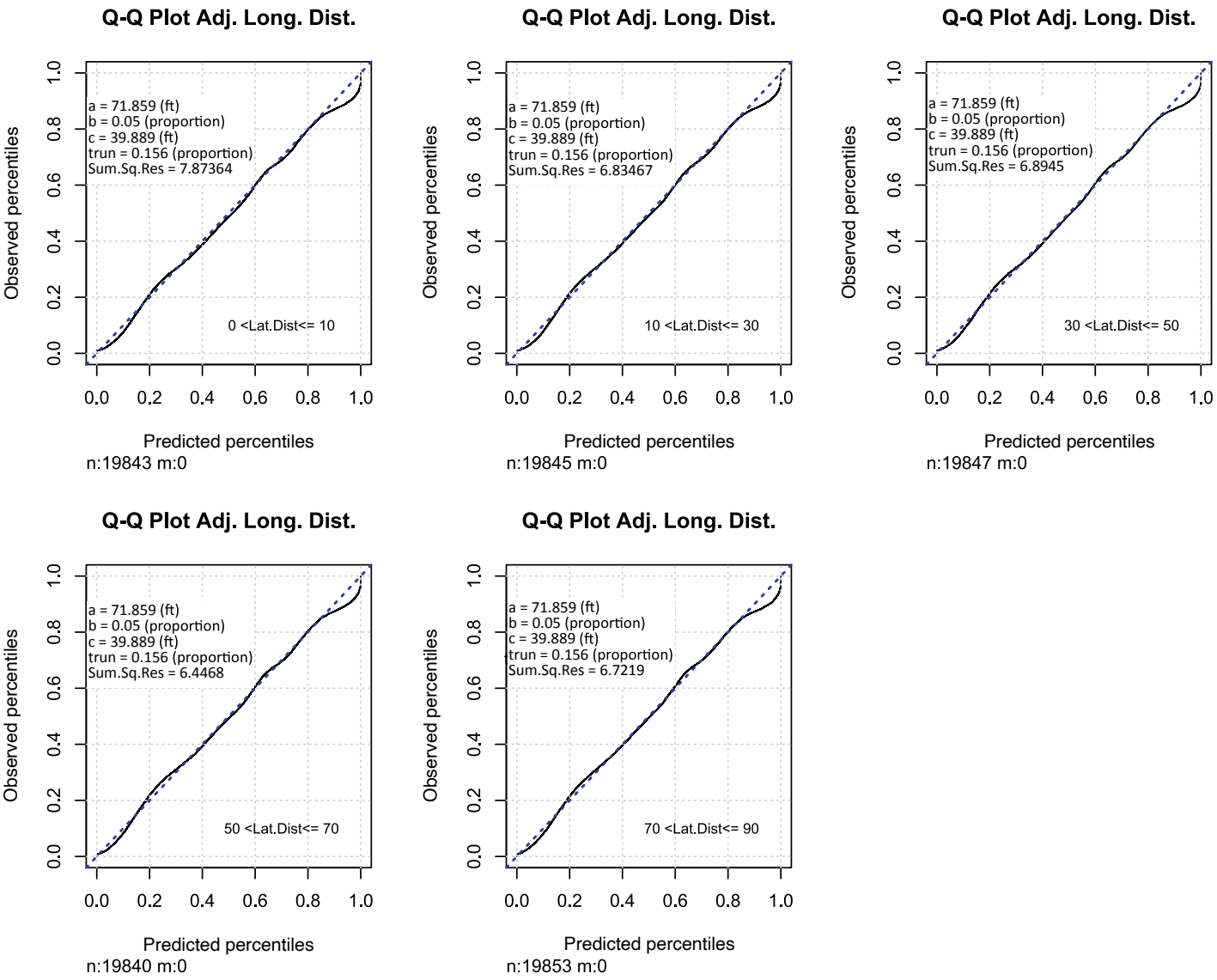

Figure 35. Q-q plots for observed versus adjusted predicted longitudinal distance distributions (sample model) for SUVs at 4D roads. Sum.Sq.Res. = sum of the squares of the residuals (estimate of the error between the observed and predicted).

Impact Speed Models

The Impact Speed Models determine the speed at which an encroaching vehicle would hit an object at different clear zone distances. This information is subsequently used within the severity module to determine the severity of the impact.

The simulated encroachment data was further analyzed to develop speed distributions for the encroaching vehicles that reach a given lateral offset. As noted, the speed distributions will be used to estimate crash severity (i.e., injury probability) for an impact with a fixed object encountered at the lateral distance of interest. Figure 36 and Figure 37 present the density and boxplot distribution of resultant speed for the encroaching vehicles that reach the prescribed lateral distance. It can be observed in Figure 36 that five peaks exist, which are defined by the values of encroachment speed used in the simulation matrix. The simulation matrix involved five encroachment speeds: 25 mph (40 kph), 35 mph (56 kph), 45 mph (72 kph), 55 mph (89 kph), and 65 mph (105 kph).

Figure 37 shows a boxplot of the absolute speeds of the vehicles at different lateral offsets. It can be observed that overall, the median value ranged between 39 mph (62 kph) and 41 mph (66 kph).

Incorporating Posted Speed Limit in the Impact Speed Models

The research team also worked on incorporating posted speed limits into the Impact Speed Models. The intent is to be able to distinguish clear zone guidance by posted speed limit along with other roadway and roadside design variables.

First, the team developed a relationship between the departure speed and the posted speed limit using the crash database from *NCHRP Web-Only Document 341* (*3*). The purpose was

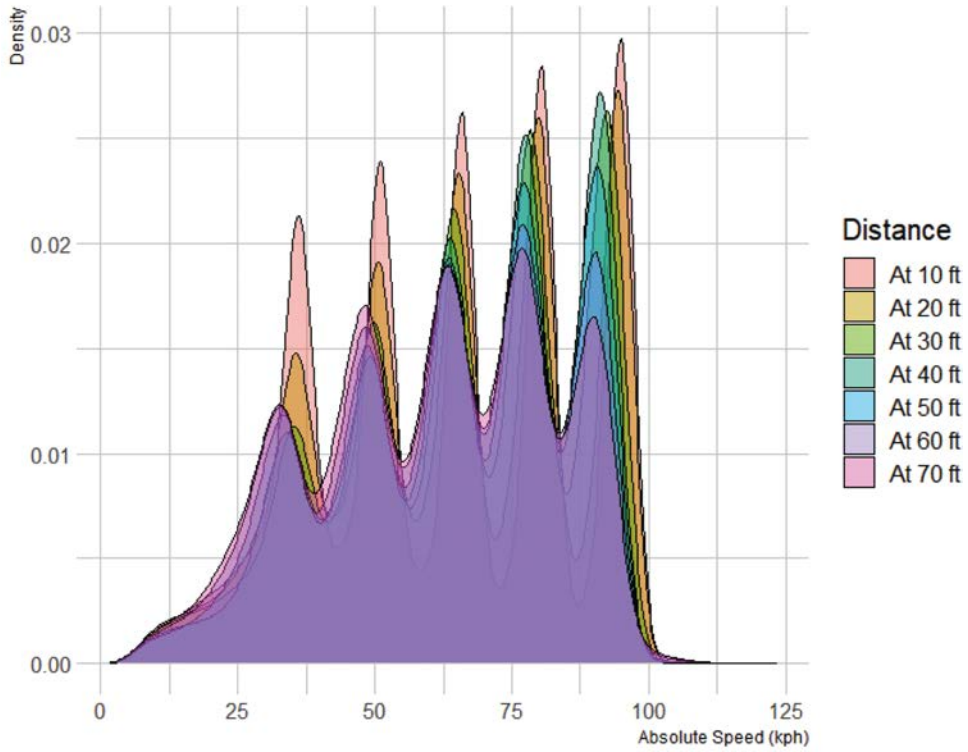

Figure 36. Absolute speed distribution.

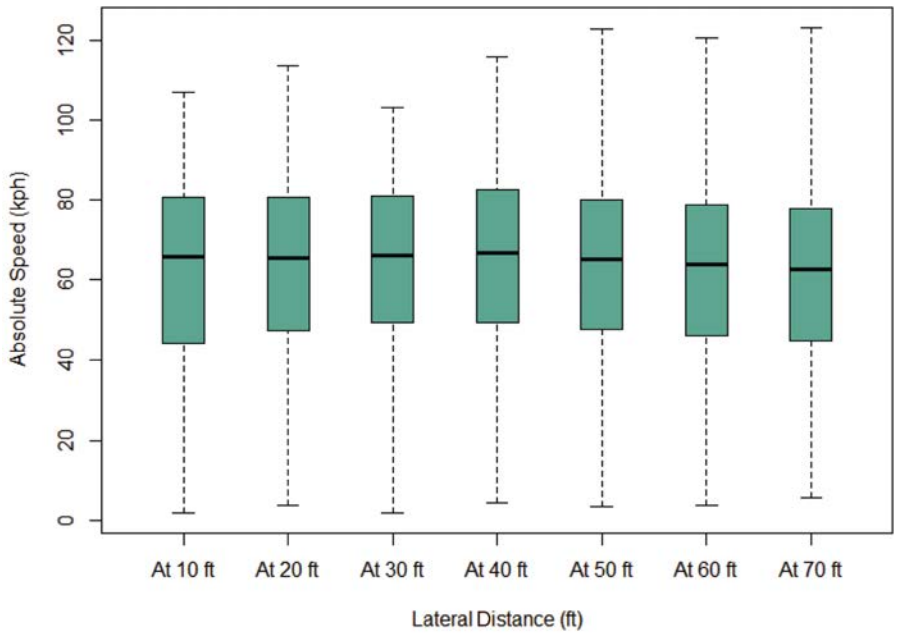

Figure 37. Boxplot of the absolute speed by lateral distances.

two-fold: improve the prediction of impact speeds for the analysis and provide sensitivity to speed limit ranges in the risk calculations. A total of 373 right-departure, fixed-object crashes was used to estimate the corresponding model presented in Table 21. The relationship associated with the model is shown graphically in Figure 38.

The developed relationship was then used to predict the posted speed limit given the departure speed and other parameters used in the simulation analysis. The predicted speed limit is treated as "point" data, meaning it is the average of all predicted speeds given the existing conditions. Table 22 presents the distribution of the predicted mean posted speed limit by facility type. It can be observed that the predicted mean posted speed limit is slightly higher for 4D facilities than for 2U facilities.

Further, given the developed speed model, the research team simulated the speed limit to produce a weighted speed limit. This enables the model to cover a wider range of data than simply relying on the mean predicted speed limit. The simulated posted speed limit data were divided

Table 21. Posted speed model derived from *NCHRP Web-Only Document 341* data (*3*).

Parameter	Estimate	Standard Error	z-Value	P-Value	Significance
Intercept	45.160170	3.188638	14.163	< 2e-16	***
Departure Speed	0.346342	0.088586	3.910	0.00011	***
Shoulder Width	2.094883	1.020895	2.052	0.04088	*
Departure Speed Squared	–0.000800	0.000548	–1.452	0.14743	—
Unknown Shoulder Condition	10.464750	4.457715	2.348	0.01943	*
Departure Speed*No Shoulder Condition	–0.137420	0.029335	–4.684	3.96E-06	***
Departure Speed Squared*4D	0.000611	0.000258	2.364	0.01859	*

NOTE: * in the left column indicates interaction between the variables; *** = statistically significant at the 99% confidence interval; * in the table = statistically significant at the 95% confidence interval; — = not statistically significant at the 90% confidence interval.

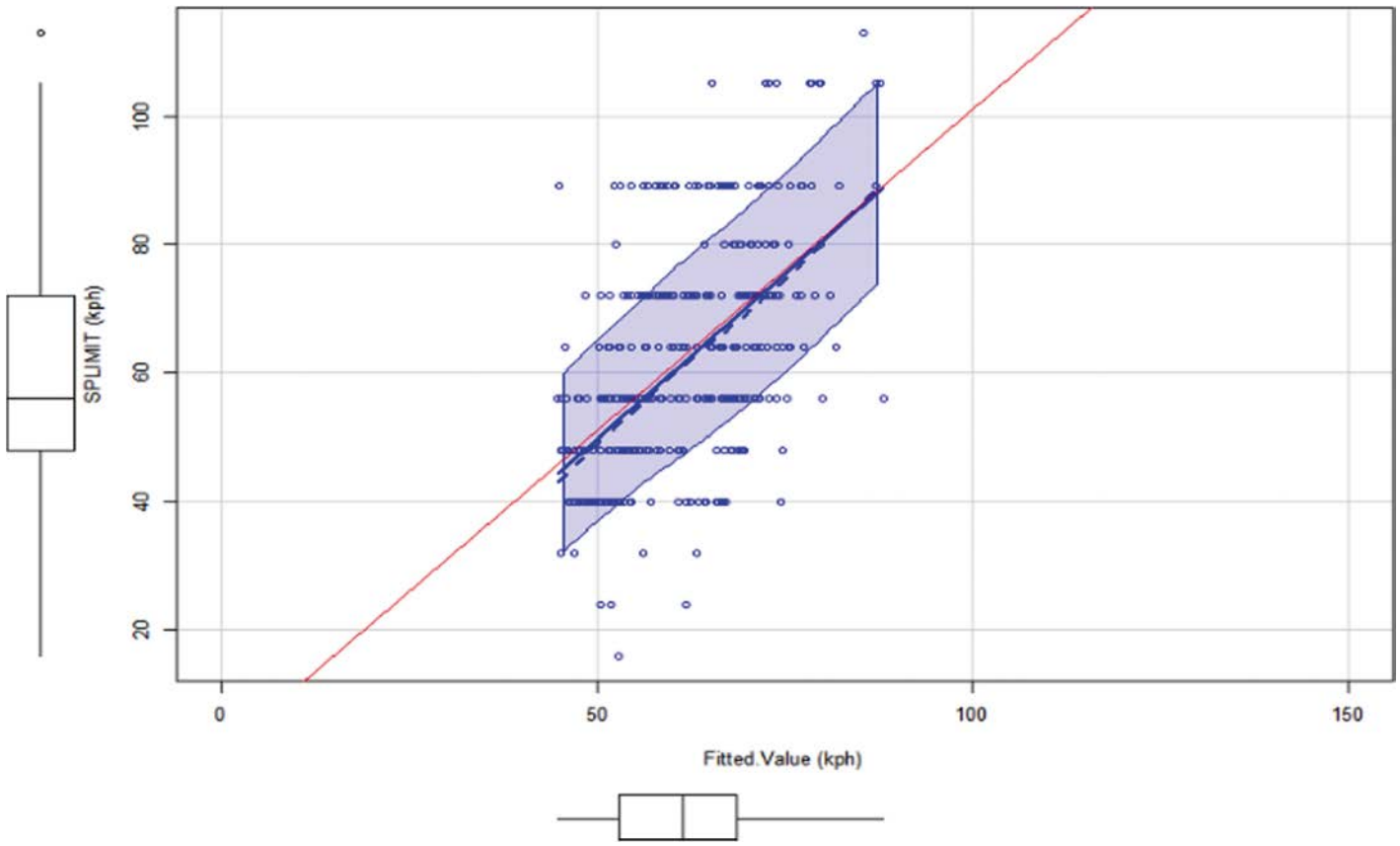

Figure 38. Actual versus predicted posted speed.

into three categories of speed limits: low speed limit (less than 45 mph), medium speed limit (45–55 mph), and high speed limit (greater than or equal to 60 mph).

Table 23 through Table 30 present the resulting Impact Speed Models. Two ranges of posted speed limits were incorporated into the model: the medium speed limit of 45–55 mph and the high speed limit greater than or equal to 60 mph. It can be observed that an increase in speed limit is associated with increased impact speed. The crash database in *NCHRP Web-Only Document 341* did not support additional categorization of posted speed (*3*).

It can be noted that the magnitude of impact speed increase varies by facility type (i.e., 2U and 4D) and the posted-speed-limit category. It can be observed that an increase in impact speed is indicated by the positive coefficients associated with the 45–55 mph and 60 mph speed limit categories. Vertical grade, a decrease in foreslope rate, an increase in foreslope, and ditch bottom width increase the impact speed. Conversely, horizontal curvature, an increase in shoulder width, and increasing lateral and longitudinal distance from the point of departure are associated with a decrease in impact speed.

Table 22. Distribution of predicted mean posted speed limit (mph) by facility type.

Facility	Minimum	1st Quartile	Median	Mean	3rd Quartile	Maximum
2U	38.75	46.11	51.35	50.84	57.01	61.14
4D	39.37	47.91	52.46	53.36	59.01	65.32

Table 23. Sedan speed model for 2U facility.

Fixed Effects	Estimate	Standard Error	z-Value
Intercept	6.38E+01	1.48E-01	431.552
Vertical Grade	5.35E-02	2.36E-03	22.673
Horizontal Curve Radius	–1.33E+00	5.82E-02	–22.841
Shoulder Width	–1.69E+00	1.48E-02	–114.647
Foreslope	4.65E-02	1.73E-02	2.688
Foreslope Width	3.02E-02	6.13E-03	4.925
Bottom Ditch Width	2.63E-02	5.96E-03	4.415
Lateral Distance	–1.68E-01	6.29E-04	–267.679
Longitudinal Distance	–5.65E-02	2.59E-04	–217.810
Simulated Speed Limit 45–55 mph	2.59E+01	5.66E-02	456.937
Simulated Speed Limit ≥ 60 mph	3.16E+01	6.80E-02	464.491
Shoulder Width*Foreslope	–4.75E-03	2.24E-03	–2.118
Lateral Distance*Longitudinal Distance	6.24E-04	3.56E-06	175.157
Random Effects		**Variance**	**Standard Deviation**
Intercept		247.87	15.744
Residual		15.94	3.993
Number of Observations	1,697,198		

NOTE: *indicates an interaction between the variables.

Table 24. Sedan speed model for 4D facility.

Fixed Effects	Estimate	Standard Error	z-Value
Intercept	7.05E+01	1.64E-01	429.604
Vertical Grade	5.26E-02	2.64E-03	19.899
Horizontal Curve Radius	–1.56E+00	6.51E-02	–23.975
Shoulder Width	–9.89E-01	1.64E-02	–60.293
Foreslope	9.58E-02	1.94E-02	4.948
Foreslope Width	2.13E-02	6.87E-03	3.102
Bottom Ditch Width	2.07E-02	6.68E-03	3.092
Lateral Distance	–1.64E-01	6.46E-04	–254.536
Longitudinal Distance	–5.18E-02	2.43E-04	–213.482
Simulated Speed Limit 45–55 mph	6.56E+00	3.42E-02	192.130
Simulated Speed Limit ≥ 60 mph	1.73E+01	5.77E-02	300.377
Shoulder Width*Foreslope	–9.49E-03	2.51E-03	–3.774
Lateral Distance*Longitudinal Distance	5.57E-04	3.38E-06	164.893
Random Effects		**Variance**	**Standard Deviation**
Intercept		261.28	16.164
Residual		16.44	4.054
Number of Observations	1,697,198		

NOTE: *indicates interaction between the variables.

Table 25. Pickup speed model for 2U facility.

Fixed Effects	Estimate	Standard Error	z-Value
Intercept	6.60E+01	1.47E-01	448.269
Vertical Grade	6.53E-02	2.33E-03	28.049
Horizontal Curve Radius	–1.65E+00	5.73E-02	–28.787
Shoulder Width	–1.84E+00	1.46E-02	–126.184
Foreslope	4.61E-02	1.71E-02	2.695
Foreslope Width	–1.32E-03	6.05E-03	–0.218
Bottom Ditch Width	4.62E-03	5.89E-03	0.785
Lateral Distance	–1.75E-01	6.61E-04	–264.428
Longitudinal Distance	–7.11E-02	2.79E-04	–254.737
Simulated Speed Limit 45–55 mph	2.68E+01	5.69E-02	470.423
Simulated Speed Limit ≥ 60 mph	3.36E+01	6.93E-02	484.217
Shoulder Width*Foreslope	–8.98E-03	2.21E-03	–4.067
Lateral Distance*Longitudinal Distance	9.20E-04	3.72E-06	247.676
Random Effects		**Variance**	**Standard Deviation**
Intercept		250.19	15.818
Residual		21.48	4.635
Number of Observations	1,892,359		

NOTE: *indicates interaction between the variables.

Table 26. Pickup speed model for 4D facility.

Fixed Effects	Estimate	Standard Error	z-Value
Intercept	7.24E+01	1.61E-01	448.770
Vertical grade	6.48E-02	2.58E-03	25.118
Horizontal Curve Radius	–2.01E+00	6.33E-02	–31.812
Shoulder Width	–1.15E+00	1.60E-02	–71.803
Foreslope	1.06E-01	1.90E-02	5.595
Foreslope Width	–1.36E-02	6.70E-03	–2.025
Bottom Ditch Width	–2.82E-03	6.52E-03	-0.433
Lateral Distance	–1.67E-01	6.67E-04	–250.449
Longitudinal Distance	–6.64E-02	2.60E-04	–255.769
Simulated Speed Limit 45–55 mph	7.44E+00	3.53E-02	210.541
Simulated Speed Limit ≥ 60 mph	1.99E+01	5.97E-02	333.097
Shoulder Width*Foreslope	–1.53E-02	2.45E-03	–6.270
Lateral Distance*Longitudinal Distance	8.48E-04	3.48E-06	243.764
Random Effects		**Variance**	**Standard Deviation**
Intercept		312.18	17.669
Residual		22.85	4.781
Number of Observations	1,892,359		

NOTE: *indicates interaction between the variables.

Table 27. SUV speed model for 2U facility.

Fixed Effects	Estimate	Standard Error	z-Value
Intercept	6.32E+01	1.47E-01	428.670
Vertical Grade	5.61E-02	2.34E-03	23.997
Horizontal Curve Radius	–1.24E+00	5.74E-02	–21.583
Shoulder Width	–1.88E+00	1.47E-02	–127.952
Foreslope	1.00E-01	1.72E-02	5.820
Foreslope Width	3.96E-02	6.07E-03	6.521
Bottom Ditch Width	4.23E-02	5.91E-03	7.164
Lateral Distance	–2.28E-01	6.95E-04	–328.279
Longitudinal Distance	–5.92E-02	2.37E-04	–250.007
Simulated Speed Limit 45–55 mph	2.78E+01	5.80E-02	479.124
Simulated Speed Limit ≥ 60 mph	3.51E+01	7.11E-02	493.317
Shoulder Width*Foreslope	–8.07E-03	2.22E-03	–3.637
Lateral Distance*Longitudinal Distance	6.75E-04	3.65E-06	185.091
Random Effects		**Variance**	**Standard Deviation**
Intercept		247.2	15.722
Residual		17.9	4.231
Number of Observations	1,568,715		

NOTE: *indicates interaction between the variables.

Table 28. SUV speed model for 4D facility.

Fixed Effects	Estimate	Standard Error	z-Value
Intercept	7.00E+01	1.61E-01	433.890
Vertical Grade	5.51E-02	2.58E-03	21.356
Horizontal Curve Radius	–1.65E+00	6.32E-02	–26.070
Shoulder Width	–1.21E+00	1.61E-02	–75.090
Foreslope	1.51E-01	1.90E-02	7.974
Foreslope Width	1.88E-02	6.70E-03	2.806
Bottom Ditch Width	2.89E-02	6.52E-03	4.437
Lateral Distance	–2.22E-01	6.97E-04	–318.562
Longitudinal Distance	–5.34E-02	2.14E-04	–249.141
Simulated Speed Limit 45–55 mph	8.07E+00	3.68E-02	219.384
Simulated Speed Limit ≥ 60 mph	2.12E+01	6.18E-02	343.382
Shoulder Width*Foreslope	–1.29E-02	2.45E-03	–5.265
Lateral Distance*Longitudinal Distance	5.90E-04	3.34E-06	176.451
Random Effects		**Variance**	**Standard Deviation**
Intercept		306.47	17.51
Residual		19.09	4.37
Number of Observations	1,568,715		

NOTE: *indicates interaction between the variables.

Table 29. CUV speed model for 2U facility.

Fixed Effects	Estimate	Standard Error	z-Value
Intercept	6.48E+01	1.51E-01	428.044
Vertical Grade	5.61E-02	2.41E-03	23.332
Horizontal Curve Radius	–7.87E-01	5.90E-02	-13.335
Shoulder Width	–1.71E+00	1.50E-02	–114.116
Foreslope	2.24E-02	1.77E-02	1.265
Foreslope Width	2.75E-02	6.25E-03	4.402
Bottom Ditch Width	2.64E-02	6.08E-03	4.339
Lateral Distance	–1.73E-01	6.59E-04	–263.036
Longitudinal Distance	–6.67E-02	2.69E-04	–247.665
Simulated Speed Limit 45–55 mph	2.53E+01	5.72E-02	441.401
Simulated Speed Limit ≥ 60 mph	3.09E+01	6.80E-02	453.800
Shoulder Width*Foreslope	–3.77E-03	2.28E-03	–1.653
Lateral Distance*Longitudinal Distance	6.73E-04	3.48E-06	193.387
Random Effects		**Variance**	**Standard Deviation**
Intercept		265.32	16.289
Residual		16.19	4.023
Number of Observations	1,748,198		

NOTE: *indicates interaction between the variables.

Table 30. CUV speed model for 4D facility.

Fixed Effects	Estimate	Standard Error	z-Value
Intercept	7.18E+01	1.68E-01	427.135
Vertical Grade	5.55E-02	2.70E-03	20.539
Horizontal Curve Radius	–1.18E+00	6.61E-02	–17.801
Shoulder Width	–9.82E-01	1.67E-02	–58.902
Foreslope	6.99E-02	1.99E-02	3.518
Foreslope Width	1.67E-02	7.02E-03	2.377
Bottom Ditch Width	2.10E-02	6.83E-03	3.074
Lateral Distance	–1.59E-01	6.80E-04	–232.993
Longitudinal Distance	–6.43E-02	2.55E-04	–252.066
Simulated Speed Limit 45–55 mph	5.84E+00	3.29E-02	177.520
Simulated Speed Limit ≥ 60 mph	1.62E+01	5.66E-02	286.801
Shoulder Width*Foreslope	–8.60E-03	2.56E-03	–3.360
Lateral Distance*Longitudinal Distance	5.87E-04	3.33E-06	176.146
Random Effects		**Variance**	**Standard Deviation**
Intercept		339.0	18.413
Residual		17.4	4.171
Number of Observations	1,748,198		

NOTE: *indicates interaction between the variables.

Impact Angle Models

The impact angle model determines the angle at which a vehicle would hit an object at different clear zone distances. This information is subsequently used as part of the determination of impact probability with fixed objects at the clear zone edge by defining a vehicle projection envelope based on the impact angle, vehicle CG position, and vehicle width.

To determine the impact angle at a given distance, the team selected the vehicle CG coordinates at three points along the vehicle trajectory at or near the prescribed lateral offset distance. Statistical models were then developed to predict the impact angles for 2U and 4D facilities.

Table 31 through Table 38 present the model results for 2U and 4D facilities for the four different vehicle types (crossover or CUV, SUV, pickup, and sedan). Design variables associated with greater impact angles are wider foreslope and ditch bottom, wider shoulder, flatter backslope, and horizontal

Table 31. CUV impact angle model for 2U facility.

Fixed Effects	Estimate	Standard Error	z-Value
Intercept	4.16E+00	3.77E-03	1105.86
Foreslope Width	1.03E-02	1.23E-04	83.48
Bottom Ditch Width	4.80E-03	1.19E-04	40.23
Lateral Distance	–9.16E-03	5.16E-05	–177.70
Longitudinal Distance	–1.44E-02	1.68E-05	–858.75
Foreslope	–3.95E-03	1.84E-04	–21.50
Shoulder Width	8.88E-03	1.20E-04	74.19
Vertical Grade	–9.00E-05	8.51E-05	–1.06
Horizontal Curve Radius	1.74E-03	1.97E-03	0.88
Backslope	2.10E-02	3.32E-04	63.12
Backslope Width	–3.20E-03	1.23E-04	–26.05
Lateral Distance*Longitudinal Distance	1.77E-04	2.70E-07	656.63
Horizontal Curve Radius*Vertical Grade	–4.89E-04	1.12E-04	–4.36
Random Effects		**Variance**	**Standard Deviation**
Intercept		0.05837	0.2416
Residual		0.11534	0.3396
Number of Observations	1,759,850		

NOTE: *indicates interaction between the variables.

Table 32. CUV impact angle model for 4D facility.

Fixed Effects	Estimate	Standard Deviation	z-Value
Intercept	4.02E+00	3.76E-03	1068.55
Foreslope Width	1.06E-02	1.24E-04	85.33
Bottom Ditch Width	4.81E-03	1.21E-04	39.86
Lateral Distance	–7.02E-03	5.18E-05	–135.31
Longitudinal Distance	–1.34E-02	1.56E-05	–856.15
Foreslope	–4.60E-03	1.86E-04	–24.74
Shoulder Width	8.76E-03	1.21E-04	72.32
Vertical Grade	–1.55E-04	8.64E-05	–1.79
Horizontal Curve Radius	–1.67E-03	2.00E-03	–0.84
Backslope	2.03E-02	3.36E-04	60.54
Backslope Width	–3.10E-03	1.24E-04	–25.00
Lateral Distance*Longitudinal Distance	1.63E-04	2.53E-07	643.17
Horizontal Curve Radius*Vertical Grade	–3.86E-04	1.14E-04	–3.40
Random Effects		**Variance**	**Standard Deviation**
Intercept		0.06585	0.2566
Residual		0.1182	0.3438
Number of Observations	1,759,850		

NOTE: *indicates interaction between the variables.

Table 33. SUV impact angle model for 2U facility.

Fixed Effects	Estimate	Standard Deviation	z-Value
Intercept	3.87E+00	4.36E-03	887.67
Foreslope Width	1.10E-02	1.49E-04	74.15
Bottom Ditch Width	5.78E-03	1.45E-04	39.99
Lateral Distance	–1.44E-02	5.82E-05	–248.37
Longitudinal Distance	–1.31E-02	1.65E-05	–790.83
Foreslope	9.80E-04	2.22E-04	4.42
Shoulder Width	7.18E-03	1.45E-04	49.59
Vertical Grade	7.84E-04	1.04E-04	7.56
Horizontal Curve Radius	9.48E-02	2.38E-03	39.89
Backslope	1.82E-02	4.02E-04	45.36
Backslope Width	–1.55E-03	1.48E-04	–10.45
Lateral Distance*Longitudinal Distance	1.87E-04	3.04E-07	615.46
Horizontal Curve Radius*Vertical Grade	–9.72E-04	1.36E-04	–7.14
Random Effects		**Variance**	**Standard Deviation**
Intercept		0.08844	0.2974
Residual		0.13978	0.3739
Number of Observations	1,578,153		

NOTE: *indicates interaction between the variables.

Table 34. SUV impact angle model for 4D facility.

Fixed Effects	Estimate	Standard Deviation	z-Value
Intercept	3.64E+00	4.46E-03	815.67
Foreslope Width	1.20E-02	1.55E-04	77.33
Bottom Ditch Width	6.14E-03	1.50E-04	40.84
Lateral Distance	–1.32E-02	5.78E-05	–228.03
Longitudinal Distance	–1.14E-02	1.50E-05	–756.26
Foreslope	2.43E-04	2.31E-04	1.05
Shoulder Width	7.89E-03	1.51E-04	52.40
Vertical Grade	8.25E-04	1.08E-04	7.64
Horizontal Curve Radius	1.12E-01	2.48E-03	45.03
Backslope	1.78E-02	4.18E-04	42.67
Backslope Width	–1.49E-03	1.54E-04	–9.67
Lateral Distance*Longitudinal Distance	1.67E-04	2.78E-07	601.59
Horizontal Curve Radius*Vertical Grade	–1.07E-03	1.42E-04	–7.52
Random Effects		**Variance**	**Standard Deviation**
Intercept		0.1078	0.3283
Residual		0.1455	0.3814
Number of Observations	1,578,153		

NOTE: *indicates interaction between the variables.

Table 35. Pickup impact angle model for 2U facility.

Fixed Effects	Estimate	Standard Deviation	z-Value
Intercept	4.00E+00	3.29E-03	1216.49
Foreslope Width	9.00E-03	1.09E-04	82.31
Bottom Ditch Width	5.49E-03	1.06E-04	51.64
Lateral Distance	–5.82E-03	4.02E-05	–144.85
Longitudinal Distance	–1.35E-02	1.35E-05	–996.62
Foreslope	–3.74E-04	1.64E-04	-2.29
Shoulder Width	8.40E-03	1.07E-04	78.79
Vertical Grade	–1.78E-04	7.63E-05	–2.33
Horizontal Curve Radius	2.17E-02	1.76E-03	12.36
Backslope	2.28E-02	2.95E-04	77.07
Backslope Width	–2.62E-03	1.09E-04	–23.97
Lateral Distance*Longitudinal Distance	1.55E-04	2.19E-07	706.86
Horizontal Curve Radius*Vertical Grade	–1.12E-04	1.00E-04	–1.12
Random Effects		**Variance**	**Standard Deviation**
Intercept		0.04965	0.2228
Residual		0.08892	0.2982
Number of Observations	1,900,968		

NOTE: *indicates interaction between the variables.

Table 36. Pickup impact angle model for 4D facility.

Fixed Effects	Estimate	Standard Deviation	z-Value
Intercept	3.85E+00	3.30E-03	1166.103
Foreslope Width	9.43E-03	1.11E-04	85.023
Bottom Ditch Width	5.61E-03	1.08E-04	51.997
Lateral Distance	–4.15E-03	4.03E-05	–102.884
Longitudinal Distance	–1.25E-02	1.26E-05	–988.250
Foreslope	–9.85E-04	1.66E-04	–5.933
Shoulder Width	8.47E-03	1.08E-04	78.271
Vertical Grade	–2.35E-04	7.76E-05	–3.023
Horizontal Curve Radius	2.65E-02	1.79E-03	14.844
Backslope	2.20E-02	3.00E-04	73.397
Backslope Width	–2.52E-03	1.11E-04	–22.723
Lateral Distance*Longitudinal Distance	1.43E-04	2.04E-07	701.485
Horizontal Curve Radius*Vertical Grade	–6.79E-05	1.02E-04	–0.667
Random Effects		**Variance**	**Standard Deviation**
Intercept		0.0555	0.2356
Residual		0.0940	0.3066
Number of Observations	1,900,968		

NOTE: *indicates interaction between the variables.

Table 37. Sedan impact angle model for 2U facility.

Fixed Effects	Estimate	Standard Deviation	z-Value
Intercept	4.15E+00	4.46E-03	928.854
Foreslope Width	9.40E-03	1.51E-04	62.170
Bottom Ditch Width	3.15E-03	1.47E-04	21.467
Lateral Distance	–9.13E-03	5.22E-05	–175.074
Longitudinal Distance	–1.40E-02	1.79E-05	–783.619
Foreslope	–7.57E-03	2.26E-04	–33.450
Shoulder Width	6.89E-03	1.48E-04	46.669
Vertical Grade	–1.76E-04	1.06E-04	–1.664
Horizontal Curve Radius	2.76E-02	2.43E-03	11.381
Backslope	1.92E-02	4.09E-04	46.990
Backslope Width	–3.13E-03	1.51E-04	–20.699
Lateral Distance*Longitudinal Distance	1.69E-04	2.86E-07	589.263
Horizontal Curve Radius*Vertical Grade	–1.62E-05	1.39E-04	–0.117
Random Effects		**Variance**	**Standard Deviation**
Intercept		0.1025	0.3202
Residual		0.1197	0.3460
Number of Observations	1,709,512		

NOTE: *indicates interaction between the variables.

Table 38. Sedan impact angle model for 4D facility.

Fixed Effects	Estimate	Standard Error	z-Value
Intercept	3.96E+00	4.45E-03	889.466
Foreslope Width	9.93E-03	1.53E-04	65.065
Bottom Ditch Width	3.19E-03	1.48E-04	21.556
Lateral Distance	–7.99E-03	5.18E-05	–154.195
Lateral Distance Squared	–1.25E-02	1.65E-05	–761.250
Longitudinal Distance	–8.12E-03	2.28E-04	–35.553
Foreslope	7.19E-03	1.49E-04	48.220
Shoulder Width	–2.06E-04	1.07E-04	–1.929
Vertical Grade	3.60E-02	2.46E-03	14.672
Horizontal Curve Radius	1.84E-02	4.12E-04	44.595
Backslope	–3.01E-03	1.52E-04	–19.767
Backslope Width	1.53E-04	2.65E-07	577.641
Horizontal Curve Radius*Vertical Grade	–2.55E-05	1.40E-04	–0.182
Random Effects		**Variance**	**Standard Deviation**
Intercept		0.1127	0.3357
Residual		0.1224	0.3499
Number of Observations	1,709,512		

NOTE: *indicates interaction between the variables.

curvature. Increased lateral and longitudinal distance, flatter foreslope, wider backslope, and vertical grade are associated with smaller impact angles. The lateral and longitudinal distance traveled by the encroaching vehicle has a significant interactive relationship with the angle of impact.

Rollover Probability Models

The team developed logistic regression models to predict the likelihood of rollover before reaching a certain lateral threshold (clear zone distance). All roadway and roadside design variables and various combinations thereof were considered in the model. Only variables that were statistically significant at a 95% confidence interval were retained in the final models.

Table 39 through Table 46 present the models for rollover probability before reaching a given lateral distance for all vehicle types expressed in terms of statistically significant design variables

Table 39. CUV rollover probability model for 2U roads.

Fixed Effects	Estimate	Standard Error	z-Value	P-Value
Intercept	–1.711	0.204	–8.37	<0.001
Shoulder Width	–0.082	0.005	–15.35	<0.001
Foreslope	–0.642	0.058	–11.03	<0.001
Foreslope Squared	0.035	0.004	7.71	<0.001
Foreslope Width	–0.062	0.005	–11.75	<0.001
Backslope	–0.276	0.015	–17.98	<0.001
Bottom Ditch Width	–0.111	0.005	–20.54	<0.001
Lateral Distance	0.264	0.007	37.43	<0.001
Lateral Distance Squared	–0.003	0.0001	–33.03	<0.001
Model Summary				
Number of Observations	3,628,800			
AIC	18			

NOTE: AIC = Akaike information criteria.

Table 40. CUV rollover probability model for 4D roads.

Fixed Effects	Estimate	Standard Error	z-Value	P-Value
Intercept	–1.900	0.203	–9.35	<0.001
Shoulder Width	–0.081	0.005	–15.27	<0.001
Foreslope	–0.626	0.058	–10.78	<0.001
Foreslope Squared	0.034	0.004	7.54	<0.001
Foreslope Width	–0.065	0.005	–12.41	<0.001
Backslope	–0.279	0.015	–18.15	<0.001
Bottom Ditch Width	–0.108	0.005	–20.10	<0.001
Lateral Distance	0.277	0.007	39.20	<0.001
Lateral Distance Squared	–0.003	0.0001	–34.46	<0.001
Model Summary				
Number of Observations	3,628,800			
AIC	18			

NOTE: AIC = Akaike information criteria.

Table 41. Pickup rollover probability model for 2U roads.

Fixed Effects	Estimate	Standard Error	z-Value	P-Value
Intercept	–0.054	0.306	–0.18	0.860
Shoulder Width	–0.076	0.008	–9.74	<0.001
Foreslope	–1.005	0.092	–10.89	<0.001
Foreslope Squared	0.054	0.007	7.41	<0.001
Foreslope Width	–0.070	0.008	–9.00	<0.001
Backslope	–0.560	0.027	–20.72	<0.001
Bottom Ditch Width	–0.163	0.009	–18.90	<0.001
Lateral Distance	0.238	0.010	23.70	<0.001
Lateral Distance Squared	–0.003	0.0001	–20.95	<0.001
Model Summary				
Number of Observations	3,628,800			
AIC	18			

NOTE: AIC = Akaike information criteria.

Table 42. Pickup rollover probability model for 4D roads.

Fixed Effects	Estimate	Standard Error	z-Value	P-Value
Intercept	–0.525	0.3050	–1.72	0.085
Shoulder Width	–0.068	0.0080	–8.83	<0.001
Foreslope	–1.005	0.0910	–11.01	<0.001
Foreslope Squared	0.055	0.0070	7.59	<0.001
Foreslope Width	–0.069	0.0080	–9.01	<0.001
Backslope	–0.579	0.0270	–21.39	<0.001
Bottom Ditch Width	–0.162	0.0080	–19.12	<0.001
Lateral Distance	0.267	0.0100	25.66	<0.001
Lateral Distance Squared	–0.003	0.0001	–22.59	<0.001
Model Summary				
Number of Observations	3,628,800			
AIC	18			

NOTE: AIC = Akaike information criteria.

Table 43. SUV rollover probability model for 2U roads.

Fixed Effects	Estimate	Standard Error	z-Value	P-Value
Intercept	–0.371	0.2330	–1.59	0.112
Shoulder Width	–0.109	0.0060	–17.87	<2e-16
Foreslope	–0.917	0.0670	–13.64	<2e-16
Foreslope Squared	0.050	0.0050	9.67	<2e-16
Foreslope Width	–0.093	0.0060	–15.46	<2e-16
Backslope	–0.527	0.0200	–26.98	<2e-16
Bottom Ditch Width	–0.201	0.0070	–29.60	<2e-16
Lateral Distance	0.322	0.0090	35.99	<2e-16
Lateral Distance Squared	–0.004	0.0001	–31.01	<2e-16
Model Summary				
Number of Observations	3,628,800			
AIC	18			

NOTE: AIC = Akaike information criteria.

Table 44. SUV rollover probability model for 4D roads.

Fixed Effects	Estimate	Standard Error	z-Value	P-Value
Intercept	–0.734	0.232	–3.16	0.002
Shoulder Width	–0.107	0.006	–17.58	<0.001
Foreslope	–0.889	0.0670	–13.24	<0.001
Foreslope Squared	0.049	0.0050	9.33	<0.001
Foreslope Width	–0.095	0.0060	–15.81	<0.001
Backslope	–0.504	0.0190	–26.12	<0.001
Bottom Ditch Width	–0.195	0.0070	–29.06	<0.001
Lateral Distance	0.341	0.0090	37.32	<0.001
Lateral Distance Squared	–0.004	0.0001	–32.11	<0.001
Model Summary				
Number of Observations	3,628,800			
AIC	18			

NOTE: AIC = Akaike information criteria.

Table 45. Sedan rollover probability model for 2U roads.

Fixed Effects	Estimate	Standard Error	z-Value	P-Value
Intercept	–0.694	0.2830	–2.45	0.014
Shoulder Width	–0.084	0.0070	–11.87	<0.001
Foreslope	–0.998	0.0820	–12.11	<0.001
Foreslope Squared	0.056	0.0060	8.61	<0.001
Foreslope Width	–0.032	0.0070	–4.52	<0.001
Backslope	–0.637	0.0250	–25.06	<0.001
Bottom Ditch Width	–0.163	0.0080	–21.12	<0.001
Lateral Distance	0.270	0.0100	28.28	<0.001
Lateral Distance Squared	–0.003	0.0001	–24.39	<0.001
Model Summary				
Number of Observations		3,628,800		
AIC		18		

NOTE: AIC = Akaike information criteria.

Table 46. Sedan rollover probability model for 4D roads.

Fixed Effects	Estimate	Standard Error	z-Value	P-Value
Intercept	–1.113	0.2860	–3.89	<0.001
Shoulder Width	–0.083	0.0070	–11.47	<0.001
Foreslope	–0.969	0.0830	–11.62	<0.001
Foreslope Squared	0.054	0.0070	8.21	<0.001
Foreslope Width	–0.036	0.0070	–5.04	<0.001
Backslope	–0.595	0.0250	–23.72	<0.001
Bottom Ditch Width	–0.152	0.0080	–19.82	<0.001
Lateral Distance	0.281	0.0100	29.03	<0.001
Lateral Distance Squared	–0.003	0.0001	–24.97	<0.001
Model Summary				
Number of Observations		3,628,800		
AIC		18		

NOTE: AIC = Akaike information criteria.

for 2U and 4D roadways. Overall, results suggest that the probability of rollover increases as the lateral distance increases as indicated by the positive coefficients associated with the lateral distance variable in Table 39 through Table 46. However, the coefficient of the square of the lateral distance variable is negative, indicating that at a certain distance, the rollover probability starts to decline. Upon further investigation, it was found that the rollover probabilities started to decline approximately 40 ft from the edge of the roadway. This may be due to an associated reduction in speed or interaction with the ditch backslope.

Other variables of interest that were found to be statistically significant in terms of rollover prediction include shoulder width, foreslope ratio, foreslope width, backslope ratio, and ditch bottom width. The presence of the square of the foreslope ratio indicates that the relationship is quadratic rather than linear. Irrespective of the vehicle type and facility type, a wider shoulder width is associated with a lower rollover probability. Likewise, the model indicates that a flatter foreslope or backslope ratio is also associated with a lower likelihood of rollover.

CHAPTER 6

Clear Zone Guideline Assistance Program

The original research plan was to modify and use the updated Roadside Safety Analysis Program (RSAPv3) as the main analysis tool to conduct the risk analysis from which the clear zone guidelines would be developed (*25*). RSAP is an encroachment-probability-based model that follows an analysis approach that is structured into four modules:

- Encroachment Module,
- Crash Prediction Module,
- Severity Prediction Module, and
- Benefit-Cost Module.

The analytical methodology uses a series of conditionally independent probabilities to represent a roadside encroachment event. This includes the probability of an encroachment occurring, the conditional probability of a crash given a roadside encroachment has occurred, the probable severity of a crash if one occurs, and the expected crash risk or cost of the roadside design alternative that is being investigated.

The following conditional probability model is used for each design alternative:

$$E\left(CC\right)\mathrm{N,M} = ADT \bullet \mathrm{LN} \bullet P(Encr) \bullet P\left(Cr \middle| Encr\right) \bullet P\left(Sev_s \middle| Cr\right) \bullet E\left(CC_s \middle| Sev_s\right)$$

where:

$E(CC)$N,M = Expected annual crash cost on segment N for alternative M,
ADT = Average daily traffic in vehicles/day,
LN = Length of segment N in miles,
$P(Encr)$ = Probability that a vehicle will encroach on the segment,
$P(Cr|Encr)$ = Probability that a crash will occur given that an encroachment has occurred,
$P(Sev_s|Cr)$ = Probability that a crash of severity s occurs given that a crash has occurred, and
$E(CC_s|Sev_s)$ = Expected cost of a crash of severity s.

RSAPv3 is written as a series of Visual Basic for Applications (VBA) macros within a Microsoft Excel environment. Users can provide input data in the accessible worksheets, while macros conduct the analyses' tasks in the background. Most of the data tables where the information is stored and used by the macros are in worksheets. Although changes and updates can be made to default values in the data tables, completely rewriting various aspects of the code to incorporate new crash prediction and severity prediction modules is more complicated.

The researchers explored the possibility of adding a function into the RSAPv3 code to import data from outside the software and populate the data tables using the developed relationships from Chapter 5. Another option that was explored was to bypass the crash prediction module, independently perform the crash prediction analysis using the newly developed encroachment models, and pass the needed crash probability information to the severity module.

However, after further analysis, the modification of RSAPv3 was considered inefficient for this project. Most of the RSAPv3 programming was being replaced by the new encroachment models derived from the computer simulation data. It was, therefore, more straightforward to use the same programming language and architecture used to develop the encroachment models for the overall risk analysis methodology.

A new risk-based analysis tool referred to as the Clear Zone Guideline Assistant Program (CZ-GAP) was developed to assist with the clear zone guideline development process. Details of CZ-GAP are provided in the sections below.

Framework

CZ-GAP is built in R, a programming language known for statistical computing and graphics. The encroachment models described in Chapter 5 form the basis of the analysis modules. The analysis modules include

1. Crash Probability Module,
2. Severity Prediction Module, and
3. Risk Determination Module.

The variable input data includes the selected roadway and roadside design variables. These include facility type, posted speed category, horizontal curvature, vertical grade, shoulder width, foreslope ratio, foreslope width, ditch bottom width, backslope ratio, backslope width, and clear zone distance, each having its specific range.

This data is used in all the models as common variables. For each design scenario, the models are fed with this data, and the probability predictions are output. Finally, the probability outputs are transferred to the Severity Prediction Module where the overall risk of a serious injury or a fatal crash for the design configuration is calculated.

Crash Probability

The Crash Probability Model computes the probability of an encroaching vehicle impacting a hazard at the clear zone edge. This module was programmed to predict the probability of reaching the clear zone and the probability of hitting the hazards (i.e., trees) at the clear zone edge. It consists of three models: the lateral distance model, the longitudinal distance model, and the impact angle model.

The probability of reaching a selected lateral distance or clear zone is schematically shown in Figure 39. The lateral distance model is used to determine the probability of each vehicle type reaching the prescribed distance based on the design characteristics of the roadway segment (common variables). The probability obtained for each vehicle is multiplied by the vehicle's weight factor and summed to arrive at the total probability of reaching the lateral distance of interest for a particular facility type (2U or 4D).

If an encroaching vehicle reaches the clear zone distance of interest, the next step in the analysis tool is to calculate the probability of impact with an obstacle at the clear zone edge. The obstacles are defined by a line of trees at a specified spacing, S. Different tree spacings are used to represent a range of hazard levels. The wider the spacing, the lower the probability of impact with a tree and vice-versa.

When a vehicle departs the roadway at a specific location, the encroachment conditions and roadside design configuration will influence its trajectory. For a given terrain configuration,

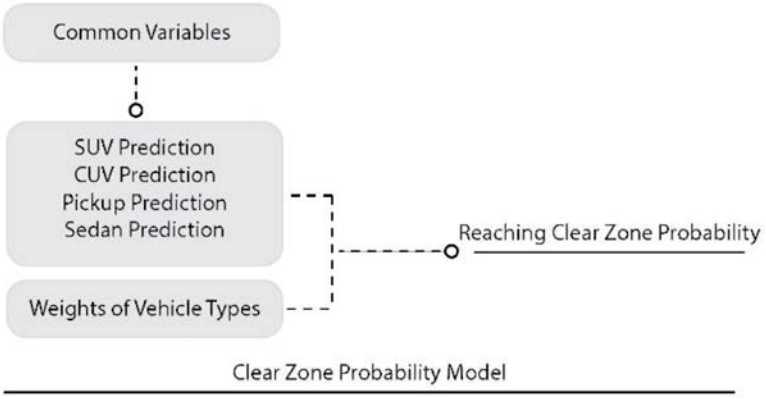

Figure 39. Clear zone probability model.

the different encroachment conditions (vehicle type, encroachment speed and angle, and driver input) define different trajectories. At a given lateral offset or clear zone edge, these multiple trajectories create a longitudinal distance distribution as illustrated in Figure 40.

This distribution defines the probability of a vehicle reaching a certain longitudinal distance for a prescribed lateral offset distance. The longitudinal distance distributions are biased toward the point of departure and have a longer tail on the downstream side. These distributions predict the probability of the encroaching vehicle crossing the clear zone edge at a given longitudinal distance.

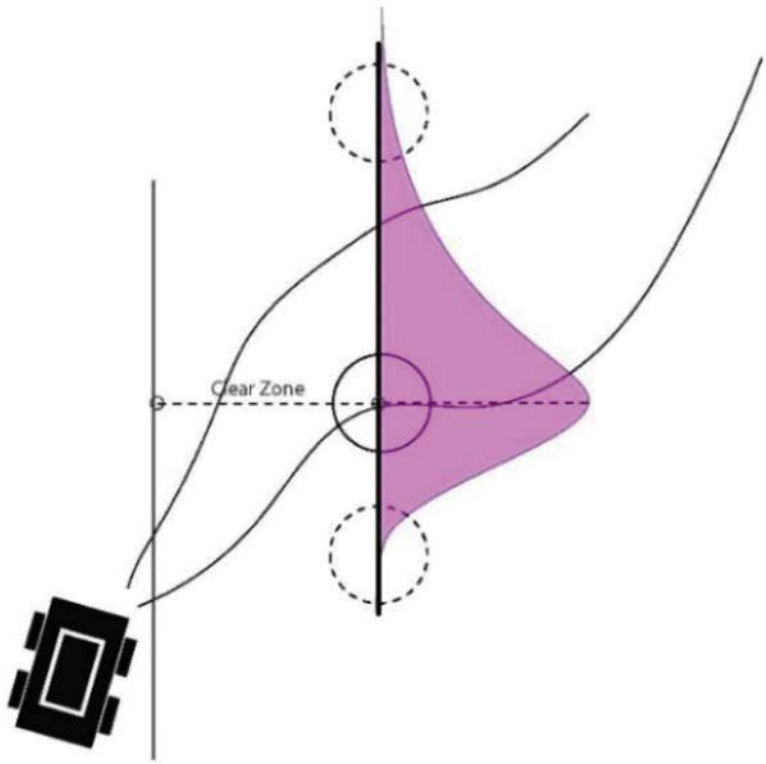

Figure 40. Illustration of longitudinal distance distribution for vehicle crossing a prescribed clear zone edge.

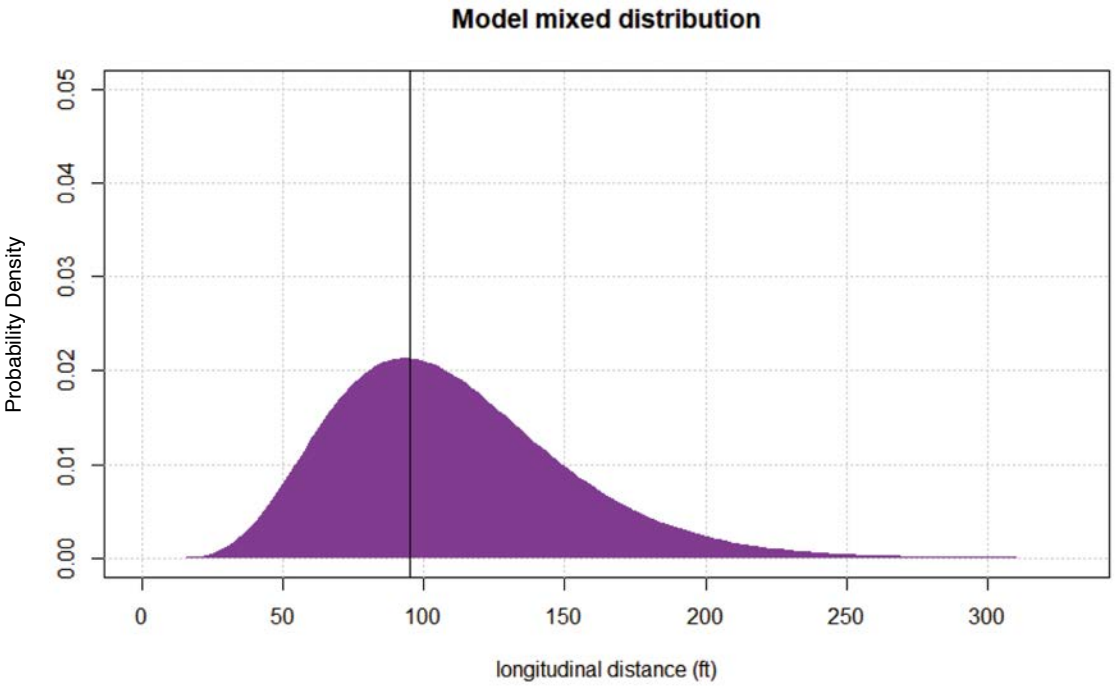

Figure 41. Typical longitudinal distance distribution for a defined design configuration and lateral offset distance.

Figure 41 shows a mixed distribution for one design scenario at a given lateral offset distance. The distribution provides longitudinal distance versus probability density. The mode (peak) of the distribution is indicated by the vertical line. The hazards at the clear zone edge, represented by a line of trees at a prescribed spacing, are mapped onto the longitudinal distribution.

The process of computing the crash probability for a given facility type, design scenario, and clear zone distance is schematically illustrated in Figure 42. First, the relevant longitudinal distribution is determined based on the design variables, and its mode is established. Next, an obstacle (tree) is aligned with the mode of the distribution, and other obstacles (trees) are then defined to the left and right of the mode based on the prescribed obstacle spacing.

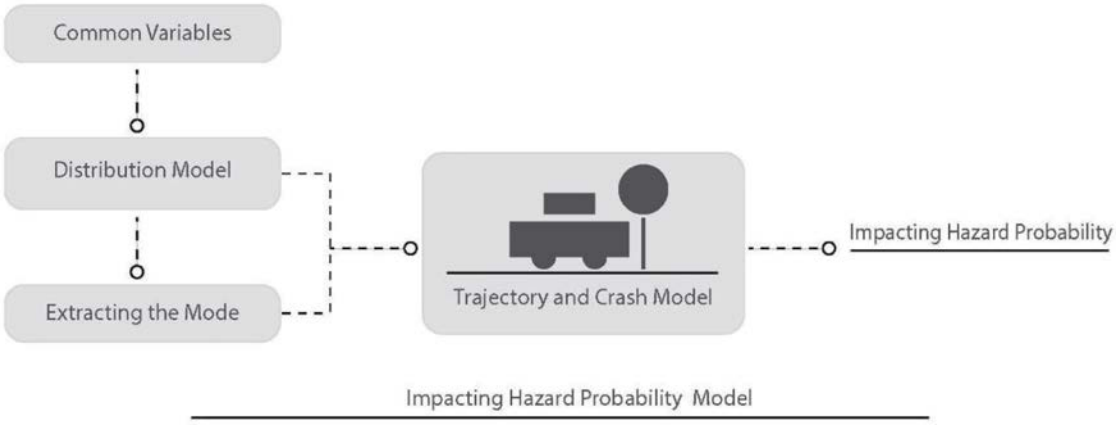

Figure 42. Illustration of impact probability model.

The diameter of the trees and the distance between them are assigned as variables in the program. The probability of impact with each obstacle that intersects the longitudinal distribution is calculated as the area under the distribution with the width of the area equal to the vehicle width, W.

Note that the calculated probabilities at this point relate to a single point of departure from the roadway. In reality, the vehicle has an equal likelihood of departing the roadway anywhere along its length, provided the characteristics of the roadway segment are consistent. What is desired for the risk analysis is an average probability of striking a particular obstacle (tree) for the roadway segment.

So, the next step is to iterate the point of departure from the roadway. The calculation is cycled for 10 points of departure in increments of S/10, where *S* is the obstacle (tree) spacing. This permits calculating an average risk for multiple points of departure. At each point of departure, the probability of impacting obstacles (trees) that overlap the longitudinal distance distribution is determined. Note that because the trees are modeled as a continuous line hazard, the probability of impact becomes cyclical as the point of departure is iterated along the roadway segment. In other words, when the point of departure has moved a distance equal to the spacing of the trees, the next tree in the line of trees will now be at the mode of the distribution, which is the same as the starting point of the analysis. This concept is illustrated in Figure 43.

The leftmost image in Figure 43 shows an obstacle (tree) placed at the mode of the distribution to define the initial point of departure, with other trees equally spaced upstream and downstream from this point. The longitudinal distance distribution is used to calculate the impact probability for each tree that falls within the distribution. The image in the middle shows a downstream iteration at a point of departure equal to half the tree spacing. A different probability of impact is calculated for each tree that overlaps the distribution. In the rightmost image, another iteration of the departure point equal to half the tree spacing has placed the next obstacle (tree) at the mode of the distribution again. The impact probabilities for the trees at this point are the same as the initial probabilities calculated for the leftmost image. The average probability of hitting a particular obstacle (tree) is taken as the summation of the probabilities at each departure point divided by the number of departure points (iterations).

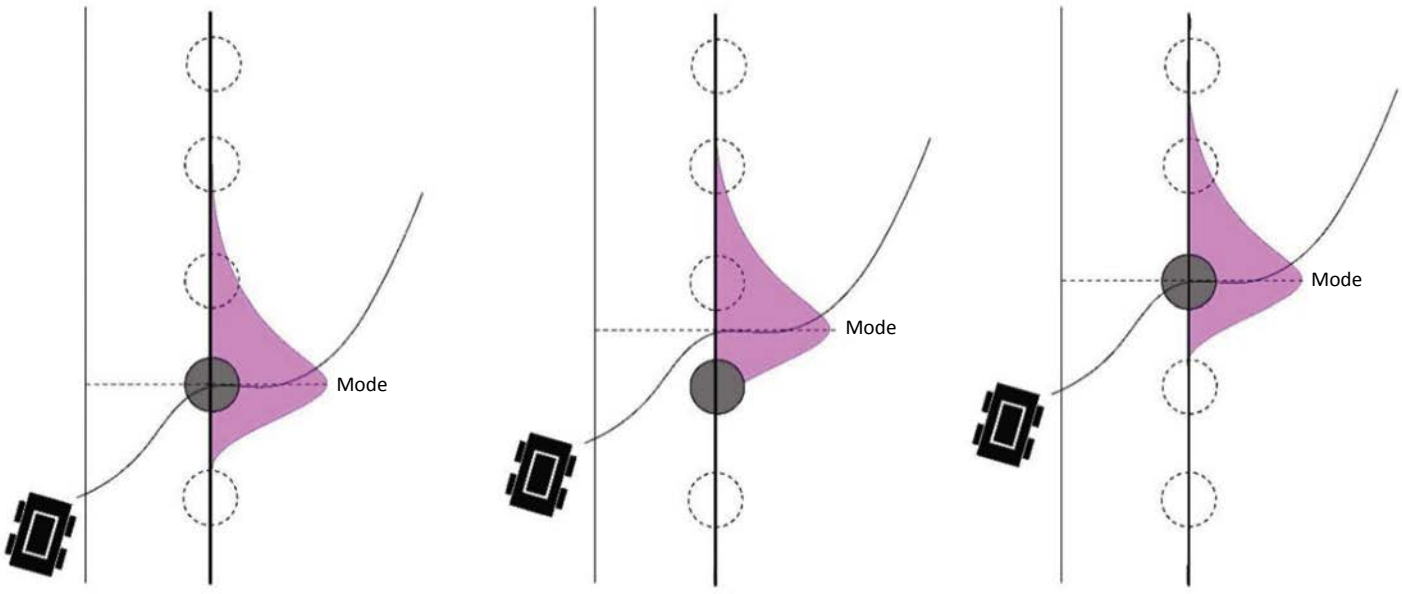

Figure 43. Iteration of point of departure for calculation of average impact probability.

Figure 44 presents an example of the point of departure (POD) cycling relative to the obstacles (trees) at the clear zone edge. It can be seen in this example that as the longitudinal distance of the tree (represented by the blue curve) increases from the POD, the effective width around the tree (indicated by the hashed red lines) increases. Also, the area under the blue curve indicates that only a few trees (roughly, from the fourth tree through the tenth tree, counting from the POD) have a probability of being impacted. It can also be seen that with each additional point of departure, the tree positions are slightly shifted toward the left relative to the longitudinal distance distribution, and that for POD 11 the position of the trees and their effective areas under the curve is equivalent to the positions from POD 1. Thus, the probabilities of hitting trees begins to repeat after 10 PODs.

The calculations of the crash probability involve the estimation of the distributions of longitudinal distance reached at a given lateral offset (i.e., the clear zone under evaluation). Because the estimated distribution is expressed as a probability density function, the area under that curve for a range of longitudinal distance values represents the probability of a trajectory reaching the clear zone within that range of longitudinal distances. The final element of the crash probability process is determining the range of probable vehicle exposure for a given fixed object at the clear

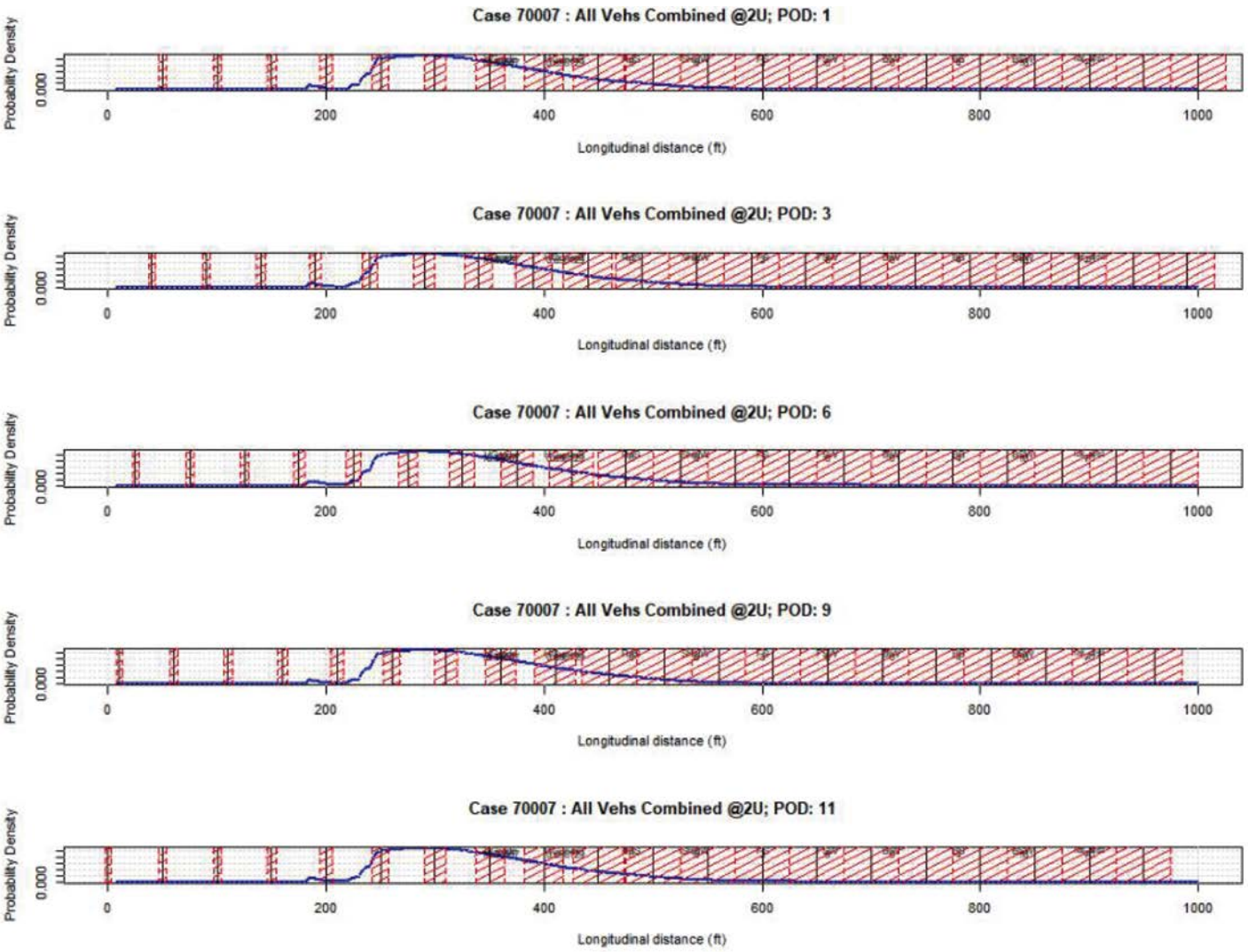

Figure 44. POD cycling to calculate cumulative impact probability for each obstacle (tree).

zone line. This exposure provides a projection or envelope that is mapped onto the longitudinal distance distribution to determine the probability of impact with a given tree at the clear zone line.

After further analysis, the research team determined the need to modify the initially assumed profile of vehicle exposure to the risk of hitting a tree in a line of trees. Initially, the exposure profile was determined based on the assumption of a tracking vehicle approaching the fixed object, as shown on the left side of Figure 45. However, some departures are not necessarily expected to arrive at the clear zone line while tracking. Therefore, the team decided to generalize the profile of vehicle exposure to represent the average expected impact angle of the vehicle CG trajectory with respect to the line of hazards, as shown on the right side of Figure 45. The orange dot in the figure represents the hazard, e.g., a tree.

For the non-tracking condition, it can be shown that the adjusted profile is governed by the relationship given in Eq. 1 involving the width (W) and length (L) of the vehicle as well as the yaw or sideslip angle with respect to the path of the vehicle.

$$Adjusted.Profile.Width_{trajectory} = W \times \cos\theta + L \times \sin\theta \quad (1)$$

where: θ = slip (sliding) angle relative to the CG trajectory of the vehicle.

The research team reviewed the *NCHRP Web-Only Document 341* database to determine the mean value of *Adjusted.Profile.Width* given the data provides sufficient information to determine the θ values expected from actual crashes (*3*). The average vehicle design dimensions for the vehicle models simulated in this project are 6.19 ft for width (W) and 15.83 ft for length (L). From this analysis, the average adjusted profile width was found to be 1.35 times the width of the vehicle.

After further discussion, the research team agreed on the need to also introduce some overlap with the fixed object to ensure that the adjusted profile width results in a significant crash with potential for severe outcomes, as opposed to a grazing or minimal impact. The amount of overlap was agreed to be 2.4 times the width of the design's fixed object (1 ft diameter tree), as shown on

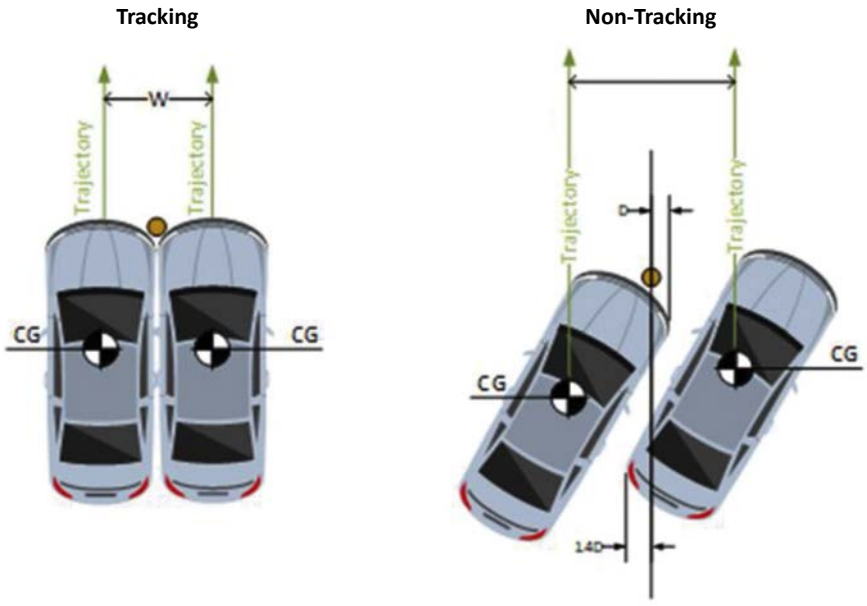

Figure 45. Comparison of vehicle exposure to hazard for tracking (left) and non-tracking (right) conditions.

the right side of Figure 45. Therefore, for this project, the adjusted profile width relative to the trajectory was set as given in Eq. 2:

$$Adjusted.Profile.Width_{trajectory} = 1.35 \times W - 2.4 \times D \quad (2)$$

where: D = Diameter of a tree.

Furthermore, the research team determined that an additional adjustment was needed in the calculations to account for the angle of the trajectory at the point of impact with respect to the line of fixed objects under consideration, as shown in Figure 46. The adjusted profile width was projected over the line of trees that is assumed to be parallel with the road. This quantity was considered as the effective exposure width along the tree line ($Eff.W_{treeline}$). As shown for the two scenarios, a narrower angle of impact (scenario on the left) will result in a longer projection over the tree line, compared to a wider angle of impact (scenario on the right). It can be shown that this relationship between the adjusted profile width and the angle of impact is governed by Eq. 3.

$$Eff.W_{treeline} = \frac{Adjusted.Profile.Width_{trajectory}}{\sin\phi} \quad (3)$$

where: ϕ = impact angle.

The research team again consulted the *NCHRP Web-Only Document 341* data to get a sense of the impact of this adjustment on the calculations. The average value of the impact angle, ϕ, in that dataset was found to be 13.01 degrees (including the sampling weights in that dataset). As shown in Eq. 4, the adjustment results in an effective exposure width of 26.46 ft, which is a significant value compared to the vehicle dimensions.

$$Eff.W_{treeline} = \frac{Adjusted.Profile.Width_{trajectory}}{\sin 13.01^{\circ}} = \frac{1.35W - 2.4D}{\sin 13.01^{\circ}} = 26.46 \text{ ft} \quad (4)$$

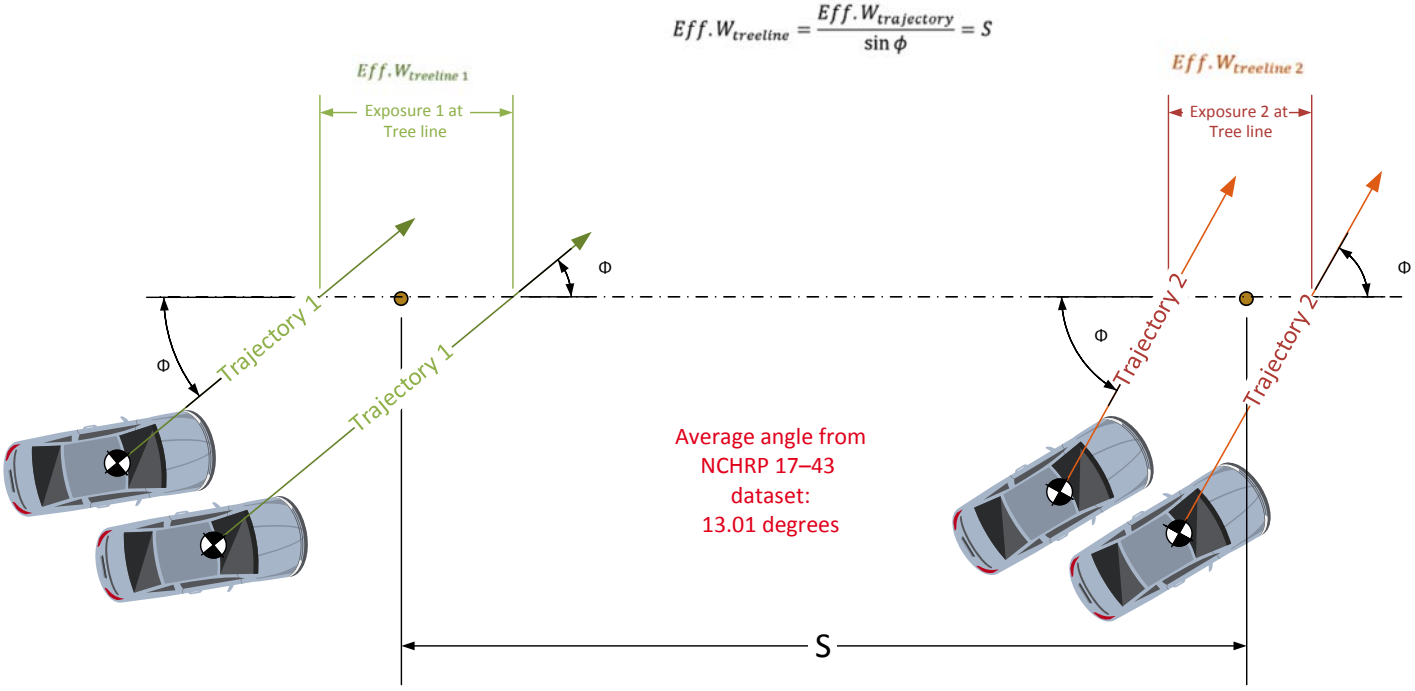

Figure 46. Effective exposure width based on vehicle trajectory angle.

The research team performed a small sensitivity analysis to explore how the separation between trees (closely tied to the tree density in the tree line) relates to the maximum impact angle that would ensure an impact with one tree [i.e., the maximum angle for which P(hit a tree)=1.0]. Therefore, in Eq. 5 and Eq. 6, the angle of impact makes the resulting $Eff.W_{treeline}$ equal to S, the obstacle spacing.

$$Eff.W_{treeline} = \frac{Adjusted.Profile.Width_{trajectory}}{\sin \phi} = S \tag{5}$$

$$\phi = \sin^{-1}\left(\frac{Adjusted.Profile.Width_{trajectory}}{S}\right) = \sin^{-1}\left(\frac{1.35W - 2.4D}{S}\right) \tag{6}$$

Table 47. Critical vehicle trajectory angle for different obstacle spacings.

S (ft)	Critical Impact Angle (degrees)
30	11.45
60	5.70
100	3.41
150	2.28

Table 47 shows the critical impact angle for different values of obstacle (tree) spacing, *S*.

It is not surprising that as the separation between trees increases, the maximum angle that ensures an impact decreases. For example, with trees spaced every 30 ft, any trajectory arriving at the line of trees at an angle of 11.45 degrees or less would be certain to result in a tree impact. On the other extreme, for a line of trees spaced every 150 ft, only trajectories arriving at the tree line at an angle of 2.28 degrees or less would be certain to result in an impact.

The impact angle model described in Chapter 5 was incorporated into the crash probability analysis procedure. The model was integrated into the CZ-GAP analysis tool such that it permits the selection of an impact angle percentile for use in the risk analysis. For purposes of this project, the mean impact angle from the modeled impact angle distribution corresponding to a given lateral and longitudinal distance was used.

The impact angle model is used in conjunction with the lateral and longitudinal distance models to determine the probability of hitting an object along the clear zone edge following the methodology described above. This information is passed to the Risk Determination Module where it is used as part of the computation of the probability of a serious injury or fatal crash for a given design condition at a prescribed clear zone distance and defined obstacle spacing at the clear zone edge.

Rollover Probability

The rollover probability for the different design vehicles was programmed in two separate functions by facility type (i.e., 2U and 4D). In each function, the rollover probability for each vehicle type is calculated and then multiplied by their representative weights. The result is the sum of vehicle model predictions and a combined rollover probability for a given design configuration at a given lateral offset distance. This architecture is shown in Figure 47. This information is passed to the Risk Determination Module where it can be used as part of the computation of the overall probability of a serious injury or fatal crash for a given design condition at a prescribed lateral offset (clear zone) distance.

Severity Prediction

The Impact Speed Models described in Chapter 5 were incorporated into the CZ-GAP analysis tool to calculate the mean speed of a vehicle at the lateral clear zone distance of interest and for the longitudinal distance associated with a given obstacle (tree) at the clear zone edge. In other words, each obstacle location defined by a prescribed lateral and longitudinal distance will have an associated mean impact speed defined by the Impact Speed Models.

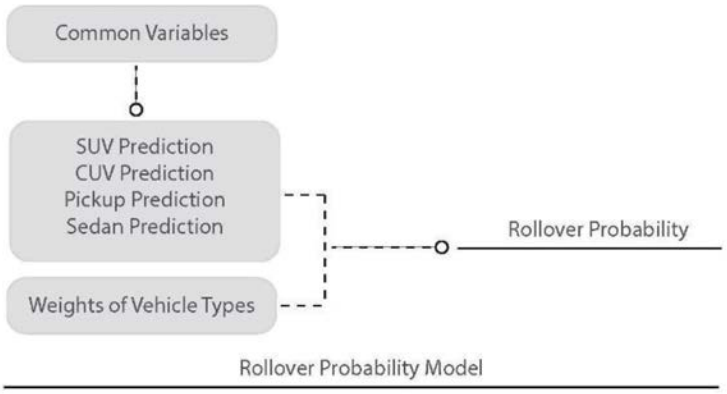

Figure 47. Rollover probability algorithm architecture.

The design (common) variables are used to fit the impact speed regression models for a given facility type, roadway and roadside terrain configuration, lateral clear zone distance, and longitudinal hazard location. The mean and standard deviation are then extracted from the models for each vehicle type. The final mean impact speed for a given hazard is the average of the mean impact speed for each vehicle multiplied by its representative weight factor. This process is schematically illustrated in Figure 48.

Development of Impact Speed-Severity Relationship for Fixed Objects

The Severity Prediction Module calculates the risk of a fatal or severe injury crash [P(K+A)] by using the mean speed from the Impact Speed Model as the impact speed with a given obstacle (tree). The Severity Prediction Module then determines the P(K+A) crash injury risk for each hazard using a fixed-object relationship between impact speed and injury probability. The P(K+A) tree crash risk for each obstacle is then multiplied by the outcome probabilities from the Crash Probability Module to generate a weighted P(K+A) tree crash risk that is summed over the number of hazards.

The research team used the crash database from *NCHRP Web-Only Document 341* to determine the relationship between impact speed and injury severity. For the subset of data that included right-side departures, the team identified 290 crashes on 2U roads and 37 crashes on 4D roads. Preliminary analyses were performed using the 2U data. The 2U and 4D data were

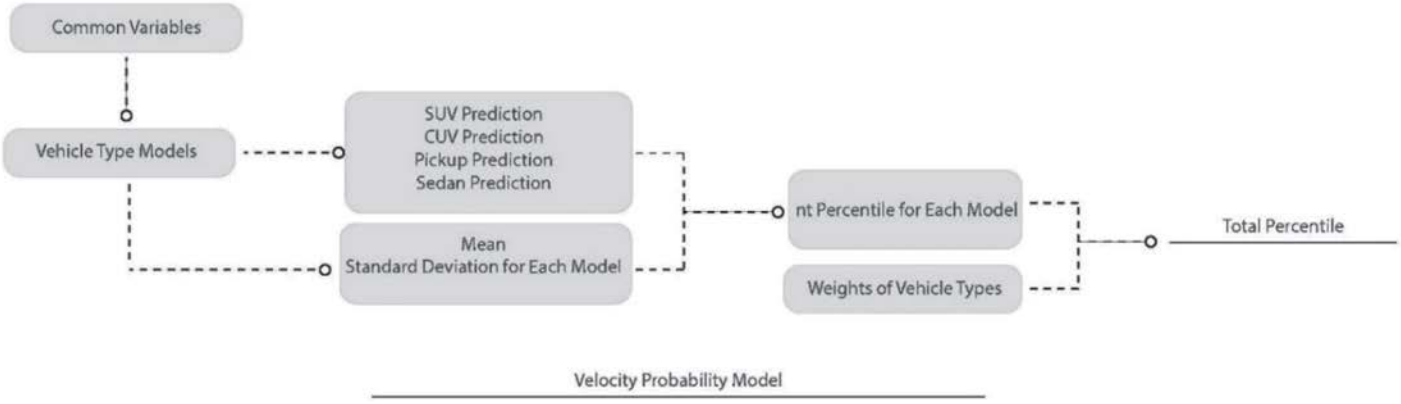

Figure 48. Impact speed prediction model.

later combined because the impact speed–injury severity relationship should be independent of facility type.

The research team identified at least two possible ways to define the severity of a crash using this database: the AAIS variable and the AINJSER variable. The definitions for these two variables are presented in Figure 49 (*14*).

Out of the 290 crashes identified on 2U facilities, 274 crashes had valid fields for the AAIS variable and 158 had valid values for the AINJSER variable. The research team elected to develop the severity relationship based on the AAIS variable, both for consistency with past work as well as for sample size purposes. The AAIS variable is based on the maximum known injury in a crash based on the Abbreviated Injury Scale (AIS).

Figure 50 shows the relationship developed when considering levels 4 through 6 of the AAIS scale to define a severe or fatal crash. Similarly, Figure 51 shows the relationships when considering levels 3 to 6 in the definition of a severe or fatal crash. After some discussion, the team decided to move forward with the definition that uses levels 3 to 6, which seems to provide better correlation with the definition of a serious injury crash. The relationship is based on 307 crashes including 274 crashes on 2U roads and 33 crashes on 4D roads combined.

The team verified that the severity relationship derived from *NCHRP Web-Only Document 341* data resembles the shape of a curve developed by Ray et al. shown in Figure 52, albeit the ordinate in that curve is cost, rather than severity (*3, 26*).

Development of Severity Relationship for Rollovers

The research team filtered rollover events from 2U and 4D facilities from the *NCHRP Web-Only Document 341* database to develop a severity relationship for rollover events (*3*). The dataset

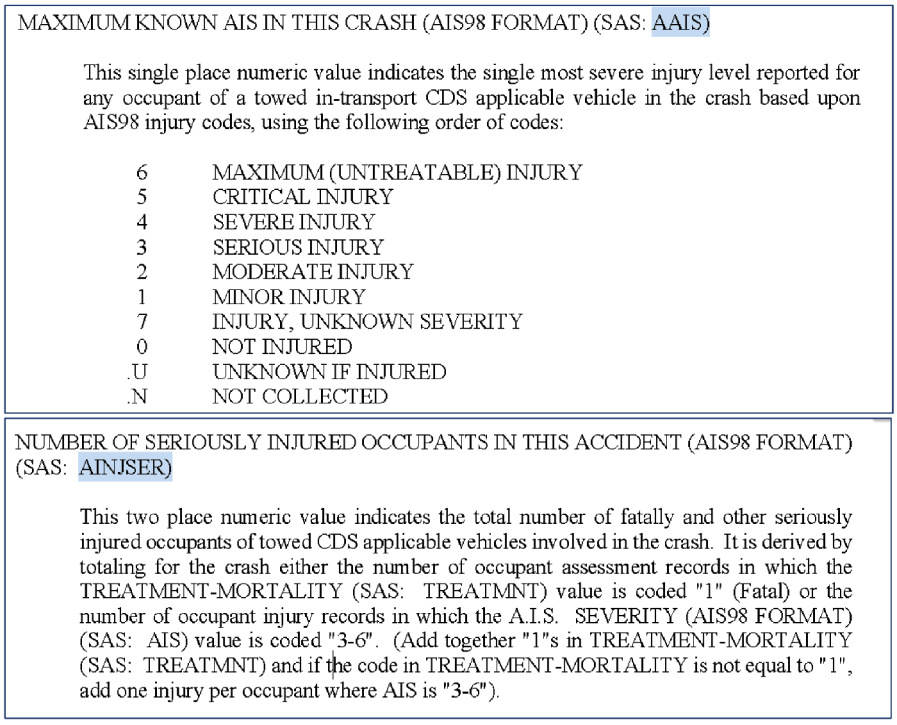

MAXIMUM KNOWN AIS IN THIS CRASH (AIS98 FORMAT) (SAS: AAIS)

This single place numeric value indicates the single most severe injury level reported for any occupant of a towed in-transport CDS applicable vehicle in the crash based upon AIS98 injury codes, using the following order of codes:

6	MAXIMUM (UNTREATABLE) INJURY
5	CRITICAL INJURY
4	SEVERE INJURY
3	SERIOUS INJURY
2	MODERATE INJURY
1	MINOR INJURY
7	INJURY, UNKNOWN SEVERITY
0	NOT INJURED
.U	UNKNOWN IF INJURED
.N	NOT COLLECTED

NUMBER OF SERIOUSLY INJURED OCCUPANTS IN THIS ACCIDENT (AIS98 FORMAT) (SAS: AINJSER)

This two place numeric value indicates the total number of fatally and other seriously injured occupants of towed CDS applicable vehicles involved in the crash. It is derived by totaling for the crash either the number of occupant assessment records in which the TREATMENT-MORTALITY (SAS: TREATMNT) value is coded "1" (Fatal) or the number of occupant injury records in which the A.I.S. SEVERITY (AIS98 FORMAT) (SAS: AIS) value is coded "3-6". (Add together "1"s in TREATMENT-MORTALITY (SAS: TREATMNT) and if the code in TREATMENT-MORTALITY is not equal to "1", add one injury per occupant where AIS is "3-6").

Figure 49. Injury code definitions (14). SAS = Statistical Analysis System.

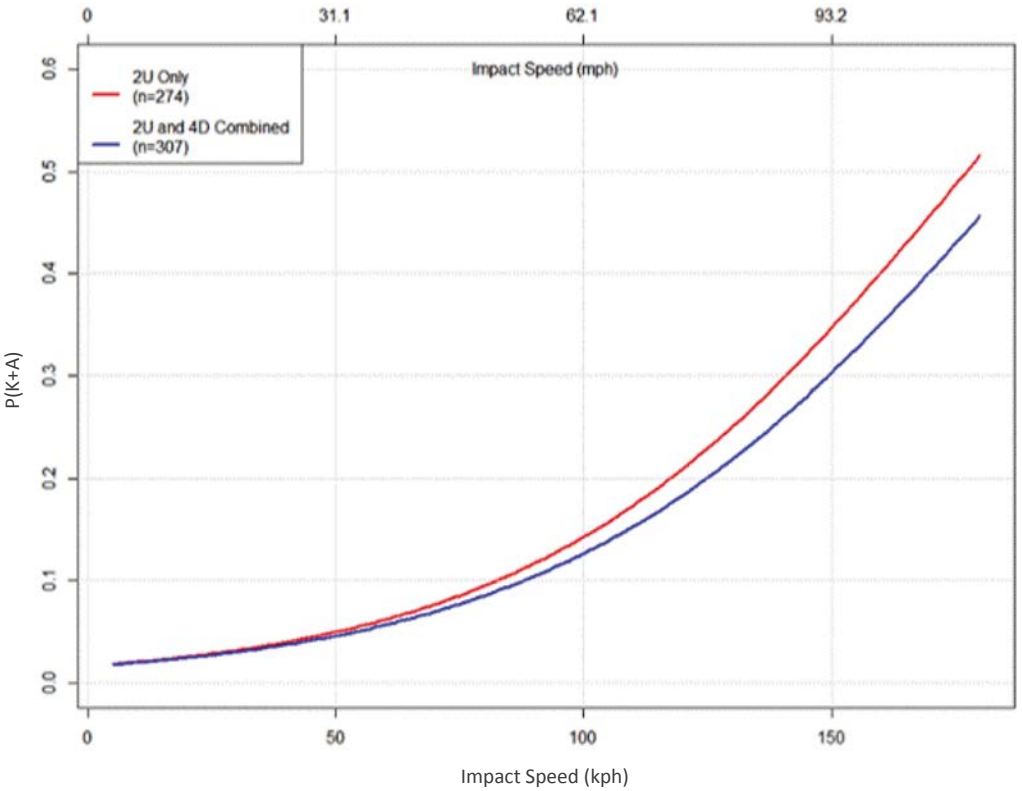

Figure 50. Fixed object K+A injury probability versus impact speed for AAIS 4–6.

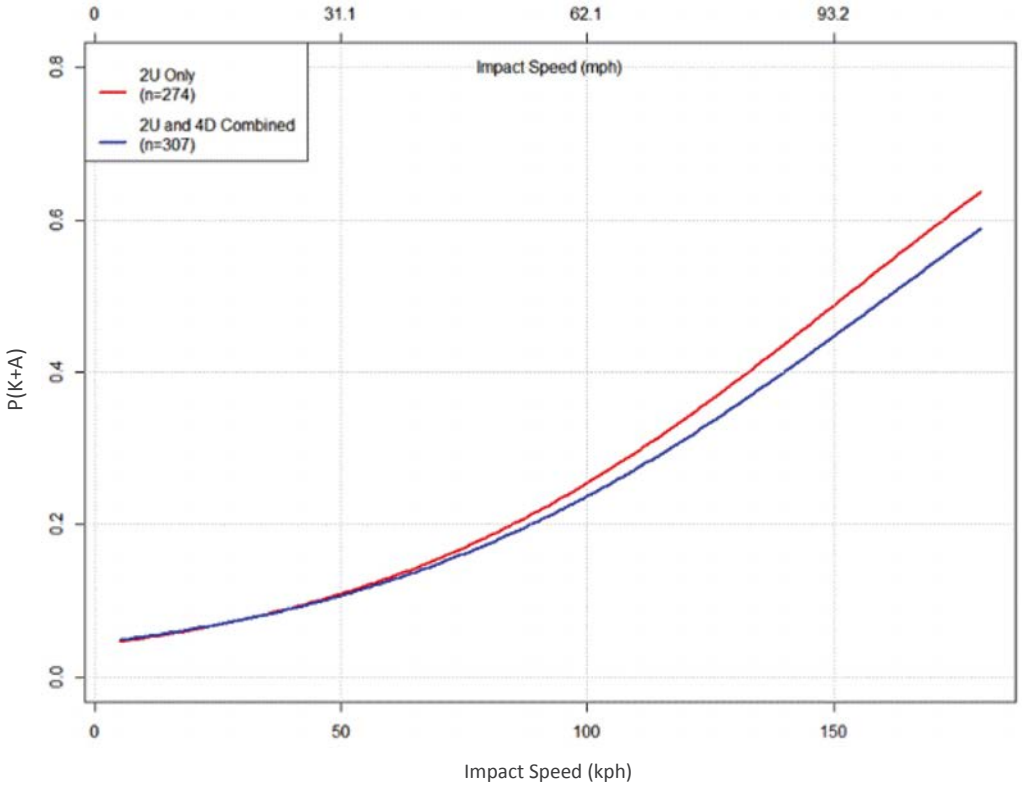

Figure 51. Fixed object K+A injury probability versus impact speed for AAIS 3–6.

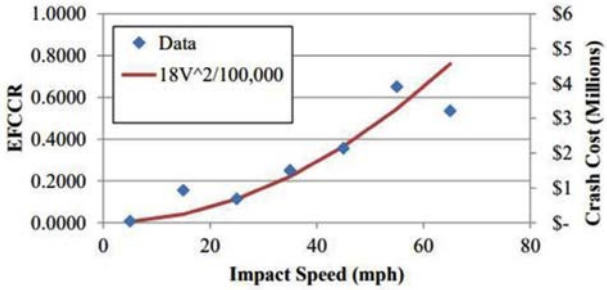

Figure 52. Cost versus impact speed for narrow fixed objects from the* NCHRP Report 665 *data (*16*). EFCCR = Effective Fatal Crash Cost Ratio.

contained rollover events and fixed-object crashes. Moreover, the vehicle speed at rollover and the impact speed with the fixed objects were available. The data were analyzed using a logistic regression model whose coefficients are indicated in Table 48. It can be observed that the rollover events have a lower likelihood of K+A crashes compared to the fixed-object crashes.

Furthermore, Figure 53 provides the resulting rollover severity relationship based on rollover speed compared to the severity of impacting a fixed object, which is plotted versus impact speed. The rollover relationship is relatively flat in the range of data available. In the programming of the CZ-GAP risk analysis tool, the team applied an average severity value for rollovers that are sensitive to the speed limit rather than making it a function of actual speed at rollover, which would significantly complicate the analysis procedure.

Risk Determination

For purposes of this project, "risk" is defined in terms of the probability of serious or fatal injury P(K+A) based on the KABCO scale. The KABCO scale is a descending scale of injury severity where a K-injury is a fatality and an O-crash results in "no apparent injury" and is often referred to as property damage only. A, B, and C refer to decreasing levels of injury severities, which are currently defined as "suspected serious injury," "suspected minor injury," and "possible injury," respectively. These injury levels are defined in the *MMUCC Guideline: Model Minimum Uniform Crash Criteria* (*27*).

The injury severity is determined for each design configuration for different clear zone distances and obstacle spacing beyond the clear zone edge. As the clear zone increases, the probability of impacting a fixed object at or beyond the clear zone edge decreases, and, thus, the risk decreases. The probability of impacting a fixed object and, hence, the injury risk associated with a given roadway segment and clear zone distance are also a function of the nature of the obstacles at the clear zone edge. Consequently, risk was determined for different obstacle spacings. As

Table 48. Regression model for rollover severity derived from the *NCHRP Web-Only Document 341* database (*3*).

Parameter	Estimate	Standard Error	z-Value	P-Value	Significance
Intercept	–2.641380	0.450441	–5.864	4.52E-09	***
Impact speed	0.016056	0.005978	2.686	0.00723	**
Rollover event	–1.247500	0.756489	–1.649	0.09913	~

NOTE: *** = statistically significant at the 99% confidence interval; ** = statistically significant at the 95% confidence interval; ~ = statistically significant at the 90% confidence interval.

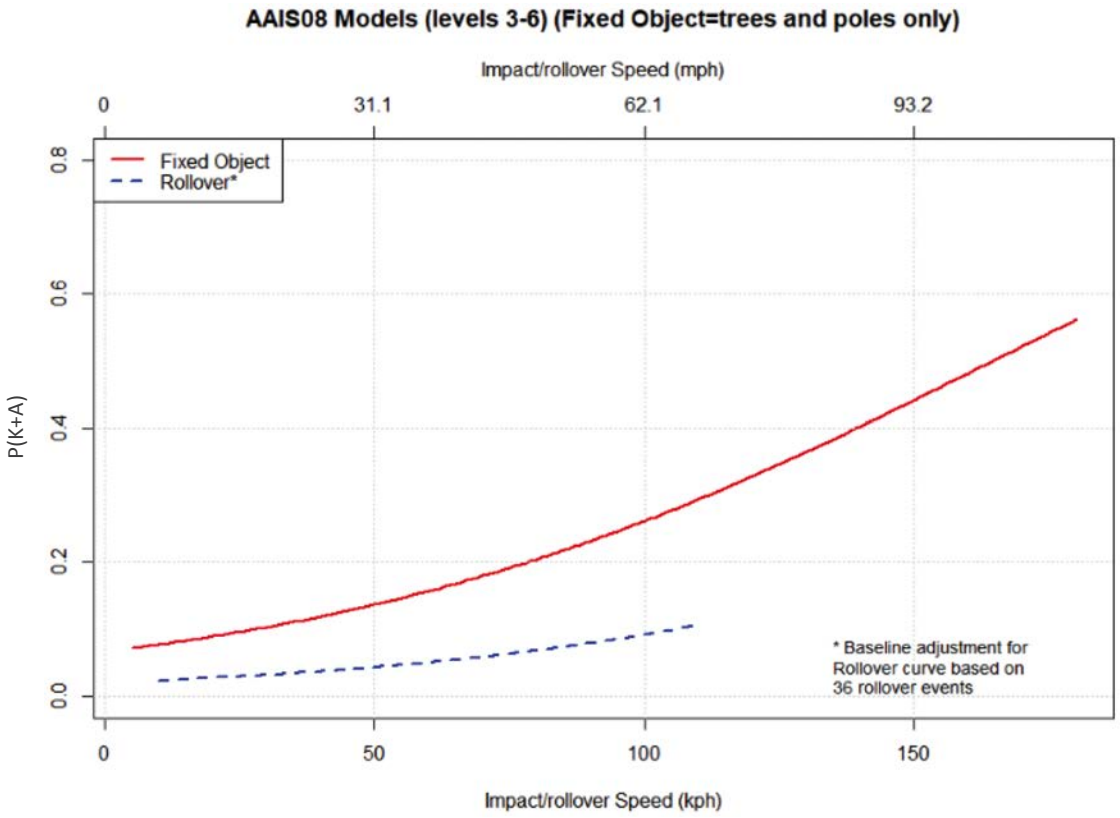

Figure 53. Comparison of rollover severity with severity of impacting a fixed object.

noted previously, the hazards were defined as a line of trees having a diameter sufficient for them to behave as "fixed objects." For practical purposes, the obstacle spacing can be considered the average spacing of trees, or other fixed-object types, along a roadway segment. A higher density of trees (i.e., closer spacing) will result in a higher probability of an impact. Conversely, a lower tree density (i.e., larger spacing) will have a lower probability of impact and a lower overall level of risk.

There are two basic approaches for using risk-based analysis results to develop guidelines. The first is based on absolute risk, where the calculated risk of the roadway segment is compared to a risk target that is considered acceptable by the owner agency. If the risk associated with a given clear zone for a defined roadway segment and the ADT is less than the target, the risk is considered acceptable, and the clear zone distance is satisfactory.

The second approach is based on relative risk. When hazards on the roadside are shielded by a barrier such as guardrail, the guardrail has an associated level of risk. The general roadside design philosophy is that the risk associated with the barrier should be less than the risk associated with the unshielded roadside. Thus, in the context of clear zone guidelines, a given clear zone distance is considered acceptable for a roadway segment if its relative risk associated with impacting obstacles at the clear zone edge is less than the risk of shielding the segment with guardrail.

As previously discussed, the Severity Prediction Module predicts the overall probability of a serious injury or fatal crash for an encroachment occurring along the predefined roadway segment for the selected clear zone distance and obstacle spacing. The Severity Prediction Module has two submodules: the Rollover Severity submodel and the Impact Severity submodel. The Rollover Severity submodel predicts the probability a given encroachment will result in a rollover before the vehicle reaches the clear zone edge of interest. This probability is then assigned

a rollover crash injury severity based on the relationship derived from the *NCHRP Web-Only Document 341* crash database (*3*).

The Impact Severity submodel uses the Impact Speed Model to determine the mean impact speed for each obstacle (tree) of interest. The Impact Speed-Severity relationship derived from the *NCHRP Web-Only Document 341* database (*3*) is then used to determine a P(K+A) for each obstacle (tree). This P(K+A) value is multiplied by the probability of an impact for each obstacle (tree), which is calculated using the Crash Probability Module. These weighted tree P(K+A) values are then summed over the number of obstacles.

The sum of the K+A tree crash risks and K+A rollover crash risk is the total K+A crash risk for the given design configuration, clear zone distance, and obstacle spacing. This is expressed mathematically in Eq. 7.

$$P\left(K+A\right)_{CZ} = \left[P\left(Roll\right)_{CZ} * P\left(K+A\right)_{Roll}\right] + \left[P\left(Reach\right)_{CZ} * \sum_{i=1}^{n} P\left(Tree\ Impact\right)_{i} * P\left(K+A\right)_{Tree}\left(\overline{V}_{i}\right)\right] \tag{7}$$

where:

$P(K+A)_{CZ}$ = Weighted total K+A crash risk P(K+A) for the clear zone distance of interest given an encroachment has occurred.
$P(Roll)_{CZ}$ = Probability of rollover before reaching the clear zone edge of interest.
$P(K+A)_{Roll}$ = Probability of a fatal or severe injury from a rollover.
$P(Reach)_{CZ}$ = Probability of an encroachment reaching the clear zone edge of interest.
n = Total number of trees in segment of interest.
$P(Tree\ Impact)_i$ = Probability of impacting i-th tree given an encroachment has reached the clear zone edge of interest.
$P(K+A)_{Tree}(\overline{V}_i)$ = Risk of a fatal or severe injury from a tree crash adjusted for the impact velocity with i-th tree.
V_i = Mean impact velocity given a crash has occurred with i-th tree.

However, since guidelines have historically been developed based only on roadside obstacle impact risk, the research team decided to exclude rollover risk in the development of clear zone guidelines in this project. This simplified Eq. 7 in the form presented in Eq. 8.

$$P\left(K+A\right)_{CZ} = P\left(Reach\right)_{CZ} * \sum_{i=1}^{n} P\left(Tree\ Impact\right)_{i} * P\left(K+A\right)_{Tree}\left(\overline{V}_{i}\right) \tag{8}$$

As a result, CZ-GAP used Eq. 8 to generate the K+A crash risk values for all the configurations considered. After further variable sensitivity and importance analysis, these P(K+A) values were then used to generate the clear zone guidelines that will be made available for consideration for inclusion in the RDG.

CHAPTER 7

Variable Sensitivity and Importance

As described in the preceding chapters, a wide array of roadway and roadside design variables were incorporated into the encroachment simulation matrix as well as the various encroachment relationship models. The variables include horizontal curvature, vertical grade, shoulder width, foreslope ratio, foreslope width, ditch bottom width, backslope ratio, and backslope width. While it is desirable to have clear zone guidance expressed in terms of key, significant design variables, the addition of variables with little significance to clear zone risk can unnecessarily complicate the guidelines. Thus, it is important to understand the key variables that have a great impact on the determination of P(K+A) during a vehicle encroachment.

A sensitivity analysis was performed to understand the change in P(K+A) for a change in the value of each design variable. The general approach involved defining various design configurations and varying the individual variables within the CZ-GAP risk analysis tool to examine the effects of changes in P(K+A) across a range of clear zone distances. If varying a roadway or roadside parameter is found to have little or no influence on P(K+A), it can be removed from the guideline development process and assigned a fixed value representative of common practice. This helps streamline the presentation of the resulting clear zone guidelines without significantly changing the resulting clear zone distance. The fewer the number of variables, the simpler the presentation and implementation of the guidelines.

A variable-importance analysis was also performed to provide insight into the impact of each variable. The variable-importance analysis ranks the variables according to their contribution to the prediction of P(K+A).

Variable Sensitivity

Using the CZ-GAP risk analysis tool, the team performed sensitivity analyses to better understand the influence of impact angle percentiles, impact speed percentiles, and tree spacings on P(K+A). The impact speed and angle models developed from the encroachment simulation data and described in Chapter 5 provide distributions for the variable at different lateral and longitudinal offset distances. A selection of the percentile value to use in the clear zone risk analysis was part of the overall clear zone analysis plan. For example, for impact speed, a median or 85th percentile value could be used, with the 85th percentile representing higher impact speeds and, thus, being more conservative. Similarly, a median or 15th-percentile impact angle could be utilized in the analysis. The 15th-percentile angle would be more conservative because it projects a wider contact envelope onto the tree line at the clear zone edge and, thus, increases the probability of impact. The tree spacing is intended to represent a relative obstacle density at the edge of the clear zone. The intent was to select values of obstacle spacing to represent low, medium, and high hazard levels for the clear zone guidelines.

Figure 54 through Figure 57 present the P(K+A) relationships for different impact speed and impact angle percentile combinations for different clear zone distances. This analysis was performed for a particular roadway and roadside terrain configuration as noted in the figures. As can be observed, the P(K+A) associated with tree impacts at the clear zone edge decreases as the vehicle encroaches further onto the roadside. This is intuitive given that increased lateral offset distances are generally associated with lower impact speed.

It can also be observed that P(K+A) due to rollover increases with lateral distance. The P(K+A) due to rollover is computed based on the probability of the rollover for a given terrain configuration and lateral offset distance. As a vehicle encroaches further onto the roadside, the probability of rollover increases.

It can be further observed that the change of the speed distribution metrics from the mean speed (Figure 54) to the 85th percentile speed (Figure 55) is associated with an increase in the P(K+A) for trees. Similarly, as observed by comparing Figure 54 and Figure 56, a change in the angle distribution metrics from the mean angle (Figure 54) to the 15th percentile angle (Figure 56) results in an increase in the P(K+A) for trees. Figure 57 presents P(K+A) for both 85th percentile speed and 15th percentile angle, which is the most conservative combination and results in the highest P(K+A).

The research team also performed a sensitivity analysis for tree spacing. In this analysis, the spacing of trees varied from 20 ft to 500 ft, and the average impact angle and 85th percentile speed were used to develop the P(K+A) curves. As can be observed from Figure 58 through Figure 62, as the spacing between trees increases, the magnitude of P(K+A), due to tree impacts, decreases. As expected, the spacing of trees has a significant influence on the estimate of P(K+A).

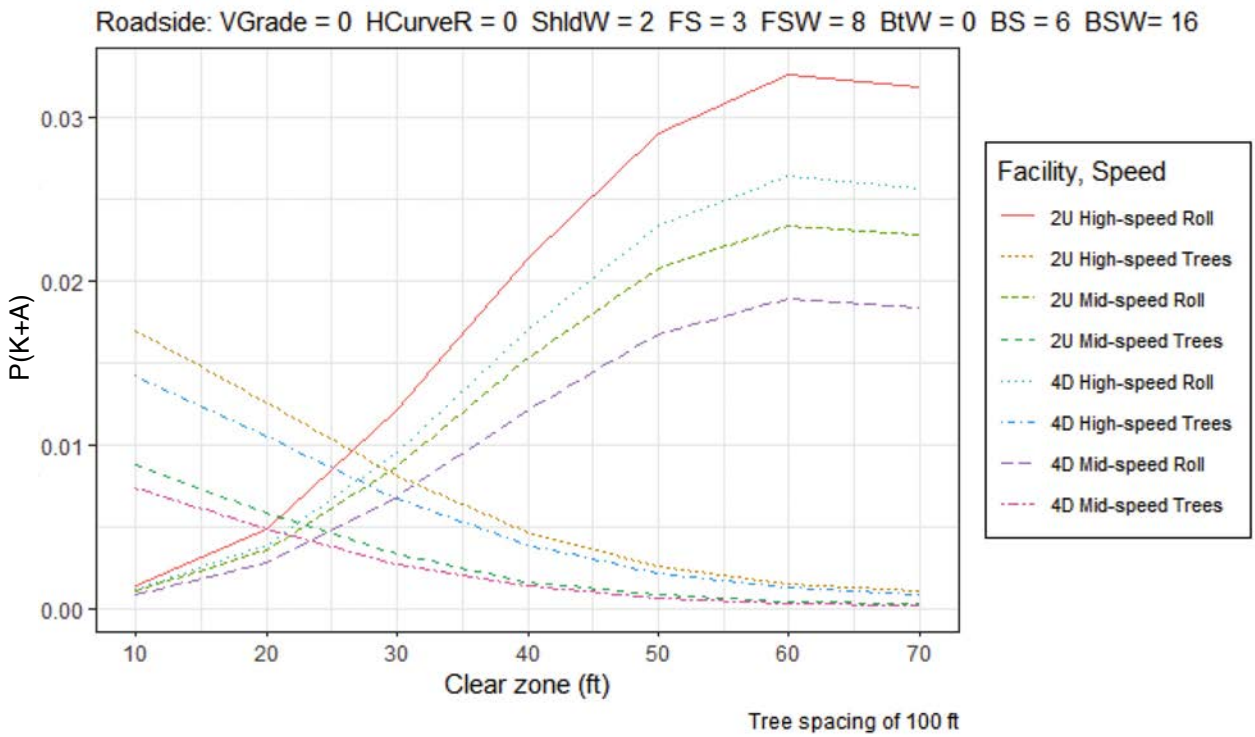

NOTE: VGrade (% downgrade) = vertical grade; HCurveR (degree of curvature) = horizontal curvature; ShldW (ft) = shoulder width; FS (H in ratio 1V:H) = foreslope ratio; FSW (ft) = foreslope width; BtW (ft) = ditch bottom width; BS (H in ratio 1V:H) = backslope; and BSW (ft) = backslope width.

Figure 54. P(K+A) for the average impact speed and average impact angle.

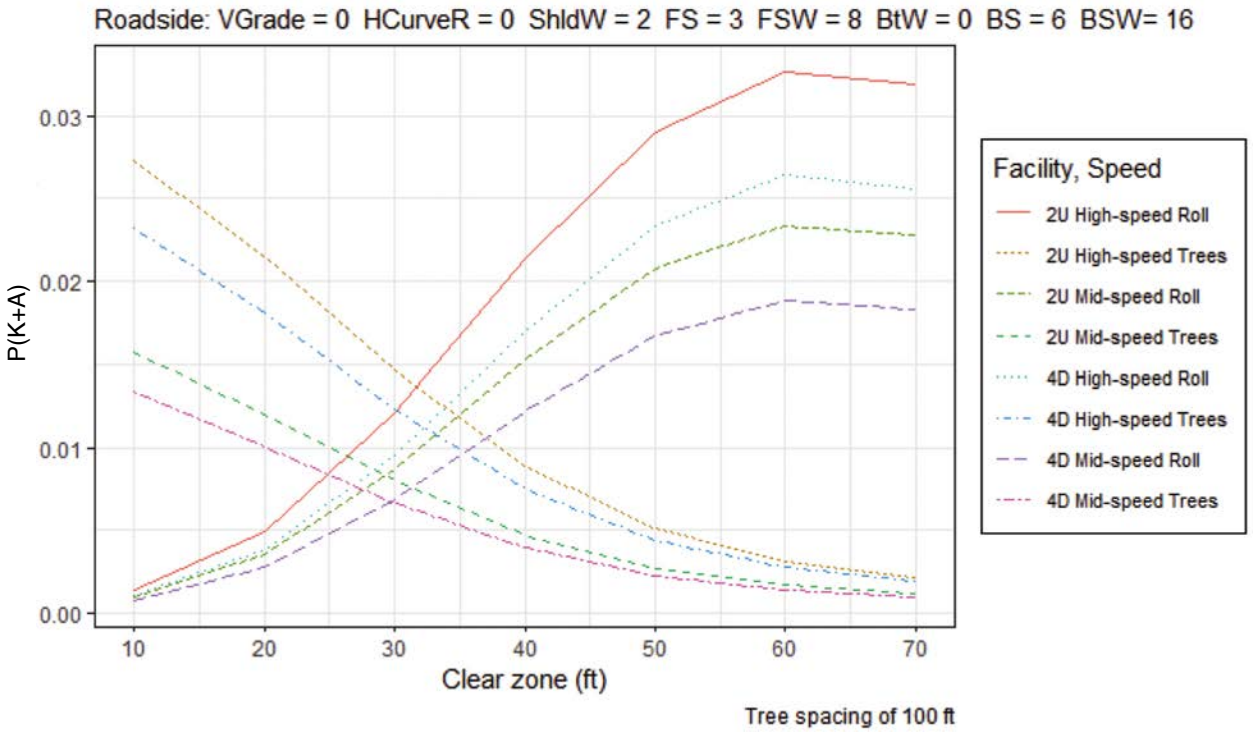

NOTE: VGrade (% downgrade) = vertical grade; HCurveR (degree of curvature) = horizontal curvature; ShldW (ft) = shoulder width; FS (H in ratio 1V:H) = foreslope ratio; FSW (ft) = foreslope width; BtW (ft) = ditch bottom width; BS (H in ratio 1V:H) = backslope; and BSW (ft) = backslope width.

Figure 55. P(K+A) for the 85th percentile impact speed and average impact angle.

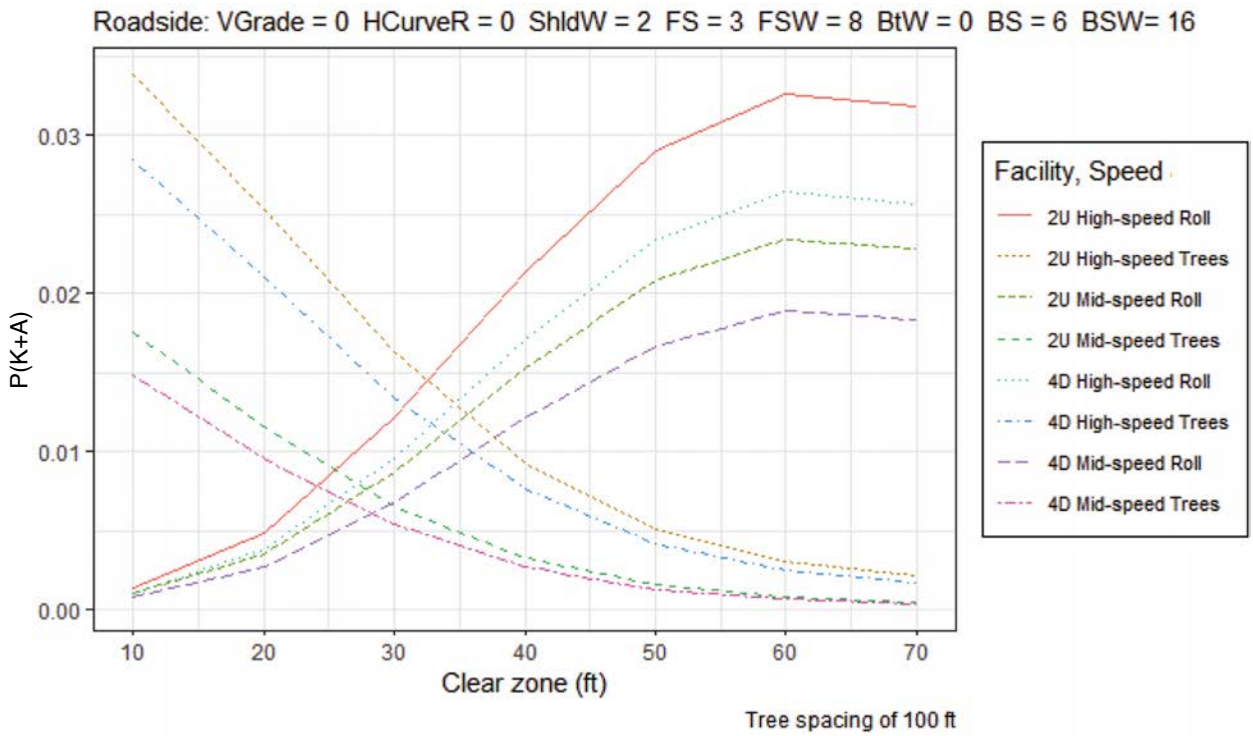

NOTE: VGrade (% downgrade) = vertical grade; HCurveR (degree of curvature) = horizontal curvature; ShldW (ft) = shoulder width; FS (H in ratio 1V:H) = foreslope ratio; FSW (ft) = foreslope width; BtW (ft) = ditch bottom width; BS (H in ratio 1V:H) = backslope; and BSW (ft) = backslope width.

Figure 56. P(K+A) for the average impact speed and 15th percentile impact angle.

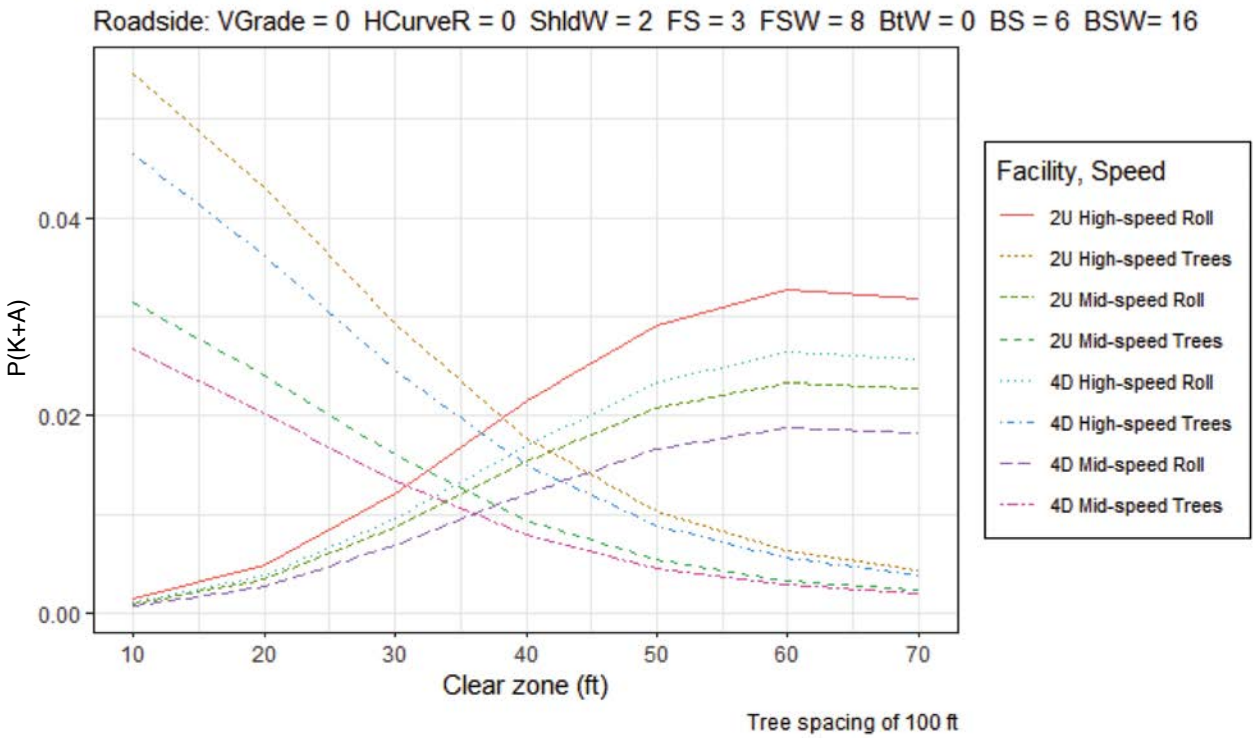

NOTE: VGrade (% downgrade) = vertical grade; HCurveR (degree of curvature) = horizontal curvature; ShldW (ft) = shoulder width; FS (H in ratio 1V:H) = foreslope ratio; FSW (ft) = foreslope width; BtW (ft) = ditch bottom width; BS (H in ratio 1V:H) = backslope; and BSW (ft) = backslope width.

Figure 57. P(K+A) for the 85th percentile impact speed and 15th percentile impact angle.

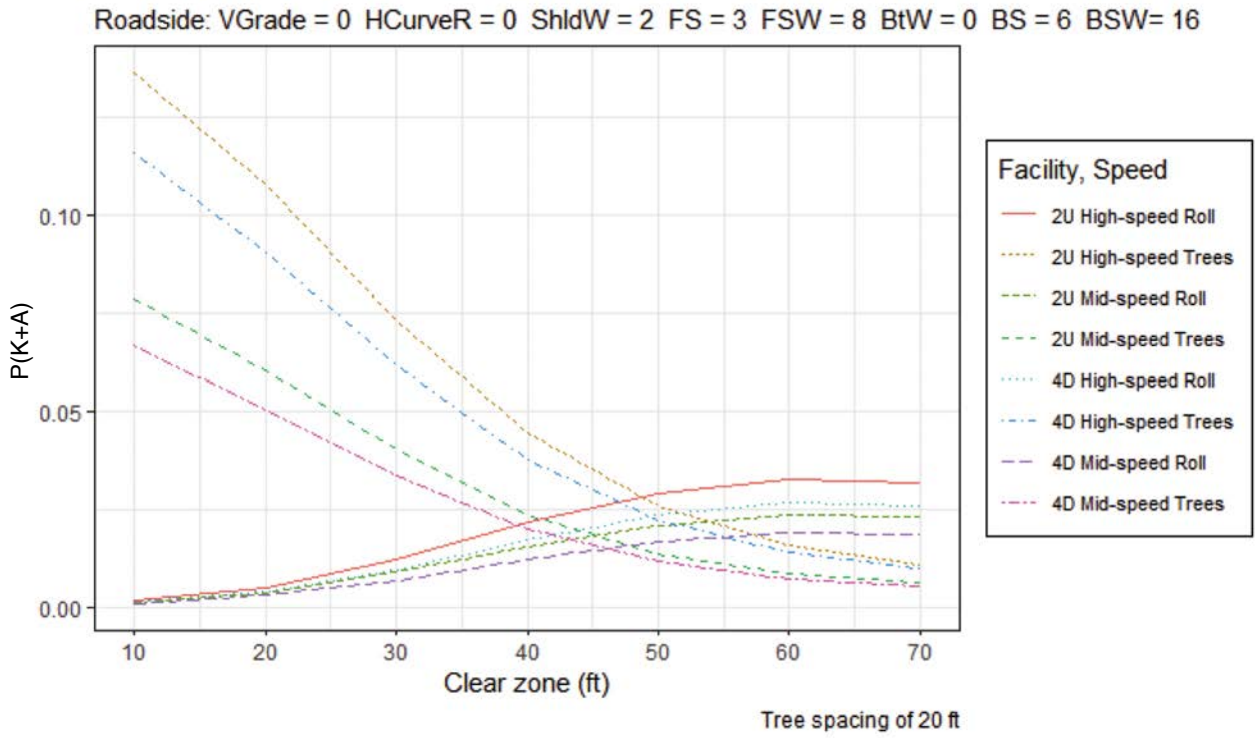

NOTE: VGrade (% downgrade) = vertical grade; HCurveR (degree of curvature) = horizontal curvature; ShldW (ft) = shoulder width; FS (H in ratio 1V:H) = foreslope ratio; FSW (ft) = foreslope width; BtW (ft) = ditch bottom width; BS (H in ratio 1V:H) = backslope; and BSW (ft) = backslope width.

Figure 58. P(K+A) for 20 ft spacing between trees.

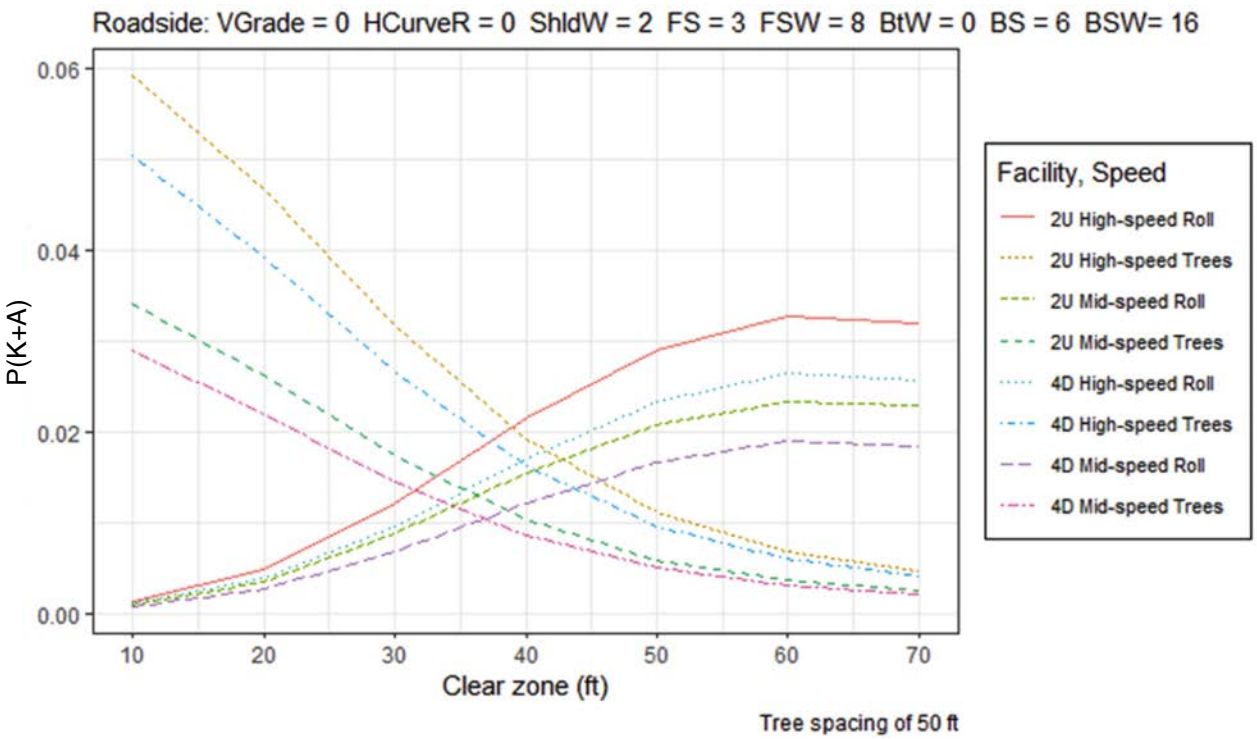

NOTE: VGrade (% downgrade) = vertical grade; HCurveR (degree of curvature) = horizontal curvature; ShldW (ft) = shoulder width; FS (H in ratio 1V:H) = foreslope ratio; FSW (ft) = foreslope width; BtW (ft) = ditch bottom width; BS (H in ratio 1V:H) = backslope; and BSW (ft) = backslope width.

Figure 59. P(K+A) for 50 ft spacing between trees.

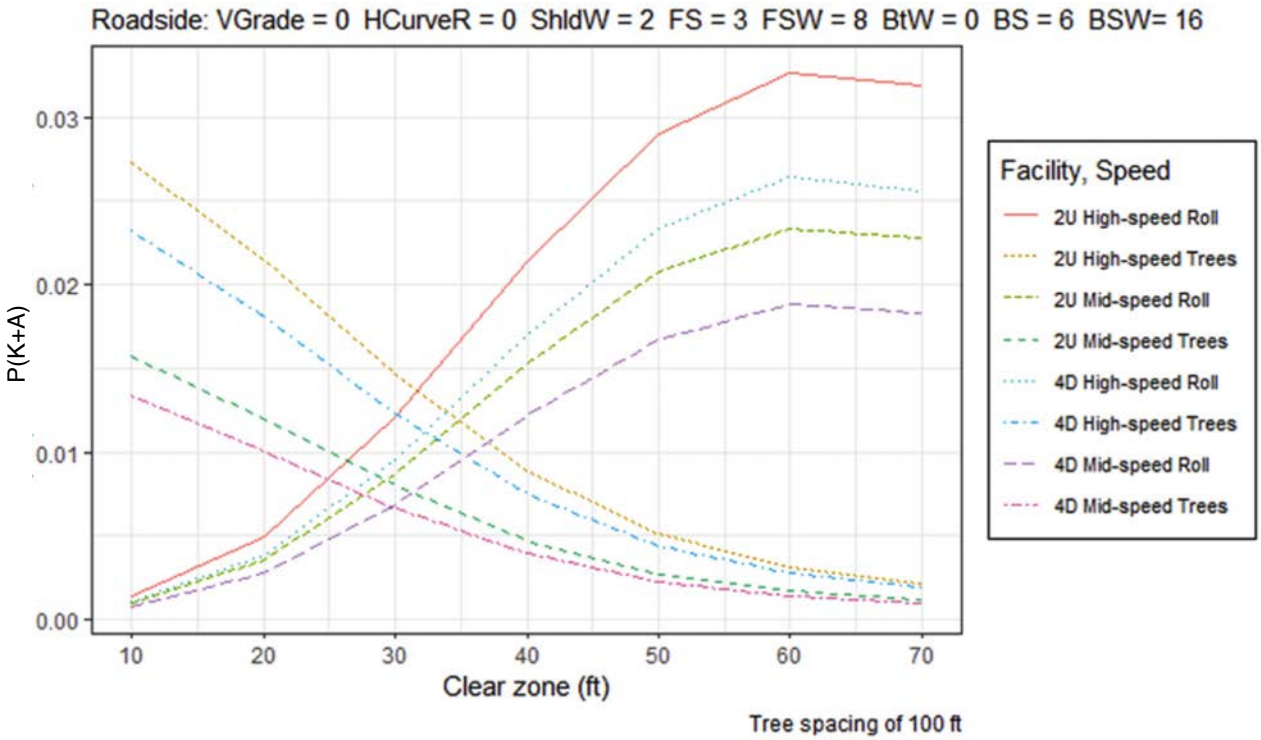

NOTE: VGrade (% downgrade) = vertical grade; HCurveR (degree of curvature) = horizontal curvature; ShldW (ft) = shoulder width; FS (H in ratio 1V:H) = foreslope ratio; FSW (ft) = foreslope width; BtW (ft) = ditch bottom width; BS (H in ratio 1V:H) = backslope; and BSW (ft) = backslope width.

Figure 60. P(K+A) for 100 ft spacing between trees.

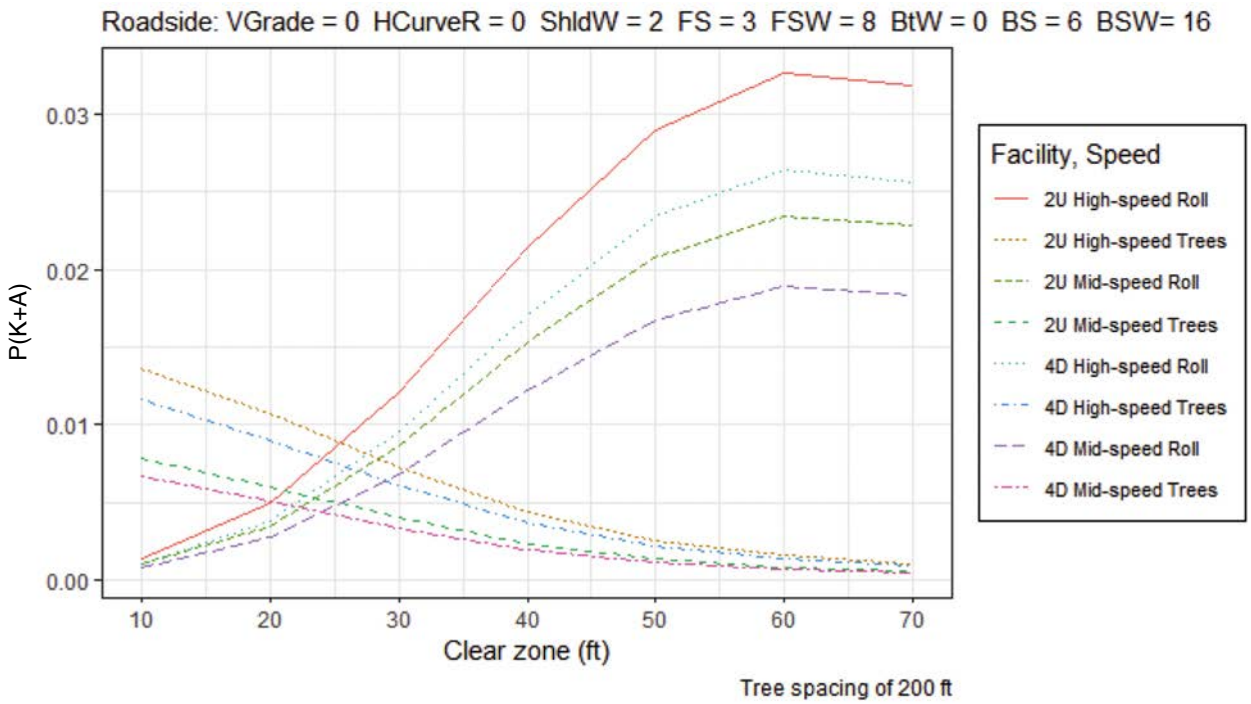

NOTE: VGrade (% downgrade) = vertical grade; HCurveR (degree of curvature) = horizontal curvature; ShldW (ft) = shoulder width; FS (H in ratio 1V:H) = foreslope ratio; FSW (ft) = foreslope width; BtW (ft) = ditch bottom width; BS (H in ratio 1V:H) = backslope; and BSW (ft) = backslope width.

Figure 61. P(K+A) for 200 ft spacing between trees.

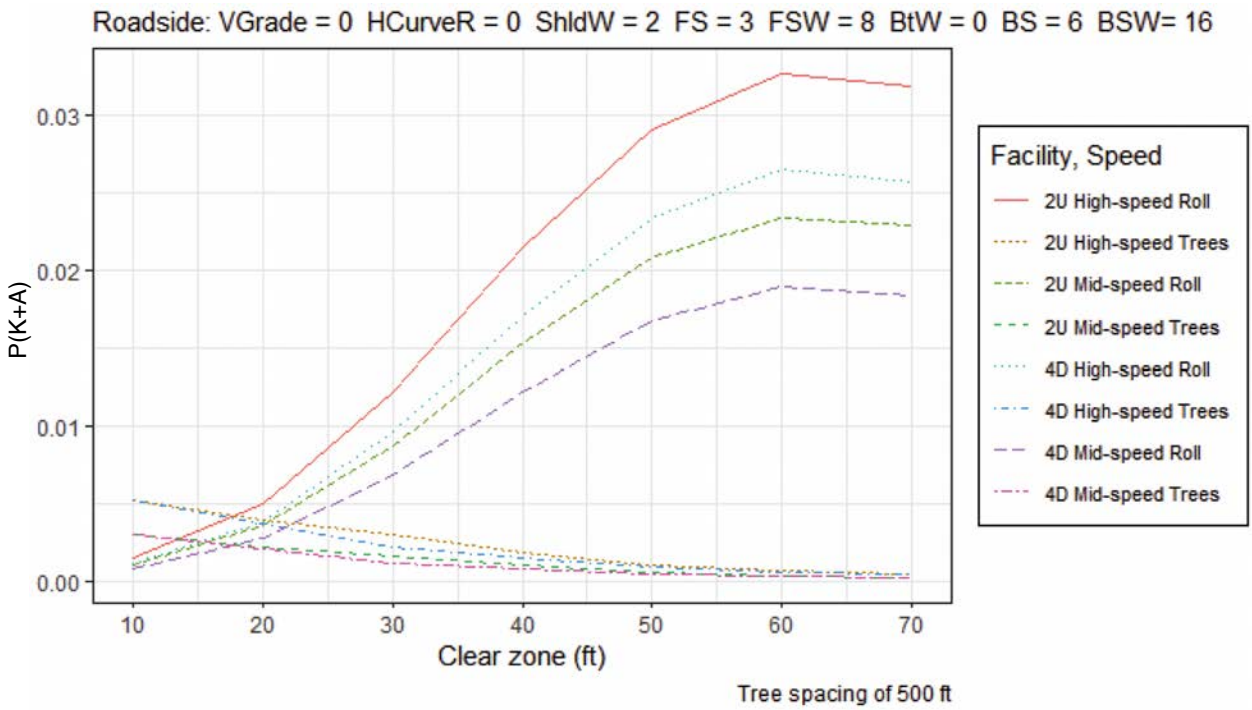

NOTE: VGrade (% downgrade) = vertical grade; HCurveR (degree of curvature) = horizontal curvature; ShldW (ft) = shoulder width; FS (H in ratio 1V:H) = foreslope ratio; FSW (ft) = foreslope width; BtW (ft) = ditch bottom width; BS (H in ratio 1V:H) = backslope; and BSW (ft) = backslope width.

Figure 62. P(K+A) for 500 ft spacing between trees.

The research team also performed a sensitivity analysis on the various roadside and roadway design variables. The sensitivity analysis was based on the probability of a fatal or serious injury crash given a vehicle hit a tree P(K+A). The median impact speed and angle and a tree spacing of 100 ft were used in the analyses.

Three roadside configurations were selected to cover the range of terrain variations within the design variable matrix. These configurations generally represent flat, moderate, and steep terrain. The design parameter values selected for each case are presented in Table 49. The key difference for the three terrains relates to the foreslope and backslope values. For the flat terrain condition, the flattest slopes in the simulation design matrix were used. These are a 1V:10H foreslope and a 1V:6H backslope. The moderate terrain used a 1V:6H foreslope and a 1V:4H backslope. The steep terrain used the steepest slope values in the simulation design variable matrix, which were a 1V:3H foreslope and a 1V:2H backslope.

For each terrain configuration, each design variable was parametrically varied using the values from the simulation matrix, and the P(K+A) was plotted for a range of clear zone distances. Separate graphs were prepared for 2U and 4D facility types. A high posted-speed-limit condition was used since that is believed to show the most sensitivity to injury probability.

A qualitative comparison of the curves was performed for the different terrain configurations and facility types. Additionally, the percentage of change between the maximum and minimum P(K+A) for the different values of the design variable was computed at a selected clear zone distance of 30 ft to provide a quantitative assessment. For instance, if the shoulder width was being assessed, the overall change in P(K+A) for the minimum (2 ft) and maximum (12 ft) shoulder widths was considered. The following sections present the results for each roadway and roadside design variable.

Vertical Alignment

Figure 63 through Figure 68 present the distribution of the probability of a fatal or serious injury crash [P(K+A)] for varying values (0, 4%, 6%) of vertical downgrades. Note that for programming purposes, the vertical downgrade (VGrade) is expressed as 1/% grade multiplied by a factor of 100. In the figures, VGrade = 16.667 = 6% of downgrade and VGrade = 25 = 4% of downgrade. Figure 63 presents the P(K+A) curves for a 2U facility type and flat terrain. Figure 64 presents the P(K+A) curves for a 4D facility type on flat terrain. Similar pairs of graphs are presented for moderate and sharp terrain in Figure 65 through Figure 68.

Across the facility type, the P(K+A) is higher for the 2U facility than the 4D facility. The observed differences in P(K+A) for different vertical grade values are not significant, irrespective of the facility type. In general, the difference increases slightly as clear zone distance increases. Table 50 provides the P(K+A) values at a clear zone distance of 30 ft and the percent

Table 49. Roadside configuration for test cases.

Variable	Case 1 (Flat)	Case 2 (Moderate)	Case 3 (Steep)
Vertical Alignment	0	0	0
Horizontal Alignment	0	0	0
Shoulder Width	2	2	2
Foreslope	1V:10H	1V:6H	1V:3H
Foreslope Width	16	16	16
Bottom Ditch Width	0	0	0
Backslope	6:1	4:1	2:1
Backslope Width	8	8	8

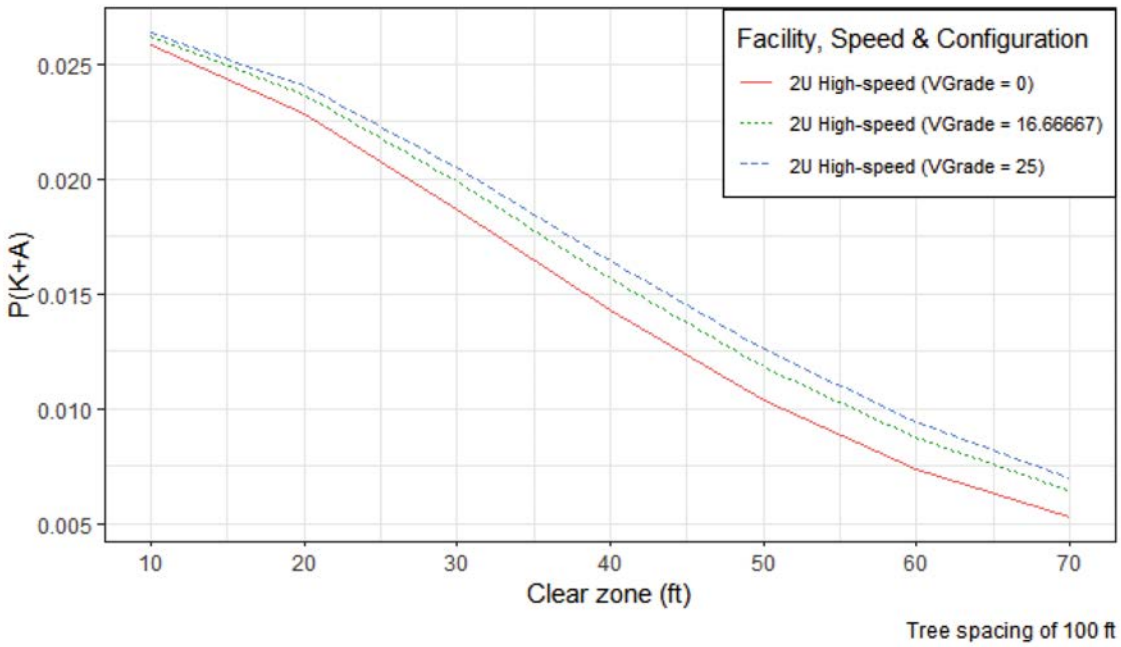

Figure 63. P(K+A) for 2U facility with varying vertical alignments (VGrade) (flat).

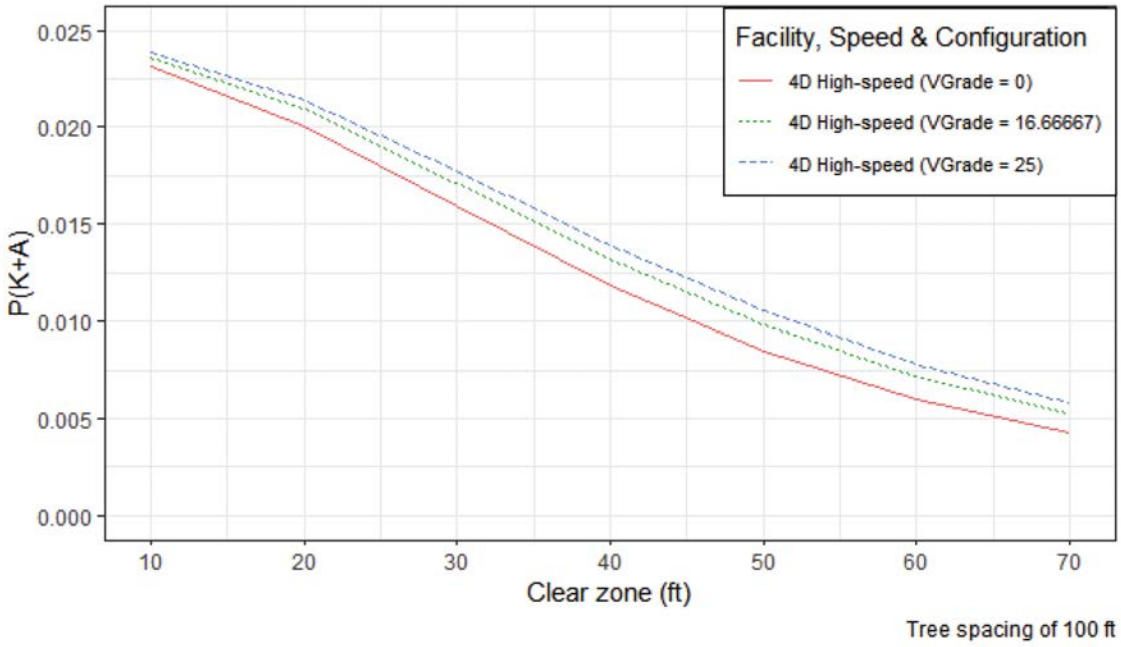

Figure 64. P(K+A) for 4D facility with varying vertical alignments (VGrade) (flat).

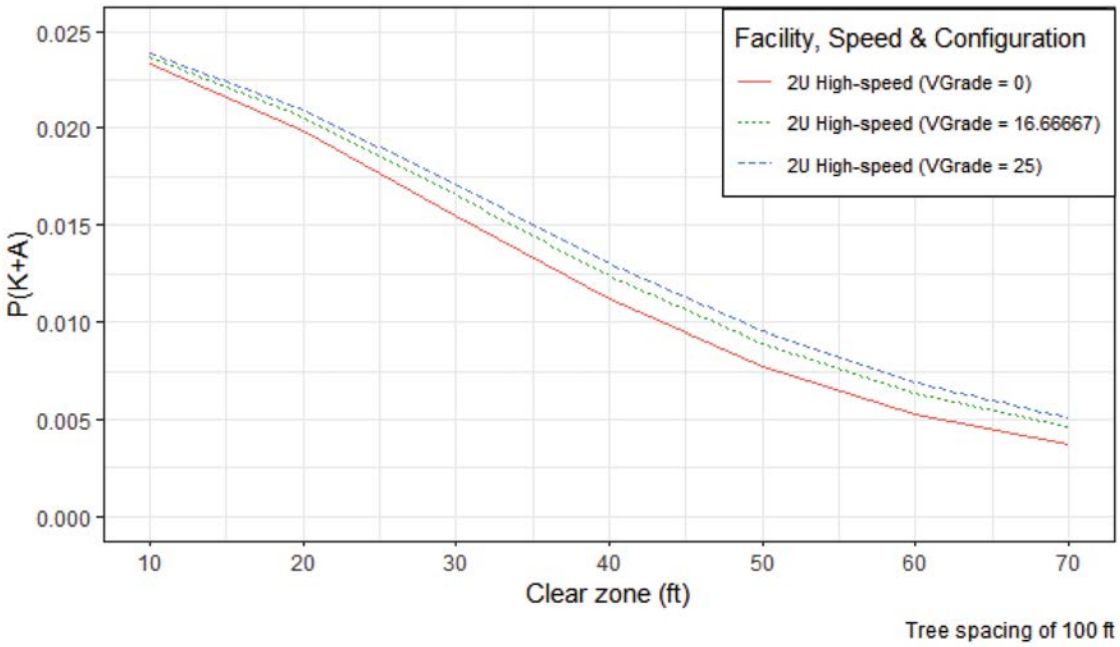

Figure 65. P(K+A) for 2U facility with varying vertical alignments (VGrade) (moderate).

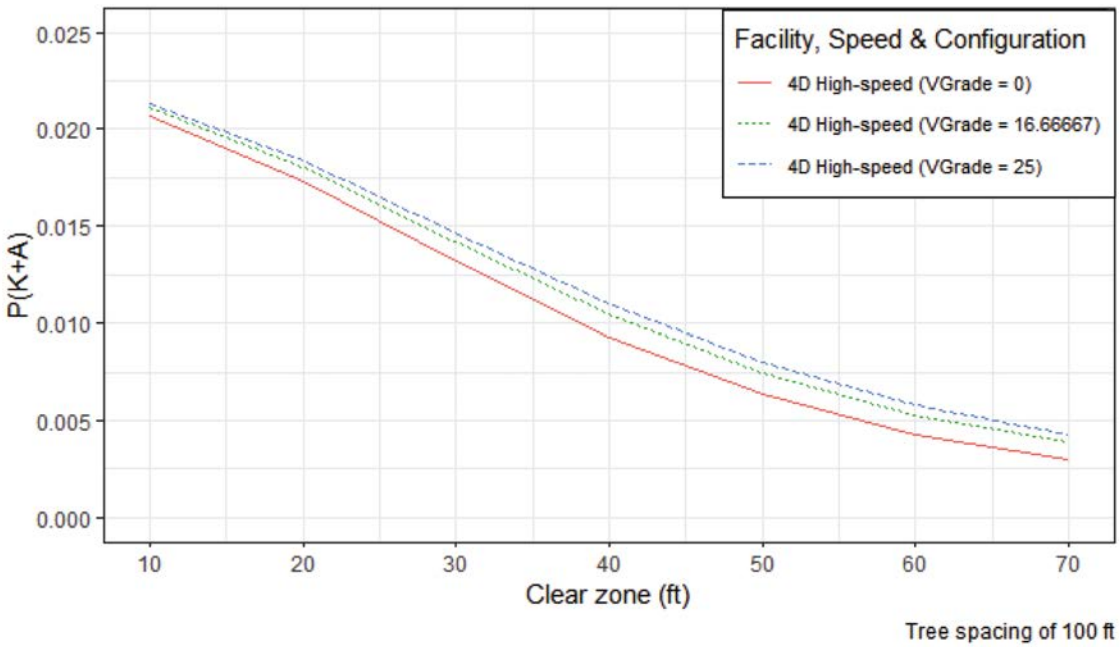

Figure 66. P(K+A) for 4D facility with varying vertical alignments (VGrade) (moderate).

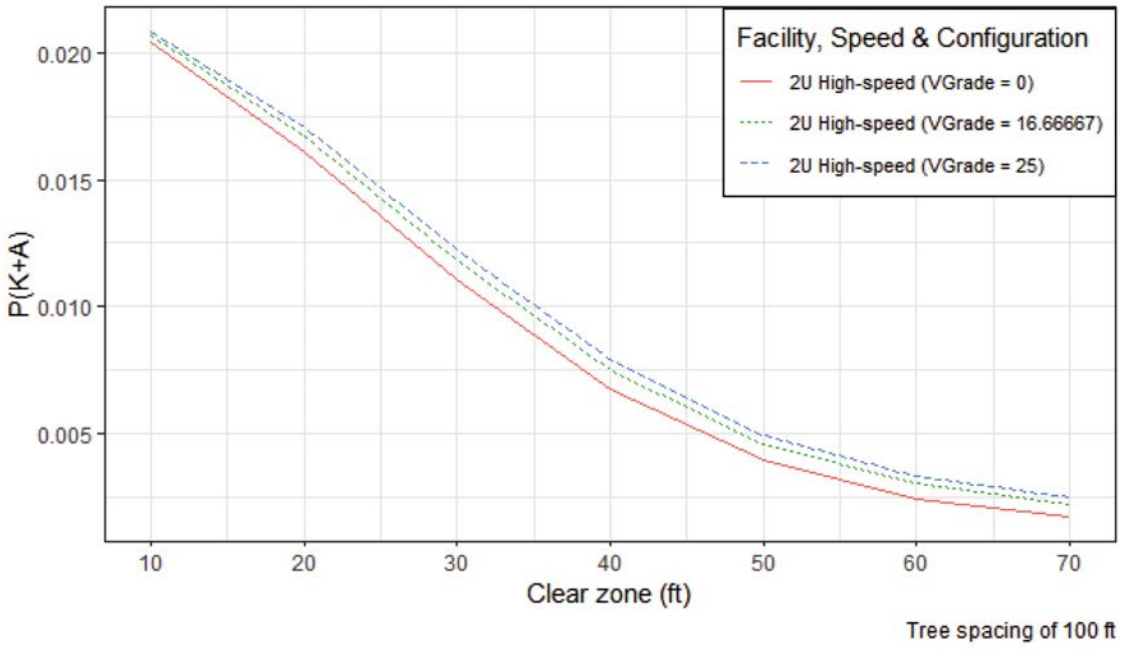

Figure 67. P(K+A) for 2U facility with varying vertical alignments (VGrade) (steep).

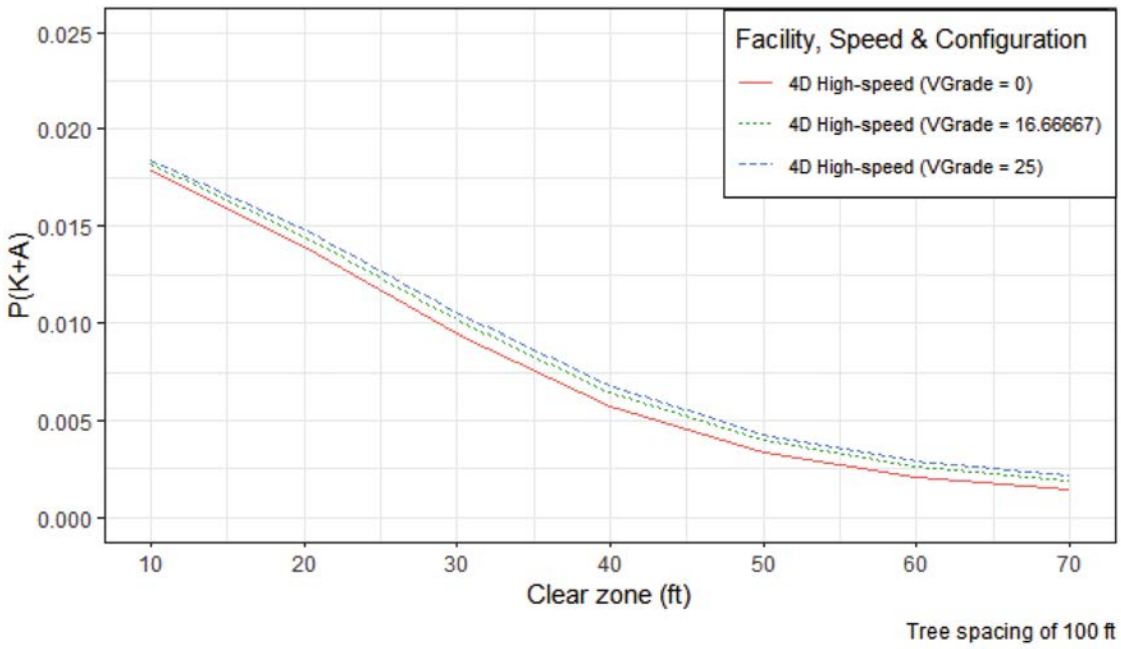

Figure 68. P(K+A) for 4D facility with varying vertical alignments (VGrade) (steep).

Table 50. Sensitivity of P(K+A) at a 30-ft clear zone with respect to vertical grade (VGrade).

Case	Facility, Speed, and Configuration	P(K+A)	Difference
Case 1			
(Flat)	2U high-speed (VGrade = –4%)	0.0205	9.8%
	2U high-speed (VGrade = 0)	0.0187	
	4D high-speed (VGrade = –4%)	0.0178	11.3%
	4D high-speed (VGrade = 0)	0.0160	
Case 2			
(Moderate)	2U high-speed (VGrade = –4%)	0.0171	10.6%
	2U high-speed (VGrade = 0)	0.0155	
	4D high-speed (VGrade = –4%)	0.0147	11.6%
	4D high-speed (VGrade = 0)	0.0132	
Case 3			
(Steep)	2U high-speed (VGrade = –4%)	0.0123	11.2%
	2U high-speed (VGrade = 0)	0.0110	
	4D high-speed (VGrade = –4%)	0.0106	12.0%
	4D high-speed (VGrade = 0)	0.0094	

difference between the minimum and maximum P(K+A) values for the range of vertical grade values. The maximum percent difference among the various terrain and facility types is only 12%.

Horizontal Alignment

Figure 69 through Figure 74 present the distribution of P(K+A) for 2U and 4D facilities and various terrain configurations for different values of roadway horizontal curvature. The horizontal curvature (HCurve) is commonly expressed in either the degree of curvature or radius of curvature. The values used in the analyses were 4 degrees of curvature (radius of curvature = 1,432 ft) and 6 degrees of curvature (radius of curvature = 1,432 ft). It can be observed that horizontal curvature has a significant impact on the P(K+A) irrespective of the facility and terrain type. The segments with the highest horizontal curvature (HCurve = 6 deg = 1,432 ft) were

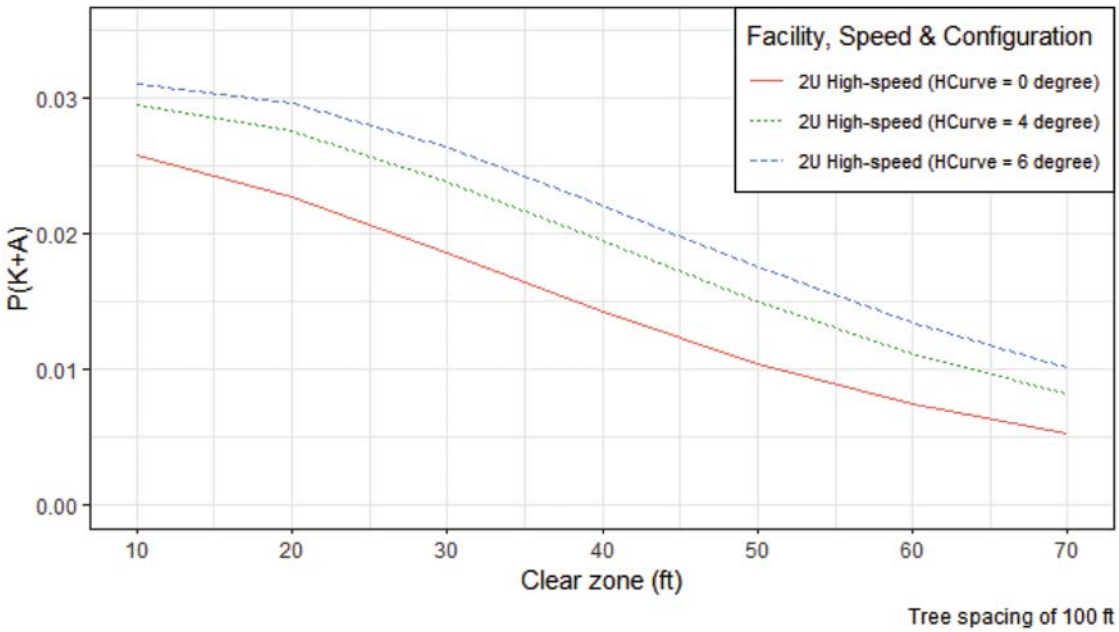

Figure 69. P(K+A) for 2U facility with varying horizontal alignments (HCurve) (flat).

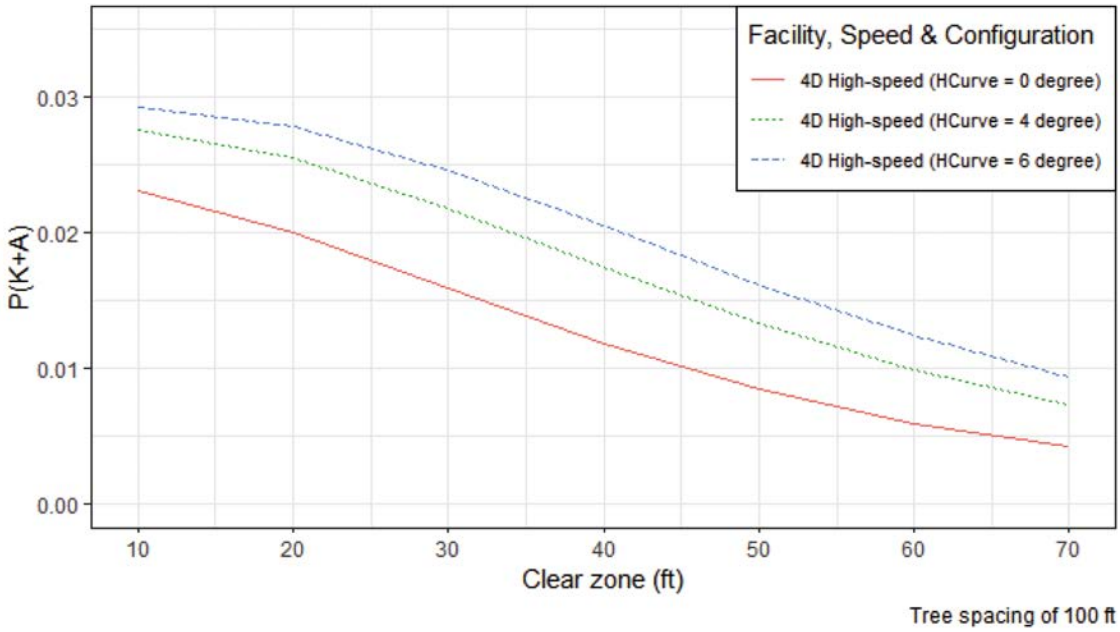

Figure 70. P(K+A) for 4D facility with varying horizontal alignments (HCurve) (flat).

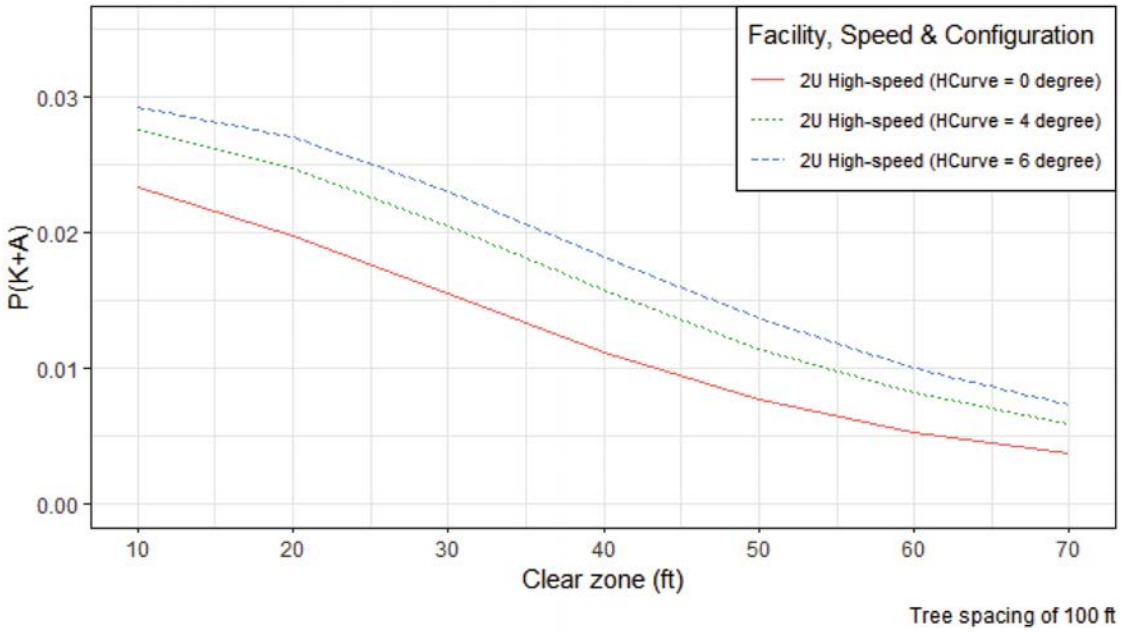

Figure 71. Probability of fatal/injury crash for 2U facility with varying horizontal alignments (HCurve) (moderate).

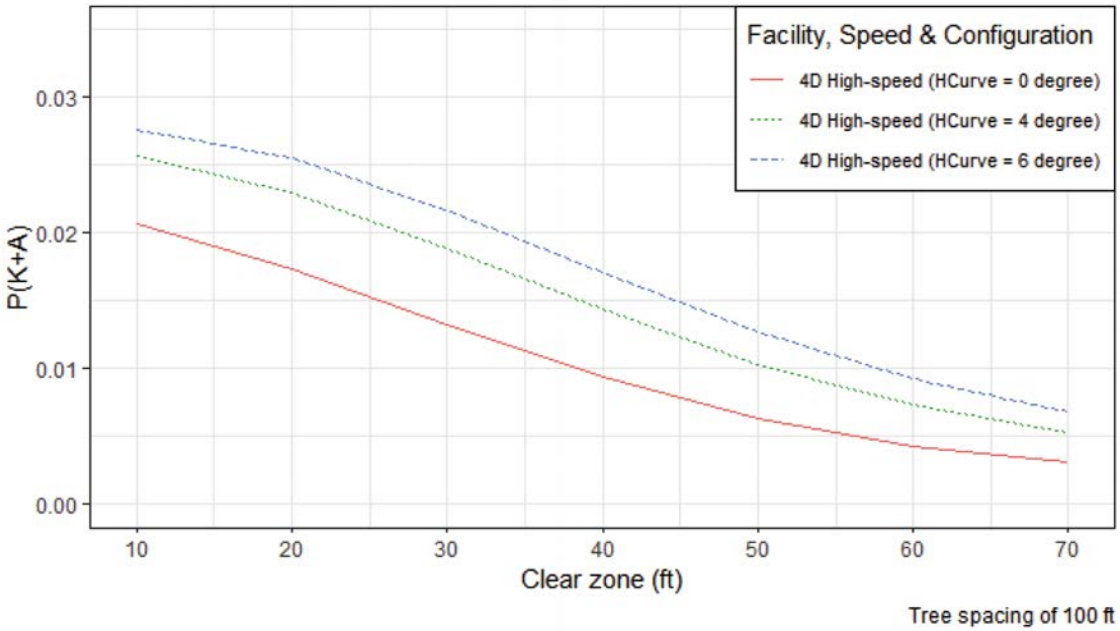

Figure 72. P(K+A) for 4D facility with varying horizontal alignments (HCurve) (moderate).

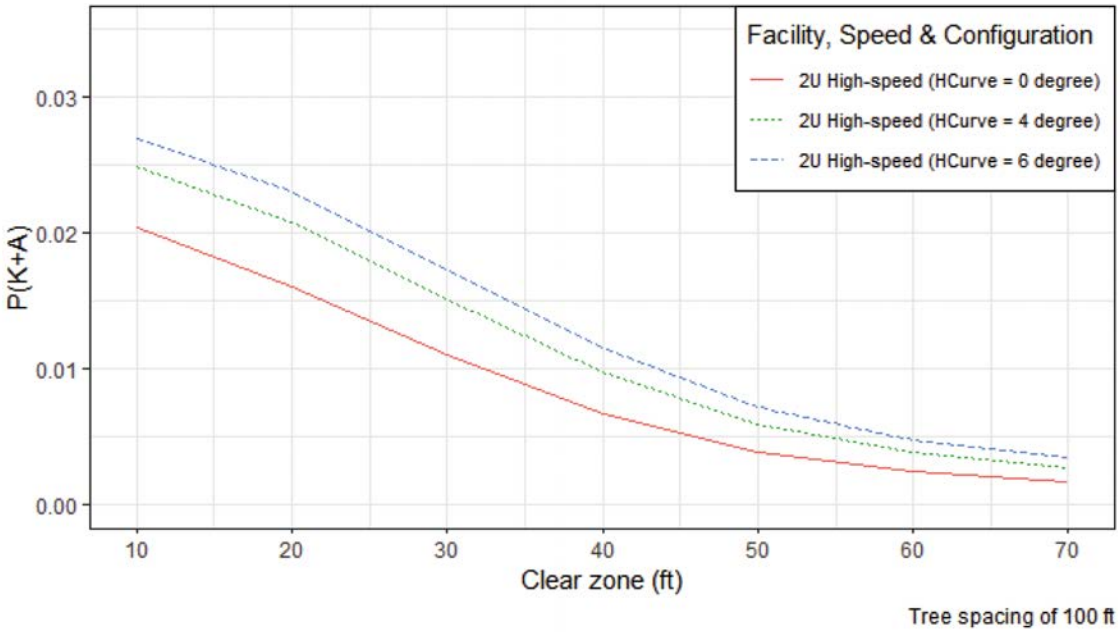

Figure 73. P(K+A) for 2U facility with varying horizontal alignments (HCurve) (steep).

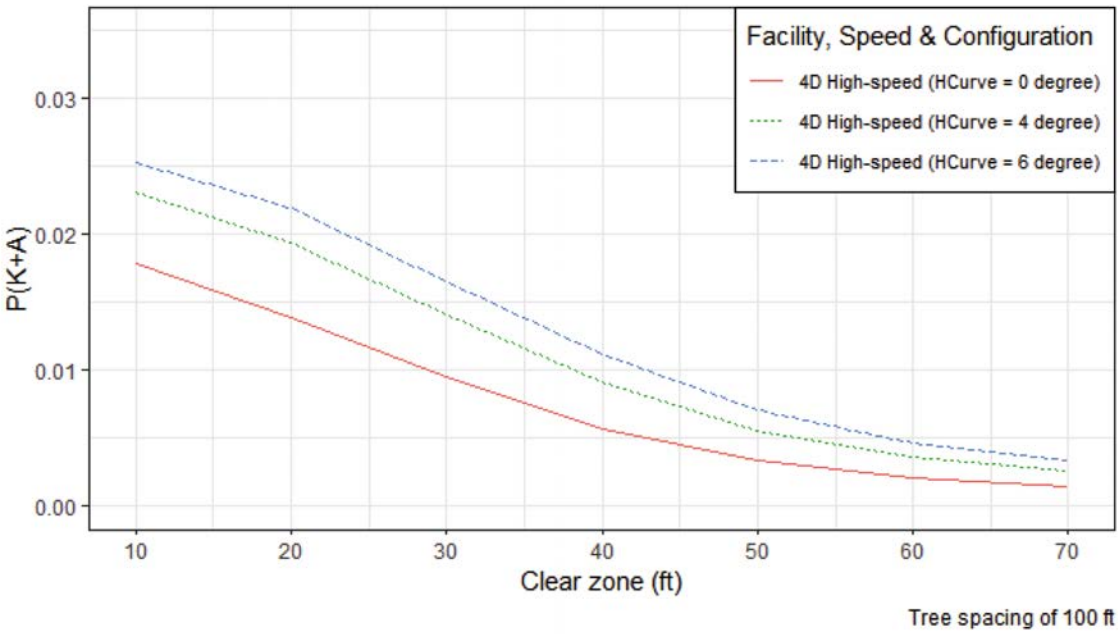

Figure 74. P(K+A) for 4D facility with varying horizontal alignments (HCurve) (steep).

associated with the highest P(K+A) across the entire clear zone distance spectrum. On the other hand, the tangent segments have the lowest P(K+A) values. Further, the 2U facilities have a slightly higher P(K+A) compared to 4D facilities, but the sensitivity [range of P(K+A)] is greater for 4D than 2U. Table 51 shows a significant percent difference for all terrain types, with the steep terrain on a 4D facility type having a difference of 76%.

Shoulder Width

The variation of P(K+A) with changes in shoulder width is presented in Figure 75 through Figure 80. As can be seen in these figures, the change in shoulder width over a range from 2 ft to 12 ft has only a small impact on the P(K+A) irrespective of the facility type or terrain configuration. The P(K+A) values are slightly higher for 2U facilities compared to 4D facilities.

Table 51. Sensitivity of P(K+A) at a 30-ft clear zone with respect to horizontal alignment (HCurve).

Case	Facility, Speed, and Configuration	P(K+A)	Difference
Case 1			
(Flat)	2U high-speed (HCurve = 6 deg/955 ft radius)	0.0264	41.5%
	2U high-speed (HCurve = 0)	0.0187	
	4D high-speed (HCurve = 6 deg/955 ft radius)	0.0246	54.4%
	4D high-speed (HCurve = 0)	0.0160	
Case 2			
(Moderate)	2U high-speed (HCurve = 6 deg/955 ft radius)	0.0231	48.9%
	2U high-speed (HCurve = 0)	0.0155	
	4D high-speed (HCurve = 6 deg/955 ft radius)	0.0217	64.8%
	4D high-speed (HCurve = 0)	0.0132	
Case 3			
(Steep)	2U high-speed (HCurve = 6 deg/955 ft radius)	0.0173	57.0%
	2U high-speed (HCurve = 0)	0.0110	
	4D high-speed (HCurve = 6 deg/955 ft radius)	0.0166	75.9%
	4D high-speed (HCurve = 0)	0.0094	

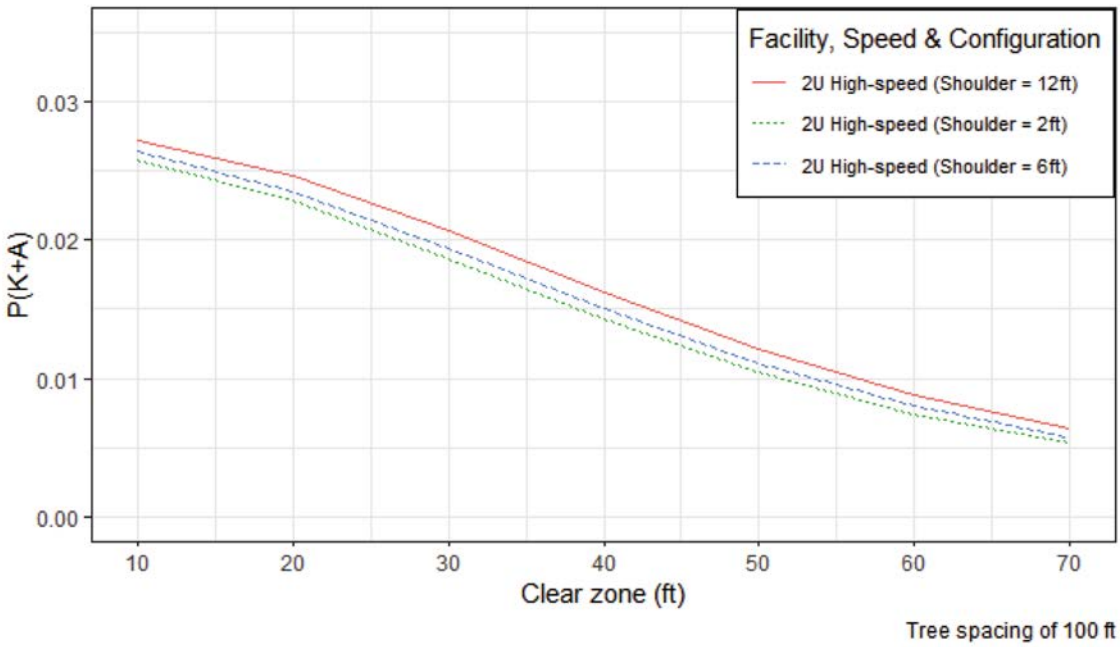

Figure 75. P(K+A) for 2U facility with varying shoulder widths (flat).

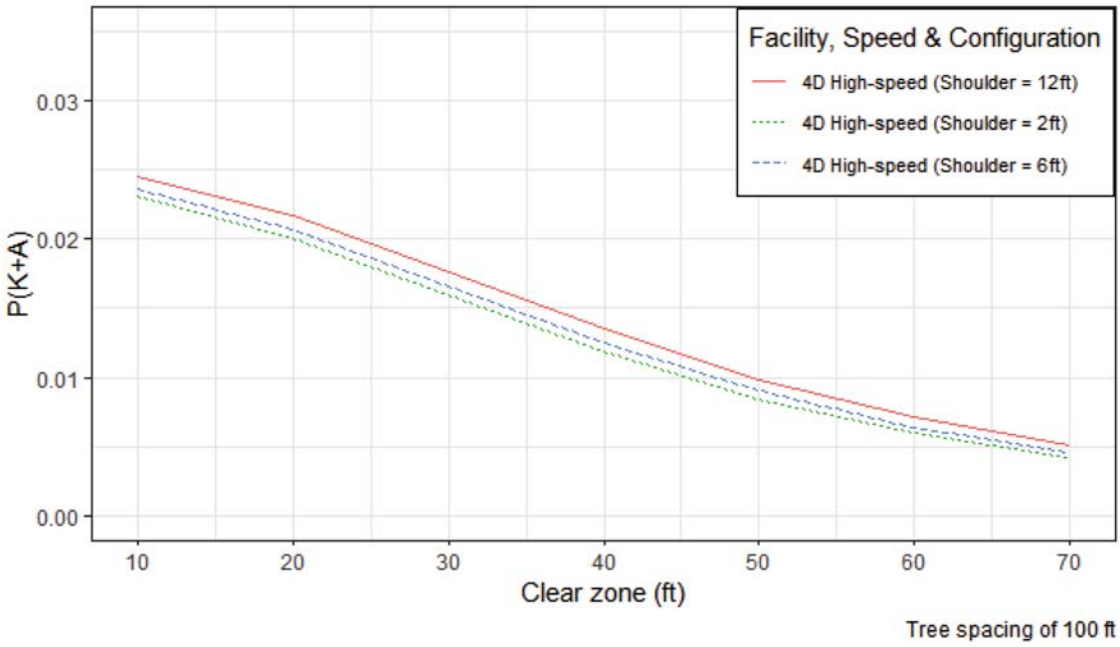

Figure 76. P(K+A) for 4D facility with varying shoulder widths (flat).

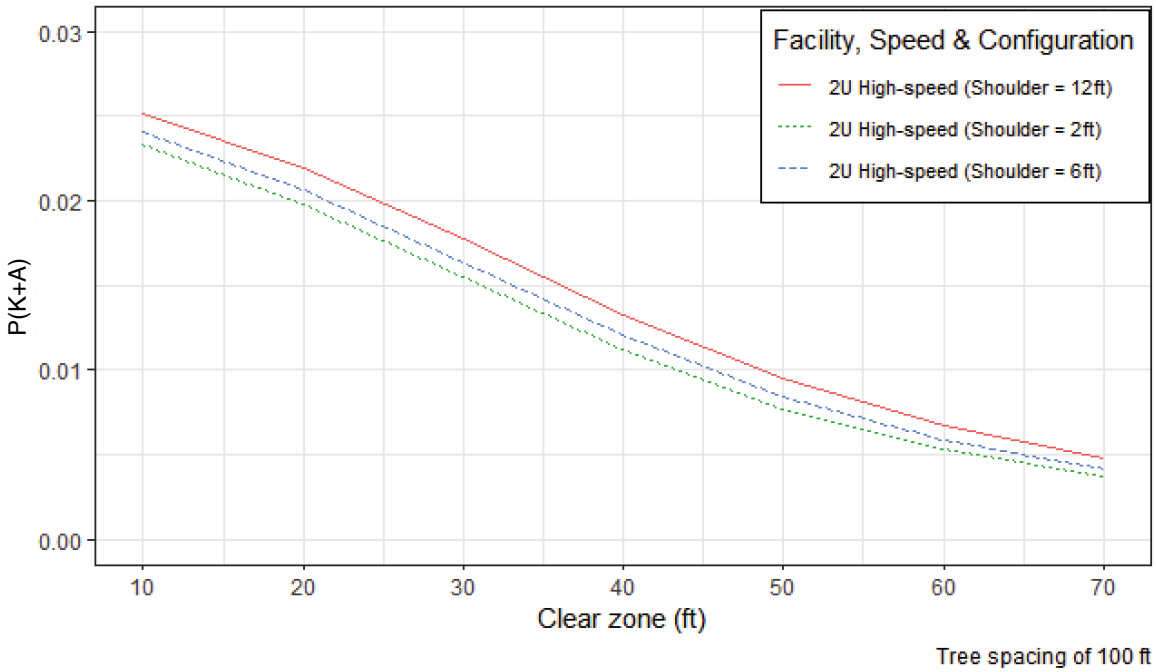

Figure 77. P(K+A) for 2U facility with varying shoulder widths (moderate).

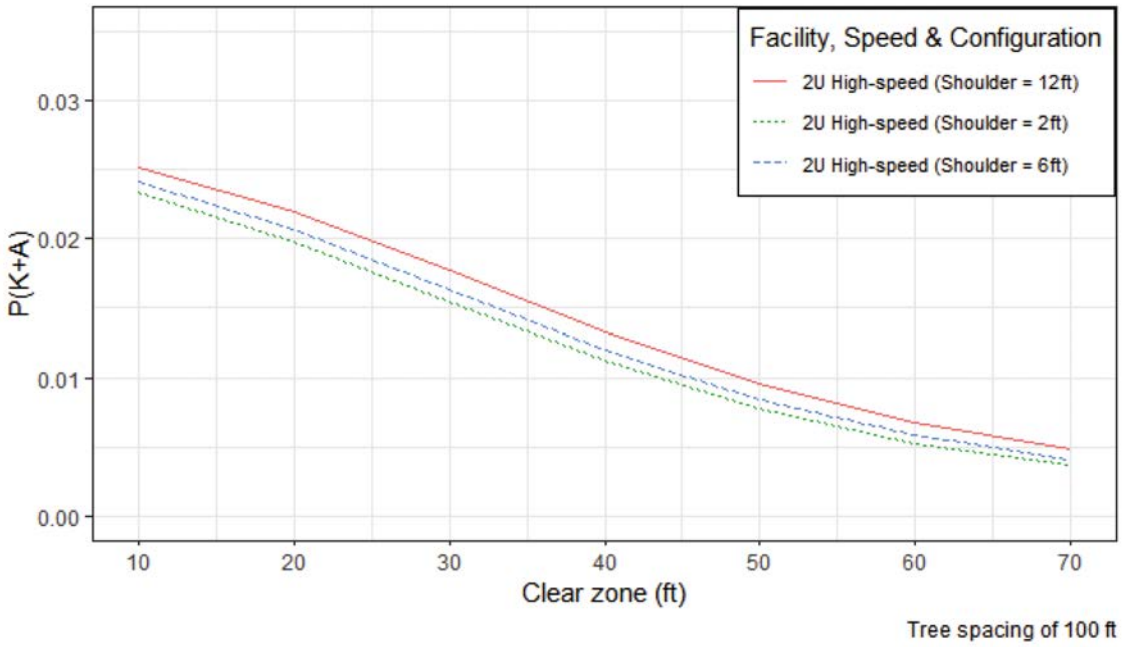

Figure 78. P(K+A) for 4D facility with varying shoulder widths (moderate).

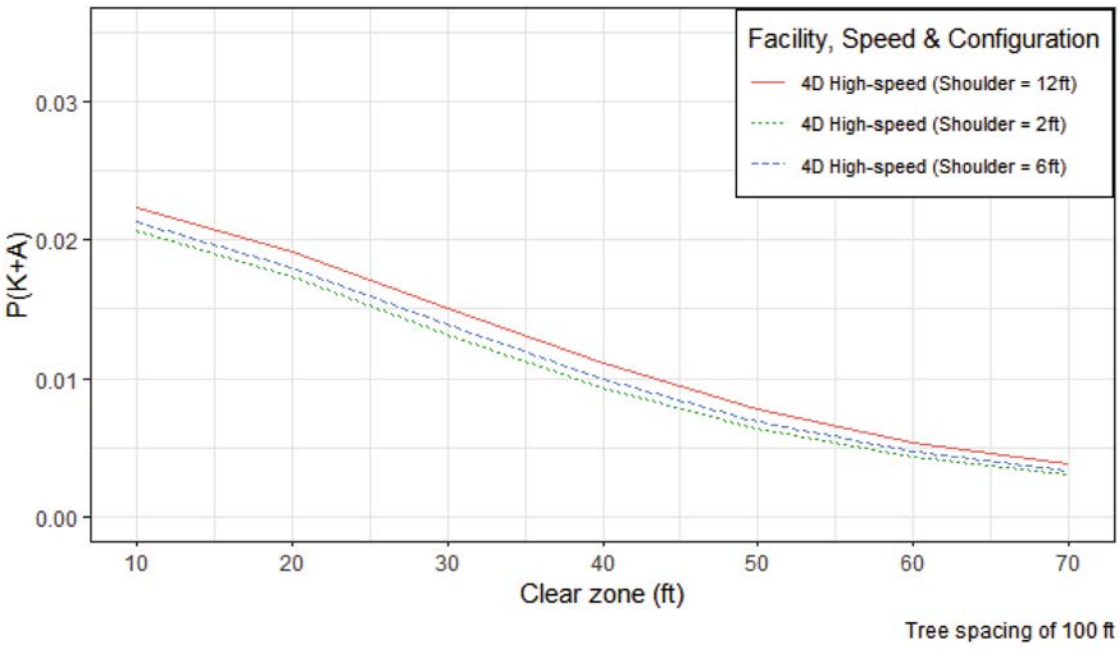

Figure 79. P(K+A) for 2U facility with varying shoulder widths (steep).

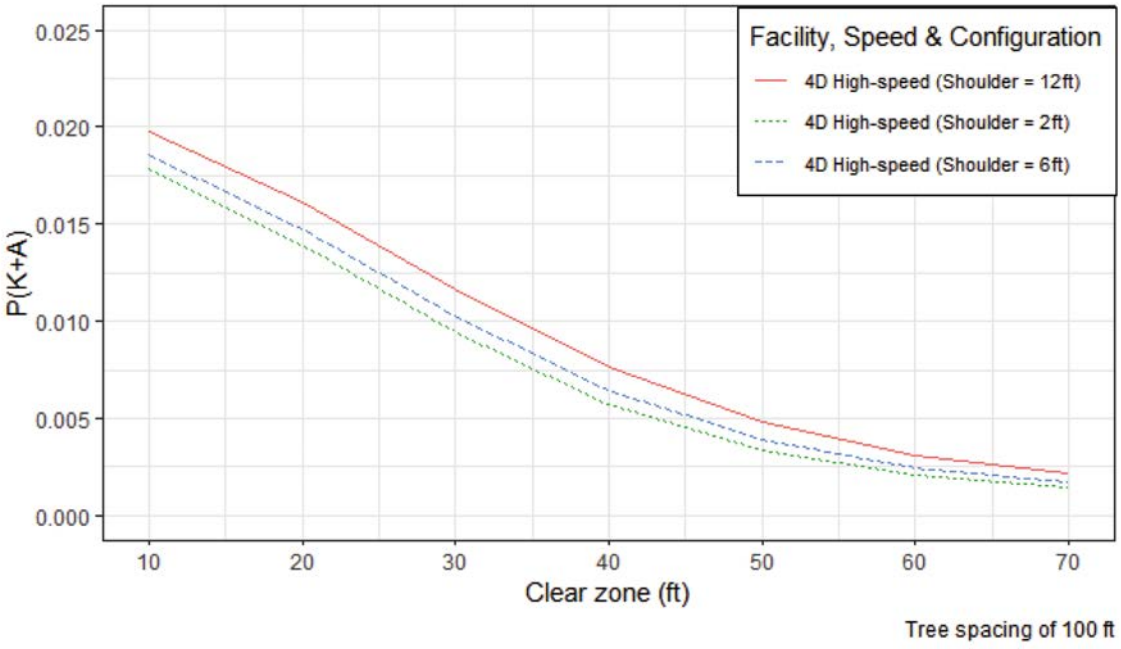

Figure 80. P(K+A) for 4D facility with varying shoulder widths (steep).

Table 52. Sensitivity of P(K+A) at a 30-ft clear zone with respect to shoulder widths.

Case	Facility, Speed, and Configuration	P(K+A)	Difference
Case 1 (Flat)	2U high-speed (shoulder width = 12 ft)	0.0206	10.5%
	2U high-speed (shoulder width = 2 ft)	0.0187	
	4D high-speed (shoulder width = 12 ft)	0.0177	10.6%
	4D high-speed (shoulder width = 2 ft)	0.0160	
Case 2 (Moderate)	2U high-speed (shoulder width = 12 ft)	0.0177	14.4%
	2U high-speed (shoulder width = 2 ft)	0.0155	
	4D high-speed (shoulder width = 12 ft)	0.0151	14.3%
	4D high-speed (shoulder width = 2 ft)	0.0132	
Case 3 (Steep)	2U high-speed (shoulder width = 12 ft)	0.0138	24.8%
	2U high-speed (shoulder width = 2 ft)	0.0110	
	4D high-speed (shoulder width = 12 ft)	0.0116	23.3%
	4D high-speed (shoulder width = 2 ft)	0.0094	

Table 52 shows the percent difference in P(K+A) values for the different facility types and terrain configurations at a clear zone distance of 30 ft. The highest variation of 24.8% occurs for the steep terrain.

Foreslope Ratio

Figure 81 through Figure 86 present the distribution of P(K+A) for varying foreslope ratios. Overall, steeper slopes have a lower impact on P(K+A). It can be observed that foreslope ratios of 1V:10H and 1V:6H have the smallest change, while the largest change in P(K+A) occurs between 1V:4H and 1V:3H slopes. Table 53 shows the largest relative difference (16.6%) is associated with the steep terrain case.

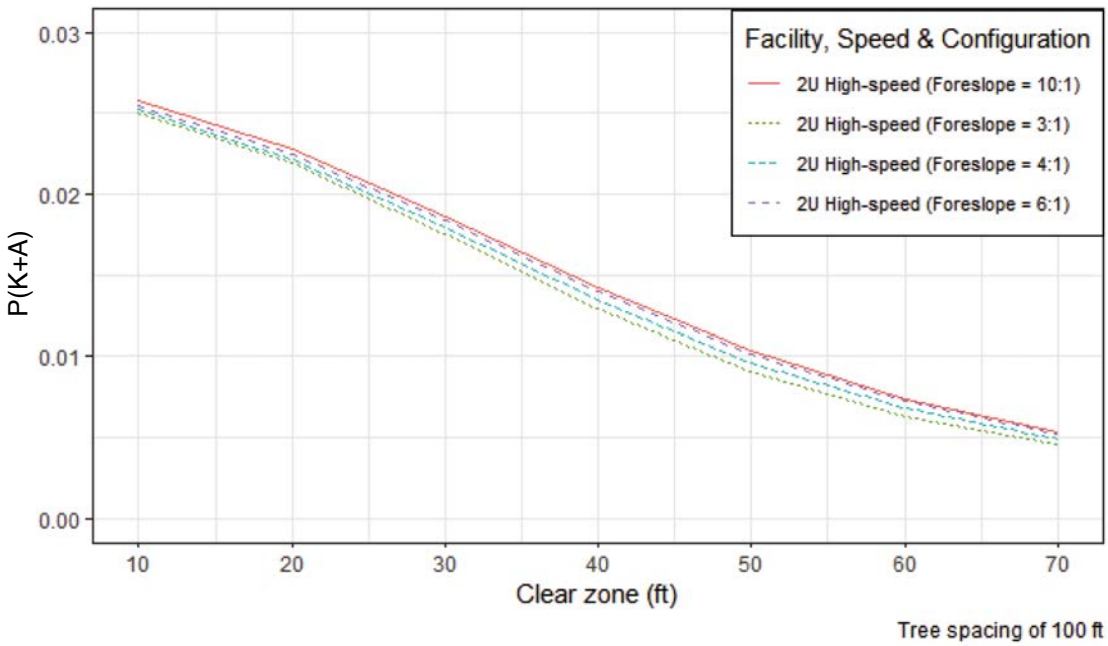

Figure 81. P(K+A) for 2U facility with varying foreslope ratio (flat).

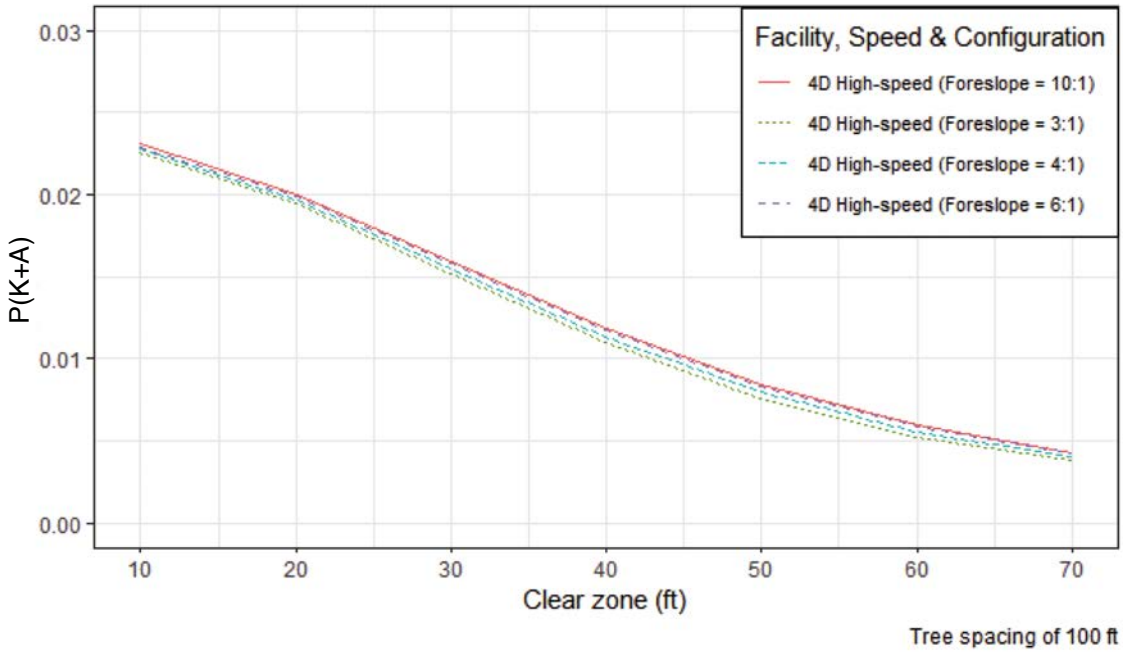

Figure 82. P(K+A) for 4D facility with varying foreslope ratio (flat).

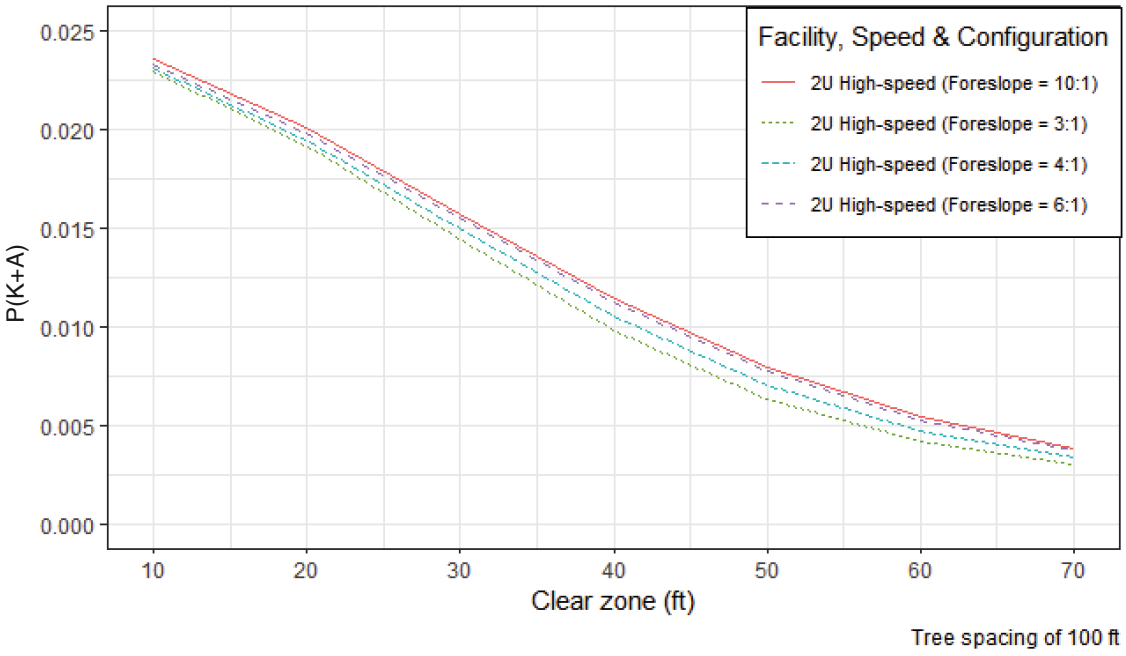

Figure 83. P(K+A) for 2U facility with varying foreslope ratio (moderate).

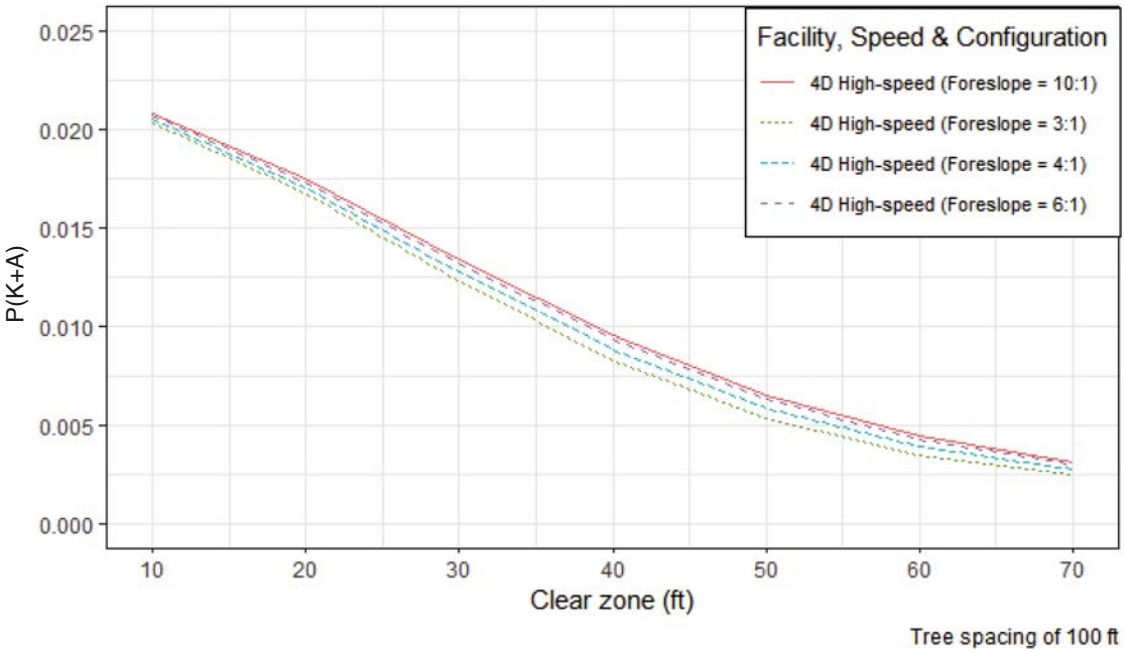

Figure 84. P(K+A) for 4D facility with varying foreslope ratio (moderate).

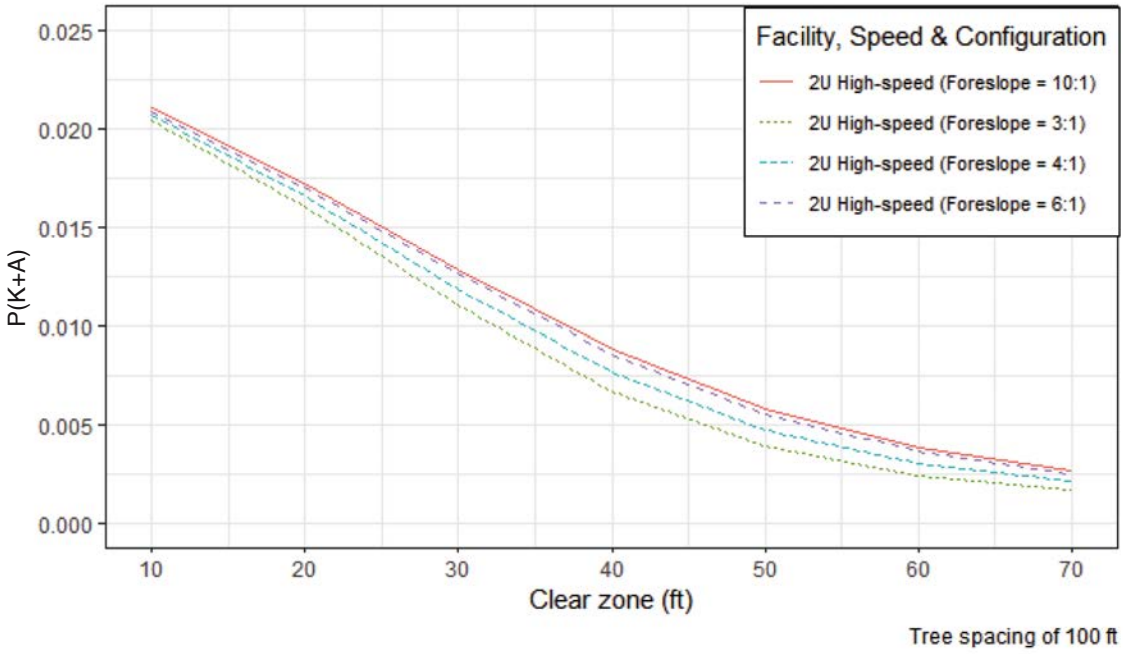

Figure 85. P(K+A) for 2U facility with varying foreslope ratio (steep).

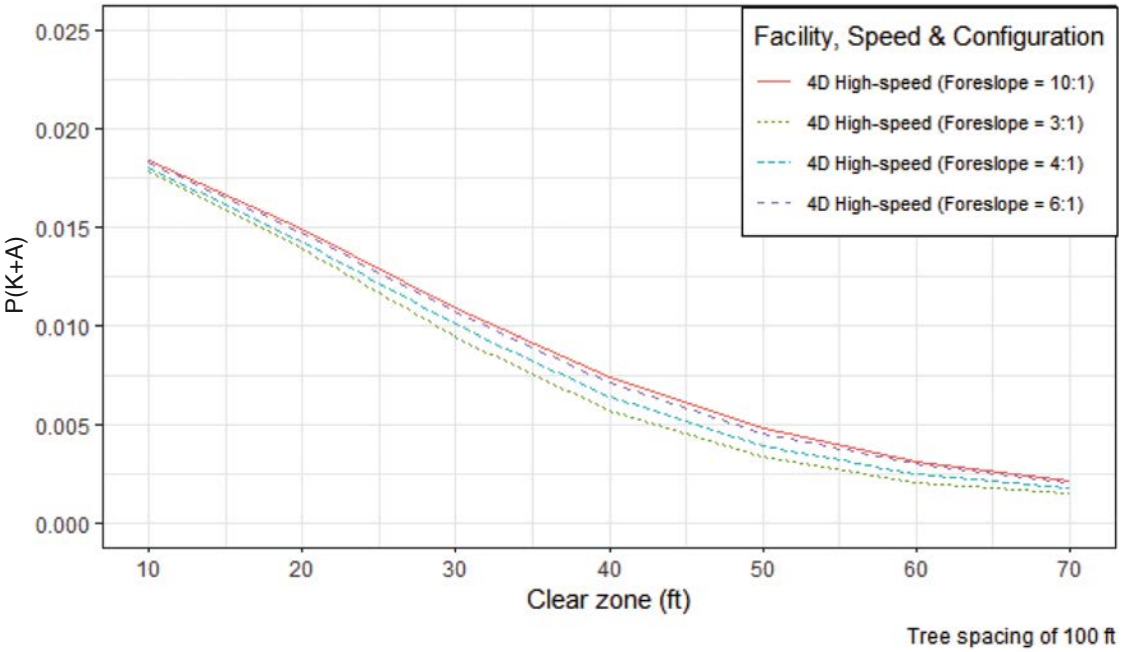

Figure 86. P(K+A) for 4D facility with varying foreslope ratio (steep).

Foreslope Width

As shown in Figure 87 through Figure 92, wider foreslopes are associated with higher P(K+A) irrespective of the facility type and terrain configuration. The differences in P(K+A) for the two facility types are relatively similar, but the 2U facility has a higher magnitude of P(K+A) compared to 4D facilities. Table 54 shows that 4D facilities have a relatively higher percent change in P(K+A), with the highest difference (27.6%) observed for the steep terrain.

Ditch Bottom Width

Figure 93 through Figure 98 show that wider ditch bottoms are associated with higher P(K+A) irrespective of facility type or terrain configuration. This is likely attributed to the

Table 53. Sensitivity of P(K+A) at a 30-ft clear zone with respect to foreslope ratio.

Case	Facility, Speed, and Configuration	P(K+A)	Difference
Case 1			
(Flat)	2U high-speed (foreslope = 1V:10H)	0.0187	6.3%
	2U high-speed (foreslope = 1V:3H)	0.0176	
	4D high-speed (foreslope = 1V:10H)	0.0160	4.9%
	4D high-speed (foreslope = 1V:3H)	0.0152	
Case 2			
(Moderate)	2U high-speed (foreslope = 1V:10H)	0.0157	9.2%
	2U high-speed (foreslope = 1V:3H)	0.0144	
	4D high-speed (foreslope = 1V:10H)	0.0133	8.1%
	4D high-speed (foreslope = 1V:3H)	0.0123	
Case 3			
(Steep)	2U high-speed (foreslope = 1V:10H)	0.0129	16.6%
	2U high-speed (foreslope = 1V:3H)	0.0110	
	4D high-speed (foreslope = 1V:10H)	0.0109	15.1%
	4D high-speed (foreslope = 1V:3H)	0.0094	

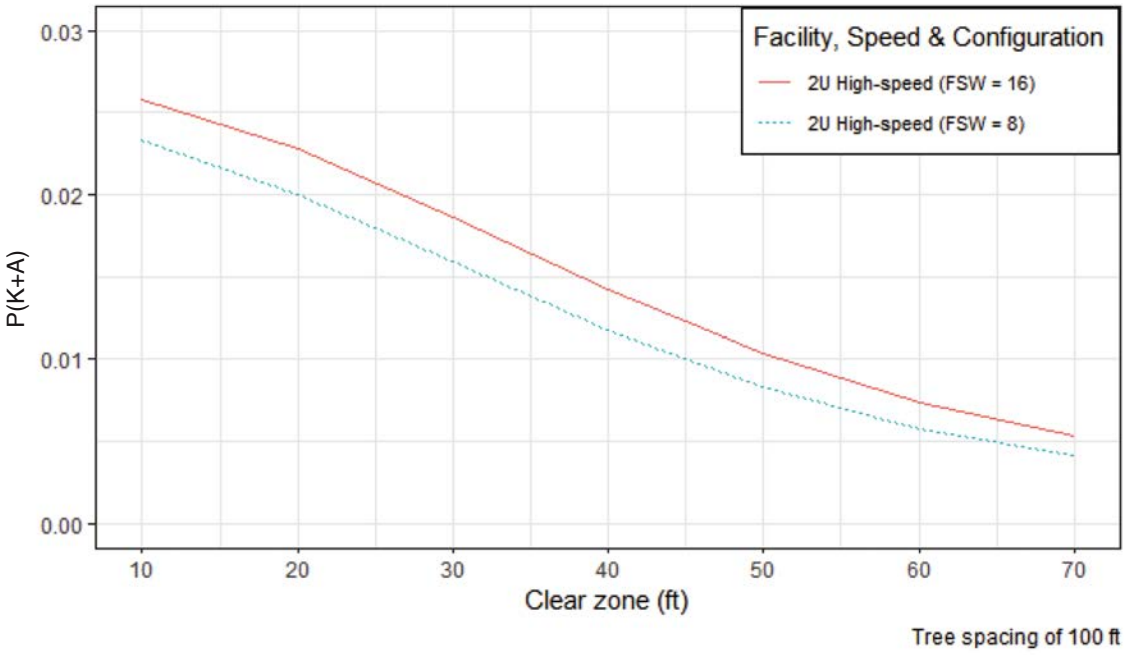

Figure 87. P(K+A) for 2U facility with varying foreslope widths (FSW) (flat).

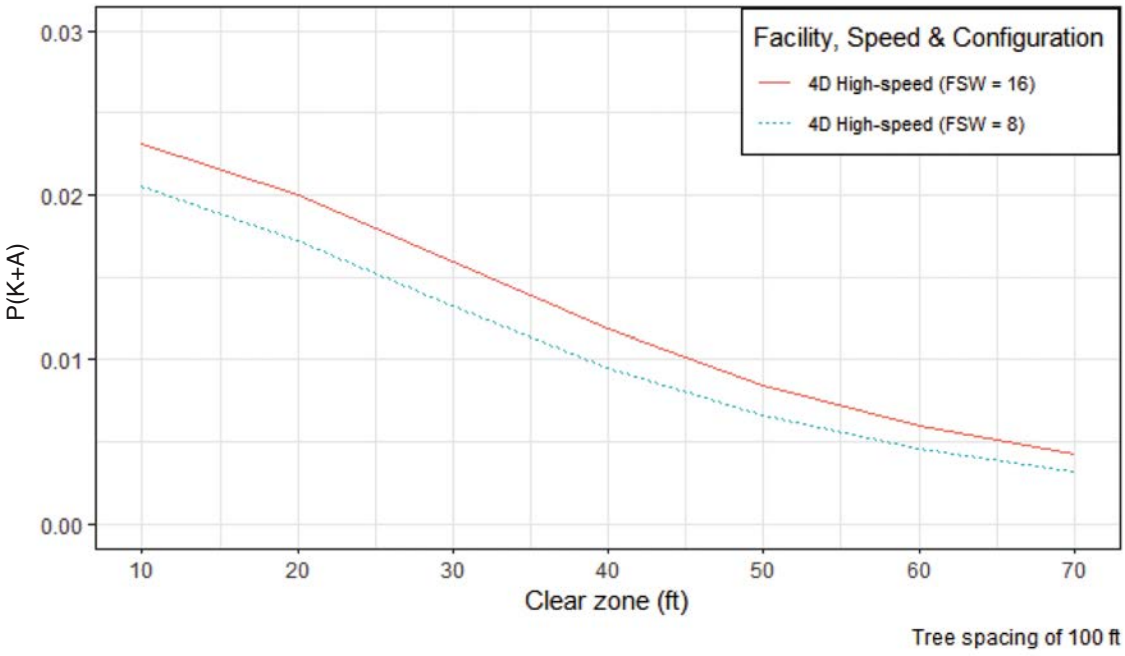

Figure 88. P(K+A) for 4D facility with varying foreslope widths (FSW) (flat).

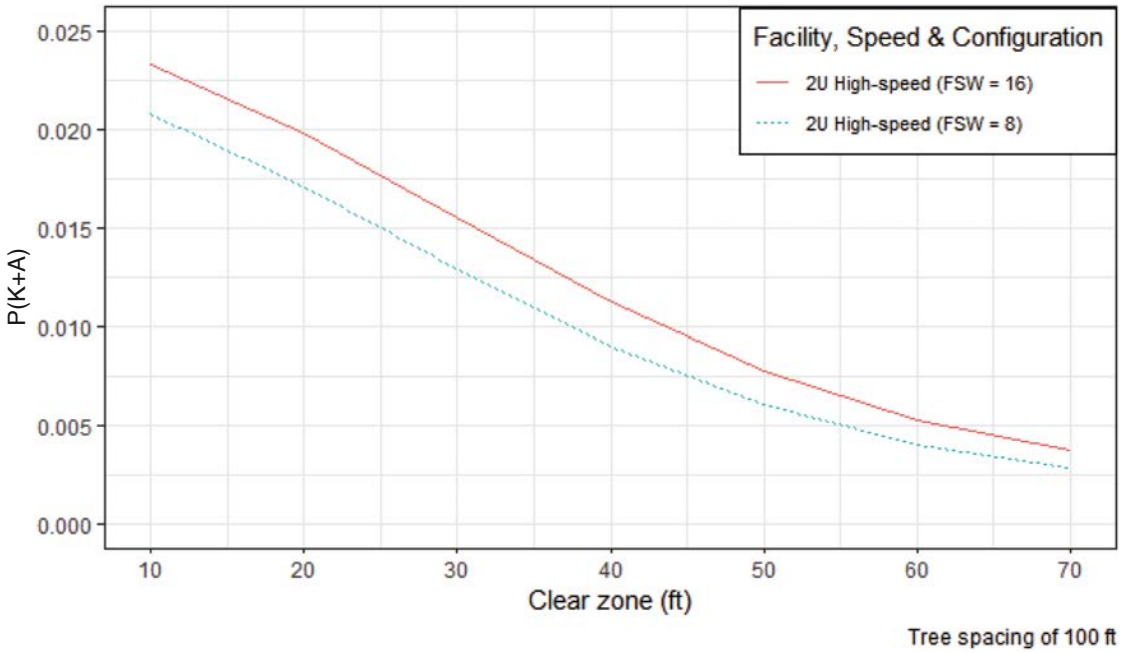

Figure 89. P(K+A) for 2U facility with varying foreslope widths (FSW) (moderate).

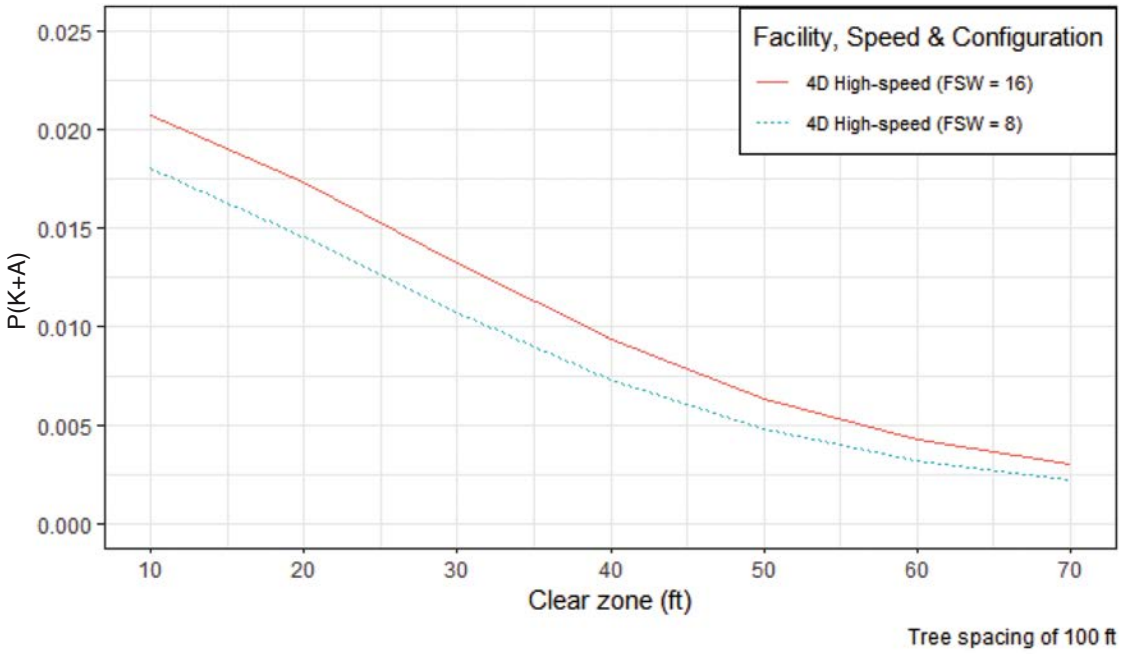

Figure 90. P(K+A) for 4D facility with varying foreslope widths (FSW) (moderate).

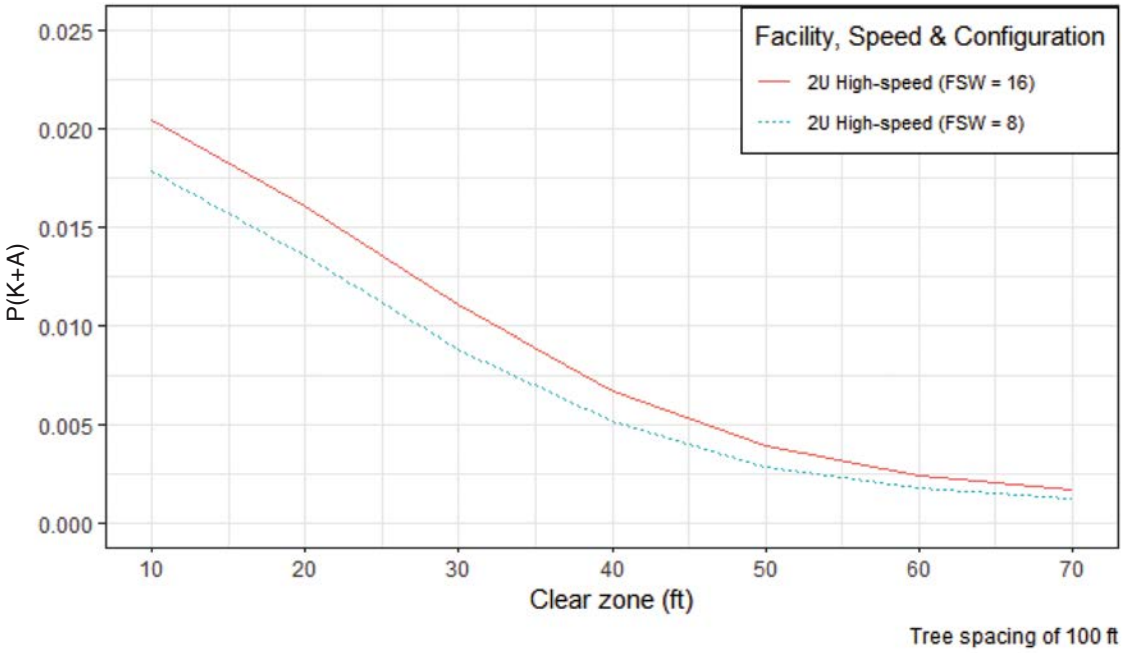

Figure 91. P(K+A) for 2U facility with varying foreslope widths (FSW) (steep).

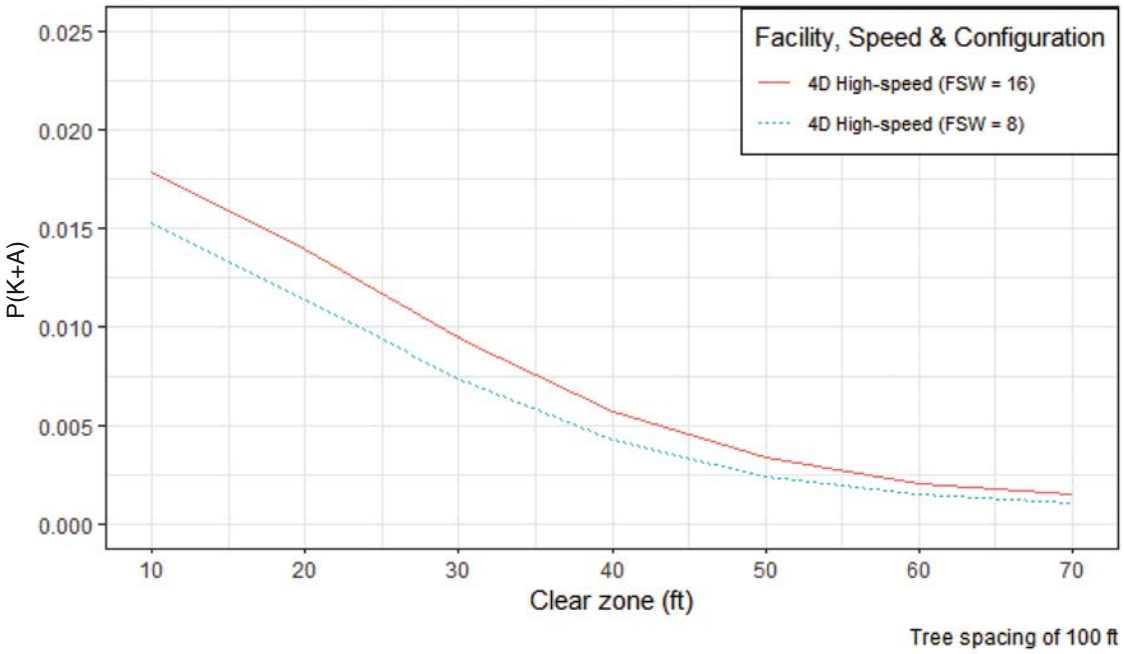

Figure 92. P(K+A) for 4D facility with varying foreslope widths (FSW) (steep).

Table 54. Sensitivity of P(K+A) at a 30-ft clear zone with respect to foreslope widths (FSW).

Case	Facility, Speed, and Configuration	P(K+A)	Difference
Case 1			
(Flat)	2U high-speed (FSW = 16 ft)	0.0187	17.5%
	2U high-speed (FSW = 8 ft)	0.0159	
	4D high-speed (FSW = 16 ft)	0.0160	20.6%
	4D high-speed (FSW = 8 ft)	0.0132	
Case 2			
(Moderate)	2U high-speed (FSW = 16 ft)	0.0155	19.9%
	2U high-speed (FSW = 8 ft)	0.0129	
	4D high-speed (FSW = 16 ft)	0.0132	23.1%
	4D high-speed (FSW = 8 ft)	0.0107	
Case 3			
(Steep)	2U high-speed (FSW = 16 ft)	0.0110	24.8%
	2U high-speed (FSW = 8 ft)	0.0089	
	4D high-speed (FSW = 16 ft)	0.0094	27.6%
	4D high-speed (FSW = 8 ft)	0.0074	

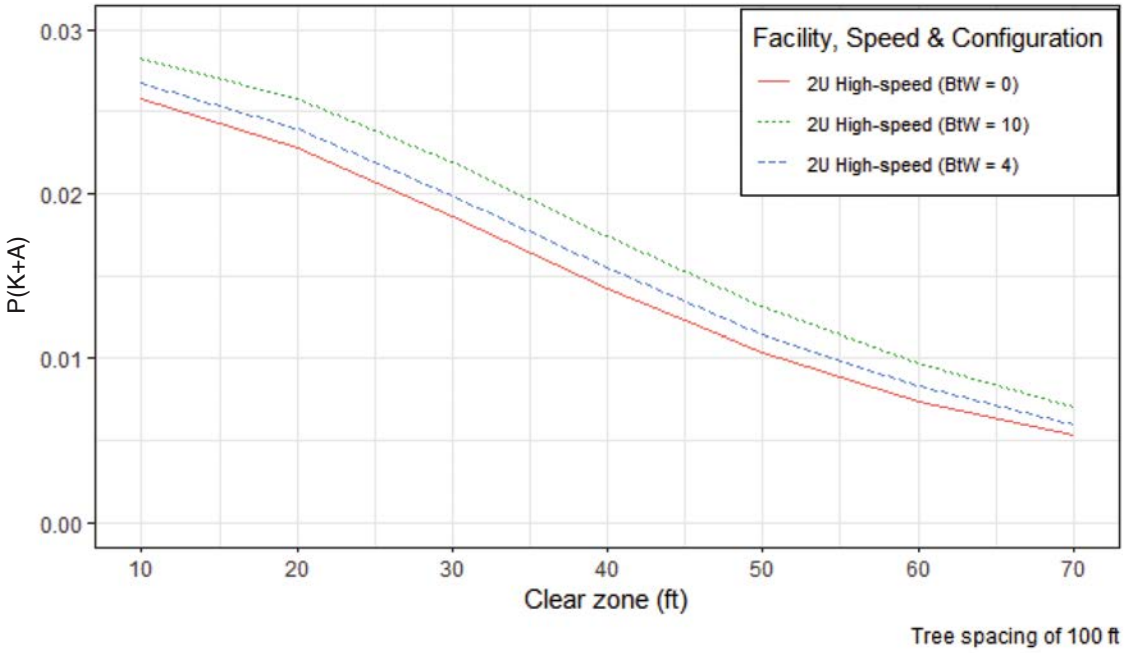

Figure 93. P(K+A) for 2U facility with varying ditch bottom widths (BtW) (flat).

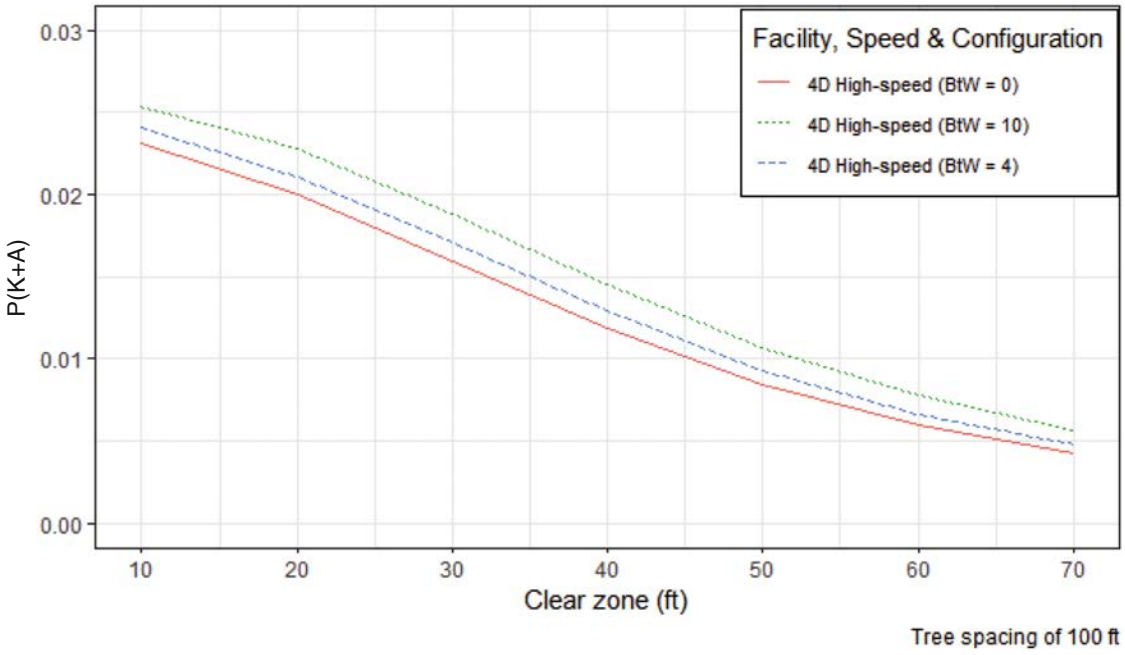

Figure 94. P(K+A) for 4D facility with varying ditch bottom widths (BtW) (flat).

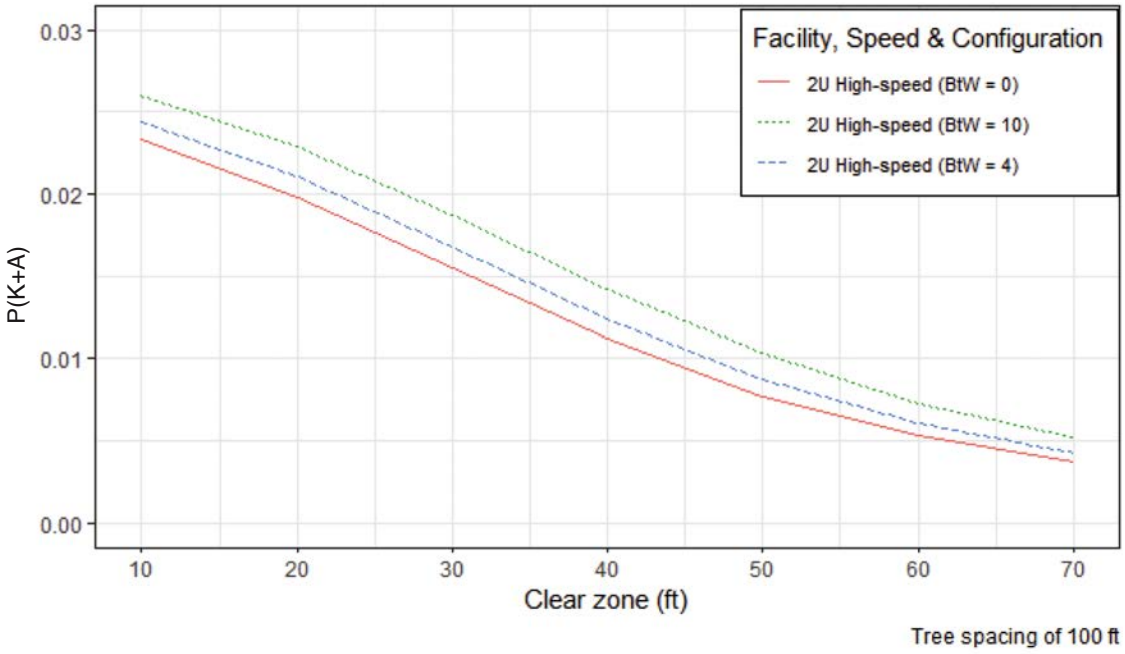

Figure 95. P(K+A) for 2U facility with varying ditch bottom widths (BtW) (moderate).

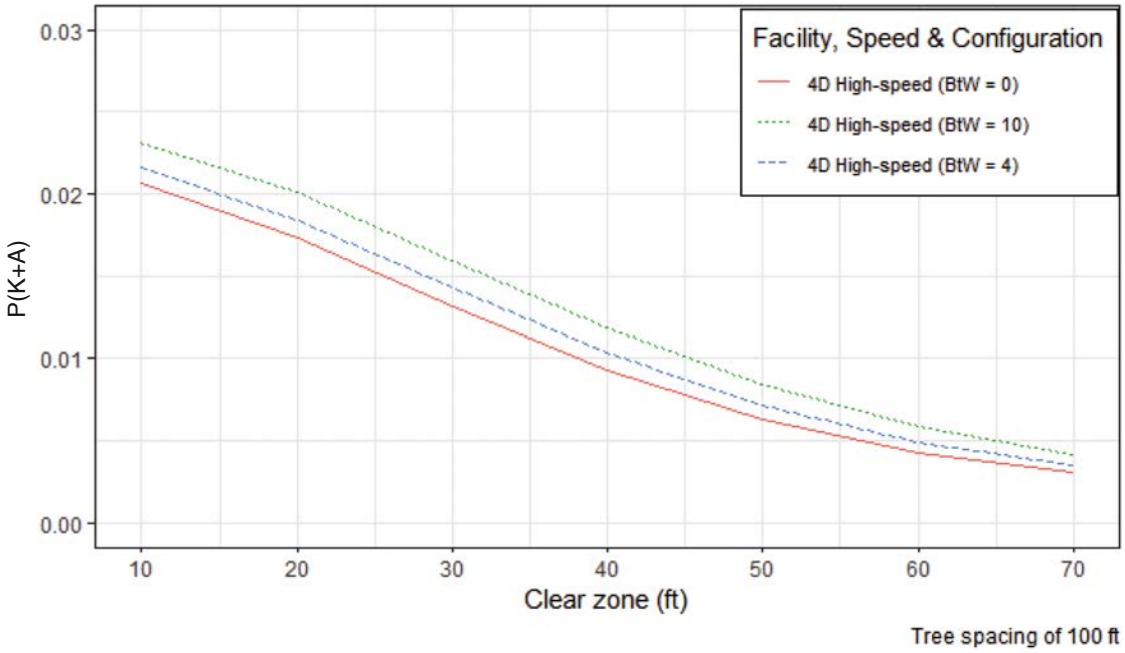

Figure 96. P(K+A) for 4D facility with varying ditch bottom widths (BtW) (moderate).

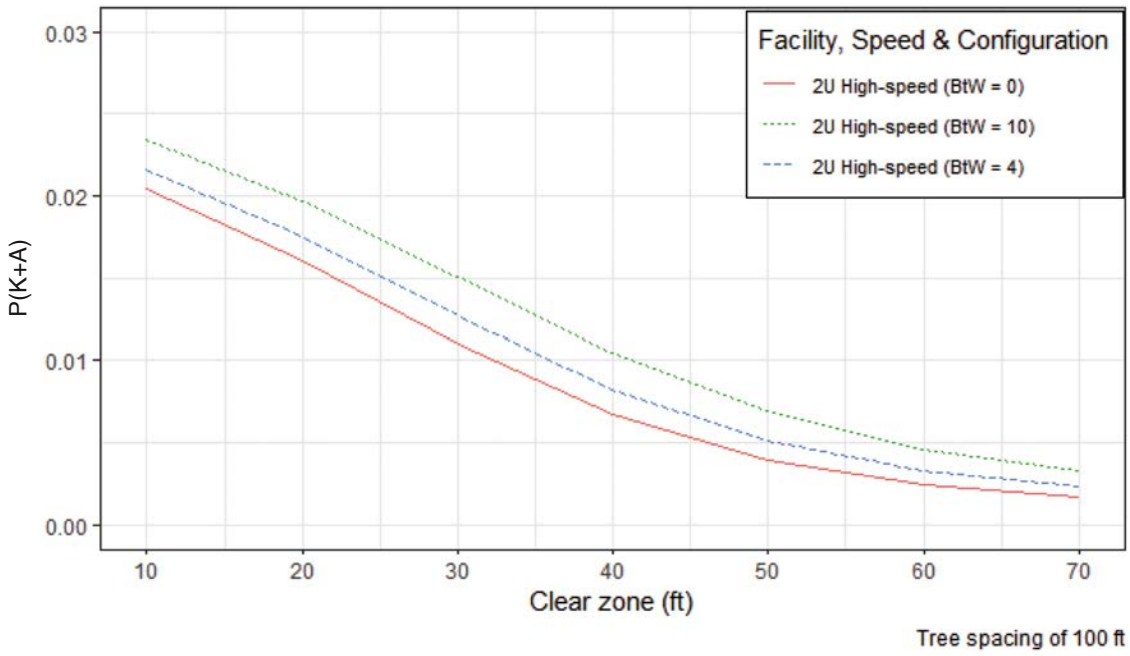

Figure 97. P(K+A) for 2U facility with varying ditch bottom widths (BtW) (steep).

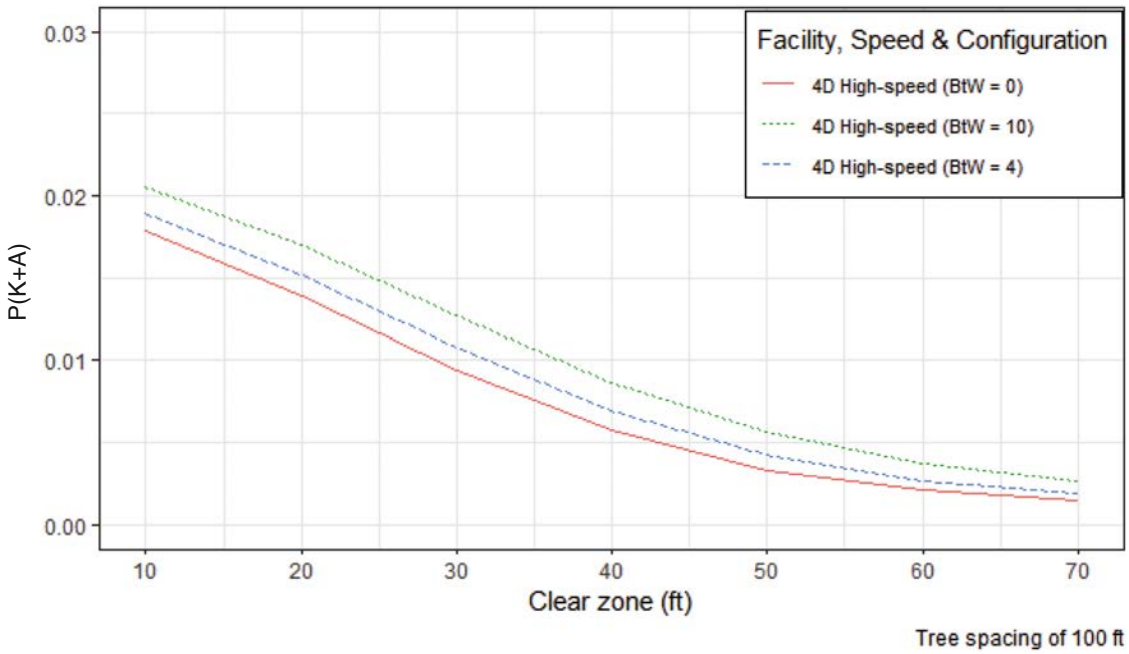

Figure 98. P(K+A) for 4D facility with varying ditch bottom widths (BtW) (steep).

vehicle maintaining more speed based on the further offset of the backslope. The lowest values of P(K+A) are obtained for the V-ditch profiles (BtW = 0). Table 55 shows a 36.2% difference in P(K+A) values at a 30-ft clear zone distance for the steep terrain case.

Backslope Ratio

Figure 99 through Figure 104 show that flatter backslope ratios have higher P(K+A) compared to steeper backslopes. This is likely attributed to a steeper backslope producing a greater reduction in vehicle speed prior to impacting an obstacle at the clear zone edge. Additionally, the sensitivity results in Table 56 show significant differences in P(K+A) with changes in the backslope ratio with the highest change (61.1%) occurring for the steep terrain case.

Table 55. Sensitivity of P(K+A) at a 30-ft clear zone with respect to ditch bottom widths (BtW).

Case	Facility, Speed, and Configuration	P(K+A)	Difference
Case 1			
(Flat)	2U high-speed (BtW = 10 ft)	0.0219	17.4%
	2U high-speed (BtW = 0)	0.0187	
	4D high-speed (BtW = 10 ft)	0.0188	17.8%
	4D high-speed (BtW = 0)	0.0160	
Case 2			
(Moderate)	2U high-speed (BtW = 10 ft)	0.0187	20.8%
	2U high-speed (BtW = 0)	0.0155	
	4D high-speed (BtW = 10 ft)	0.0160	21.1%
	4D high-speed (BtW = 0)	0.0132	
Case 3			
(Steep)	2U high-speed (BtW = 10 ft)	0.0150	36.2%
	2U high-speed (BtW = 0)	0.0110	
	4D high-speed (BtW = 10 ft)	0.0127	34.2%
	4D high-speed (BtW = 0)	0.0094	

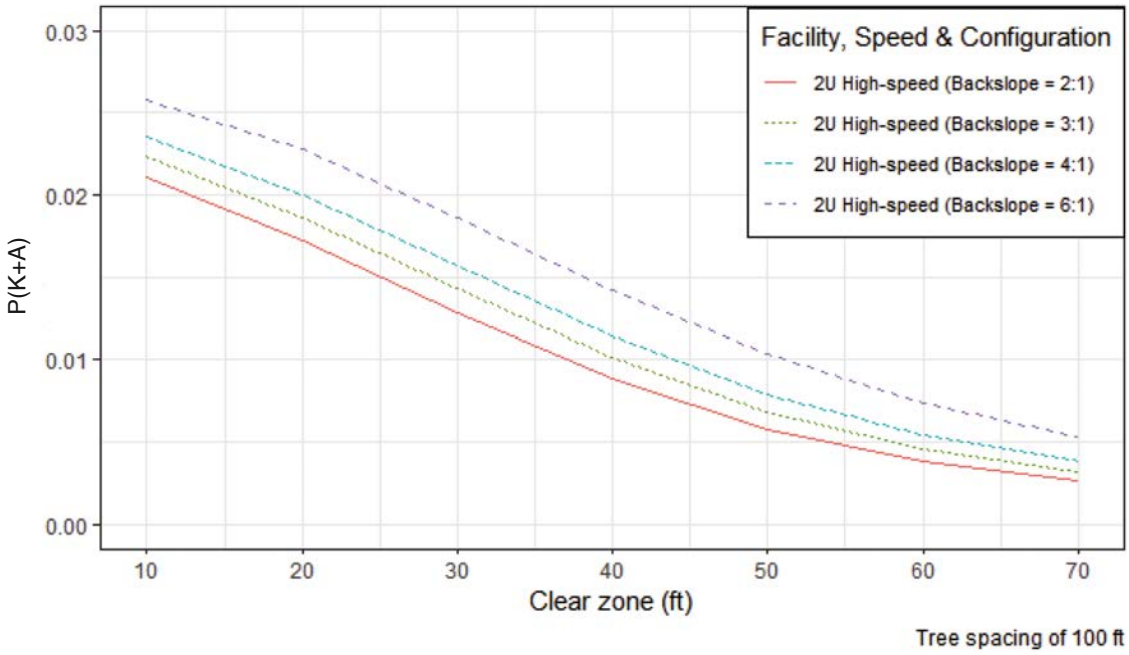

Figure 99. P(K+A) for 2U facility with varying backslope ratio (flat).

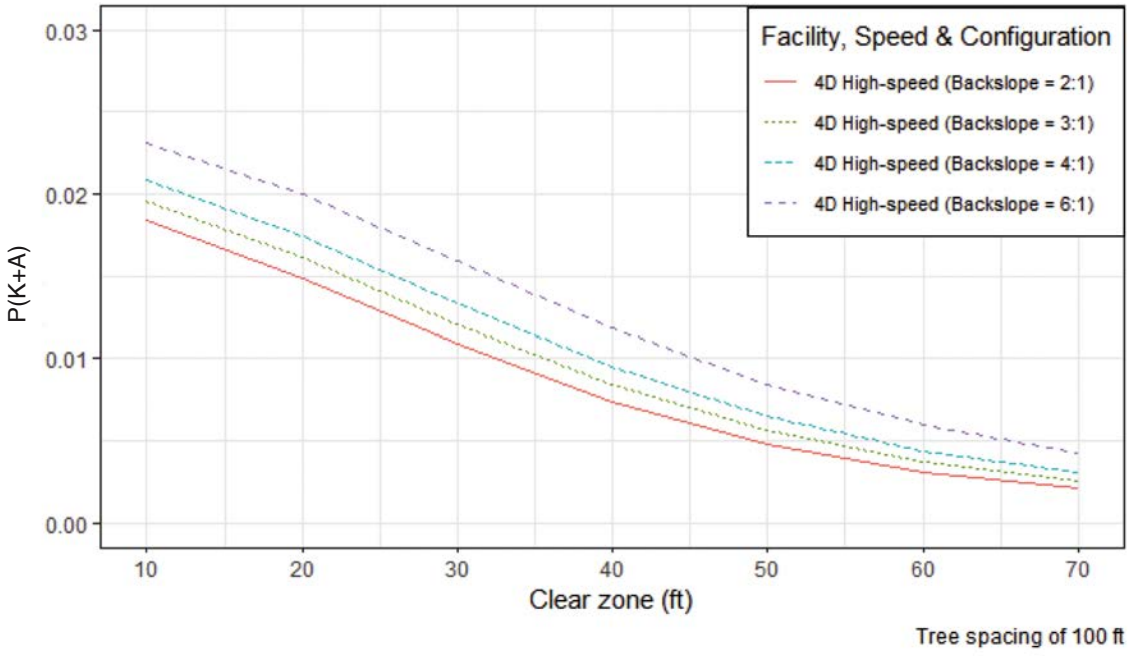

Figure 100. P(K+A) for 4D facility with varying backslope ratio (flat).

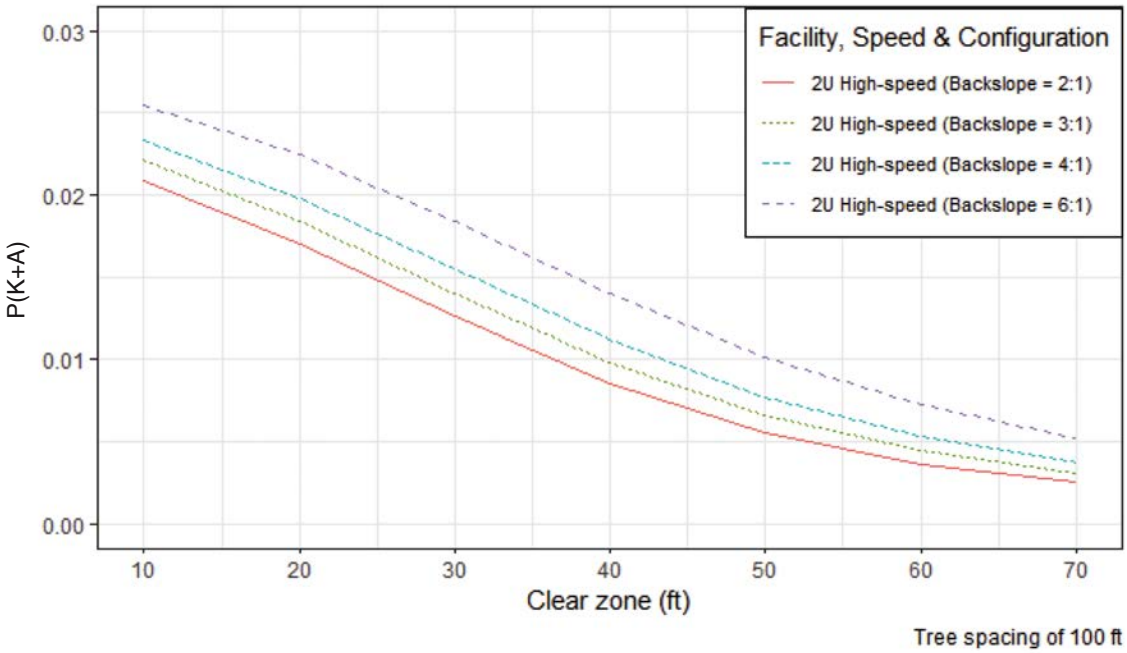

Figure 101. P(K+A) for 2U facility with varying backslope ratio (moderate).

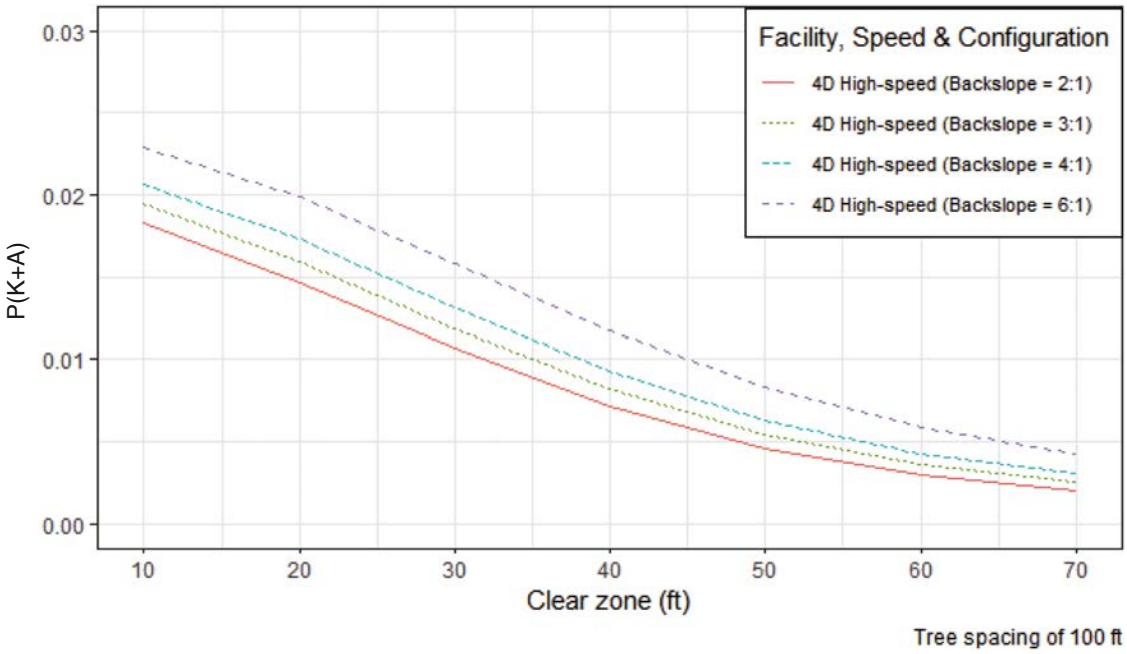

Figure 102. P(K+A) for 4D facility with varying backslope ratio (moderate).

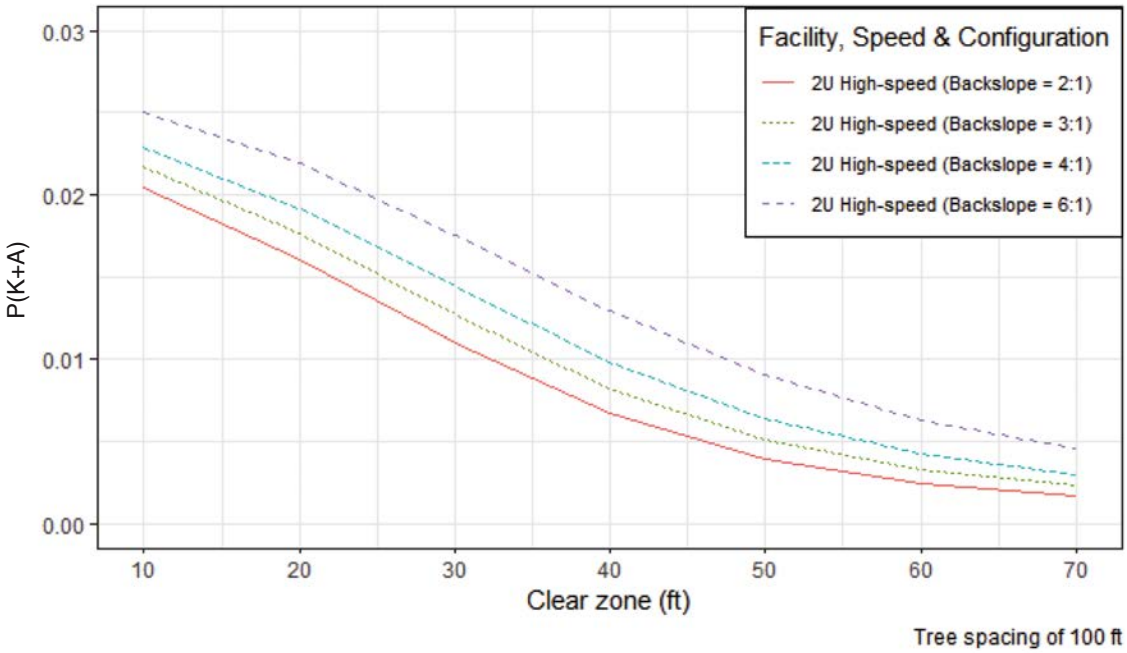

Figure 103. P(K+A) for 2U facility with varying backslope ratio (steep).

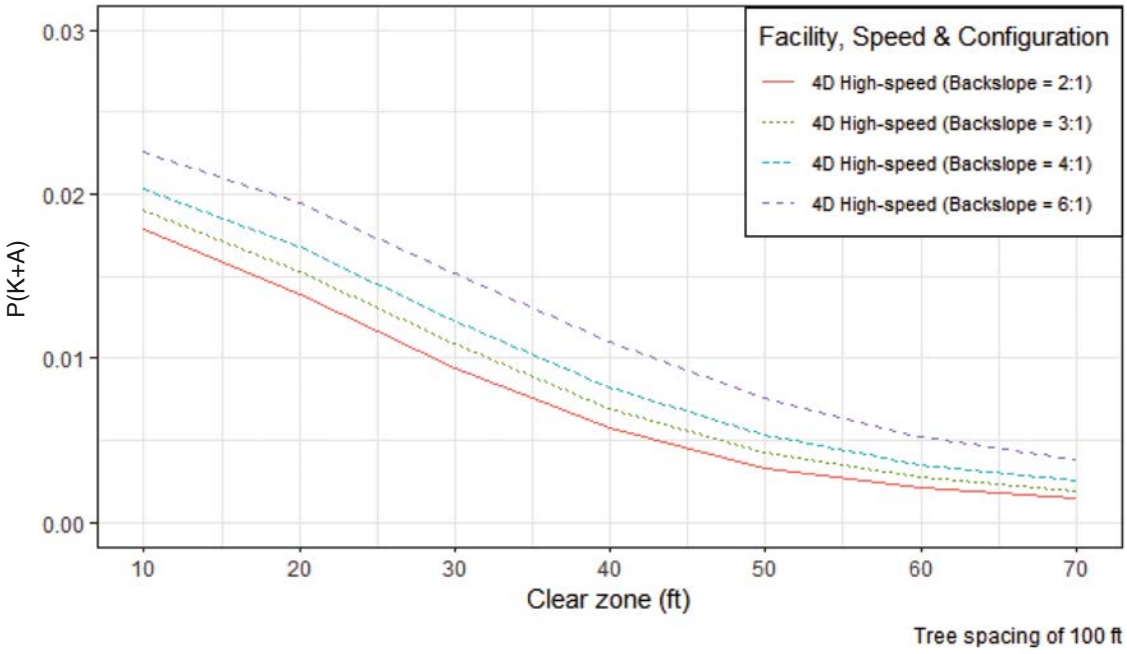

Figure 104. P(K+A) for 4D facility with varying backslope ratio (steep).

Table 56. Sensitivity of P(K+A) at a 30-ft clear zone with respect to backslope ratio.

Case	Facility, Speed, and Configuration	P(K+A)	Difference
Case 1			
(Flat)	2U high-speed (backslope ratio = 1V:6H)	0.0187	44.9%
	2U high-speed (backslope ratio = 1V:2H)	0.0129	
	4D high-speed (backslope ratio = 1V:6H)	0.0160	46.8%
	4D high-speed (backslope ratio = 1V:2H)	0.0109	
Case 2			
(Moderate)	2U high-speed (backslope ratio = 1V:6H)	0.0184	45.6%
	2U high-speed (backslope ratio = 1V:2H)	0.0126	
	4D high-speed (backslope ratio = 1V:6H)	0.0158	48.5%
	4D high-speed (backslope ratio = 1V:2H)	0.0107	
Case 3			
(Steep)	2U high-speed (backslope ratio = 1V:6H)	0.0176	59.0%
	2U high-speed (backslope ratio = 1V:2H)	0.0110	
	4D high-speed (backslope ratio = 1V:6H)	0.0152	61.1%
	4D high-speed (backslope ratio = 1V:2H)	0.0094	

Backslope Width

The variation of P(K+A) with changes in backslope width is presented in Figure 105 through Figure 110. As can be seen in these figures, the changes in P(K+A) associated with backslope widths of 8 ft and 16 ft are consistently small. As shown in Table 57, the maximum percent difference in P(K+A) for backslope widths analyzed is less than 10%.

Summary

An analysis was performed to investigate the relative sensitivity of parameters—such as impact speed percentile, impact angle percentile, and tree spacing—on the risk of a fatal or serious injury crash [P(K+A)]. As anticipated, it was found that the P(K+A) is highly sensitive to these parameters.

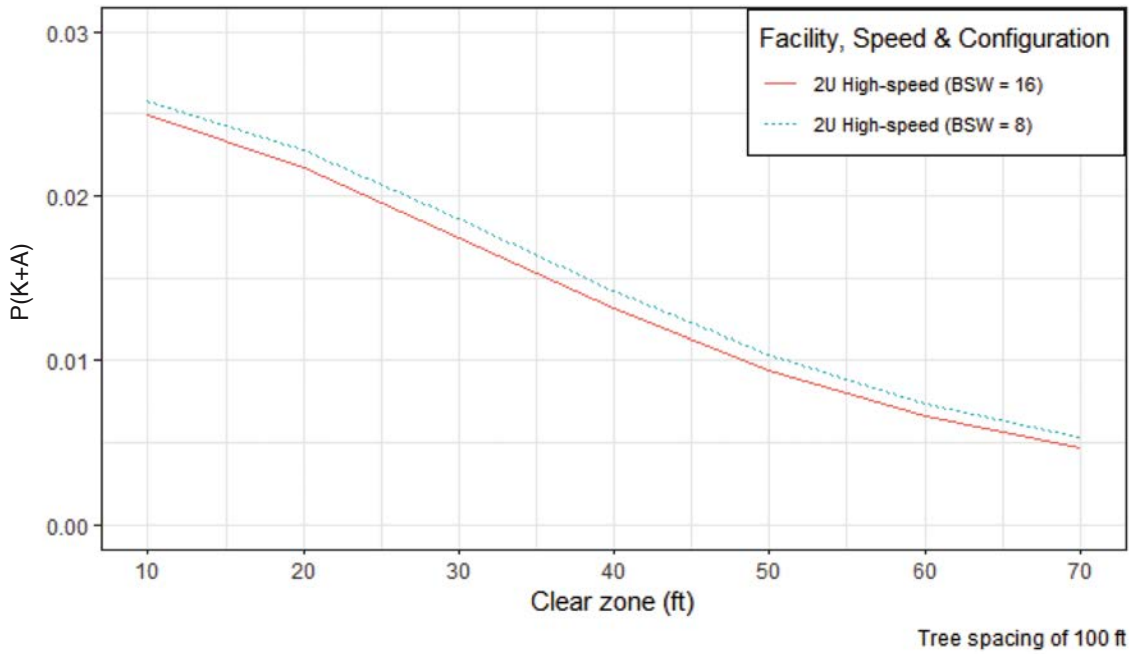

Figure 105. P(K+A) for 2U facility with varying backslope widths (BSW) (flat).

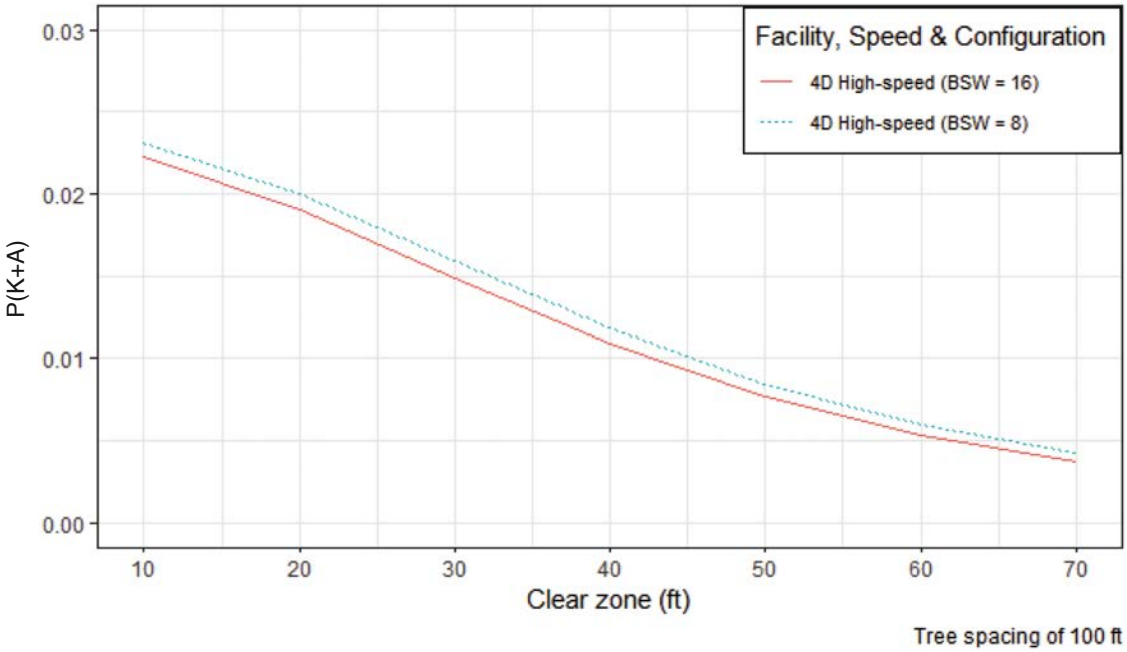

Figure 106. P(K+A) for 4D facility with varying backslope widths (BSW) (flat).

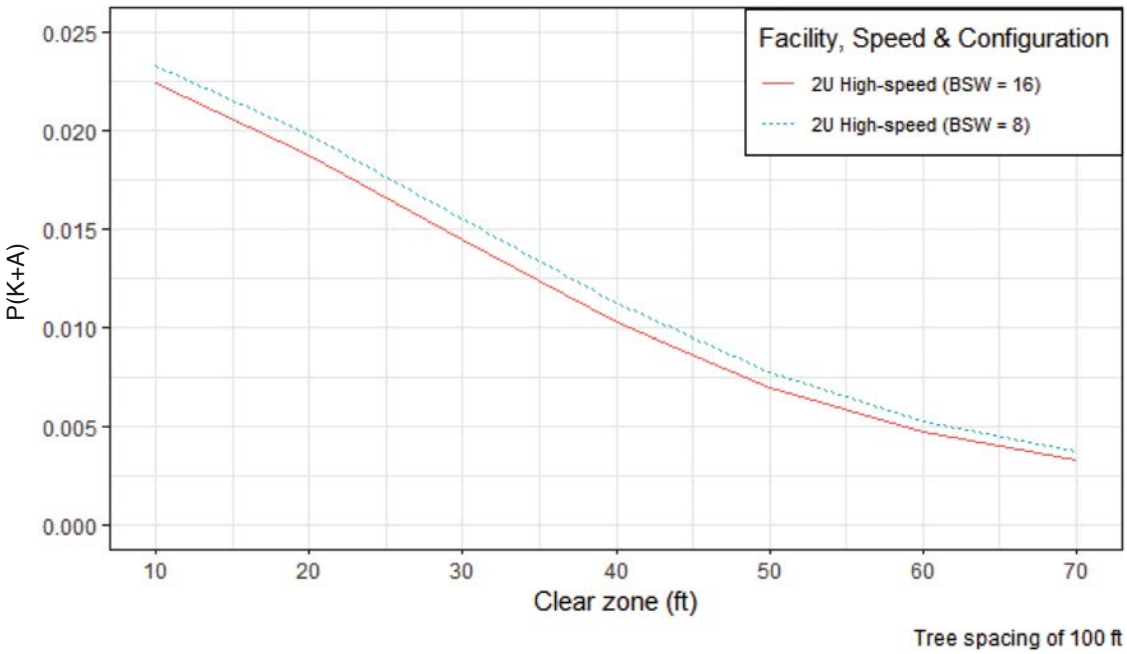

Figure 107. P(K+A) for 2U facility with varying backslope widths (BSW) (moderate).

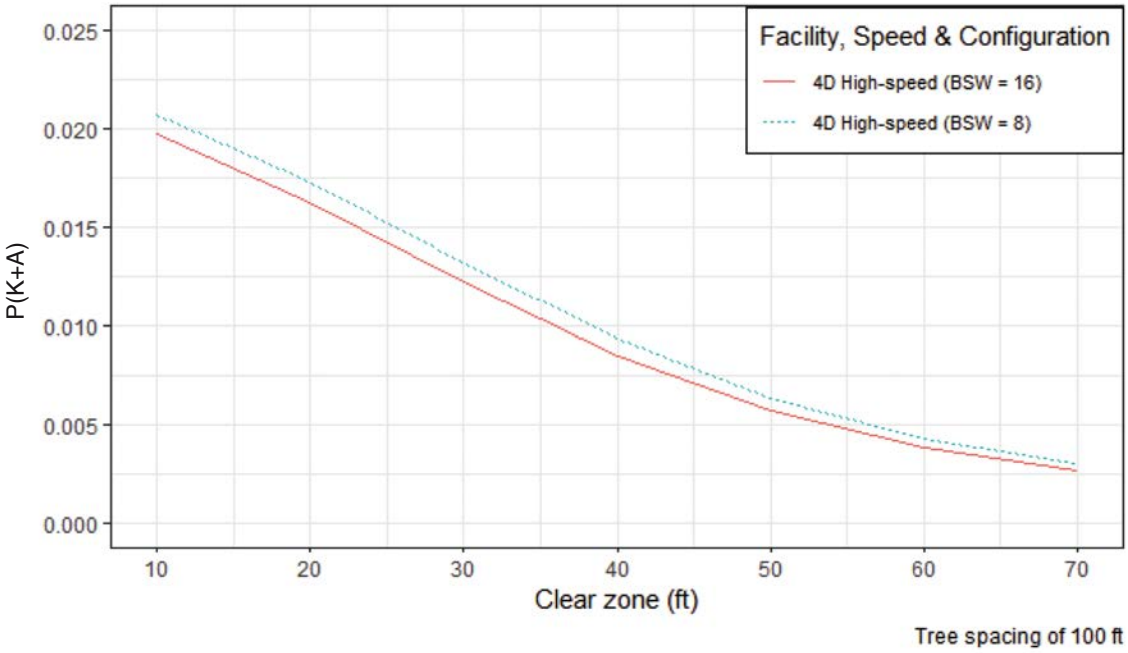

Figure 108. P(K+A) for 4D facility with varying backslope widths (BSW) (moderate).

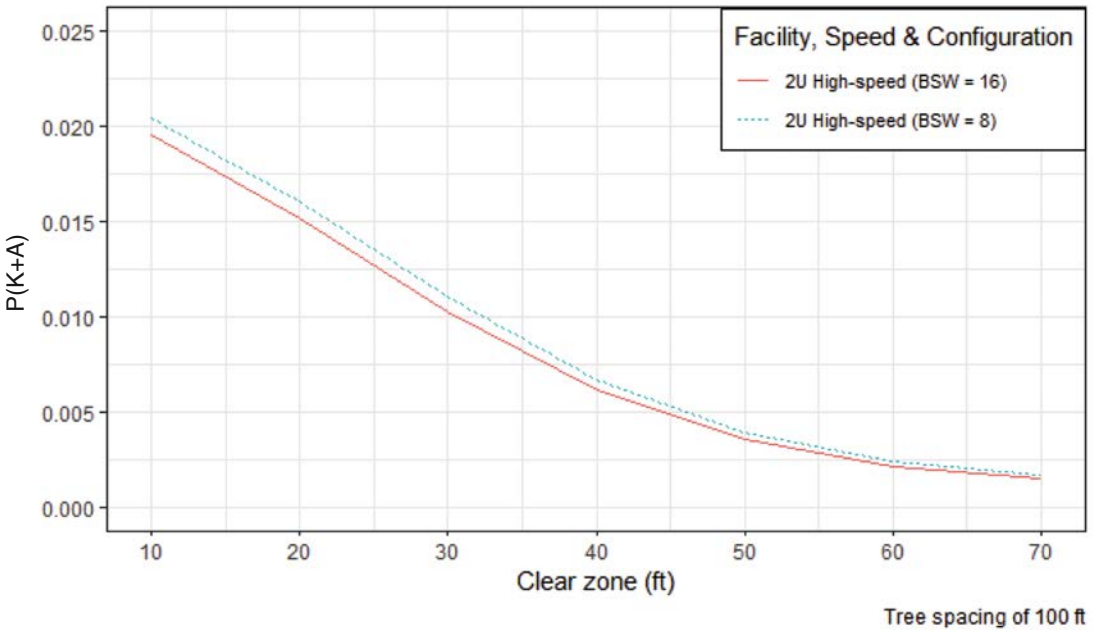

Figure 109. P(K+A) for 2U facility with varying backslope widths (BSW) (steep).

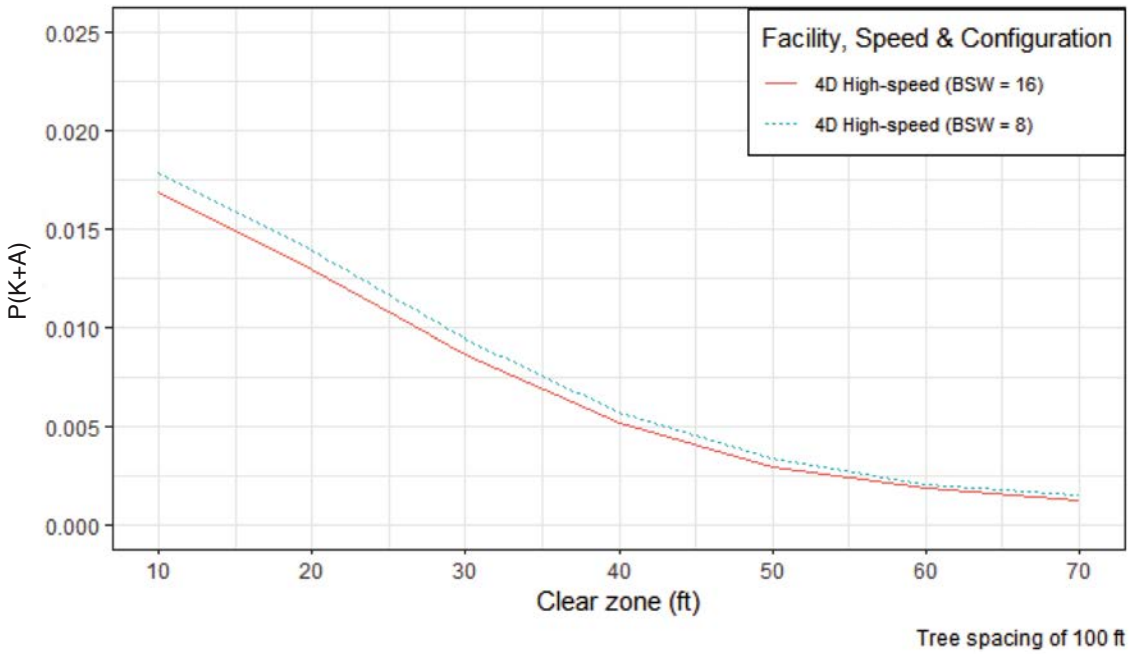

Figure 110. P(K+A) for 4D facility with varying backslope widths (BSW) (steep).

When selecting values for these parameters for use in the final risk analysis, the researchers wanted to avoid making the guidelines too conservative so that they are no longer practical. Since the weight factors or marginal probabilities determined for the various encroachment variables were based on reported crashes, they tend to be conservative because they do not account for unreported crashes or encroachments. This led the researchers to select the median impact speed and impact angle for use in the guideline development process. Precedence for the use of median or average impact speed and angle percentiles was also found in RSAPv3 (*25*).

When selecting tree spacings to represent different hazard levels at the clear zone edge, consideration was given to capturing a reasonable range of conditions from relatively dense to sparse. An initial selection of 100 ft, 200 ft, and 300 ft tree spacings to represent high, medium, and low hazard ratings was later expanded to include tree spacings ranging from 50 ft to 500 ft in the clear

Table 57. Sensitivity of P(K+A) at a 30-ft clear zone with respect to backslope width (BSW).

Case	Facility, Speed, and Configuration	P(K+A)	Difference
Case 1			
(Flat)	2U High-speed (BSW = 8 ft)	0.0187	6.8%
	2U High-speed (BSW = 16 ft)	0.0175	
	4D High-speed (BSW = 8 ft)	0.0160	7.1%
	4D High-speed (BSW = 16 ft)	0.0149	
Case 2			
(Moderate)	2U High-speed (BSW = 8 ft)	0.0155	7.2%
	2U High-speed (BSW = 16 ft)	0.0144	
	4D High-speed (BSW = 8 ft)	0.0132	8.2%
	4D High-speed (BSW = 16 ft)	0.0122	
Case 3			
(Steep)	2U High-speed (BSW = 8 ft)	0.0110	7.7%
	2U High-speed (BSW = 16 ft)	0.0103	
	4D High-speed (BSW = 8 ft)	0.0094	9.3%
	4D High-speed (BSW = 16 ft)	0.0086	

zone development process. Note that below a certain spacing or density of trees, the projected vehicle envelope (which is a function of the impact angle) ensures an impact will occur if the encroaching vehicle reaches the clear zone edge.

A sensitivity analysis was also performed for the different roadway and roadside design variables across different terrain configurations intended to represent relatively flat, moderate, and steep slope conditions. One purpose of the analysis was to identify less-sensitive variables and remove them from the guideline development process given that the risk analysis results will need to be simplified into a practical set of clear zone guidelines. This typically involves reducing the number of variables at some stage in the analysis. The sensitivity analysis permitted some of these decisions to be made prior to the final risk analysis, which simplified the clear zone guideline development process. Design variables with a high level of sensitivity tend to dominate those with lower sensitivity. Any variable with a relatively low sensitivity is still represented in the analysis but with a single value rather than a variable value.

The research team used a 25% variation as the cutoff for design variable inclusion. If the maximum percent change of a design variable across its values in the analysis matrix was less than 25%, the variable was excluded from the guideline development and assigned a mean value in the risk analysis. As presented above, the maximum percent change was typically associated with the steep terrain configuration, which utilized a 1V:3H foreslope and 1V:2H backslope combination. The moderate and flat terrain configurations were generally associated with smaller percent differences in P(K+A).

Based on this process, the research team concluded that vertical grade (9.8%–12%), foreslope ratio (6.3%–16.6%), and backslope width (6.8%–9.3%) should be excluded from the guideline development analysis based on their relatively low sensitivity compared to the other design variables. Note that the percent differences shown for each variable represent the range of differences in P(K+A) obtained across the various facility types and terrain configurations.

The variables retained for the initial guideline development analysis include horizontal curvature (41.5%—75.9%), shoulder width (10.5%—24.8%), foreslope width (17.5%—27.6%), ditch bottom width (17.4%—36.2%), and backslope ratio (44.9%—61.1%).

Variable Importance

To further aid in the selection of the key variables with significant influence on clear zone estimation, the research team applied the variable-importance approach. In this approach, a linear regression model was prepared, and the capability of the model to predict the P(K+A) was determined.

To determine the important variables, the team divided the data into two sets: a training set and a testing set. The training data were used to develop the model, while the testing set was used to examine the prediction capability of the developed model. The training data contained 70% of the entire risk analysis dataset, while the testing data contained the remaining 30%. The team developed linear models for the lower- and higher-posted-speed-limit categories using the training data and tested the accuracy of the model using the testing dataset. The resulting mean square error (MSE) for the lower-posted-speed-limit category was 0.043, while that of the higher-posted-speed-limit category was 0.042. These MSE are small, which implies that the predicted and observed P(K+A) are very similar.

The research team then estimated the importance of each variable, which is the relative influence of each variable used in the model in making accurate predictions of P(K+A). Figure 111 presents the relative importance of the various roadway and roadside design variables.

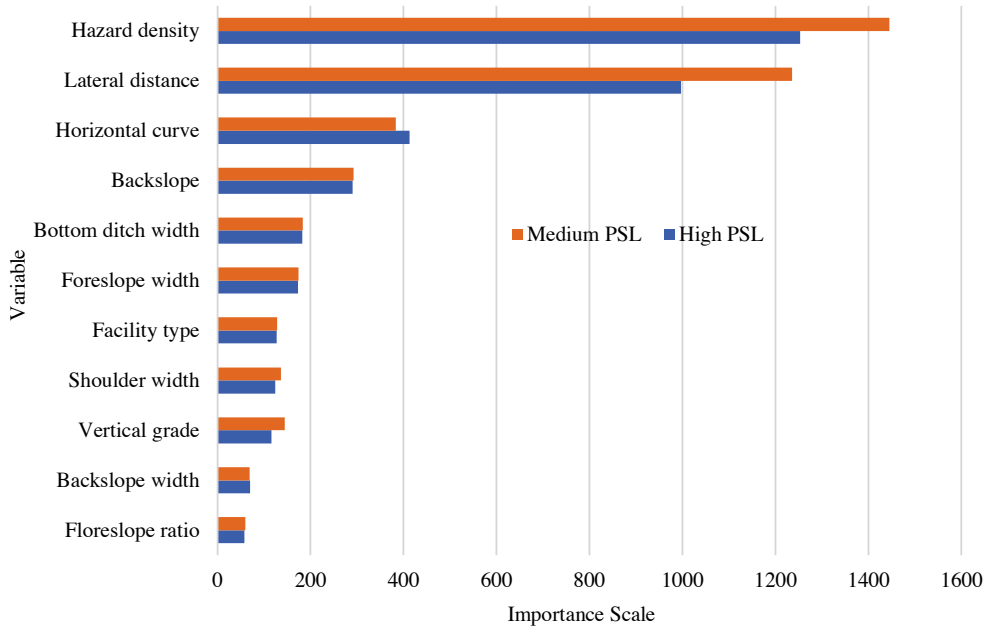

Figure 111. Model variable importance. PSL = posted speed limit.

It can be observed that hazard density and lateral distance are the most important predictors of P(K+A). Horizontal curvature, backslope ratio, ditch bottom width, and foreslope width have the higher importance values. On the other hand, the foreslope ratio and backslope width have low importance in the prediction of P(K+A). Further, facility type, shoulder width, and vertical grade have intermediate importance. It was interesting to note that the importance analysis supported the results of the sensitivity analysis.

CHAPTER 8

Recovery Area Guideline Development

The CZ-GAP risk analysis tool was used to estimate P(K+A) for encroachments occurring on various roadway and roadside design configurations for various clear zone distances and obstacle spacing at the edge of the clear zone. The results obtained from the risk analysis were developed into guidelines for recommended clear recovery distances using the relative risk approach. The basic premise of the relative risk approach is that the risk associated with an unshielded roadside should be less than the risk of shielding that roadway segment with guardrail.

The guidelines provide recommended clear recovery distances based on a given set of roadway and roadside characteristics while also considering the obstacle spacing that exists at the clear zone edge. As the spacing of the obstacles at the clear zone edge increases, the risk of impact with a hazard and, hence, the probability of a severe or fatal injury crash, P(K+A), decreases. Thus, the recommended clear zone distance is determined as the distance at which the injury risk associated with impacting a hazard at the clear zone edge drops below the injury risk associated with impacting a guardrail. For wide enough obstacle spacing, the risk associated with guardrail is greater than the risk associated with impacting an obstacle at a given lateral offset.

Note that rollover risk was not explicitly included in the guideline development process. Although the CZ-GAP analysis tool was developed with the capability of estimating rollover risk for different design configurations, rollover risk is related to the traversability of a given terrain configuration rather than the clear zone distance. While slope or ditch traversability is another important aspect of roadside design, this issue has recently been addressed under previous research (*18, 19*). Including it in the clear zone guidelines would be, in some ways, superseding the previous research and would be a fundamental shift in clear zone philosophy that has historically been based on reducing crashes with fixed objects on the roadside.

The guidelines were developed in two forms to present different options for a designer. The first form consists of equations derived using statistical regression analysis. The equations allow the user to calculate the minimum recommended clear zone distance for a given set of variables. The second form consists of charts in which multiple variables of interest are displayed. The charts provide the user with the ability to find the minimum recommended clear zone distance as well as understand the magnitude of the relative risk.

Guideline Equations

Given that the risk of injury is highly sensitive to obstacle spacing, a greater range of spacings from 50 ft to 500 ft was incorporated into the statistical models used to develop the equations for the recommended clear zone distance.

Table 58. Linear regression results for P(K+A) for roadways with high posted speed limit.

Fixed Effects	Estimate	Standard Error	z-Value	P-Value
Vertical Grade	0.006	4.46E-05	131.19	<0.001
Horizontal Curve	0.494	1.06E-03	464.77	<0.001
Shoulder Width	0.016	1.13E-04	140.63	<0.001
Foreslope	0.011	1.73E-04	64.81	<0.001
Foreslope Width	0.023	1.16E-04	195.71	<0.001
Bottom Ditch Width	0.023	1.13E-04	205.08	<0.001
Backslope	0.103	3.13E-04	328.12	<0.001
Backslope Width	−0.009	1.16E-04	−79.13	<0.001
Lateral Distance	−0.026	2.32E-05	−1,117.95	<0.001
Hazard Density	−0.005	3.11E-06	−1,546.74	<0.001
Facility Type	0.127	9.26E-04	136.97	<0.001
Intercept	3.977	3.09E-03	−1,285.64	<0.001
Model Performance Metrics				
Multiple R-Squared	0.9043			
Adjusted R-Squared	0.9043			
F-Statistic	3.739e+05			
Degree of Freedom	435,444			
P-Value	< 0.001			

Table 58 and Table 59 present the linear regression results for the probability of fatal and injury crashes [P(K+A)] for the high and low categories of the posted speed limit, respectively. The high-speed range includes posted speed limits of 60 mph and above, and the low-speed range represents posted speed limits from 45 mph to 55 mph.

Along with the coefficients/estimates for each of the design variables, the tables also present the model performance metrics. It can be observed that the R-squared values for the two models are relatively high. The implication is that the design variables are able to explain the variability in P(K+A) by about 90% and 92% for high- and low-posted-speed-limit ranges, respectively.

The research team utilized these statistical models to develop equations that can calculate a recommended clear zone distance for a given roadway and roadside design configuration. The

Table 59. Linear regression results for P(K+A) for roadways with low posted speed limit.

Fixed Effects	Estimate	Standard Error	z-Value	P-Value
Vertical Grade	0.007	4.48E-05	164.65	<0.001
Horizontal Curve	0.465	1.07E-03	434.72	<0.001
Shoulder Width	0.017	1.13E-04	153.66	<0.001
Foreslope	0.012	1.74E-04	67.47	<0.001
Foreslope Width	0.023	1.16E-04	198.58	<0.001
Bottom Ditch Width	0.024	1.13E-04	208.42	<0.001
Backslope	0.105	3.15E-04	332.87	<0.001
Backslope Width	–0.009	1.16E-04	−79.86	<0.001
Lateral Distance	–0.038	2.33E-05	−1,635.44	<0.001
Hazard Density	–0.005	3.12E-06	−1,538.80	<0.001
Facility Type	0.129	9.31E-04	138.15	<0.001
Intercept	–4.542	3.11E-03	−1,460.73	<0.001
Model Performance Metrics				
Multiple R-Squared	0.9267			
Adjusted R-Squared	0.9267			
F-Statistic	5.005e+05			
Degree of Freedom	435,444			
P-Value	< 0.001			

Feature	K_{65}	KA_{65}	KAB_{65}	$KABC_{65}$
Longitudinal Barriers				
Cable Barrier	0.0009	0.0050	0.0297	0.0849
Strong-Post W-Beam Barrier	0.0015	0.0094	0.0422	0.0977
Weak-Post W-Beam Barrier	0.0006	0.0091	0.0321	0.1187
Closed Faced Concrete Barriers	0.0021	0.0159	0.0810	0.1667

NOTE: subscript 65 = 65mph.

Figure 112. Severity probabilities for longitudinal barriers from* NCHRP Research Report 972 *(28).

clear zone distance is defined as the distance at which the P(K+A) associated with the obstacles at the clear zone edge is equal to the P(K+A) associated with a guardrail at the roadway edge. The team adopted the guardrail P(K+A) values from *NCHRP Research Report 972: Development of Safety Performance-Based Guidelines for the* Roadside Design Guide (*28*). Figure 112 shows values of P(K+A) at 65 mph for different longitudinal barriers. The research team selected the P(K+A) for the strong-post W-beam barrier to represent the guardrail risk for guideline development.

For roadways within the higher-posted-speed-limit category (i.e., ≥ 60 mph), the team chose to use the guardrail P(K+A) for a 65-mph posted speed limit, which is given as 0.0094. For roadways within the lower-posted-speed-limit category (i.e., 45 mph ≤ PSL ≤ 55 mph, where PSL = posted speed limit), a guardrail P(K+A) associated with a 50-mph posted speed limit was selected.

To calculate the guardrail P(K+A) at 50 mph, Eq. 9 from *NCHRP Research Report 972* was used (*28*). The guardrail P(K+A) at 50 mph was calculated as follows:

$$P\left(K+A\right)_{50} = P\left(K+A\right)_{65} * \left(\frac{50^3}{65^3}\right) = 0.0043 \tag{9}$$

The clear zone distance equations were determined by setting the regression equations for P(K+A) equal to the guardrail risk value for the appropriate posted-speed-limit category and solving for the lateral distance. Furthermore, the research team used default values for the variables that had little significance on the prediction of the P(K+A) estimate as determined by the sensitivity and importance analyses presented in Chapter 7. The default values adopted in the clear zone equation development process for these variables are:

- Backslope width = 12 ft,
- Foreslope ratio = 1V:6H, and
- Vertical grade = 0 percent.

The team developed two equations for estimating clear zone distance. Each equation applies to a range of posted speed limits to be used.

For the higher-posted-speed-limit category (i.e., ≥60 mph), Eq. 10 should be used to determine a recommended clear zone distance (CZ_D):

$$CZ_D = 19013.4 * \frac{1}{HCurveR} + 0.610 * ShldW + 0.872 * FSW + 0.889 * DBtW + 3.950 * BS - 0.185 * ObS + 4.881 * FType + 24.894 \tag{10}$$

For the lower-posted-speed-limit category (i.e., 45 mph ≤ PSL ≤ 55 mph), Eq. 11 should be used to determine the recommended clear zone distance:

$$CZ_D = 12232.9 * \frac{1}{HCurveR} + 0.458 * ShldW + 0.608 * FSW + 0.621 * DBtW + 2.758 * BS - 0.126 * ObS + 3.384 * FType + 22.786 \quad (11)$$

where:

HCurveR = Radius of horizontal curve (ft),
ShldW = Shoulder width (ft),
FSW = Foreslope width (ft),
DBtW = Ditch bottom width (ft) (= 0 for V-ditch),
BS = Backslope ratio = horizontal component of slope (e.g., BS = 6 for 1V:6H slope),
ObS = Average obstacle spacing at clear zone edge (ft), and
FType = Facility type = $\begin{cases} 1 \text{ for } 2U; \\ 0 \text{ for } 4D. \end{cases}$

To determine a clear zone distance, the user inputs values for the indicated roadway and roadside design variables using the equation associated with the appropriate speed limit category for the facility. The backslope ratio (*BS*) is input as the horizontal component of the slope. For example, for a 1V:6H backslope, BS = 6 in the equations. The obstacle spacing (*ObS*) at the clear zone edge is input as an average obstacle spacing (e.g., tree spacing). The facility type (*FType*) is a binary variable depending on whether the facility is 2U or 4D.

Guideline Charts

Several different formats were evaluated for chart-based clear zone guidelines. Despite the challenge of having a large number of variables involved, the researchers managed to develop guidelines in the form of meaningful and legible charts. In addition to providing the minimum required clear zone distance, some of the charts also display the relative risk values for different clear zone distances for each design configuration. Use of these numbers can assist a designer with understanding the change in relative risk if different clear zone distances are contemplated based on engineering, environmental, or cost factors.

It was important to generate charts that were practical to use, reasonable in number, and legible within acceptable page margins. To address these challenges, the researchers introduced an innovative chart style that permitted the integration of multiple variables onto a single chart. Several of the design variables that were shown to have little importance in determining clear zone distance in Chapter 7 were excluded from the charts to assist with meeting the chart objectives. For the excluded variables, default values were used to compute the associated P(K+A) and relative risk for a given design configuration. The variables that were excluded and their associated default values used in the clear zone guideline chart development are

- Backslope width = 8 ft,
- Foreslope ratio = 1V:6H,
- Vertical grade = 0 percent,
- Shoulder width = 6 ft, and
- Facility type = 2U.

The charts are populated with values of relative risk defined as a ratio of P(K+A) associated with impacting obstacles at the clear zone edge over the P(K+A) of a guardrail impact. The P(K+A) values associated with impacting obstacles at the clear zone edge were generated from

CZ-GAP for each design configuration and respective posted-speed-limit category. As discussed in the previous section, the P(K+A) values for a guardrail impact were adopted from *NCHRP Research Report 972* for each posted speed limit category (*28*).

A risk ratio less than or equal to 1 indicates a recommended clear zone distance. A risk ratio greater than 1 indicates a larger clear zone value, or shielding the roadway segment with a guardrail should be considered. This relationship is presented in Eq. 12.

$$Relative\ Risk\ Ratio = \frac{P\left(K+A\right)_{Tree}}{P\left(K+A\right)_{Guadrail}} = \begin{cases} \leq 1, Clear\ Zone\ Recommended \\ > 1, Shielding\ Recommended \end{cases} \quad (12)$$

One chart-based guideline format contains three charts with each being associated with a different obstacle spacing at the clear zone edge. Figure 113, Figure 114, and Figure 115 show clear zone selection guideline charts for obstacle spacings of less than 150 ft, 150 ft to 300 ft, and greater than 300 ft, respectively.

The most significant design variables are located along the left and right sides of these charts. The primary outcome of interest is the recommended clear zone distance, which is located at the bottom of the charts. When a risk ratio is greater than 1, the cell containing the value is shaded, indicating that the clear zone distance is not recommended for that design configuration. The recommended clear zone distance is the leftmost unshaded cell among the group of cells associated with a particular roadway and roadside configuration.

Another chart-based guideline that combines all three obstacle spacing ranges into a single chart is presented in Figure 116 in a landscape layout. A similar, alternative chart format without the risk ratio values is shown in Figure 117, also in a landscape layout. Presenting the clear zone guidelines in a single chart provides for a more compact presentation.

An advantage of having the risk ratios included in Figure 116 is that the chart can be updated for different guardrail risk values that might become available from future research. This can be accomplished by multiplying the relative risk in the chart by the original guardrail P(K+A) value to return to the original P(K+A) associated with impacting obstacles at the clear zone edge and dividing by the new guardrail P(K+A).

The equations can be similarly updated in the future to account for a new guardrail P(K+A), but this requires the use of the regression models presented in this chapter to formulate the new equations.

Guideline Examples

A set of examples is provided to demonstrate the use of both the clear zone guideline chart and clear zone guideline equations.

Example 1

Given: Facility type: 2U
Posted speed limit: 50 mph
Horizontal curvature: 0 degrees (none)
Shoulder width: 2 ft
Foreslope width: 10 ft
Ditch Bottom width: 0 ft (V-ditch)
Backslope ratio: 1V:4H
Average obstacle spacing at clear zone edge: 200 ft

Backslope Ratio (H:V)	Ditch Bottom Width (ft)	<150 ft Obstacle Spacing at Clear Zone Edge — Posted Speed Limit — Low (45-55 mph)							High (≥ 60 mph)							Horizontal Curvature (deg)	Foreslope Width (ft)
2:1	≤4	2.31	1.63	1.04	0.61	0.34	0.19	0.12	2.03	1.62	1.18	0.79	0.50	0.33	0.23	<2	≤12
	>4	2.66	1.96	1.32	0.83	0.50	0.29	0.18	2.33	1.94	1.49	1.06	0.72	0.49	0.34		
	≤4	2.90	2.16	1.47	0.91	0.53	0.31	0.19	2.55	2.16	1.67	1.18	0.79	0.53	0.37	2-5	
	>4	3.22	2.51	1.80	1.19	0.74	0.45	0.28	2.83	2.50	2.04	1.54	1.10	0.77	0.54		
	≤4	3.16	2.43	1.69	1.08	0.64	0.38	0.23	2.78	2.42	1.93	1.41	0.97	0.66	0.47	>5	
	>4	3.46	2.77	2.04	1.39	0.89	0.55	0.34	3.04	2.76	2.31	1.81	1.33	0.95	0.68		
	≤4	2.63	1.92	1.27	0.78	0.45	0.26	0.16	2.31	1.90	1.43	0.99	0.66	0.43	0.30	<2	>12
	>4	2.97	2.26	1.58	1.03	0.63	0.38	0.24	2.60	2.24	1.77	1.31	0.92	0.63	0.44		
	≤4	3.19	2.46	1.73	1.11	0.67	0.40	0.25	2.80	2.45	1.96	1.44	1.00	0.69	0.49	2-5	
	>4	3.49	2.81	2.08	1.43	0.92	0.57	0.36	3.06	2.79	2.34	1.84	1.36	0.98	0.70		
	≤4	3.42	2.72	1.96	1.30	0.81	0.49	0.31	3.01	2.71	2.23	1.69	1.21	0.85	0.61	>5	
	>4	3.69	3.05	2.32	1.64	1.09	0.69	0.44	3.25	3.03	2.62	2.12	1.61	1.19	0.87		
4:1	≤4	2.61	1.92	1.30	0.81	0.48	0.29	0.18	2.29	1.91	1.46	1.04	0.70	0.48	0.33	<2	≤12
	>4	2.95	2.25	1.59	1.04	0.65	0.40	0.25	2.59	2.23	1.78	1.33	0.95	0.66	0.47		
	≤4	3.16	2.46	1.76	1.16	0.72	0.44	0.27	2.77	2.45	1.99	1.50	1.07	0.75	0.54	2-5	
	>4	3.45	2.79	2.08	1.45	0.95	0.60	0.38	3.03	2.77	2.35	1.86	1.40	1.02	0.74		
	≤4	3.39	2.71	1.99	1.35	0.87	0.54	0.34	2.98	2.70	2.26	1.76	1.29	0.93	0.67	>5	
	>4	3.65	3.02	2.32	1.66	1.12	0.73	0.47	3.21	3.01	2.63	2.15	1.66	1.24	0.91		
	≤4	2.92	2.22	1.55	1.00	0.62	0.37	0.23	2.56	2.20	1.74	1.28	0.90	0.62	0.44	<2	>12
	>4	3.24	2.56	1.86	1.27	0.82	0.51	0.33	2.84	2.53	2.09	1.61	1.18	0.84	0.60		
	≤4	3.42	2.75	2.03	1.39	0.90	0.56	0.36	3.00	2.73	2.29	1.79	1.33	0.96	0.69	2-5	
	>4	3.69	3.06	2.36	1.70	1.15	0.75	0.49	3.24	3.04	2.66	2.18	1.69	1.27	0.93		
	≤4	3.62	2.98	2.26	1.60	1.06	0.68	0.44	3.18	2.97	2.56	2.06	1.57	1.16	0.86	>5	
	>4	3.86	3.28	2.60	1.92	1.34	0.90	0.59	3.39	3.25	2.92	2.46	1.97	1.52	1.14		
6:1	≤4	2.90	2.21	1.56	1.03	0.64	0.40	0.25	2.54	2.19	1.75	1.31	0.93	0.66	0.47	<2	≤12
	>4	3.21	2.54	1.87	1.28	0.84	0.53	0.34	2.81	2.52	2.09	1.63	1.21	0.87	0.63		
	≤4	3.38	2.73	2.04	1.42	0.93	0.60	0.38	2.97	2.72	2.30	1.83	1.38	1.01	0.74	2-5	
	>4	3.65	3.04	2.36	1.72	1.18	0.78	0.51	3.20	3.02	2.66	2.20	1.73	1.31	0.97		
	≤4	3.58	2.96	2.27	1.63	1.10	0.72	0.47	3.15	2.95	2.57	2.10	1.63	1.23	0.91	>5	
	>4	3.81	3.25	2.59	1.93	1.37	0.93	0.62	3.35	3.22	2.91	2.48	2.01	1.57	1.19		
	≤4	3.18	2.51	1.83	1.25	0.81	0.51	0.33	2.79	2.49	2.05	1.59	1.17	0.84	0.61	<2	>12
	>4	3.48	2.84	2.15	1.53	1.03	0.67	0.44	3.05	2.80	2.40	1.93	1.48	1.09	0.80		
	≤4	3.62	3.00	2.31	1.67	1.14	0.75	0.49	3.18	2.98	2.61	2.14	1.67	1.26	0.94	2-5	
	>4	3.85	3.29	2.64	1.98	1.41	0.96	0.64	3.38	3.26	2.95	2.52	2.04	1.59	1.21		
	≤4	3.79	3.21	2.54	1.88	1.32	0.89	0.59	3.32	3.19	2.86	2.42	1.94	1.50	1.14	>5	
	>4	3.99	3.48	2.85	2.20	1.60	1.12	0.76	3.51	3.44	3.19	2.80	2.33	1.87	1.46		
		10	20	30	40	50	60	70	10	20	30	40	50	60	70		

Clear Zone (ft)

Figure 113. Guidelines for less than 150 ft of obstacle spacing at clear zone edge. Clear zone distance, in feet, is the row across the bottom of each chart.

Backslope Ratio (H:V)	Ditch Bottom Width (ft)	150 - 300 ft Obstacle Spacing at Clear Zone Edge — Posted Speed Limit — Low (45-55 mph)							High (≥ 60 mph)							Horizontal Curvature (deg)	Foreslope Width (ft)
2:1	≤4	1.16	0.82	0.52	0.31	0.17	0.10	0.06	1.02	0.81	0.59	0.39	0.25	0.16	0.11	<2	≤12
	>4	1.33	0.98	0.66	0.42	0.25	0.15	0.09	1.17	0.97	0.74	0.53	0.36	0.24	0.17		
	≤4	1.45	1.08	0.73	0.45	0.26	0.15	0.09	1.27	1.08	0.83	0.59	0.39	0.26	0.18	2-5	
	>4	1.61	1.26	0.90	0.60	0.37	0.23	0.14	1.42	1.25	1.02	0.77	0.55	0.39	0.27		
	≤4	1.58	1.22	0.85	0.54	0.32	0.19	0.12	1.39	1.21	0.96	0.70	0.48	0.33	0.23	>5	
	>4	1.73	1.39	1.02	0.70	0.45	0.28	0.17	1.52	1.38	1.16	0.90	0.67	0.48	0.34		
	≤4	1.32	0.96	0.64	0.39	0.22	0.13	0.08	1.15	0.95	0.72	0.50	0.33	0.22	0.15	<2	>12
	>4	1.49	1.13	0.79	0.51	0.32	0.19	0.12	1.30	1.12	0.89	0.65	0.46	0.32	0.22		
	≤4	1.59	1.23	0.87	0.56	0.34	0.20	0.12	1.40	1.23	0.98	0.72	0.50	0.34	0.24	2-5	
	>4	1.75	1.40	1.04	0.71	0.46	0.29	0.18	1.53	1.39	1.17	0.92	0.68	0.49	0.35		
	≤4	1.71	1.36	0.98	0.65	0.40	0.25	0.15	1.51	1.36	1.12	0.85	0.60	0.42	0.30	>5	
	>4	1.85	1.52	1.16	0.82	0.54	0.35	0.22	1.62	1.51	1.31	1.06	0.81	0.59	0.43		
4:1	≤4	1.31	0.96	0.65	0.40	0.24	0.14	0.09	1.15	0.95	0.73	0.52	0.35	0.24	0.17	<2	≤12
	>4	1.48	1.13	0.80	0.52	0.33	0.20	0.13	1.29	1.12	0.89	0.67	0.47	0.33	0.23		
	≤4	1.58	1.23	0.88	0.58	0.36	0.22	0.14	1.39	1.22	1.00	0.75	0.54	0.38	0.27	2-5	
	>4	1.73	1.40	1.04	0.72	0.48	0.30	0.19	1.52	1.39	1.17	0.93	0.70	0.51	0.37		
	≤4	1.70	1.36	0.99	0.68	0.43	0.27	0.17	1.49	1.35	1.13	0.88	0.65	0.46	0.34	>5	
	>4	1.83	1.51	1.16	0.83	0.56	0.36	0.23	1.61	1.50	1.31	1.07	0.83	0.62	0.46		
	≤4	1.46	1.11	0.78	0.50	0.31	0.19	0.12	1.28	1.10	0.87	0.64	0.45	0.31	0.22	<2	>12
	>4	1.62	1.28	0.93	0.63	0.41	0.26	0.16	1.42	1.27	1.04	0.80	0.59	0.42	0.30		
	≤4	1.71	1.37	1.01	0.70	0.45	0.28	0.18	1.50	1.37	1.15	0.90	0.66	0.48	0.35	2-5	
	>4	1.85	1.53	1.18	0.85	0.58	0.38	0.24	1.62	1.52	1.33	1.09	0.84	0.63	0.47		
	≤4	1.81	1.49	1.13	0.80	0.53	0.34	0.22	1.59	1.48	1.28	1.03	0.79	0.58	0.43	>5	
	>4	1.93	1.64	1.30	0.96	0.67	0.45	0.29	1.70	1.63	1.46	1.23	0.99	0.76	0.57		
6:1	≤4	1.45	1.11	0.78	0.51	0.32	0.20	0.13	1.27	1.10	0.88	0.65	0.47	0.33	0.23	<2	≤12
	>4	1.61	1.27	0.93	0.64	0.42	0.27	0.17	1.41	1.26	1.05	0.81	0.60	0.44	0.31		
	≤4	1.69	1.37	1.02	0.71	0.47	0.30	0.19	1.49	1.36	1.15	0.92	0.69	0.51	0.37	2-5	
	>4	1.83	1.52	1.18	0.86	0.59	0.39	0.25	1.60	1.51	1.33	1.10	0.86	0.65	0.49		
	≤4	1.79	1.48	1.14	0.81	0.55	0.36	0.23	1.57	1.47	1.29	1.05	0.82	0.61	0.46	>5	
	>4	1.91	1.63	1.29	0.97	0.68	0.46	0.31	1.68	1.61	1.46	1.24	1.01	0.78	0.59		
	≤4	1.59	1.26	0.92	0.62	0.40	0.26	0.16	1.39	1.24	1.03	0.79	0.58	0.42	0.30	<2	>12
	>4	1.74	1.42	1.08	0.76	0.52	0.34	0.22	1.52	1.40	1.20	0.97	0.74	0.55	0.40		
	≤4	1.81	1.50	1.16	0.83	0.57	0.37	0.24	1.59	1.49	1.30	1.07	0.83	0.63	0.47	2-5	
	>4	1.93	1.65	1.32	0.99	0.70	0.48	0.32	1.69	1.63	1.48	1.26	1.02	0.80	0.61		
	≤4	1.89	1.61	1.27	0.94	0.66	0.44	0.29	1.66	1.60	1.43	1.21	0.97	0.75	0.57	>5	
	>4	2.00	1.74	1.42	1.10	0.80	0.56	0.38	1.75	1.72	1.60	1.40	1.17	0.94	0.73		
		10	20	30	40	50	60	70	10	20	30	40	50	60	70		

Clear Zone (ft)

Figure 114. Guidelines for 150 ft to 300 ft of obstacle spacing at clear zone edge. Clear zone distance, in feet, is the row across the bottom of each chart.

Backslope Ratio (H:V)	Ditch Bottom Width (ft)	>300 ft Obstacle Spacing at Clear Zone Edge — Posted Speed Limit — Low (45-55 mph)							High (≥ 60 mph)							Horizontal Curvature (deg)	Foreslope Width (ft)
2:1	≤4	0.81	0.55	0.36	0.21	0.11	0.06	0.04	0.71	0.55	0.40	0.27	0.17	0.11	0.08	<2	≤12
	>4	0.98	0.65	0.43	0.27	0.16	0.10	0.06	0.86	0.64	0.49	0.35	0.24	0.16	0.11		
	≤4	1.11	0.73	0.50	0.31	0.18	0.10	0.06	0.97	0.72	0.56	0.40	0.27	0.18	0.12	2-5	
	>4	1.19	0.88	0.59	0.39	0.24	0.15	0.09	1.05	0.87	0.67	0.50	0.36	0.25	0.18		
	≤4	1.19	0.84	0.56	0.35	0.21	0.13	0.08	1.05	0.84	0.63	0.46	0.32	0.22	0.15	>5	
	>4	1.21	1.00	0.69	0.47	0.30	0.18	0.11	1.06	1.00	0.78	0.61	0.45	0.32	0.22		
	≤4	0.96	0.63	0.42	0.25	0.15	0.09	0.05	0.84	0.63	0.47	0.32	0.22	0.15	0.10	<2	>12
	>4	1.13	0.76	0.54	0.35	0.21	0.13	0.08	0.99	0.75	0.60	0.44	0.31	0.21	0.14		
	≤4	1.19	0.85	0.57	0.36	0.22	0.13	0.08	1.04	0.85	0.65	0.47	0.33	0.22	0.16	2-5	
	>4	1.21	1.01	0.70	0.48	0.31	0.20	0.12	1.07	1.01	0.79	0.62	0.46	0.33	0.24		
	≤4	1.21	0.98	0.66	0.44	0.28	0.17	0.10	1.07	0.97	0.75	0.57	0.41	0.29	0.20	>5	
	>4	1.30	1.11	0.80	0.54	0.36	0.23	0.15	1.14	1.10	0.90	0.70	0.53	0.40	0.29		
4:1	≤4	0.93	0.63	0.42	0.26	0.16	0.10	0.06	0.82	0.62	0.47	0.34	0.23	0.16	0.11	<2	≤12
	>4	1.10	0.76	0.54	0.35	0.22	0.13	0.08	0.96	0.75	0.60	0.45	0.32	0.22	0.16		
	≤4	1.20	0.84	0.58	0.38	0.24	0.15	0.09	1.05	0.84	0.66	0.49	0.35	0.25	0.18	2-5	
	>4	1.23	1.00	0.70	0.49	0.32	0.20	0.13	1.08	0.99	0.79	0.63	0.48	0.34	0.24		
	≤4	1.23	0.96	0.66	0.46	0.29	0.18	0.11	1.08	0.96	0.76	0.59	0.44	0.31	0.22	>5	
	>4	1.28	1.11	0.80	0.55	0.37	0.25	0.16	1.12	1.10	0.90	0.71	0.55	0.42	0.31		
	≤4	1.08	0.74	0.52	0.34	0.21	0.12	0.08	0.95	0.74	0.58	0.43	0.30	0.21	0.15	<2	>12
	>4	1.19	0.88	0.61	0.41	0.27	0.17	0.11	1.04	0.87	0.69	0.53	0.39	0.28	0.20		
	≤4	1.23	0.97	0.68	0.47	0.31	0.19	0.12	1.08	0.97	0.77	0.60	0.45	0.32	0.23	2-5	
	>4	1.29	1.11	0.81	0.56	0.38	0.25	0.16	1.13	1.10	0.91	0.72	0.56	0.42	0.31		
	≤4	1.26	1.10	0.77	0.52	0.35	0.23	0.15	1.11	1.09	0.87	0.68	0.52	0.39	0.29	>5	
	>4	1.37	1.14	0.92	0.65	0.45	0.29	0.19	1.20	1.13	1.04	0.83	0.66	0.50	0.38		
6:1	≤4	1.04	0.74	0.52	0.35	0.22	0.13	0.08	0.92	0.73	0.59	0.44	0.32	0.22	0.16	<2	≤12
	>4	1.20	0.87	0.62	0.42	0.28	0.18	0.11	1.05	0.86	0.69	0.53	0.40	0.29	0.21		
	≤4	1.24	0.96	0.68	0.48	0.32	0.20	0.13	1.09	0.95	0.77	0.62	0.47	0.33	0.24	2-5	
	>4	1.26	1.11	0.81	0.56	0.39	0.26	0.17	1.11	1.10	0.91	0.72	0.57	0.44	0.33		
	≤4	1.25	1.07	0.77	0.53	0.37	0.24	0.16	1.10	1.07	0.87	0.69	0.54	0.42	0.31	>5	
	>4	1.34	1.14	0.92	0.65	0.45	0.31	0.21	1.18	1.13	1.03	0.84	0.67	0.52	0.40		
	≤4	1.19	0.85	0.61	0.41	0.26	0.17	0.11	1.04	0.84	0.69	0.52	0.38	0.27	0.20	<2	>12
	>4	1.23	1.00	0.72	0.51	0.35	0.23	0.15	1.08	0.99	0.80	0.65	0.50	0.37	0.27		
	≤4	1.25	1.09	0.79	0.55	0.38	0.25	0.17	1.10	1.08	0.89	0.70	0.55	0.42	0.32	2-5	
	>4	1.36	1.14	0.94	0.67	0.47	0.31	0.21	1.19	1.13	1.04	0.85	0.68	0.52	0.40		
	≤4	1.33	1.13	0.90	0.63	0.44	0.29	0.20	1.16	1.13	1.01	0.81	0.65	0.49	0.38	>5	
	>4	1.43	1.20	0.99	0.77	0.54	0.38	0.25	1.26	1.19	1.11	0.98	0.78	0.63	0.48		
		10	20	30	40	50	60	70	10	20	30	40	50	60	70		

Clear Zone (ft)

Figure 115. Guidelines for greater than 300 ft of obstacle spacing at clear zone edge. Clear zone distance, in feet, is the row across the bottom of each chart.

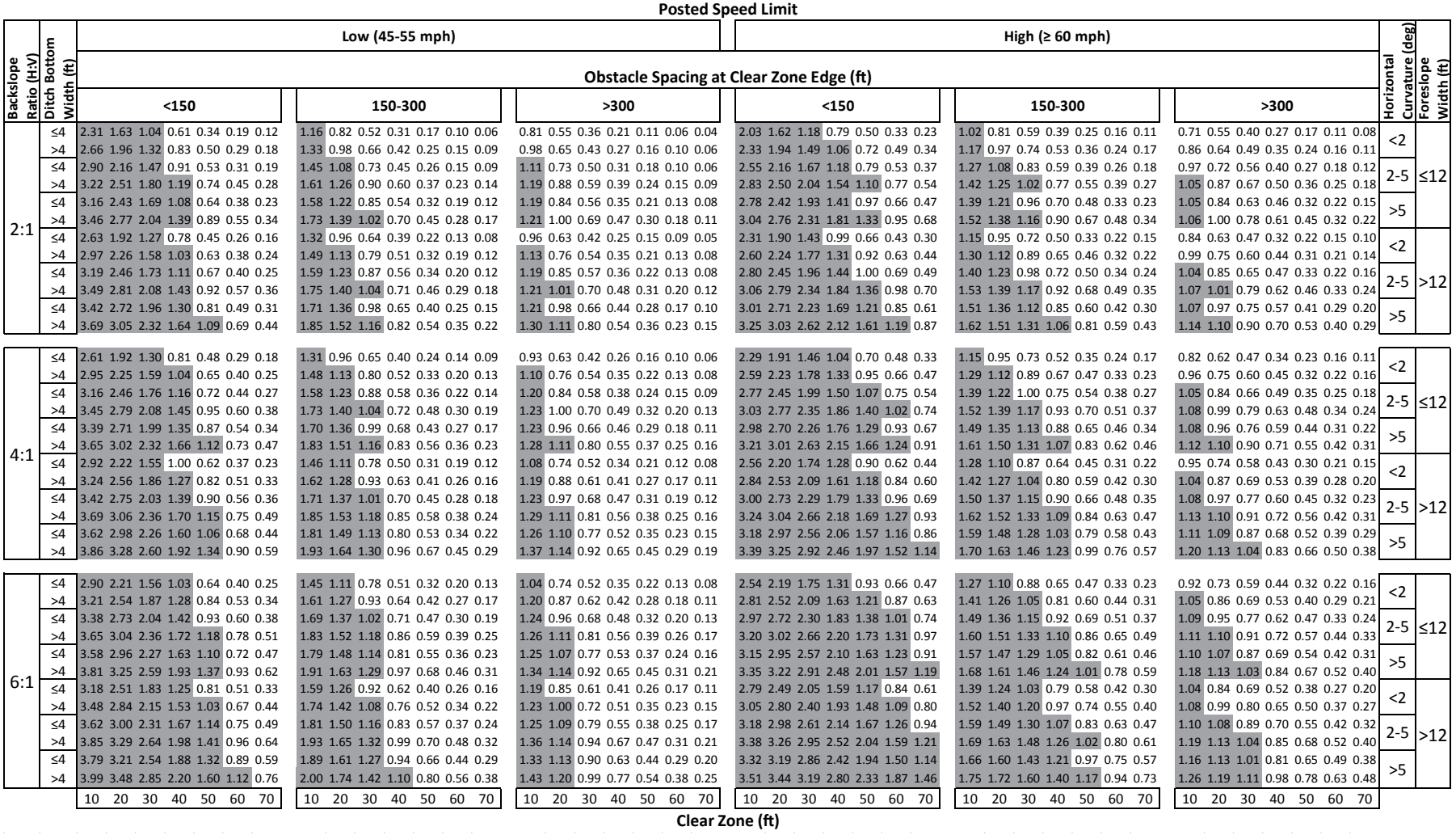

Figure 116. Combined chart for ranges of obstacle spacing at clear zone edge.

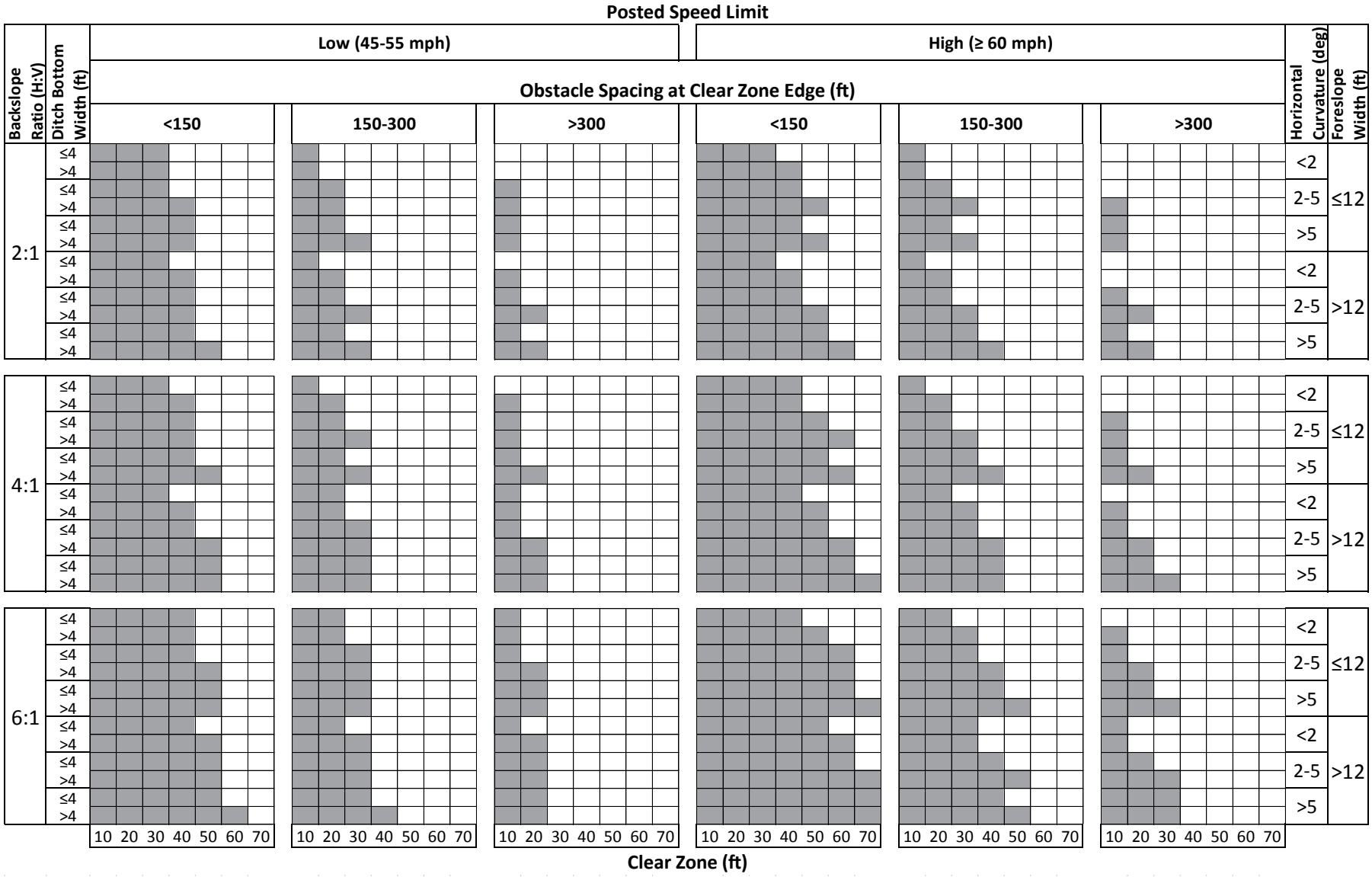

Figure 117. Alternative combined chart for ranges of obstacle spacing at clear zone edge without risk ratios.

Use of Clear Zone Guideline Chart

The chart presented in Figure 116 is used for purposes of this example. An illustrated, step-by-step procedure for finding the applicable clear zone distance for the prescribed roadway and roadside configuration is as follows.

Step 1 – For the given PSL = 50 mph, observe only the three major columns on the left side of the chart corresponding to Low PSL (45–55 mph) (see Figure 118).
Step 2 – For the given average Obstacle Spacing at Clear Zone Edge = 200 ft, select the middle major column in this group corresponding to 150–300 ft (see Figure 119).
Step 3 – For the given Backslope Ratio = 1V:4H, select the second (or middle) major row. This now defines a prescribed box or group of numbers (see Figure 119).
Step 4 – For the given Foreslope Width = 10 ft, reduce to the top six rows of the identified box of numbers corresponding to ≤ 12 ft (see Figure 120).
Step 5 – For the given Horizontal Curvature = 0 degrees, reduce to only the top two rows corresponding to < 2 degrees (see Figure 120).
Step 6 – For the given Ditch Bottom Width = 0 ft, reduce to the top row corresponding to ≤ 4 ft. This row provides the range of relative risk ratios for the given roadway and roadside design configuration, which range from 1.31 on the left to 0.09 on the right (see Figure 121).
Step 7 – Select the leftmost unshaded value in the final row, which for this example is 0.96 (see Figure 121).
Step 8 – Project down the minor column containing the risk value of 0.96 to obtain the recommended Clear Zone distance = 20 ft (see Figure 121).

Use of Clear Zone Equations

Now consider determining the recommended clear zone distance for the same example using the clear zone guideline equations. For the given lower-posted-speed-limit category (i.e., 45 mph ≤ PSL ≤ 55 mph), Eq. 11 should be used to determine the recommended clear zone distance. The design values to use in the equation are as follows.

$HCurveR$ = Radius of horizontal curve = 0 (i.e., no curvature).
$ShldW$ = Shoulder width = 2 ft.
FSW = Foreslope width = 10 ft.
$DBtW$ = Ditch bottom width = 0 (i.e., V-ditch).
BS = Backslope ratio = 4 (horizontal component of slope ratio).
ObS = Average obstacle spacing at clear zone edge = 200 ft.
$FType$ = Facility type = 1 (2U).

Entering these values into Eq. 11 yields Eq. 13 as follows:

$$CZ_D = 12232.9 * 0 + 0.458 * 2 + 0.608 * 10 + 0.621 * 0 + 2.758 * 4 - 0.126 * 200 + 3.384 * 1 + 22.786 = 19 \text{ ft} \quad (13)$$

The recommended clear zone distance using the clear zone guideline equation for the example roadway segment is 19 ft, which is similar to the result from the chart. Note that the equations may not always yield the same result as the chart, because the chart is based on ranges of the design variable values and increments of clear zone distance, whereas the equation computes the recommended clear zone value for specific values of the design variables.

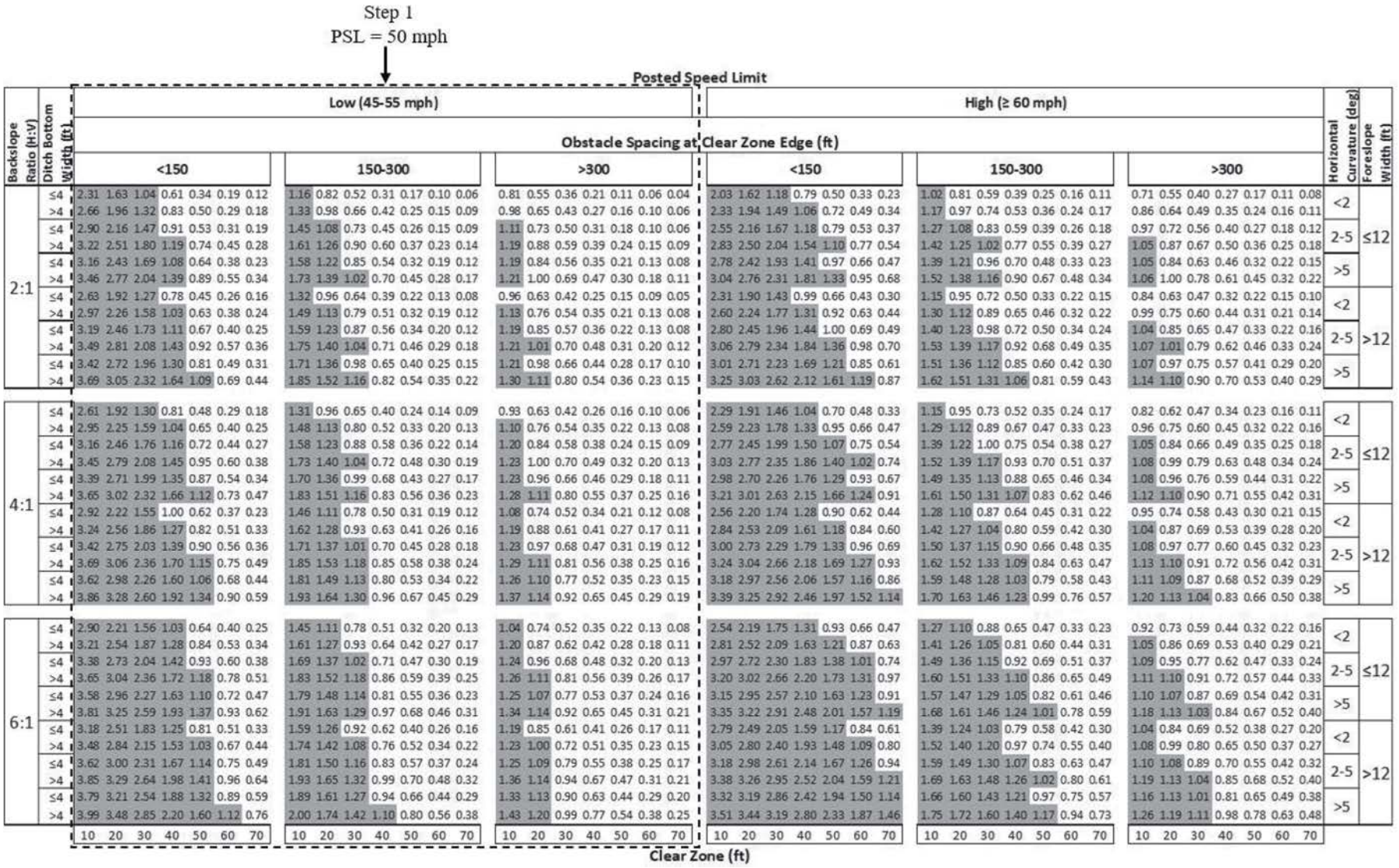

Figure 118. Example of Step 1.

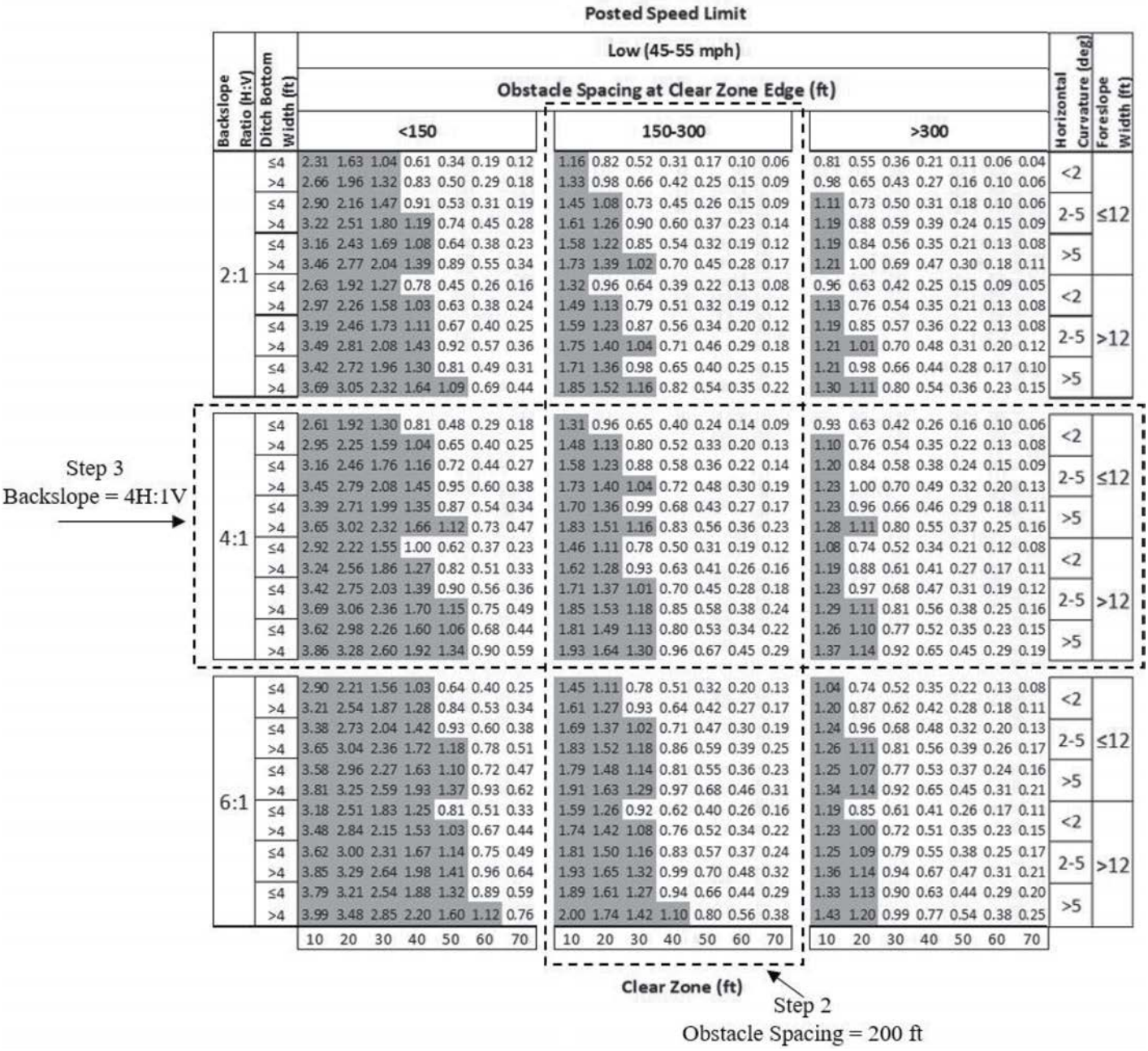

Figure 119. Example of Step 2 and Step 3.

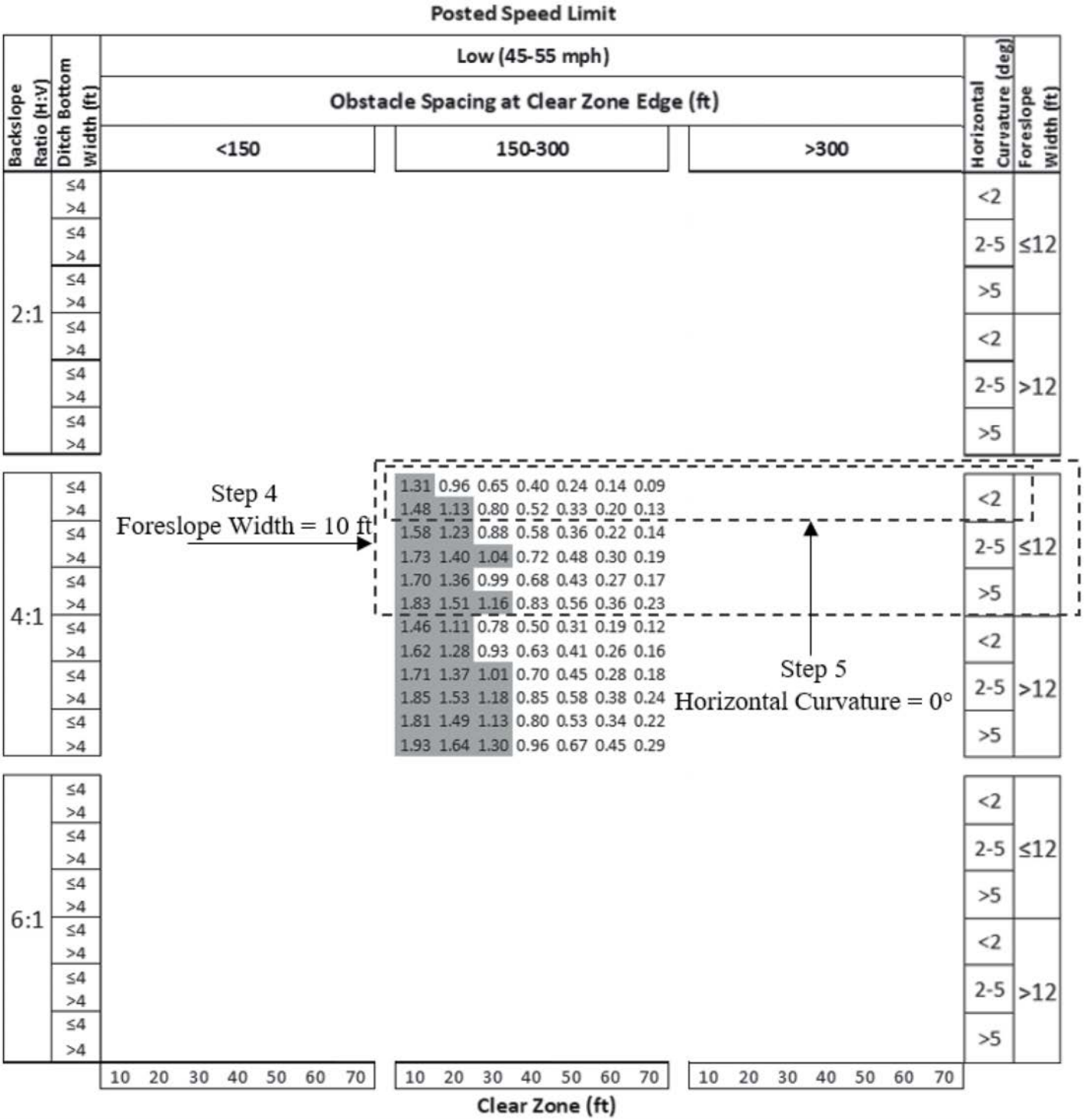

Figure 120. Example of Step 4 and Step 5.

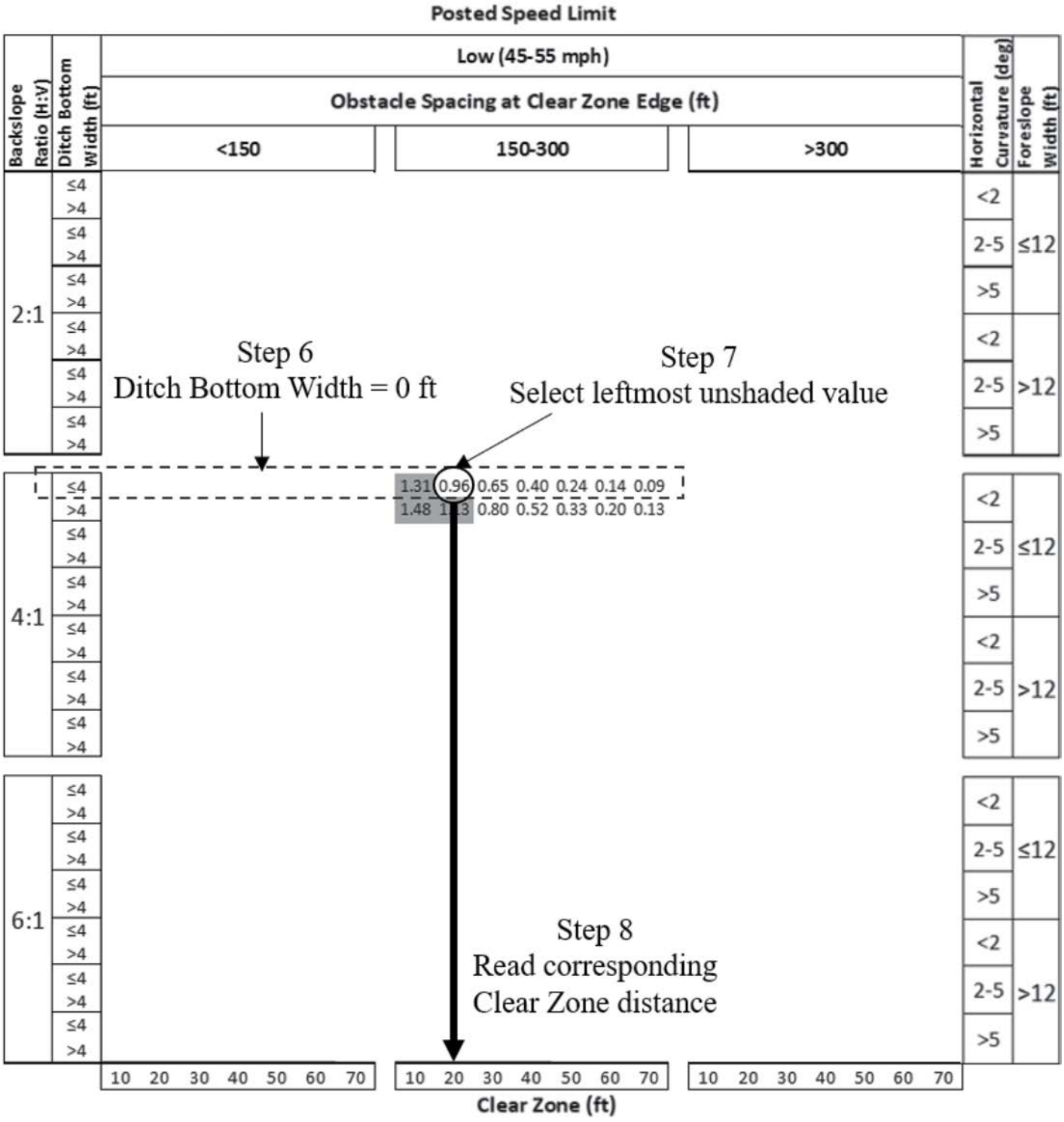

Figure 121. Example of Step 6, Step 7, and Step 8.

CHAPTER 9

Conclusions, Recommendations, and Suggested Research

Summary and Conclusions

Under this project, guidelines for roadside clear zones were developed in terms of key roadway and roadside design parameters. Due to the limitations inherent in using crash data for this purpose, an innovative methodology was used that combined encroachment simulations, crash data, statistical modeling, and risk analysis.

A simulation matrix, consisting of over 2 million encroachments, was executed using a vehicle dynamics code enhanced by the researchers to more accurately account for various vehicle-terrain interactions that can occur during vehicle traversal of roadside terrain features. Use of computer simulation permitted a detailed analysis of vehicle trajectory and resulted in vehicle kinematics for a wide range of variables for which data are not otherwise available. The variables in the simulation matrix included vehicle type, encroachment speed and angle, vehicle orientation at departure (i.e., tracking or non-tracking), driver input (e.g., steering and/or braking), horizontal curvature, vertical grade, shoulder width, foreslope ratio, foreslope width, ditch bottom width, backslope ratio, and backslope width. Simulation output included lateral distance traveled, vehicle stability outcome, trajectory data, and velocity data.

Real-world crash data were used to develop probability distributions for the selected encroachment variables. The results were used to determine marginal probabilities for the values of the encroachment variables used in the simulation matrix that were applied as weighting factors to the simulation results. A probability matrix for vehicle type was developed using vehicle sales data.

Encroachment relationships were derived from the simulation results in terms of significant roadway and roadside design variables to assist with the determination of the probability and severity of an impact given an encroachment has occurred onto the roadside. Models were developed for lateral and longitudinal distance traveled by the encroaching vehicle, rollover probability, and speed and angle at a prescribed lateral and longitudinal offset. These relationships were developed for two ranges of posted speed and two facility types.

The encroachment relationships were incorporated into a risk analysis tool to estimate the probability of a fatal or serious injury crash [P(K+A)] with fixed objects at the clear zone edge. An encroachment-based analysis methodology was used to estimate the conditional probability of a crash given a roadside encroachment has occurred and the probable severity of the crash.

Sensitivity analyses were performed using the risk analysis tool to evaluate the sensitivity of the design variables to the estimation of risk and the relative importance of the variables to the overall determination of P(K+A). The results of the sensitivity analyses were used to determine which variables to retain or exclude from the clear zone guideline development process.

Analyses were parametrically executed using the risk analysis tool to cover combinations of facility type, posted speed limit, roadway and roadside design variables, clear zone distance, and

obstacle spacing beyond the clear zone edge. A relative risk approach was used to define a clear zone distance for a given design configuration that has a P(K+A) risk equal to that of a guardrail.

The final clear recovery area guidelines were developed in both chart and equation form in terms of the most significant design variables. The guidelines can be used to determine a recommended clear recovery distance for a given set of roadway and roadside characteristics and the obstacle spacing beyond the clear zone edge.

For Consideration

The clear zone guidelines developed under the project were formatted and presented in a manner deemed suitable for consideration in a future edition of the AASHTO *Roadside Design Guide* (RDG). The guidelines are presented in both equation and chart-based forms to provide options for a designer.

The guidelines are based on a relative risk assessment. The risk associated with impacting fixed objects at the clear zone edge is compared to the risk associated with impacting a guardrail on the edge of the roadway.

The risk-based guideline is a different approach from the previous guideline. When obstacle spacing is sufficiently large, the risk of a K+A crash is low, and the guideline may recommend a very small clear zone, even for high-speed conditions. Conversely, for very small obstacle spacing, the probability of impacting an obstacle can approach 1.0, and there may not be a practical recommended clear zone distance. In such situations, shielding the roadside with a guardrail could be considered by the designer.

Previous risk-based guidelines have been developed for other design scenarios, such as determining the need and appropriate test levels for median barrier (*29*), bridge rails (*30*), and shielding bridge piers (*31*). The clear zone guidelines developed under this project can be considered for inclusion in a future update of the RDG that incorporates a risk-based philosophy for roadside design.

Suggested Research

The clear zone guidelines developed under this project are based on the injury risk associated with striking fixed objects at the clear zone edge. Another aspect of injury risk associated with roadside encroachments is rollover crashes. The vehicle type, terrain conditions, and driver input can all influence the probability of a rollover crash. This is related to the traversability of a given terrain configuration, which is another aspect of roadside design.

Future research could be performed to incorporate rollover into the clear zone guidelines. Under this project, the weight encroachment simulation data was used to develop a regression model for the probability of rollover based on lateral offset and statistically significant design variables. In addition to being influenced by variables such as shoulder width, foreslope ratio and width, ditch bottom width, and backslope ratio, it was observed that rollover increases nonlinearly with increasing lateral distance. Additionally, a relationship between rollover speed and injury severity was developed under this project using the crash database in *NCHRP Web-Only Document 341* (*3*).

The rollover probability model and rollover severity relationship were incorporated into the Clear Zone Guideline Assistance Program (CZ-GAP) for use in future risk-based analyses. A comprehensive risk-based analysis that includes rollover risk could potentially result in a guideline that encompasses terrain traversability, clear zones, and guardrail need.

References

1. American Association of State Highway and Transportation Officials (AASHTO). *Guide for Selecting, Locating, and Designing Traffic Barriers*. Washington, DC, 1977.
2. American Association of State Highway and Transportation Officials (AASHTO). *Roadside Design Guide*. Washington, DC, 1989.
3. Riexinger, L.E., H.C. Gabler, N. Johnson, K. Kusano, S. Kusano, A. Daniello, and R. Thomson. *NCHRP Web-Only Document 341: Roadside Database Coding Manual.* Transportation Research Board, Washington, DC, 2023.
4. Stonex, K.A. "Roadside Design for Safety." *Highway Research Board Proceedings*, Volume 39. Highway Research Board, Washington, DC, 1960.
5. Stonex, K.A. "Relation of Cross-Section Design and Highway Safety." Presented at the 35th Annual Highway Conference, University of Colorado, Denver, CO, February 1962.
6. American Association of State Highway Officials (AASHO). *Highway Design and Operational Practices Related to Highway Safety*. Washington, DC, 1967.
7. American Association of State Highway and Transportation Officials (AASHTO). *Highway Design and Operational Practices Related to Highway Safety*, 2nd ed. Washington, DC, 1974.
8. Graham, J.L., and D.W. Hardwood. *NCHRP Report 247: Effectiveness of Clear Recovery Zones.* TRB, National Research Council, Washington, DC, May 1982.
9. Zegeer, C.V., J. Hummer, D.W. Reinfurt, L. Herf, and W.W. Hunter. *Safety Effects of Cross-Section Design for Two-Lane Roads*. Report No. FHWA/RD-87-008. Federal Highway Administration, Washington, DC, October 1987.
10. Ross, H.E. Jr., T.L. Kohutek, and J. Pledger. *Guide for Selecting, Locating, and Designing Traffic Barriers*, Volumes I and II. Final Report, U.S. Department of Transportation, Contract FH-11-8507. Texas Transportation Institute, Texas A&M University System, College Station, TX, February 1976.
11. Segal, D.J. *Highway-Vehicle-Object Simulation Model - 1976*, Volumes I–IV. Report Numbers FHWA-RD-76-162 to 165. Federal Highway Administration, Washington, DC, 1976.
12. American Association of State Highway and Transportation Officials (AASHTO). *Roadside Design Guide*. Washington, DC, 2002.
13. American Association of State Highway and Transportation Officials (AASHTO). *Roadside Design Guide*, 4th ed. Washington, DC, 2011.
14. Radja, G.A. *National Automotive Sampling System – Crashworthiness Data System, Analytical User's Manual 2015.* No. DOT HS 812 321. National Highway Traffic Safety Administration, Washington, DC, 2016.
15. Mak, K.K., and D.L. Sicking. *NCHRP Report 492: Roadside Safety Analysis Program (RSAP)—Engineer's Manual.* TRB, National Research Council, Washington, DC, 2003.
16. Mak, K.K., D.L. Sicking, and B.A. Coon. *NCHRP Report 665: Identification of Vehicle Impact Conditions Associated with Serious Ran-Off-Road Crashes.* Transportation Research Board of the National Academies, Washington, DC, 2009.
17. Ferdous, M.R. *Placement of Traffic Barriers on Roadside and Median Slopes. Department of Civil Engineering.* Texas A&M University, College Station, TX, 2011.
18. Sheikh, N.M., S.-P. Miaou, R.P. Bligh, and D.L. Bullard, Jr. *NCHRP Web-Only Document 296: Guidelines for Cost-Effective Safety Treatments of Roadside Ditches*. Transportation Research Board, Washington, DC, 2021.
19. Sheikh, N.M., R.P. Bligh, S. Cakalli, and S-.P. Miaou. *NCHRP Research Report 911: Guidelines for Traversability of Roadside Slopes.* Transportation Research Board, Washington, DC, 2019.
20. Ross, H.E., Jr., H.S. Perera, D.L. Sicking, and R.P. Bligh. *NCHRP Report 318: Roadside Safety Design for Small Vehicles.* TRB, National Research Council, Washington, DC, 1989.

21. American Association of State Highway and Transportation Officials (AASHTO). *Manual for Assessing Safety Hardware* (MASH). Washington, DC, 2016.
22. 4N6XPRT Systems. Expert AutoStats, 2020 Release. 4N6XPRT Systems Forensic Expert Software. La Mesa, CA, 2020.
23. Highway Loss Data Institute. *Technical Appendix*. Highway Loss Data Institute, Arlington, VA, 2010. Available: https://www.iihs.org/media/80eed4d2-96e2-43b8-8381-34ca4274346c/dXp2Ww/Ratings/Protocols/current/tech_10.pdf. Retrieved September 2, 2021.
24. Stolle, C.S., K. Ronspies, R.W. Bielenberg, and R.K. Faller. *Evaluation and Update of MASH Test Vehicles*. Midwest Roadside Safety Facility, University of Nebraska–Lincoln, 2021.
25. Ray, M.H., C.E. Carrigan, C.A. Plaxico, S.-P. Miaou, and T.O. Johnson. *NCHRP Web-Only Document 319: Roadside Safety Analysis Program (RSAP) Update*. Transportation Research Board, Washington, DC, 2012.
26. Ray, M.H., C.E. Carrigan, and C. Plaxico. *Estimating Crash Costs in the Updated Roadside Safety Analysis Program*. Transportation Research Board 91st Annual Meeting, Transportation Research Board, Washington, DC, 2011.
27. NHTSA (National Highway Traffic Safety Administration). *MMUCC Guideline: Model Minimum Uniform Crash Criteria,* 5th ed. No. DOT HS 812 433. NHTSA, Washington, DC, 2017.
28. Ray, M.H., C.E. Carrigan, and E.M. Ray. *NCHRP Research Report 972: Development of Safety Performance-Based Guidelines for the* Roadside Design Guide. Transportation Research Board. Washington, DC, 2022.
29. Carrigan, C.E., and M.H. Ray. *NCHRP Research Report 996: Selection and Placement Guidelines for Test-Level 2 Through Test-Level 5 Median Barriers*. Transportation Research Board, Washington, DC, 2022.
30. Ray, M.H., and C.E. Carrigan. *NCHRP Web-Only Document 307: Guidelines for the Selection of Test-Levels 2 Through 5 Bridge Railings*. Transportation Research Board, Washington, DC, 2021.
31. Ray, M.H., C.E. Carrigan, and C. Plaxico. *NCHRP Research Report 892: Guidelines for Shielding Bridge Piers*. Transportation Research Board, Washington, DC, 2018.

List of Abbreviations

2U	2-lane undivided
4D	4-lane divided
AASHO	American Association of Highway Officials
AASHTO	American Association of State Highway and Transportation Officials
ABS	Antilock braking system
ADT	Average daily traffic
AIS	Abbreviated Injury Scale
CDS	Crashworthiness Data System
CG	Center of gravity
CPU	Central processing unit
CUV	Compact utility vehicle
CZ-GAP	Clear Zone Guideline Assistance Program
MASH	*Manual for Assessing Safety Hardware*
MMUCC	Model Minimum Uniform Crash Criteria
MSE	Mean square error
NASS	National Automotive Sampling System
NHTSA	National Highway Traffic Safety Administration
P(K+A)	Probability of fatal + serious injury crash
POD	Point of departure
PRT	Perception-reaction time
q-q	Quantile to quantile
RDG	*Roadside Design Guide*
RSAP	Roadside Safety Analysis Program
RSAPv3	Roadside Safety Analysis Program, Version 3
SIM	Simulation interface manager
SUV	Sport utility vehicle
TTI	Texas A&M Transportation Institute
VBA	Visual Basic for Applications

Abbreviations and acronyms used without definitions in TRB publications:

A4A	Airlines for America
AAAE	American Association of Airport Executives
AASHO	American Association of State Highway Officials
AASHTO	American Association of State Highway and Transportation Officials
ACI–NA	Airports Council International–North America
ACRP	Airport Cooperative Research Program
ADA	Americans with Disabilities Act
APTA	American Public Transportation Association
ASCE	American Society of Civil Engineers
ASME	American Society of Mechanical Engineers
ASTM	American Society for Testing and Materials
ATA	American Trucking Associations
CTAA	Community Transportation Association of America
CTBSSP	Commercial Truck and Bus Safety Synthesis Program
DHS	Department of Homeland Security
DOE	Department of Energy
EPA	Environmental Protection Agency
FAA	Federal Aviation Administration
FAST	Fixing America's Surface Transportation Act (2015)
FHWA	Federal Highway Administration
FMCSA	Federal Motor Carrier Safety Administration
FRA	Federal Railroad Administration
FTA	Federal Transit Administration
GHSA	Governors Highway Safety Association
HMCRP	Hazardous Materials Cooperative Research Program
IEEE	Institute of Electrical and Electronics Engineers
ISTEA	Intermodal Surface Transportation Efficiency Act of 1991
ITE	Institute of Transportation Engineers
MAP-21	Moving Ahead for Progress in the 21st Century Act (2012)
NASA	National Aeronautics and Space Administration
NASAO	National Association of State Aviation Officials
NCFRP	National Cooperative Freight Research Program
NCHRP	National Cooperative Highway Research Program
NHTSA	National Highway Traffic Safety Administration
NTSB	National Transportation Safety Board
PHMSA	Pipeline and Hazardous Materials Safety Administration
RITA	Research and Innovative Technology Administration
SAE	Society of Automotive Engineers
SAFETEA-LU	Safe, Accountable, Flexible, Efficient Transportation Equity Act: A Legacy for Users (2005)
TCRP	Transit Cooperative Research Program
TEA-21	Transportation Equity Act for the 21st Century (1998)
TRB	Transportation Research Board
TSA	Transportation Security Administration
U.S. DOT	United States Department of Transportation

Transportation Research Board
500 Fifth Street, NW
Washington, DC 20001

ADDRESS SERVICE REQUESTED

NATIONAL ACADEMIES *Sciences Engineering Medicine*

The National Academies provide independent, trustworthy advice that advances solutions to society's most complex challenges.
www.nationalacademies.org

ISBN 978-0-309-70945-3
90000
9 780309 709453